Ciclostratigrafia e tuning astronomico delle alternanze calcareo-marnosi Maastrichtiane di Zumaia e Sopelana, Paesi Baschi, N-Spagna

Sietske J. Batenburg

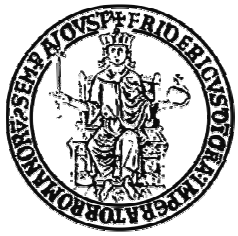

XXV ciclo dottorato

Università degli Studi di Napoli Federico II

Tutor: Mario Sprovieri

Marzo 2013

Ciclostratigrafia e tuning astronomico delle alternanze calcareo-marnosi Maastrichtiane di Zumaia e Sopelana, Paesi Baschi, N-Spagna

Cyclostratigraphy and astronomical tuning of the Maastrichtian limestone-marl alternations at Zumaia and Sopelana, Basque country, N-Spain

Sietske J. Batenburg

Abstract

We present an astronomical time scale for the Maastrichtian based on an integrated stratigraphy of the Zumaia and Sopelana sections in northern Spain. The cyclic alternations of hemipelagic limestones and marls at Sopelana and Zumaia display the range of periodicities of eccentricity-modulated precession. The rhythmic bedding pattern is primarily caused by variations in siliciclastic supply and to a lesser extent to variations in biological productivity, both of which controlled by eccentricity-modulated precession through its influence on the hydrological cycle. Together, the Zumaia and Sopelana sections span almost the entire Maastrichtian, and encompass thirteen 405-kyr cycles, spanning a total duration of 5.3 Myr. Consecutive 405-kyr minima in the lithological and geophysical data records are tuned to successive 405-kyr minima in the new La2011 eccentricity solution. Assuming a K/Pg boundary age of 65.97 Ma, we present orbitally tuned ages of biostratigraphic and magnetostratigraphic events. The bases of Chrons C29r and C30n have been reliably established at Zumaia and their astronomically tuned ages are in good agreement with previous studies. Data from Sopelana provide a refinement of the age of the base of Chron C31r. Planktonic foraminifera and calcareous nannoplankton data from Zumaia, and new calcareous nannoplankton data from Sopelana allow for worldwide correlation of the cyclostratigraphy of the Basque country. Additionally, the orbitally tuned bulk carbonate carbon isotope curve displays a remarkable amplitude of variation. Strong oscillations in $\delta^{13}C$ seem regularly paced by the 405-kyr periodicity of eccentricity modulated precession. Additionally, sharp negative shifts associated with falls in sea-level occur at regular intervals of ~1.2 Myr. We present a new global correlation of carbon isotope stratigraphies with an astronomically tuned age model based on the cyclostratigraphy of Zumaia and Sopelana and site 762C (Exmouth Plateau). The Late Campanian/Maastrichtian carbon isotope correlation scheme displays a series of trends and excursions that can be observed across the different depositional settings. We propose that the 405-kyr cycle of eccentricity, and potentially longer periodicities, paced the latest Cretaceous climate and carbon cycle.

Contents

Chapter 1. Introduction

1.1 Cyclostratigraphy and astronomical tuning

The Earth's climate is strongly controlled by the amount of energy we receive from the sun, and on long time scales, this depends on the position of the Earth. Gravitational interactions with other bodies in our solar system cause quasi-periodic variations in the Earth's orbit and axial position.

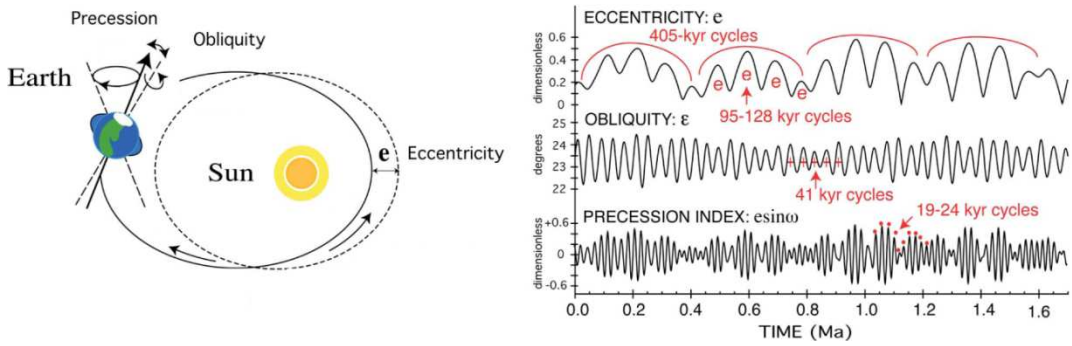

Figure 1: Modified from Hinnov and Ogg (2007). Left: The Earth's orbital parameters: eccentricity, the ellipticity of the Earth's orbit; precession of the ellipse and of the equinoxes, which describe the gradual rotation of the Earth's axis, similar to the spinning of a top; and obliquity, the tilt of the Earth's axis. Right: eccentricity, obliquity and precession over the last 1.6 Ma (Laskar et al., 2004), with main periodicities indicated in red. Due to interactions in the Earth-Moon system, and the closer position of the Moon to the Earth, the periodicities of precession and obliquity were slightly shorter for the Late Cretaceous than for the present-day, at ~21.8 for precession and ~39 kyr for obliquity.

The realisation that orbital parameters influence climate and sedimentation, initially by Adhémar (1842) and Croll (1864), has lead to great advancements in our understanding of past climate and time scales. The study of cyclic variations in the stratigraphic record, and the impact of orbital variations on paleo-environments, is

called cyclostratigraphy. The first known cyclostratigraphic study, of Cretaceous strata in Colorado, is by Gilbert (1895). The field was much advanced by Milankovitch, who calculated the first curves of insolation, the amount of energy received from the sun at the top of the Earth's atmosphere, and who developed a theory of the ice ages (Milanković, 1941). Astronomical tuning is the calibration of cyclic sedimentary variations to such astronomical target curves. The detection of orbital periodicities in land-based marine sections, mostly in the Mediterranean area, has greatly improved the Neogene and Quaternary time scale (23 to 0 Ma)(Fischer et al., 2009; Hilgen et al., 1999; Lourens et al., 2004). This has gone hand-in-hand with advancements in the astronomical solutions, which reconstruct the amount of energy received by the sun, termed insolation, over time (Berger, 1978; Laskar et al., 2004, 1993; Varadi et al., 2003). Great progress in the development of orbital time scales was made with the advent of ocean drilling, where long, continuous sedimentary records from the sea floor provide excellently preserved archives of Earth's climate, and by the development of new climate sensitive proxies such as stable oxygen isotope ratios (Emiliani, 1955). Such records have been used extensively to obtain better time control on the Cenozoic, for example for the Oligocene (33.9 to 23 Ma) (Pälike et al., 2006) and the Paleocene (Westerhold et al., 2008). Recently, the orbital tuning of Campanian-Maastrichtian ocean cores (latest Cretaceous) (Husson et al., 2011) has been incorporated in the Geologic Time Scale 2012 (Ogg and Hinnov, 2012).

1.2 The Late Cretaceous

The Cretaceous period was characterised by a warm climate and high sea-levels, with large epicontinental seas covering present day low-lying land. This vast area of shallow seas together with the rise in numbers of groups of skeleton-forming micro-organisms has led to the widespread deposition of limestone. In the boreal realm we find the seemingly homogenous white chalk or creta (Latin) or Kreide (German), from which the Cretaceous derives its name and abbreviation "K". In other settings, the deposition of limestones and marls occurred in a rhythmic fashion, sensitive to the amount of clay brought in by rivers and dust, and to the

amount of productivity by micro-organisms. Such Cretaceous rhythmic limestone-marl alternations, for example in the Umbria-Marche basin in Italy (Herbert and Fischer, 1986), have long been recognised to have frequency ratios corresponding to those of orbital parameters. However, the establishment of orbitally tuned time scales for the Cretaceous is hampered by the reliability of the astronomical solution, and only the stable 405-kyr periodicity of eccentricity-modulated precession can be used as a tuning target. Radiometric dating can provide independent age control to identify the correct 405-kyr cycle and anchor astronomical tuning efforts to the absolute time scale. Nevertheless, radiometric dating techniques can suffer from an increasing error further back in time, causing many Cretaceous tunings to remain floating (Fiet et al., 2001; Gale et al., 1999; Sprovieri et al., 2006).

1.3 Rationale

Recently, the astronomical time scale for the Maastrichtian (72.1 to 66 Ma) has been improved by tuning of geophysical records from ocean drilling cores (Husson et al., 2011). However, such cores have a limited resolution and rarely reflect the full range of orbital periodicities. This study proposes to take the orbitally tuned time scale for the Late Cretaceous to the next level, and use land-based marine sections to improve and refine the Maastrichtian time scale. Similar to the Mediterranean Neogene successions, the selected Cretaceous sections reflect the range of periodicities of eccentricity-modulated precession, and allow obtaining a cyclostratigraphic interpretation on a precessional resolution (~21.8 kyr).

1.3.1 The Maastrichtian Zumaia and Sopelana sections

The Zumaia and Sopelana sections in the Basque Country, northern Spain, contain hemipelagic limestone-marl alternations (Fig. 2) and provide an excellent opportunity to improve the Maastrichtian time scale. These sections are investigated with the aim to detect the range of orbital periodicities and the

potential expression of the stable 405-kyr periodicity of eccentricity. The continuity of the sections is investigated by analysis of the behaviour of potential longer term periodicities and analysis of stable carbon isotope ratios and comparison with existing carbon isotope stratigraphies. The reliability of a field-based cyclostratigraphic interpretation is tested by statistical analyses of high resolution geophysical data sets. After a phase relation with eccentricity is determined, the 405-kyr periodicity, as identified in the lithological and geophysical data records, is tuned to the extracted 405-kyr component of eccentricity in the latest astronomical target curve La2011 (Laskar et al., 2011).

To use the established astronomical tuning elsewhere, and to enable comparison with existing astrochronologies, magnetostratigraphic and biostratigraphic data are collected, as well as a stable carbon isotope curve, which allow for global correlation. The carbon isotope stratigraphy permits to distinguish between regional and global climatic influences on the Basque-Cantabric Basin. Finally, we aim to investigate the underlying climatic mechanisms leading to the deposition of the rhythmic limestone-marl alternations in the Basque successions of Maastrichtian and Danian (66 to 61.6 Ma).

1.4 GTSnext

This research is part of the European Commission Seveth Framework Programme - funded Initial Training Network GTSnext, “towards the next generation Geologic Time Scale”, funded under grant agreement 215458 . Within this project, nine PhD students and three Post-docs work on intercalibration of astronomical and radiometric (Ar-Ar and U/Pb) dating techniques, to better constrain the research methods and to obtain improved ages for dating standards, such as the Fish Canyon Sanidine, and stratigraphic levels, such as the Cretaceous/Paleogene boundary. These efforts are resulting in a step forward in the improvement of the Geologic Time Scale and in the training and encouragement of a new generation of geochronologists.

Fig. 2: The Maastrichtian Zumaia and Sopelana sections, Basque Country, northern Spain, containing hemipelagic limestone-marl alternations and spanning the Cretaceous/Paleogene Boundary (K/Pg)

Chapter 2. Cyclostratigraphy and astronomical tuning of the Late Maastrichtian at Zumaia (Basque country, Northern Spain)

published as:
Batenburg, S.J., Sprovieri, M., Gale, A.S., Hilgen, F.J., Hüsing, S., Laskar, J., Liebrand, D., Lirer, F., Orue-Etxebarria, X., Pelosi, N., Smit, J., 2012. Cyclostratigraphy and astronomical tuning of the Late Maastrichtian at Zumaia (Basque country, Northern Spain). *Earth and Planetary Science Letters* 359–360, 264–278.

Abstract

The standard Geological Time Scale for the Cretaceous is still largely based on seafloor anomaly profiles combined with radio-isotopic tie-points. The astronomical tuned time scale with its much higher resolution and accuracy has recently been extended to the K/Pg-boundary and is being extended into the Cretaceous. To construct such a time scale for the Cretaceous, we selected the upper Maastrichtian of the Zumaia section in the Basque country (northern Spain) which contains a cyclic alternation of limestones and marls deposited in a hemipelagic setting. The Paleogene portion of the Zumaia section has previously been studied for a joint cyclostratigraphic-radioisotopic intercalibration of the age of the K/Pg boundary. Here we present a high-resolution cyclostratigraphic framework for the upper Maastrichtian (Latest Cretaceous) of the Zumaia section in the Basque country (northern Spain), with new biostratigraphic and magnetostratigraphic data. Bed-to-bed correlation with the nearby Sopelana section provides additional bio- and magnetostratigraphic constraints. The stacking pattern of the lithologies shows a hierarchy that reflects the combined influence of the orbital parameters of precession and eccentricity. This is confirmed by time series analyses of lithological and geochemical data indicating a strong influence of eccentricity-modulated precession on latest Cretaceous climate as well. The expression of the 405-kyr eccentricity cycle serves as primary signal for astronomical tuning. We provide two

tuning options depending on absolute K/Pg-boundary ages of 65.56 and 65.97 Ma. The logged part of the section encompasses nine and a half 405-kyr cycles in total and spans 3.9 Myr. The acquired cyclostratigraphic framework provides ages for characteristic planktonic foraminiferal events, magnetic reversals and carbon isotope excursions and resolves the late Maastrichtian time scale in unprecedented detail with relative age uncertainties <100 kyr. The high resolution and large amplitude of shifts in $\delta^{13}C$ on the 405-kyr and 1.2-Myr scales allow for global correlation and may shed more light on the orbital pacing of late Cretaceous climate.

1 Introduction

Astronomical tuning of cyclic climate records of late Cretaceous age has the potential to significantly reduce current uncertainties in the Geological Time Scale. Until recently, the magnetic polarity time scale for this time interval was constructed using seafloor anomaly profiles in combination with a limited set of radio-isotopic tie-points (Gradstein et al. 2004; Cande and Kent 1995). Resultant ages typically have uncertainties up to 0.5 Myr. Astronomical tuning has allowed for a much more detailed and accurate chronology for the younger Cenozoic parts of the Geological Time Scale: most of the Neogene is tuned on the precession and obliquity scale, although uncertainties remain in its older part (Lourens et al., 2004), and most of the Paleogene to the long 405-kyr eccentricity cycle (Pälike et al., 2001; Dinarès-Turell et al., 2003; Röhl et al., 2003; Lourens et al., 2005; Pälike, Norris, et al., 2006; Pälike and Hilgen, 2008; Westerhold et al., 2008, 2012; Westerhold and Röhl, 2009; Hilgen et al., 2010). In view of recent improvements in the astronomical solution (e.g., Laskar et al., 2011), the tuning is being extended into the Late Cretaceous, using only the stable 405-kyr eccentricity cycle for age-assignment.

Herbert (1999) used the expression of the long eccentricity modulation of precessional amplitude in reflectance records of South Atlantic Deep Sea Drilling Project (DSDP) cores from sites 516F, 525A, 527 and 528 (South Atlantic) to

establish an astronomical estimate for durations of Late Cretaceous magnetochrons. This resulted in a floating chronology that gives durations, but not ages, as it was not anchored to orbital target curves. Husson et al. (2011) have recently improved and extended these estimates through direct astronomical tuning of magnetic susceptibility records from Ocean Drilling Program (ODP) Leg 207 (equatorial Atlantic) and 208 (South Atlantic), and grey level variations from ODP-Leg 122 (Indian Ocean) and DSDP-Leg 74 (South Atlantic). They presented two tuning options, following existing uncertainties in the tuning of the Paleocene (Westerhold et al. 2008; Kuiper et al. 2008; Hilgen et al. 2010).

A suitable section for independently testing the tuning of the Maastrichtian is the Zumaia section located in the Basque country in northern Spain (Fig. 1). These coastal cliffs are famous for their rhythmically bedded Late Cretaceous to Eocene deposits of hemipelagic limestones and marls and form a classical site for paleoclimatic studies, magnetostratigraphic, biostratigraphic and cyclostratigraphic studies (Herm, 1965; Percival and Fischer, 1977; Lamolda, 1990; Ward et al., 1991; Ward and Kennedy, 1993; ten Kate and Sprenger, 1993; Pujalte et al., 1995; Dinarès-Turell et al., 2003; Elorza and García-Garmilla, 1998; Gómez –Alday et al., 2008). Carbon and oxygen isotope values have been reported in low resolution for the upper Maastrichtian and lowermost Danian interval in Zumaia (Mount et al. 1986; Margolis et al. 1987), for an 85 m Mid-Maastrichtian interval (Paul and Lamolda, 2007) and for the Paleocene interval (Schmitz et al. 1997). Recently, two GSSPs have been ratified in Zumaia, marking the bases of the Thanetian and Selandian stages of the Paleocene (Schmitz et al., 2011). The Zumaia section is one of the reference sections for the K/Pg-boundary interval, which is well exposed and contains an iridium anomaly and extinction events of planktonic foraminifera (Smit & ten Kate 1982; Alvarez et al, 1982; Pujalte et al. 1995; Apellaniz et al., 1997). The section plays an important role in determining the age of the K/Pg-boundary, which is currently under discussion.

In this study, we focus on the Maastrichtian part of the Zumaia section to complement and improve the cyclostratigraphic framework and tuning of the Maastrichtian. We present a detailed magnetobiostratigraphy and continuous, high-resolution records of carbon isotopes, reflectance and magnetic susceptibility of the rhythmically bedded Maastrichtian part of the Zumaia section. Following the identification of the 405-kyr cyclicity in these records, the Zumaia section is tuned to provide astronomical ages of biostratigraphic, magnetostratigraphic and stable isotope events, for regional and global correlation. Finally, a comparison with existing time scales is made, and the astrochronologies of Husson et al. (2011) and Thibault, Husson et al. (2012) are independently tested.

2 Geological setting and sections

2.1 Basque-Cantabric basin of Spain

The Zumaia section, together with the Bidart, Hendaye and Sopelana coastal sections , as well as the Trabakua section further in-land (Pujalte et al., 1998), contains marine sediments that were deposited in the flysch trough of the Basque-Cantabric basin (Fig. 1) (Mary et al. 1991; Pujalte et al. 1995; Pujalte et al. 1998). This interplate trough was formed in the Early Campanian, as smaller basins from previous rifting stages joined at the start of the Pyrenean convergence (Pujalte et al. 1998). Whereas the lower Maastrichtian in Zumaia is represented by a thick turbidite succession, deposited during an interval of increased subsidence, the Upper Maastrichtian to Paleocene was characterised by relative tectonic stability, and only slight subsidence (Pujalte et al. 1998). Limestones, marls and occasional turbidites were deposited in a hemipelagic setting with an estimated water depth of 800-1500m. The basin opened into the Bay of Biscay to the west and was surrounded by shallow shelf areas (Pujalte et al. 1998).

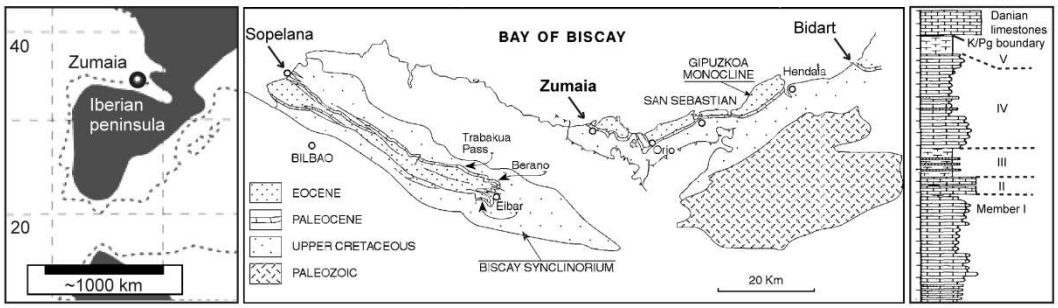

Figure 1: Paleogeographic setting (Gómez –Alday et al., 2008), simplified geologic map of the study area, from Pujalte et al. (1998) and schematic stratigraphic log from Ward et al (1991) with members as distinguished by them.

2.2 Studied sections

2.2.1 Zumaia

The Upper Maastrichtian interval at Zumaia spans 145 m and is composed of rhythmically bedded limestones and reddish marls with thin intercalated siliciclastic or calcareous turbidites. These turbidites, although they are many (ten Kate and Sprenger, 1993), do not disrupt the pattern of alternating limestones and marls in the Upper Maastrichtian portion of the section. The sequence of alternating marls and limestones reveals cyclicity on different scales, as summarised in Table 1. On a large scale of ~40 m, there are overall changes in carbonate (light) and clay (purple-red) content, which make the expression of the smallest scale alternations (~77 cm) quite variable. The ~20 m-intervals of purple marls have been interpreted in terms of sequence stratigraphy as Lowstand Slope Fan complexes, and the ~20 m grey-red limestone-marl alternations as Transgressive/Highstand Systems Tract deposits (Pujalte et al. 2000). The smallest scale (~77 cm) alternations consist of lighter and darker marls in the lowstand units and of alternating limestones and marls in the transgressive/highstand units. These small scale alternations, or couplets, are grouped in bundles of five (~4 m), and these again in groups of four (Fig. 2 and 3) that have an average thickness of ~16 m. As the thickness ratios (0.77:4:16 m

equals 1:5:20) agree with the ratio of the periodicities of eccentricity modulated precession (21.8:100:405 kyr equals 1:5:20), we interpret the individual couplets as the expression of the precessional cycle. The variations in colour and resistance, most prominent in the marly units of the couplets, were recorded in high detail in the stratigraphic log and the couplets were numbered (Fig. 3). A total of 189 precessional cycles have been identified, including four couplets with very poorly expressed marls that have been marked with "a" and "b" (Fig. 3).

Scale of alternation	Lithological expression	Interpreted depositional mechanism
~ 80 cm	Couplets of either limestone/marl alternations or marl/marl alternations with differences in resistance and colour (lightness and redness)	Individual precessional cycles of ~21kyr
~ 4 m	Bundles of five ~80-cm couplets, mostly expressed in the marlier parts of the cycles, by increased thickness, darkness and redness.	Short term eccentricity cycle of ~100kyr
~ 16 m	Groups of four ~4-m bundles, bounded by characteristic couplets with a limited and thinner expression of the marlier part of the couplet.	Long term eccentricity cycle of 405kyr, with a distinctive expression of the minima
~40 m	Variations in colour (greyness and redness) and resistance	Long term (~1.2Myr) variations in carbonate and clay content

Table 1: Different scales of lithological alternations in the Zumaia section

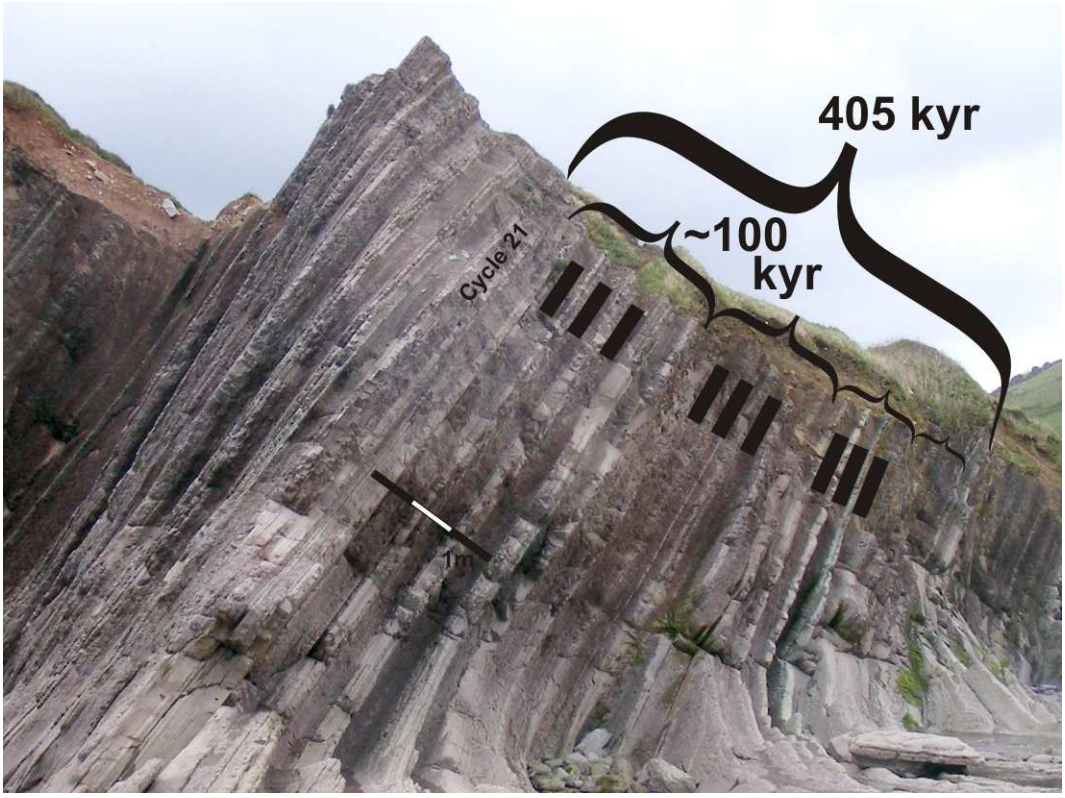

Figure 2: Part of the Zumaia section displaying the hierarchical stacking pattern with couplets in bundles of five, and these in groups of four, interpreted as the ~100-kyr and 405-kyr periodicities, respectively. The black lines indicate the most prominent marls.

2.2 Sopelana

The Sopelana section also forms part of the Basque Maastrichtian succession and shows a similar alternation of limestones and marls, without the occurrence of turbidites. The Upper Maastrichtian interval of the Sopelana section is characterised by a number of faults, but despite these, the following intervals can be correlated to the Zumaia section by recognition of patterns and marker beds: from cycle 13-29, 79-117, 145- 153, and from cycle 156 downwards, where the section is undisturbed. Only those intervals in Sopelana that have been sampled for paleomagnetism have been incorporated in the log (Fig. 3). These display excellent bed-to-bed correlation, which is in agreement with the recognition of the large-scale (~40 m) alternation as has previously been reported by Ward et al. (1991) (Fig.

3). The Sopelana section has been successfully studied for low-resolution magnetostratigraphy providing approximate locations for several reversals (Mary et al. 1991; Moreau et al. 1994).

2.2.3 Bidart

The coastal cliffs of the Bidart section in south west France, south of Biarritz, reveal faults but the succession is continuous over the K/Pg boundary interval (Galbrun and Gardin, 2004). Approximately 8 m of Maastrichtian redbrown marls and marly limestones, of which the top 30 cm are gray, are overlain by the clay-rich boundary layer, green at its base, and Danian limestones. Samples for biostratigraphic analysis have been taken in the marliest intervals of the topmost 8m of Maastrichtian sediments.

3. Materials and Methods

3.1 Sampling

To obtain climatically sensitive proxy records, samples were taken with hammer and chisel throughout the Zumaia section, in a high resolution of 5-10 samples per limestone/marl couplet (e.g. precession cycle), at an average distance of 10 cm. These samples were analysed for stable carbon isotope ratios, magnetic susceptibility and colour reflectance, after which time series analysis was applied to the records. Oriented cores were drilled for paleomagnetic analyses in both the Zumaia and Sopelana sections, and additional samples were taken in the Zumaia, Sopelana and Bidart sections for the detection of biostratigraphic marker events.

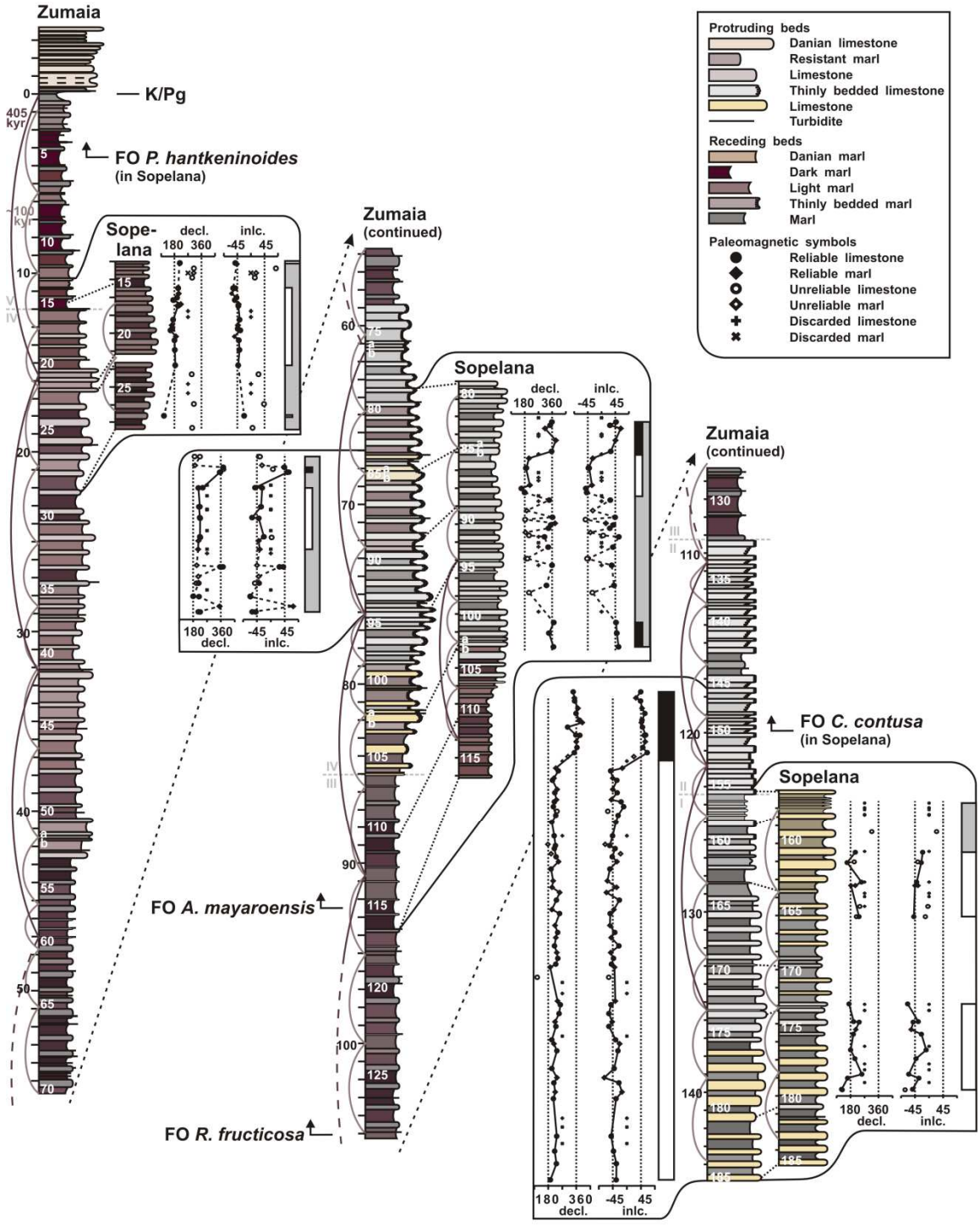

Figure 3: Stratigraphic log of the Zumaia section and selected intervals of the Sopelana section with key biostratigraphic events and magnetostratigraphy from this study. Grey roman numerals indicate the intervals identified by Ward et al. (1991). The half circles in deep purple indicate the 405-kyr eccentricity minima, the lighter half circles indicate the 100-kyr bundling. White numbers are cycle numbers.

3.2 Biostratigraphy

The first occurrences of four species of planktonic foraminifera, *Contusotruncana contusa*, *Abathomphalus mayaroensis*, *Racemiguembelina fructicosa* and *Plummerita hantkeninoides*, are recognised in the Basque sections. These species are important biostratigraphic markers, used for defining biohorizons in the Late Maastrichtian, and possess clear characteristics that allow them to be distinguished from similar species (Supplementary text).

For *A. mayaroensis*, *R. fructicosa* and *C. contusa*, samples were taken from marly lithologies in selected intervals in Zumaia and Sopelana. Hundreds of specimens were studied in the fraction 250-630µm. Samples for *P. hantkeninoides* were taken in Sopelana and in the coastal section of Bidart, France. The Bidart section has a good exposure of the K/Pg-boundary interval (Galbrun and Gardin, 2004) and the bedding pattern can be correlated to Zumaia. For *P. hantkeninoides*, thousands of specimens from the fraction 100-300µm were analysed, because of its rare occurrence along the Basque coast.

3.3 Magnetostratigraphy

With a gasoline-powered drill, 111 oriented samples were taken in the Zumaia section and 140 in Sopelana, with two samples per limestone and one per marl. Two intervals were sampled in the Zumaia section (cycle 84-94, 145-185) and three in Sopelana (cycle 13-29, 82-103 and 157-180), based on previously identified reversal boundaries by Mary et al. (1991). From each oriented sample level, one specimen was thermally demagnetized in a magnetically shielded furnace using numerous small temperature increments, at 20, 80, 120, 150, 180, 200, 220, 240, 300, 320, 340, 360°C. For some samples, the thermal demagnetization was continued up to 550°C. The natural remanent magnetization (NRM) was measured on a 2G Enterprise horizontal cryogenic magnetometer equipped with DC SQUIDS (noise level 3 x 10^{-12} Am^2) at the Paleomagnetic Laboratory Fort Hoofddijk, the Netherlands. The directions of the NRM components were calculated by principal component analysis (Zijderveld, 1967; Kirschvink, 1980). Mean directions were

determined for the individual sections using standard Fisher statistics. The 51° and 58° tilt, respectively, (bedding orientation at Zumaia 110/51 and at Sopelana 129/58; strike/dip) helped to distinguish primary (pre-tilt) from secondary (post-tilt) components and to recognize the present-day field overprint (Dec/Inc; 359/58).

3.4 Geophysical properties

Magnetic susceptibility was measured in the petrophysical laboratory of the IAMC-CNR in Naples (Italy) with a Bartington MS2E Point sensor to measure low-field magnetic susceptibility (MS) on the surface of all samples (Fig. 4). The repeatability of the measurements was good (within 0.12 %, 1σ, based on all samples) but the values show scatter, which may be due to surface irregularities and the generally low values.

The total light reflectance (L*, in %) of all samples was measured in the same laboratory with a Konica Minolta Spectrophotometer CM 2002 on the surface of the rock fragments (Fig. 4). This records the percentage of reflected energy (RSC) at 31 wavelengths in 10-nm steps, over the visible spectrum from 400 to 700 nm. The precision was estimated at 1.2% (1σ, 173 repeated samples).

3.5 Carbon isotope stratigraphy

Two samples for stable carbon isotope analysis (Fig. 5) were selected per couplet, one in each lithology. A small amount of powder was obtained with a small handheld 2 mm drill or with a micro-mill. The powders were heated to 400°C to remove organic components. Analyses were performed in the geochemistry laboratory at the IAMC-CNR (Naples, Italy) with an automated continuous flow carbonate preparation GasBenchII device and a ThermoElectron Delta Plus XP mass spectrometer. Acidification of samples was performed at 50°C. Samples were calibrated to Vienna Pee Belemnite using an internal standard (Carrara Marble with $\delta^{13}C$ = 2.43 ‰VPDB) and NBS19. The precision/repeatability of $\delta^{13}C$ measurements was estimated at 0.14 ‰ (1σ), on the basis of 41 replicate samples. All isotope data are reported in per mil (‰) relative to the VPDB standard. Measurements with

extremely negative values for $\delta^{13}C$ were repeated. Five outliers outside a 9-point moving average ±2σ were excluded.

3.6 Time series analyses

Time series analyses on all datasets (Fig. 4 and 5) were performed with the program Redfit, which is designed to estimate red noise spectra from unevenly spaced data series (Schulz and Mudelsee, 2002). Furthermore, wavelet analysis was applied to expand the time series in time frequency space (Grinsted et al. 2004) after removal of periodicities over 25 m in Matlab with the function idealfilter (Matlab 7.9.0, The MathWorks, Natick, MA, 2009). Band-pass filters centred at ~16 m were applied with AnalySeries (Paillard et al. 1996) to reveal variations in the dominant cycle.

3.6 Astronomical target curve

Until recently, orbital tuning to astronomical target curves was limited to 40 Ma, with the La2004 solution (Laskar et al., 2004). New advances in the construction of planetary ephemerides have enabled extension to 50 Ma with the La2010 solution (Laskar, Fienga, et al., 2011), and to ~55 Ma with the new astronomical solution La2011 (Laskar, Gastineau, et al., 2011), adjusted to the INPOP10a ephemeris (Fienga et al., 2011). Besides the nominal solution, different solutions were generated with changes in the initial positions of the planets and the asteroids, to evaluate the solution's stability. Earth's eccentricity cannot be precisely calculated beyond 60 Ma, and only the stable 405-kyr cycle can be used for astronomical tuning (Laskar, Gastineau, et al., 2011) The 405-kyr cycle from the La2011 solution was used by Westerhold et al. (2012) to establish an astronomical time scale for the Early Paleogene.

4 Results

4.1 Biostratigraphy

The first occurrences of four species of planktonic foraminifera are indicated in Figure 3 and 5. The FO of *C. contusa* was found in cycle 150 in Sopelana, corresponding to a stratigraphic level of 119 m in Zumaia. In the Zumaia section itself, the species was first found in cycle 149. Of *R. fructicosa*, the FO was in cycle 128 in both Zumaia and Sopelana, at 105 m depth in Zumaia. The FO of *A. mayaroensis* was found in cycle 115 in both Zumaia and Sopelana, at 92 m in Zumaia. For *P. hantkeninoides* , the FO was in cycle 5 in Sopelana, corresponding to a depth of 4 m in Zumaia. In Bidart, the species was first encountered one couplet above.

4.2 Magnetostratigraphy

4.2.1 NRM behaviour

In general, the quality of the demagnetization data is relatively poor, which hampers a reliable interpretation in several parts of the selected sections. In all samples, a randomly oriented viscous component is first removed between 20 and 80°C. Upon further heating a second component is removed, in general up to 200/220°C. The direction of the second component is random in all sections, except for some reverse samples in the upper two intervals in Sopelana, which display a present-day field overprint. Heating up to 360°C did not yield reliable directions for all samples as many samples displayed a randomly oriented increase of NRM intensity starting from 300°C (Supplementary Fig. 1, SZ17-1p). Post-depositional processes might have affected the paleomagnetic signal in the Zumaia and Sopelana sections as has been described for the Sopelana section by Moreau et al. (1994). In the case that the demagnetization revealed only one component and the NRM intensities at 220°C are extremely high (above 0.2 A/m; similar to suggestions of Moreau et al. (1994), we consider these directions as being related to the

process of re-magnetization and therefore unreliable. These samples are mainly from the marly lithology, which is conforming to the findings of Moreau et al. (1994). On the other hand, some samples could be heated up to 550°C (Supplementary Fig. 1, So3), and the resultant direction of this third component did not differ from the direction yielded between 200/220° and 300-360°C. In both intervals in Zumaia and in Sopelana from cycle 82-103, this 200-360°C temperature component has dual polarity and could be interpreted as primary characteristic remanent magnetization (ChRM) component. The mean direction of this stable magnetic component is plotted on equal area projections (Supplementary Fig. 1). These reveal a slight non-antipodality of the normal and reverse directions, but the data do not pass the reversal test. The slight non-antipodality is most likely related to the weak NRM intensities, which make it difficult to isolate the primary component from an overprint component, related to overlapping blocking temperature of the magnetic carrier. The ChRM directions of the third component are plotted in stratigraphic order (Fig. 3).

4.2.2 C30n/C29r chron boundary

The interval spanning the possible position of the C30n/C29r boundary was sampled in Sopelana, from cycle 13-29. In this section, the middle part, from cycle 16-23, seems to show reverse polarity, but the majority of the samples in the lower and upper intervals is of unreliable quality, which may be indicative of a later overprint.

4.2.3 Interval within C31n-C30n

In both the Zumaia and Sopelana section, an interval has been sampled that corresponds to a previously identified short reverse interval in Sopelana, which was thought to represent C30r (Mary et al., 1991). In Zumaia (cycle 84-94) the demagnetization data are of poor quality. At the top of the section, polarities are normal, with a reversal boundary between 68.2-69.0 m, within cycle 85b. The

following 3.5 m, cycle 86-89, seem to have reverse polarity. The lowermost ~3.5 m have uncertain polarity as normal as well as reverse directions mark this interval. In Sopelana (cycle 82-103), the top of the sampled interval also seems to show reverse polarity, with a reversal at 4.1 m, within cycle 85b. Down to cycle 88, in the interval between 6.2-4.1 m, most samples show a reverse polarity. In the interval from cycle 89-100, from 6.2-13.4 m, the samples that are considered most likely reliable have normal polarity. However, six levels, of which four within carbonates (at 11.79, 9.90, 8.61, and 7.73 m; example SZ 17-1 Supplementary Fig. 1) and two within marls (at 8.45 and 7.23 m), seem reliable and suggest a reverse polarity. Example SZ 17-1 shows an increase in NRM intensity and a diversion from a progressive decay line towards the origin upon heating above 300°C. Therefore, we indicate this interval as having uncertain polarity and we cannot exclude that the reverse polarity might extend down to cycle 100. From cycle 101 downwards, between 15 -13.4 m, the resulting polarity is normal.

4.2.4 C31r/C31n boundary

The interval spanning the C31r/C31n boundary has been sampled fully in Zumaia, and partially in Sopelana (due to the presence of faults). Plotting the ChRM of the 200-300°C components of samples ZZ 1 to 72 from cycle 145-185 from Zumaia on equal area projections (Supplementary Fig. 1) clearly shows dual polarity. Even though the directions are non-antipodal, we consider these ChRM reliable. The lower 23.5 m of this interval has reverse polarity, whereas the upper 4 m is of normal polarity. The reversal boundary is located at the top of cycle 153, at 121.5m. It is well defined and in agreement with data of Mary et al. (1991) from Sopelana. In Sopelana, samples yielded reverse polarity, from cycle 161-166, and 173-180. In the uppermost interval between 3.2 -0.5 m, the quality of the demagnetization data is too poor to yield any reliable polarity.

4.3 Cyclostratigraphy

4.3.1 Geophysical data

The magnetic susceptibility and the total reflectance record (L*) vary in close agreement to the observed alternations in the lithology (Fig. 4). For example, the ~77-cm periodicity is particularly well discernible in the magnetic susceptibility record between 60 and 80 m depth, where this signal is bundled in groups of five that vary in amplitude on the 16-m scale. Both records show remarkable shifts (-18 % in L*, +~14 SI in MS) at depths around 59 and 110 m, reflecting abrupt changes in lithology form carbonate-rich sediments below to marlier sediments above.

The magnetic susceptibility record shows main periodicities in the spectrum (estimated by Redfit) at 56 and 18.8 m, and at 84.2 and 72.5 cm (Fig. 4). In the wavelet analyses (for which periodicities larger than 25 m were removed by notch-filtering) the ~19-m periodicity is strongly present throughout the record. In two intervals, from 30-70 m and more strongly from 110-120 m, the periodicity is shifted towards smaller values, around 12 m. The wavelet analysis also shows a periodicity around 4 m, albeit of less significance, that is similarly shifted towards smaller values. The ~12-m and ~4-m periodicities are most prominently present in the record around 58 and 109 m in the stratigraphy. Finally, there are periodicities around 80cm throughout the record, except for the interval 110-120 m. The band-pass filter centred at 19 m (bandwidth 12-40 m) shows ten large-scale minima. The reflectance record (L*) has its main periodicities at 47.0 and 15.7 m and 72.3 cm (Fig. 4). The wavelet analysis shows a strongly present 16-m periodicity throughout the record, which is somewhat shifted to lower values in the interval from 50-70 m and strongly shifted to a length of ~12 m in the interval 100-120 m. There is an additional periodicity around 4 m, visibly present around 58 m and significantly present in the interval 105-120 m, where it is shifted to slightly lower values. A periodicity with a length of ~70 cm is intermittently present throughout the record. The band-pass filter centred at 15.7 m (bandwidth 12-22 m) shows ten large-scale maxima.

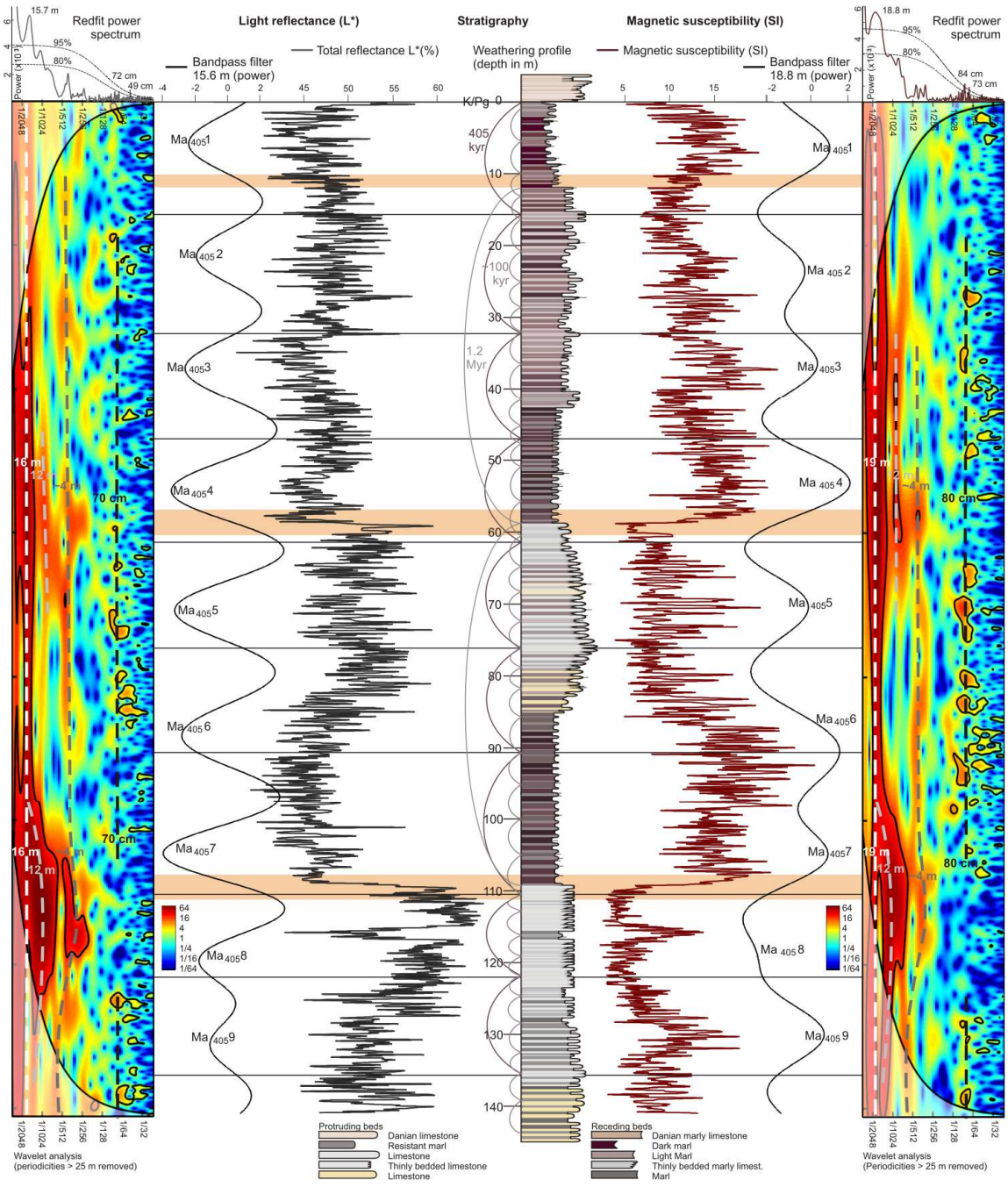

Figure 4: Stratigraphic log of the Zumaia section with total reflectance L on the left and magnetic susceptibility on the right, with three-point moving averages plotted over the data series. The data are flanked by their band-pass filters (black lines) and wavelet analyses (for the latter two a notch filter was applied to remove periodicities larger than 25 m). The band-pass filter of the reflectance is centred at 15.7 m (bandwidth 12-22 m), and the filter for magnetic susceptibility is centred at 18.9 m (bandwidth of 12-40 m). Bandwidths are broad to allow for detection of the smallest long-term periodicity of ~12 m as observed in the wavelet spectrum. The*

horizontal lines indicate the stratigraphic levels that are identified as 405-kyr minima; the black Ma_{405}no.s indicate the 405 eccentricity cycles following the nomenclature of Husson et al. (2011); the orange bands indicate major transitions in the lithology.

4.3.2 Carbon isotopes

The $\delta^{13}C$ curve from Zumaia (Fig. 5) shows an overall decreasing trend, punctuated by two types of fluctuations of 0.5-1‰. The upper half of the curve is characterised by five rises and falls with a periodicity on the order of 16 m, whereas the lower half shows longer-term oscillations on the order of 47 m. Six prominent negative shifts are indicated Figure 5 and Table 2, ranging in amplitude from 0.9-1.2‰. The sharpest shift (No.1) occurs within one cycle, and the most gradual shift (No.2) over 6 cycles (5 m).

The same time series analyses techniques were applied as for the geophysical properties (§4.3), showing main periodicities around 47.0 and 16.6 m, and at 122, 103, 101, 97.0, 92.9, 81.3 and 77.5 cm (Fig. 5). In the wavelet analyses, the 16-m periodicity is more significant in the upper half of the record, and an additional periodicity is present, although not significant, around 4 m. The resolution of the record does not allow for reliably detecting periodicities around 80 cm. The band-pass filter centred at 16.6 m (bandwidth 11-31 m) shows nine large-scale maxima.

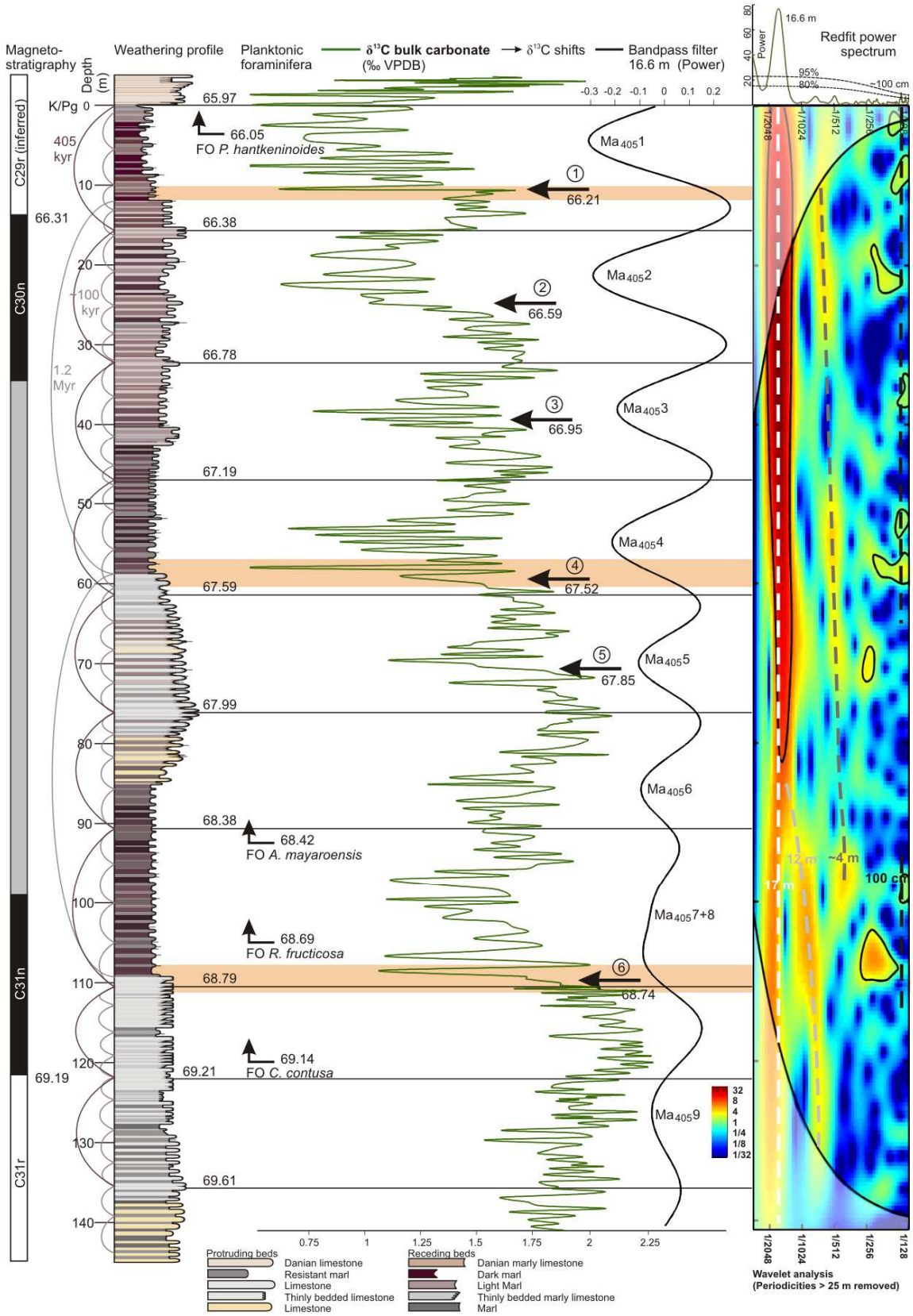

Figure 5: A Chemo-, bio-, magnetostratigraphic framework for the Zumaia section. - The $\delta^{13}C$ record, with a band-pass filter centred at 16.6m (in black, with a bandwidth of 11-31 m, to allow for detection of the smallest long-term periodicity

~12 m as indicated in the wavelet spectrum). The black Ma_{405}no.s indicate the 405 eccentricity cycles following the nomenclature of Husson et al. (2011). Prominent negative shifts, as listed in Table 2, are indicated by black arrows accompanied by their tuned ages.

- The identified 405-kyr minima with ages obtained by tuning to the new La2011 solution (Laskar, Gastineau, et al., 2011), assuming a K/Pg-boundary age of 65.97 Ma.

- The first occurrences of four species of planktonic foraminifera, of which the lower three are considered reliable global markers.

- The tuned ages of magnetic reversals C31n/C31r and C30n/C29r, the latter based on correlation to Westerhold et al. (2008) (see Supplementary Figure 2).

5 Discussion

5.1 Initial age control

An initial estimate of the time span in the Upper Maastrichtian of the Zumaia section can be made by applying the ages of Gradstein et al. (2004), and Ogg et al. (2008) for the K/Pg-boundary and the C31r/C31n reversal boundary. This gives an average sedimentation rate of 3.7 cm/year, a periodicity of 407 kyr for the ~16-m cyclicity, and a periodicity of 20.8 kyr for the ~77-cm limestone-marl alternations. These durations and the hierarchical pattern are strong indications that the different lithologies were deposited under the combined influence of the orbital periodicities of precession and eccentricity. The periodicities of precession were slightly smaller in the Cretaceous with respect to present day (Berger & Loutre 1994; Hinnov 2000), with a mean duration of 20.8 kyr (Herbert & D'Hondt 1990).

5.2 Phase relation

As the combined influence of the precession and eccentricity is clearly reflected in the rhythmic alternations in Zumaia, the phase relation with eccentricity is

unambiguous. Since eccentricity determines precessional amplitude, the eccentricity maxima can be recognised by well developed precessional cycles with distinct thick and dark marls. Eccentricity minima can be pinpointed by a poor expression of the marly part of the cycle occurring in an interval of relatively thin and carbonate-rich cycles. This is the same phase relationship as inferred by Dinarès-Turrel et al. (2003), Kuiper et al. (2008), and Hilgen et al. (2010) for the Paleocene part of the Zumaia section.

A strong marl-limestone contrast coincides with larger amplitudes in the magnetic susceptibility and reflectance variations. As increased thickness usually coincides with a darker colour of the marls, the variation amongst couplets is most likely caused by increased clay-input. This mechanism has previously been described, and lithologically tested, by Mount & Ward (1986). Increased clastic input may indicate more runoff, potentially caused by an intensified hydrological regime due to the influence of precession.

5.3 Cyclostratigraphic framework of the 405-kyr cycles

The identification of 405-kyr minima of eccentricity in the field forms the basis for a chronostratigraphic framework, which allows for more precise age determinations of bio- and magnetostratigraphic events of global importance. This field interpretation is tested by comparison to the periodicities in the generated data records. The identified 405-kyr minima are listed in Supplementary Table 1 and indicated by black lines in Figure 4 and 5. In the upper part of the section, the identified minima coincide with minima in the ~16 m band-pass filter of magnetic susceptibility and maxima in the filter of total reflectance. The carbon isotopes seem to have a lag of two to three precessional cycles (44-65 kyr) with regard to the geophysical data. Further down in the section, the variability in the thickness of the strata increases, which leads to difficulties in comparing the filtered signals with the field interpretation. Nonetheless, the overall number of nine and a half 405-kyr cycles identified in the field is in agreement with the filtered large-scale cycles, yielding an estimated time-span of 3.9 Myr for the studied interval, and an average sedimentation rate of 3.7 cm/kyr.

5.4 Astrochronology

5.4.1 Astronomically tuned age model

Now that the cyclostratigraphic framework of the 405-kyr eccentricity related cycles is established and the phase relation with eccentricity known, we can attempt to tune these cycles to 405-kyr eccentricity minima (identified with a filter centred at 405 kyr, band-width 300-623 kyr) in the new La2011 solution (Laskar, Gastineau, et al., 2011). This tuning uses the K/Pg-boundary as starting point. In fact, the younger Paleocene part of the Zumaia section played an important role in recent attempts to better determine its age. The section was first studied for cyclostratigraphy by Ten Kate and Sprenger (1993) who successfully identified the cycles around the K/Pg-boundary and established an initial tuning of part of the Maastrichtian and Danian sediments. Later, Dinarès-Turell et al. (2003) tuned the Paleocene part of the Zumaia section to the inferred expression of the long-period 2.4-Myr and ~100-kyr eccentricity cycles. Kuiper et al. (2008) tuned to the stable 405-kyr period of eccentricity, to arrive at an astronomical age of ~65.95 Ma for the K/Pg-boundary, using their newly astronomically calibrated age for the FC standard for ^{40}Ar-^{39}Ar dating. A recent direct intercalibration of the Fish Canyon Sanidine by Rivera et al. (2011) arrived at 28.172 ± 0.028 Ma, within the uncertainty of the Kuiper et al. (2008) age. The Paleocene part of the Zumaia section was combined with high resolution records from ODP-leg 198 and 208 by Westerhold et al. (2008) to suggest two main tuning options with ages of ~65.28 or ~65.68 Ma for the K/Pg-boundary. However, a recent evaluation of the astronomically tuned time scale for the Paleocene and Earliest Eocene by Hilgen et al. (2010) presents an alternative 405-kyr interpretation, arriving at a main tuning option of ~66.0 Ma for the K/Pg-boundary, although a 405-kyr younger tuning could not be excluded. Westerhold et al. (2012) recently presented a different astrochronology for the Early Paleogene, using the new La2010 and La2011 orbital solutions, with a K/Pg boundary age of 65.250 ± 0.06 Ma. New Ar-Ar and U/Pb data are expected to resolve this age problem. For the moment, however, two tuning options for the Late Maastrichtian are presented here, similar to the approach of Husson et al. (2011) with K/Pg-

boundary ages of 65.56 and 65.97 Ma, of the 65.97 Ma option in particular is in close agreement with the intercalibrated Fish Canyon Sanidine ages of Kuiper et al. (2008) and Rivera et al. (2011). The tuning options of the Paleocene (Kuiper et al, 2008; Westerhold et al, 2008, Hilgen et al, 2010) and the Maastrichtian cyclostratigraphy presented here and by Husson et al. (2011) place the K/Pg boundary in a 405-kyr eccentricity minimum.

5.4.2 Time series analysis in the time domain

A further test for the field-based age model is performed by application of spectral analyses to the proxy records after tuning. To avoid differences in durations between the tuning options, for this exercise only an age model was applied with a constant duration of 405 kyr between eccentricity minima and linear interpolation between these points. The magnetic susceptibility shows main periodicities at 1.26 Myr, and at 399, 24.1 and 19.7 kyr (Fig. 6). Time series analysis of total reflectance in the time domain shows a strong peak at 1.26 Myr. After removal of the larger periodicities, also periodicities of 404, 275, 135, 110 and 23.0 kyr are noteworthy (Fig. 6). Finally, $\delta^{13}C$ shows main periodicities at 1.26 Myr, and at 446, 26.9, 25.2, 23.1 and 21.2 kyr.

The geophysical data records show a strong expression of the precessional cycles, with periodicities between 19.7 and 24.1 kyr. These durations are, on average, slightly longer than the expected 20.8 kyr, but this can be explained by the influence of precessional amplitude on sedimentation rate. Darker marls have an increased thickness, so that the more prominent and thicker couplets will carry a stronger proxy signal. Additionally, the short ~100-kyr period of eccentricity shows up in the reflectance record, and there is high power around the 405-kyr period, albeit partly introduced by tuning. After tuning, the wavelet analyses of all data series show a very constant behaviour of the periodicities over time.

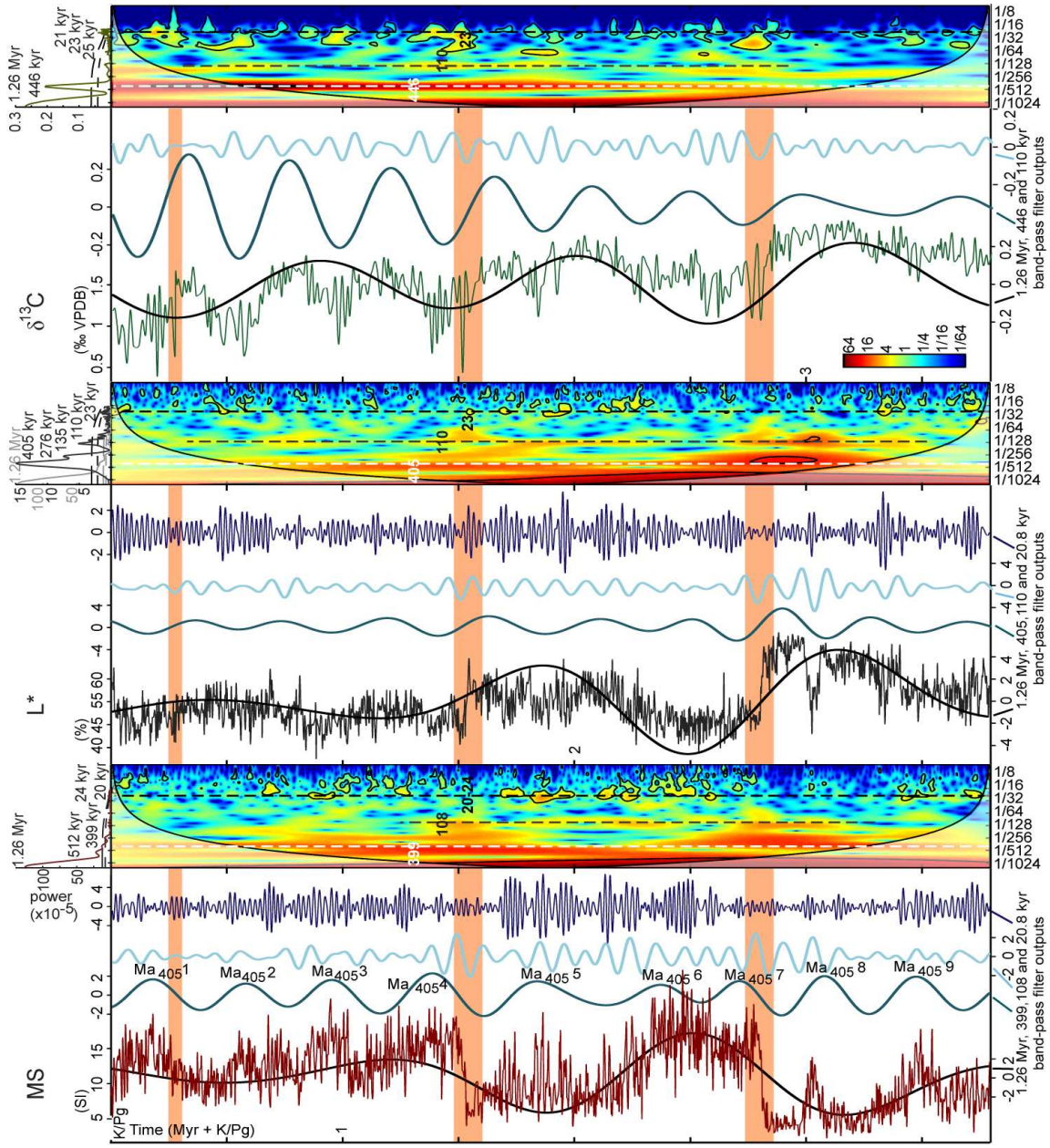

Figure 6: The magnetic susceptibility (MS), reflectance (L) and stable carbon isotope ($\delta^{13}C$) data series in the time domain, with their band-pass filters (with bandwidths of 0.0003, 0.0008, 0.003 and 0.014 yr^{-1}), the 405 eccentricity cycles (black Ma_{405}no.s)following the nomenclature of Husson et al. (2011), wavelet analyses (periodicities larger than 2 Myr were removed by notch-filtering) and Redfit spectra (dashed lines at 95 and 80 % significance levels, for the spectrum of L* periodicities larger than 2 Myr were removed by notch-filtering, the original spectrum is shown in grey).*

5.4.3 Biostratigraphy

Our orbital tuning and age model allow us to calculate astronomical ages of biostratigraphic events, stable carbon isotope shifts and magnetostratigraphic reversals (Fig. 5 and 7, Table 2). The first occurrences of planktonic foraminifera *Contusotruncana contusa*, *Abathomphalus mayaroensis*, *Racemiguembelina fructicosa* are considered reliable markers, as these species are common in the upper Maastrichtian of the Basque-Cantabric basin. As *Plummerita hantkeninoides* is very rare in the in the Basque-Cantabric basin, its first appearance does not necessarily match its global occurrence. In this study, the FOs of *A. mayaroensis* and *C. contusa* (at 68.42 Ma and 69.14 Ma, respectively) are younger with respect to reversal C31n/C31r and the K/Pg boundary than the ages reported by Gradstein et al. (2004) and Ogg et al. (2008) of 68.36 Ma and 69.49 Ma, respectively, using a K/Pg boundary age of 65.5 Ma. The FO of the planktonic foraminifer *R. fructicosa* at 68.69 Ma is considerably younger than reported by Gradstein et al (2004) at 69.62Ma, but this species is very similar to *Racemiguembelina powelli*, which occurs earlier. Other authors may consider these species synonymous and group them together, resulting in an older FO.

5.4.4 Magnetostratigraphy

The position of the C30n/C29r reversal boundary has been obtained by correlation to Westerhold et al. (2008), as the data from this study are not reliable for this interval. The seemingly reverse interval with its upper boundary within cycle 85b and its lower boundary in cycle 88 (in Sopelana), which is in agreement with Mary et al. (1991), is not likely to reflect C30r. The magnetostratigraphic results are in excellent agreement with the recently published magnetostratigraphy of Zumaia by Pérez-Rodríguez et al. (2012). The tuned durations for reversal boundaries are listed in Table 2 and Figure 7, with previously reported ages by Husson et al. (2011), Thibault, Husson et al. (Thibault, Husson, et al., 2012), the Geologic Time Scale 2004 (Gradstein et al., 2004), Cande and Kent (1995), Herbert et al. (1995) and Herbert (1999). There is a remarkably good agreement on the total amount of time

between the K/Pg-boundary and the base of C31n, estimated at 3.22 Myr in this study, 3.23 in Gradstein et al. (2004) and 3.22 by Husson et al. (2011).

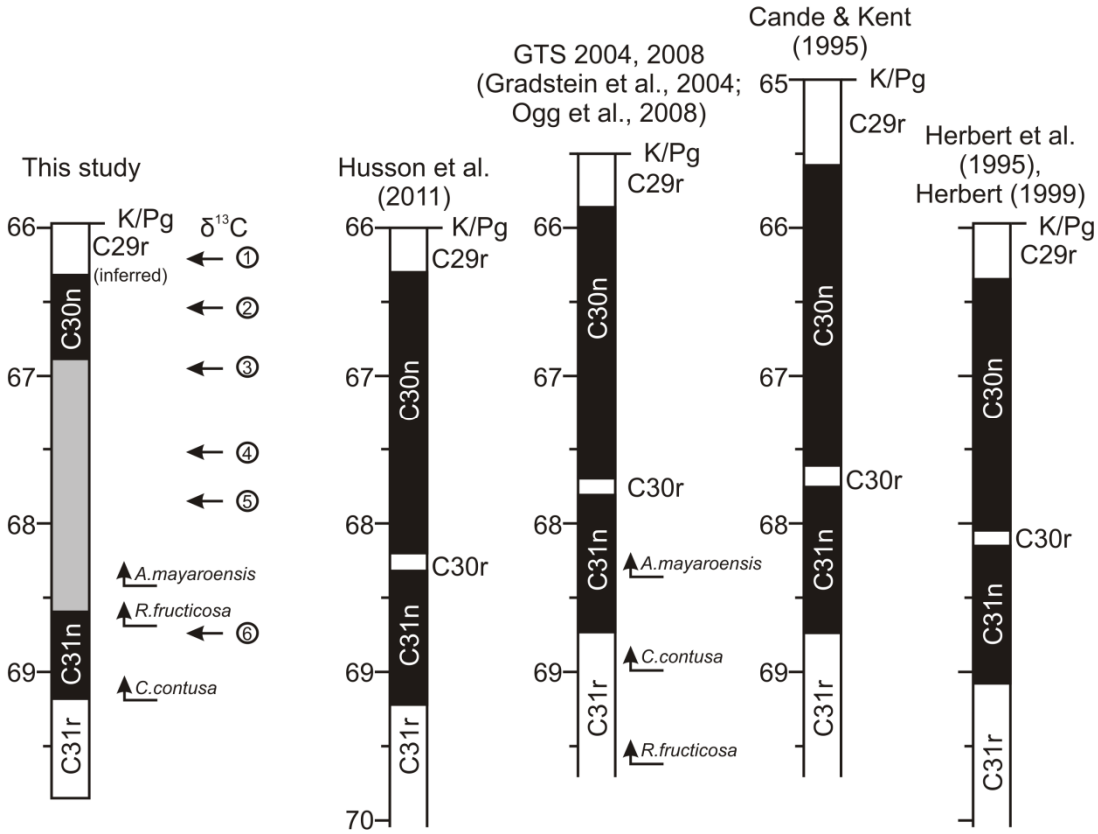

Fig 7: Late Maastrichtian time scales with magneto-, bio- and chemostratigraphic events according to option 2 of this study; option 2 of Husson et al. (2011) (both assuming a K/Pg-boundary age of 65.96 Ma); the GTS 2004 and 2008 (Gradstein et al. 2004; Ogg et al. 2008); Cande and Kent (1995), Herbert et al. (1995) and Herbert (1999). Please note that Herbert et al. (1995) and Herbert (1999) only report durations, a K/Pg-boundary age of 65.96 Ma has been assigned for comparison. For this study, the age of the base of C29r is based on correlation to Westerhold et al. (2008) (see Supplementary Figure 2).

5.4.4.1 C30r

The position of C30r in seafloor anomaly profiles is roughly at one third of the otherwise normal polarity interval C31n-C30n (based on Cande & Kent 1992; Bouligand et al. 2006), whereas the potential reverse interval in this study is about midway in both thickness and recorded time, which would imply unreasonable changes in spreading rates. Comparison to Husson et al (2011) and other previous estimates (Table 2) suggests that C30r should be located one 405-kyr cycle further down, and it is possible that our sampling does not extend far enough. Although the possibly reverse interval seems rather long (66 kyr), it may be a cryptochron that correlates to one of the "wiggles" within the C30n interval of anomaly profiles from ocean floors of different basins (Cande and Kent, 1992; Bouligand et al., 2006). Alternatively, the data may be unreliable and result from remagnetization, as samples with reversed polarities also occur within an otherwise normal interval further down (cycle 89 to 100).

5.4.4.2 Base of C29r

The samples in this interval seem to indicate reverse polarity at least down to cycle 23, which is older than most previous tunings, and may represent a more recent remagnetization. Instead, the position of the base of C29r can be obtained by correlation to IODP Sites 1262 and 1267, as done by Westerhold et al. (2008). Supplementary Figure 2 shows the reversal to correspond to three cycles above the last 45 kyr minimum before the K/Pg boundary, or 17.5 cycles below the K/Pg boundary, which is in good agreement with Herbert (1999) who found the reversal to be 18.5 cycles to the K/Pg-boundary in reflectance records from ODP-Sites 516F, 528 and 525A in the South Atlantic. It is in reasonable agreement with ten Kate and Sprenger (1993), who correlated the base of C29r from Agost, Spain (De Groot et al, 1986) and Sopelana (Mary et al. 1991).

5.4.5 Carbon isotope stratigraphy

The tuned bulk-carbonate $\delta^{13}C$ curve from Zumaia has a high resolution, which provides excellent possibilities for correlation. The $\delta^{13}C$ variations compare well with recently published high resolution bulk $\delta^{13}C$ data from northern Germany (Voigt et al. 2010), the Gubbio section in Italy (Voigt et al., 2012), two sections in Denmark (Thibault, Harlou, et al., 2012), ODP Hole 1210B on Shatsky Rise in the Tropical Pacific (Jung et al., 2012) and ODP Hole 762C in the Indian Ocean (Thibault, Husson, et al., 2012), although the carbon isotope curve from Zumaia seems to vary with a larger amplitude. The $\delta^{13}C$ curve reveals clear variations on a ~1.2 Myr scale. These variations are especially apparent in the lower half of the record, while the upper half is dominated by a strong 405-kyr cyclicity. The bulk-carbonate $\delta^{13}C$ shows a gradual decline throughout the Late Maastrichtian of approximately 0.5 permil, punctuated by six prominent negative shifts, on the order of -1 ‰ (Fig. 5). Interpretation of the carbon isotope curve is not straightforward, as the behaviour reflects a complex interplay of sea level variations (Voigt and Hilbrecht, 1997; Jarvis et al., 2006), ocean circulation (Barrera et al., 1997; Frank and Arthur, 1999; Friedrich et al., 2004), and productivity (Li & Keller 1998).

The major shifts in bulk-carbonate $\delta^{13}C$ at 59 and 109 m depth, approximately 1.2 Myr apart, coincide with lithological shifts from reddish limestone-marl alternations that have been interpreted as Transgressive or Highstand Systems Tract deposits to purple marly intervals that likely represent low-stand deposits (Pujalte et al., 1995). A drop of relative sea level, either by eustacy or local tectonics, may have exposed shallow shelf areas. This would have led to increased erosion, and an increased input of clastic material to deeper parts of the basin, where the sedimentary cycles became thicker and marlier. Erosion of sediments on shallow shelf areas, relatively rich in organic matter, may have delivered more ^{12}C to the deeper parts of the basin, causing a negative excursion in $\delta^{13}C$.

Maxima of the 405-kyr eccentricity cycle in the lithology coincide with minima in $\delta^{13}C$, which may be related to an intensified hydrology that would not only have carried more clastic material to the basin, but may also have carried relatively lighter $\delta^{13}C_{HCO3-}$. The relatively strong expression of the 405-kyr cycle in the bulk carbonate $\delta^{13}C$ record of Zumaia in comparison to other sites may be related to the slightly restricted nature of the basin, which was a narrow inter-plate trough (Pujalte et al., 1995), and to a major continental influence. The correspondence of 405-kyr maxima in the $\delta^{13}C$ record with 405-kyr minima in the lithology is in agreement with the classic response of sedimentary records to Cenozoic climate forcing. The lag of 2-3 precessional cycles compared to geophysical proxy records is similar to a lag of ~35 kyr to the 405-kyr period of eccentricity as found in Oligocene-Miocene records (Pälike et al. 2006), of 42±20 or 48±18 kyr for the Miocene (Holbourn et al. 2007), and of 40-60 kyr for the Paleocene (Westerhold et al. 2011). Such a lag is likely due to the longer residence time of carbon and consequently the longer response time of the global carbon cycle to astronomical forcing (Pälike et al. 2006).

In general, this study shows that Late Maastrichtian climate was strongly controlled by insolation at low latitudes, as the periodicities of eccentricity-modulated precession are the dominant control on the geophysical and $\delta^{13}C$ data. This is corroborated by the absence of obliquity (with a main period of 41 kyr) that would have exerted a strong control on high latitude climate. Glacio-eustacy has been suggested as controlling mechanism on Late Cretaceous sea levels (Miller et al. 2005), but the absence of a high-latitude signal in our records makes this hypothesis unlikely.

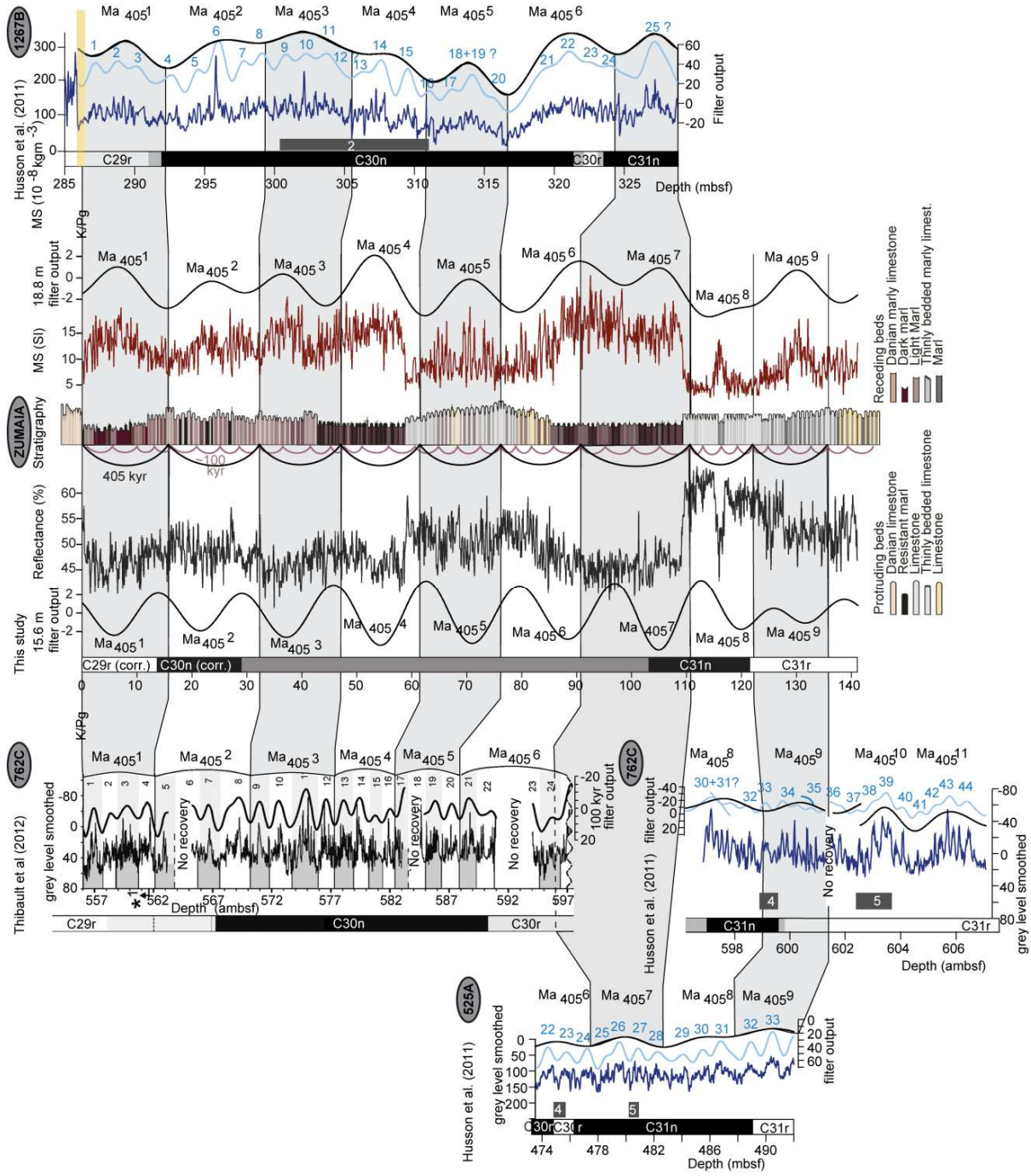

Fig. 8: Comparison of Maastrichtian astrochronologies, with grey bands indicating the identified 405-kyr cycles, numbered $Ma_{405}1$, $Ma_{405}2$, ... , from the K/Pg boundary downwards, following Husson et al. (2011). From left to right the cyclostratigraphic interpretation of Husson et al. (2011) of the grey level data of Hole 525A and Hole 762C, with their ~100 kyr and 405 kyr band-pass filters; the cyclostratigraphic framework of Thibault, Husson et al. (2012) of the grey level data of Hole 762C; the magnetostratigraphy, 15.7 m band-pass filter (bandwidth 12-22 m) of reflectance,

the reflectance data, the stratigraphic column, the magnetic susceptibility data and the 18.9 m band-pass filter of magnetic susceptibility (bandwidth 12-40m) of Zumaia (this study); the cyclostratigraphic interpretation of the magnetic susceptibility data of Hole 1267B by Husson et al. (2011).

5.5 Comparison of Maastrichtian astrochronologies

This cyclostratigraphic framework provides a refinement of the Geological Time Scale for the Late Maastrichtian, with the potential to anchor it to astronomical target curves. The recent astronomical tuning of Maastrichtian sediments from ODP Holes 1267B, 525A and 762C by Husson et al. (2011) shows a very similar duration from the base of chron C31n to the K/Pg boundary (table 2) of 3.22 Myr. Additional tuning results from Hole 762C by Thibault, Husson, et al. (2012) allow to re-evaluate the durations of chrons C29r (Cretaceous) and C30n (table2), which, added to the durations of chrons C30r and C31n by Husson et al. (2011), again gives a duration from the base of C31n to the K/Pg boundary of 3.22 Myr. The geophysical data of magnetic susceptibility (Hole 1267B) and grey level (Hole 762C and 525A) with their 100-kyr and 405-kyr band-pass filters and cyclostratigraphic interpretations by Husson et al (2011) and Thibault et al (2012) are plotted next to the geophysical data and band-pass filters of Zumaia (Figure 8), to assess the cyclostratigraphic framework. The ODP-records have a lower resolution, meaning that the precessional cycles are usually not well expressed. The cyclostratigraphic interpretation often depends on the 100-kyr cyclicity instead of the stable 405-kyr periodicity, such as in Hole 525A (Husson et al., 2011) and the upper part of Hole 762C (Thibault, Husson, et al., 2012). Also, the interpretation relies on several Sites, of which the correlation is not entirely straightforward, as the cyclostratigraphic interpretations do not agree with the positions of the magnetic reversals (Fig. 5 in Husson et al., 2011). By contrast, the Zumaia section has a much higher resolution and offers the possibility to identify the full range of periodicities of eccentricity modulated precession. This allows for a more reliable and detailed cyclostratigraphic framework that is based primarily on cycles that can be identified

directly in the lithological record. A test of this interpretation is provided by high resolution records of magnetic susceptibility, reflectance, and bulk $\delta^{13}C$. There are no indications for faulting or hiatuses, and the large scale alternation of carbonate-rich versus marly intervals is in agreement with the Sopelana section, as well as with the Bidart and Hendaye sections in France and the Trabakua section further inland (Pujalte et al., 1998) that were visited, but not logged in detail. It should be mentioned that if there are hiatuses of exactly 405 kyr, these could go unnoticed. The obtained estimate of the duration between C31r/C31n and the K/Pg boundary, however, is in close agreement with the GTS2004 and other studies (Figure 7, Table 2). For the first time, a consistent 405-kyr cyclostratigraphy is presented for the Late Maastrichtian, which is pivotal for anchoring the Geologic Time Scale of the Cretaceous.

	This study					(Gradstein et al., 2004)	Husson et al., 2011)		Thibault et al. (2012)[1]	Cande and Kent (1995)	Herbert (1995[2], 1999)
	section	cycle no.	depth (m)	option 1	option 2		option 1	option 2			
K/Pg				65.56 ± 0.02	65.97 ± 0.02	65.5	65.59 ± 0.07	66 ±0.07	65.97[3]	65	65.97[3]
magnetic reversals											
C30n/C29r	correlated	18	13.8	65.91 ± 0.09	66.31 ± 0.09	65.861	65.89 ± 0.08	66.3 ± 0.07	66.376	65.578	66.347 ± 2[1]
C30r/C30n						67.696	67.79 ± 0.08	68.2 ± 0.07	68.165	67.61	68.047
C31n/C30r						67.809	67.91 ± 0.07	68.32 ± 0.07	68.338[4]	67.735	68.152
C31r/C31n	Zumaia	152/153	121.5	68.77 ± 0.08	69.19 ± 0.08	68.732	68.81 ± 0.07	69.22 ± 0.07		68.737	69.077
duration C31r/C31n - K/Pg				3.22	3.22	3.23	3.22	3.22		3.74	3.107
planktonic foraminifera											
FO *P. hantkeninoides*	Sopelana (Bidart 1 cycle up)	5	3.6	65.64 ± 0.08	66.05 ± 0.08						
FO *A. mayaroensis*	Zumaia, Sopelana	115	92.4	68.03 ± 0.08	68.42 ± 0.08	68.36					
FO *R. fructicosa*	Zumaia, Sopelana	128	105.0	68.28 ± 0.08	68.69 ± 0.08	69.62					
FO *C. contusa*	Sopelana (Zumaia 1 cycle up)	150	119.9	68.73 ± 0.08	69.14 ± 0.08	69.49					
δ^{13}C shifts											
No.1 (-1.0 ‰)	Zumaia	13	10.5	65.80 ± 0.07	66.21 ± 0.07						
No. 2 (-1.1 ‰)	Zumaia	29-35	24.8	66.18 ± 0.07	66.59 ± 0.07						
No. 3 -0.9 ‰	Zumaia	48-51	39.4	66.54 ± 0.07	66.95 ± 0.07						
No. 4 (-1.4 ‰)	Zumaia	72-76	59.4	67.12 ± 0.07	67.52 ± 0.07						
No. 5 (-0.9 ‰)	Zumaia	86-89	70.6	67.45 ± 0.07	67.85 ± 0.07						
No. 6 (-1.2 ‰)	Zumaia	131-134	109.7	68.34 ± 0.07	68.74 ± 0.07						

Table 2: Tuned ages of chemo-, bio- and magnetostratigraphic events, compared to Husson et al. (2011), Thibault, Husson et al. (2012), the Geologic Time Scale 2004 and 2008 (Gradstein et al., 2004), Cande and Kent (1995), Herbert et al (1995) and Herbert (1992, 1999). Uncertainties in this study are based on the uncertainty in the position of an event, uncertainty in the astronomical target curve (0.023 Myr) and uncertainty in the cyclostratigraphic interpretation (two precessional cycles, 0.044 Myr). For this study, the age of the base of C29r is based on correlation to Westerhold et al. (2008) (see Supplementary Figure 2). Cycle nr and depth refer to (correlation to) the Zumaia section.[1] Uncertainties for the estimates of the durations (not for the ages) are listed in the original publication. [2] The age of the C30n/C29 reversal was taken from Herbert et al., (1995), the other ages from Herbert (1999). [3] A K/Pg-boundary age of 65.97 Ma was chosen here for comparison. [4] The duration of chron C30r is uncertain due to a recovery gap.

Appendix A. Supplementary information Chapter 2

Biostratigraphy

All studied samples from the Zumaia, Sopelana and Bidart sections are rich in well preserved planktonic foraminifera. The planktonic species represent more than 90% of all foraminifera, as expected for material deposited in deep facies. About 60 species of planktonic foraminifera can be recognised in the studied assemblages. The lowermost 52m of the logged Maastrichtian succession, before the appearance of *Abathomphalus mayaroensis*, are included in the *Gansserina gansseri* biozone. The upper 92m belong to the *A. mayaroensis* biozone. Some specialists differentiate another biozone in between, which extends from the first occurrence of *Contusotruncana contusa* until the first occurrence of *A. mayaroensis*. Additionally, some differentiate a biozone of *Plummerita hantkeninoides* from its first occurrence up to the K/Pg boundary.

Characteristics of the planktonic foraminifera *Contusotruncana contusa*, *Abathomphalus mayaroensis*, *Racemiguembelina fructicosa* and *Plummerita hantkeninoides*:

- Within the four selected species, *P. hantkeninoides* is the only Maastrichtian species with tubulospines and a surface covered with ridges and costellae.
- The name *A. mayaroensis* refers to those specimens of *Abathomphalus* that have two muricocarinas in all chambers of the last whorl.
- *R. fructicosa* is considered a species distinct from *Racemiguembelina powelli*, for having a shorter biseriate development and a larger number of chambers in the final part of the test.
- The species *C. contusa* stands apart from other large species within the genus *Contusotruncana*, for example *C. patelliformis*, because it has a higher side spiral and a larger size.

Characteristics of identified 405-kyr minima and maxima

The levels that have been identified as 405-kyr minima share the characteristics of having rather thin, very poorly developed cycles, with minimal difference between the marly and carbonaceous part of the cycles. In between the 405-kyr minima, the cycles are generally more pronounced and bundled in groups of five corresponding to the ~100-kyr periodicity. There are either two or three bundles with darker marls midway between two 405-kyr minima.
The 405-kyr minima as identified in the field have been used as starting point for the development of the age model.

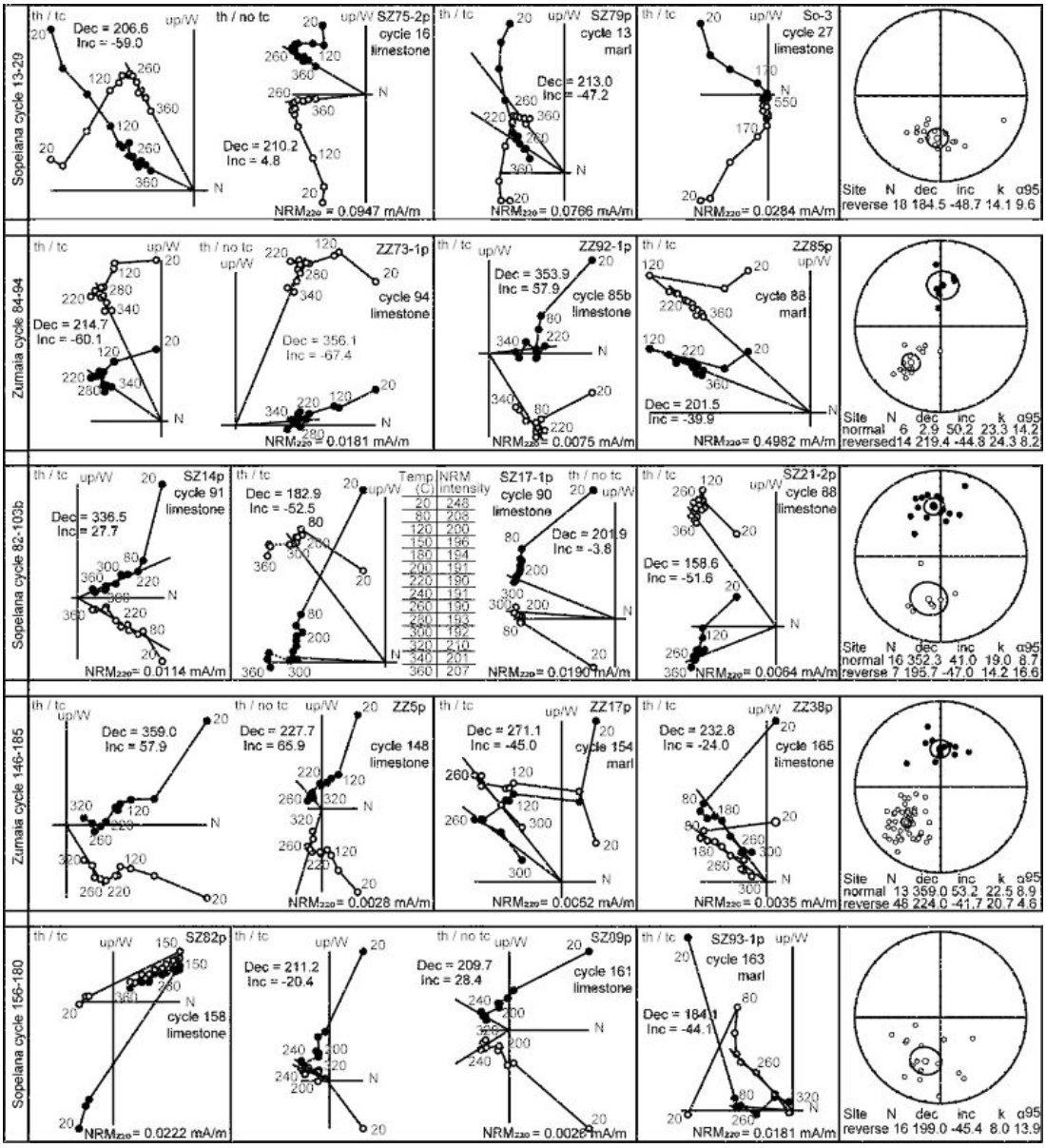

Supplementary Figure 1: Paleomagnetic results: examples of NRM behaviour and equal area projections

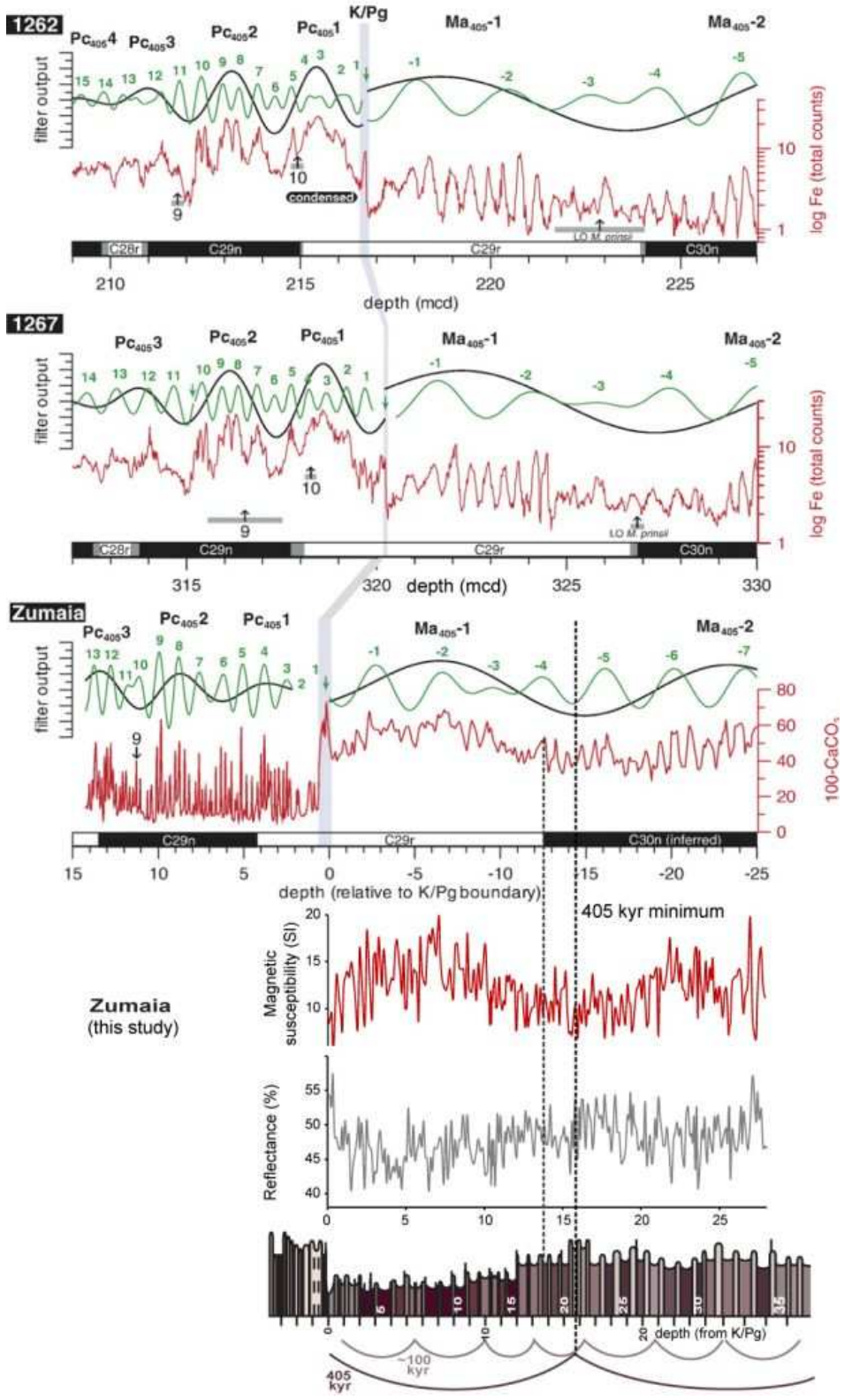

Supplementary Figure 2: Correlation of the base of C29r with the magnetic susceptibility and reflectance records from Zumaia (this study) to the carbonate content at Zumaia (ten Kate and Sprenger, 1993) and XRF data from Site 1262 and 1267 from the Walvis Ridge, as compiled by Westerhold et al. (2008).

Stratigraphic level	405 kyr cycle	Description
0 m	minimum	Cycles 1-3 are lighter and thinner than the underlying cycles. This is consistent with the identification of a 405-kyr minimum at the K/Pg-boundary by Kuiper et al. (*).
2-12 m	maximum	The marls, grouped in bundles of five, are darkest and thickest in the middle of these three bundles, and these bundles are most clearly expressed.
16 m	minimum	The marl of cycle 21, and to a lesser extent the marl of cycle 22, is lighter and thinner than the surrounding marls and form a protruding point of the cliff.
17-28 m	maximum	The marls, grouped in bundles of five, are darkest and thickest in the middle of these three bundles, and these bundles are most clearly expressed.
32 m	minimum	The marl of cycle 41 is poorly developed and the limestone of cycle 42 is very prominent, forming a slightly protruding point.
38-44 m	maximum	The marls, grouped in bundles of five, are darkest and thickest in the middle of these two bundles, and these bundles are most clearly expressed. Just below 41m, the beds are hard to distinguish, coinciding with a probable ~100-kyr minimum.
47 m	minimum	The individual cycles are very thin and the more resistant part of the cycle is very poorly expressed.
49-59 m	maximum	The marls, grouped in bundles of five, are darkest and thickest in the middle of these three bundles, and these bundles are most clearly expressed.
61 m	minimum	The individual beds are thinner and poorly expressed, especially the marlyer beds.
65-72 m	maximum	The marls, grouped in bundles of five, are darkest and thickest in the middle of these two bundles, and these bundles are most clearly expressed. At 68m there is a double limestone bed with no marl in between, coinciding with a probable ~100-kyr-minimum.
76 m	minimum	The marl of cycle 94, and to a lesser extent the marl of cycles 93 and 95, is very thin and light compared to the surrounding marls and this level forms the furthest protruding point.
80-89 m	maximum	The marls, grouped in bundles of five, are darkest and thickest in the middle of these three bundles, and these bundles are most clearly expressed compared to bundles above. At 82m, there is a very thin limestone and a very thin marl, probably coinciding with a probable ~100-kyr minimum.
91 m	minimum	The marly and less marly layers are hard to distinguish at this level, the marls are not so dark and the less marly layers are very thin and not very resistant.
96-108 m	maximum	The marls, grouped in bundles of five, are darkest and thickest in the middle of

		these two bundles, and these bundles are most clearly expressed.
111 m	minimum	The cycles are thin and difficult to identify, because the marls are very poorly expressed, and all beds are very carbonaceous
114-119	maximum	The individual cycles are easier to identify and the marls around 116 are very prominent.
122 m	minimum	The cycles are thin and difficult to identify here, because the marls are very poorly expressed, and all beds are very carbonaceous.
126-132 m	maximum	The cycles are very regular and easy to distinguish, with a very prominent marl at 128m.
135 m	minimum	The marl of cycle 173 is very thin, and the limestones of cycle 173 and 174 very prominent, forming a protruding point into sea.
137-143 m	maximum	The cycles are very clear and grouped in groups of five, with the darkest marls in these two bundles.

Supplementary Table 1: characteristics of the 405-kyr maxima and minima. Minima are used as tie-points for the age model. Underlined levels are particularly well-defined minima.

Chapter 3. An astronomical time scale for the Maastrichtian at the Zumaia and Sopelana sections (Basque country, northern Spain)

Submitted to *Earth and Planetary Science Letters*

In collaboration with: Andrew S. Gale, Mario Sprovieri, Frederik J. Hilgen, Nicolas Thibault, Myriam Boussaha, Xabier Orue-Etxebarria

Abstract

The rhythmically bedded limestone-marl alternations in the coastal cliffs of Sopelana and Zumaia in the Basque country, northern Spain, provide an excellent opportunity to test and refine existing chronologies for the Maastrichtian (latest Cretaceous). Recently, we established an astronomical time scale for the younger part of the Maastrichtian based on the Zumaia section in northern Spain. Here we present an integrated stratigraphy of the nearby Sopelana section to extend this time scale into C31n, almost to the base of the Maastrichtian. The cyclic alternations of hemipelagic limestones and marls at Sopelana show a strong influence of eccentricity-modulated precession. Together, the Zumaia and Sopelana sections span almost the entire Maastrichtian, and encompass thirteen 405-kyr cycles, spanning a total duration of 5.3 Myr. Consecutive 405-kyr minima in the lithological and geophysical data records are tuned to successive 405-kyr minima in the new La2011 eccentricity solution. Assuming a K/Pg boundary age of 65.97 Ma, we present orbitally tuned ages of biostratigraphic and magnetostratigraphic events. While the bases of Chrons C29r and C30n have been reliably established at Zumaia and their astronomically tuned ages are in good agreement with previous studies, new data from Sopelana provide a refinement of the age of the base of Chron C31r. Additional planktonic foraminifera and calcareous nannoplankton data from Zumaia, and new calcareous nannoplankton data from Sopelana allow for worldwide correlation and comparison of the cyclostratigraphy of the Basque country.

1. Introduction

1.1 *Maastrichtian chronologies*

Recently, much progress has been made in improving the temporal resolution of the Maastrichtian time scale by astronomical tuning of cyclic climate records. Originally, Ten Kate and Sprenger (1993) used variations in carbonate content above and below the Cretaceous/Paleogene (K/Pg) boundary at Zumaia to establish a cyclostratigraphic framework, extending ~1.7 Myr down into the Maastrichtian. Later, Herbert et al. (1995) and Herbert (1999) identified the eccentricity modulation of precessional cycles in reflectance records of South Atlantic Deep Sea Drilling Project (DSDP) Sites 357 (Leg 39), 516F (leg 72), 525A, 527 and 528 (Leg 74) to obtain an orbital estimate for the durations of Late Cretaceous magnetochrons C31n-C29r. Husson et al. (2011) produced an astronomical tuning of magnetic susceptibility records from Ocean Drilling Program (ODP) Hole 1258A (Equatorial Atlantic) and Hole 1267B (South Atlantic) and grey level variations from DSDP Site 525 (South Atlantic) and ODP Site 762 (Indian Ocean) and attempted to anchor this tuning to the absolute time scale. Another cyclostratigraphic framework was presented by Thibault et al. (2012b) for ODP Hole 762C based on grey level variations, with an integrated magnetostratigraphy, a bulk-carbonate $\delta^{13}C$ profile, and planktonic foraminifera and calcareous nannofossil bio-events. A global correlation of carbon isotope curves from Campanian-Maastrichtian successions by Voigt et al. (2012) allows for direct correlation to the Global Stratotype Section and Point of the Campanian-Maastrichtian boundary at Tercis les-Bains (France). Recently, a cyclostratigraphic framework for the late Maastrichtian, with magnetostratigraphy, biostratigraphy and a high resolution carbon isotope stratigraphy, has been obtained for the Zumaia section in the Basque country, northern Spain (Batenburg et al., 2012/Chapter 2). This study elaborates on that work by extending the geophysical data records of reflectance and magnetic susceptibility with new data from the lower Maastrichtian Sopelana section. We also include the calcareous nannofossil biostratigraphy for Zumaia of Pérez-

Rodríguez et al. (2012) and present new calcareous nannofossil data from Sopelana, and additional magnetostratigraphic data.

1.2 Age of the K/Pg boundary

Orbitally tuned magneto-, bio- and carbon isotope stratigraphies have recently been established for the Maastrichtian (Batenburg et al., 2012/Chapter 2; Husson et al., 2011; Thibault et al., 2012b), but must to some extent be considered floating. In the ongoing debate about the age of the K/Pg boundary (e.g., (Westerhold et al., 2012), this level has been placed in three successive minima of the 405-kyr eccentricity cycle, following different tuning options. After initial tuning efforts by (1993) and Dinarès-Turell et al. (2003), Kuiper et al. (2008) used an astronomically calibrated age of 28.201 ± 0.046 Ma for the Fish Canyon sanidine (FCs) dating standard to recalculate ^{40}Ar-^{39}Ar ages and constrain the tuning on the 405-kyr cycle scale to arrive at a K/Pg boundary age of ~65.95 Ma. A recent intercalibration attempt resulted in a FCs age of 28.172 ± 0.028 Ma (Rivera et al., 2011), within the uncertainty of the Kuiper et al. (2008) age. However, Westerhold et al. (2008) combined high resolution XRF and geophysical property records from ODP Sites 1209, 1210, and 1211 (North Pacific;) and Sites 1262 and 1267 (South Atlantic;) with the Paleocene part of the Zumaia section and suggested two main tuning options with ages of ~65.28 or ~65.68 Ma for the K/Pg boundary. Hilgen et al. (2010) re-evaluated the Paleocene and Eocene time scale, and with an alternative 405-kyr interpretation arrived at a main tuning option of ~66.0 Ma for the K/Pg-boundary, although not excluding a possible 405-kyr younger tuning. Finally, Westerhold et al. (2012) presented a different astrochronology for the Early Paleogene, using the new La2010 and La2011 orbital solutions, with a K/Pg boundary age of 65.250 ± 0.06 Ma. In this study, we adopt the 66.0 Ma age, as this is in agreement with the intercalibrated Fish Canyon Sanidine ages of Kuiper et al. (2008) and Rivera et al. (2011), but we do not exclude younger tuning options.

2. Geological setting and sections

The coastal cliffs of Zumaia and Sopelana, along the Bay of Biscay in northern Spain, display rhythmically bedded hemipelagic limestone-marl alternations, deposited in the Basque-Cantabric Basin. From the Campanian to the Eocene, this basin was a deep elongated intra-plate trough, opening to the west into the Bay of Biscay, and surrounded by shallow shelf areas (Mathey, 1988; Pujalte et al., 1998; Rat, 1988). These successions were uplifted in late Eocene times during the Pyrenean orogeny. Major outcrops of Maastrichtian strata are found in the Biscay synclinorium, with the Sopelana section on the eastern flank, and in the Gipuzkoa monocline, with the Zumaia section being the westernmost outcrop (Supplementary figure 1) (Pujalte et al., 1998).

2.1 Zumaia

The Zumaia section is located beneath the Punta Aitzgorri Headland near the town of Zumaia, in the Gipuzkoa province of northern Spain. The section is composed of rhythmically bedded deposits of hemipelagic limestones, marls and turbidites of late Cretaceous to Eocene age, and is a classical site for paleoclimatic, magnetostratigraphic, biostratigraphic and cyclostratigraphic studies (Dinarès-Turell et al., 2003; Elorza and García-Garmilla, 1998; Gómez –Alday et al., 2008; Herm, 1965; Kuiper et al., 2008; Lamolda, 1990; Percival and Fischer, 1977; Pujalte et al., 1998; ten Kate and Sprenger, 1993; Ward and Kennedy, 1993; Ward et al., 1991) and a reference section for the K/Pg boundary (Molina et al., 2009). The upper Campanian and lower Maastrichtian of the Zumaia section are characterized by a thick turbidite succession, deposited during relatively rapid subsidence, which grades into upper Maastrichtian limestone-marl alternations with intercalated turbidites, deposited during relative tectonic quiescence (Pujalte et al., 1998). The upper Maastrichtian interval was first studied for cyclostratigraphy by Ten Kate and Sprenger (1993). A new cyclostratigraphic framework for the Zumaia section, with additional bio-, magneto-, and chemostratigraphic data, was obtained recently

(Batenburg et al., 2012/Chapter 2) and is displayed in Figure 2, together with the stratigraphic log of the lower Maastrichtian interval of the Sopelana section. Recently, a high resolution calcareous nannoplankton and planktonic foraminifera stratigraphy was obtained by Pérez-Rodríguez et al. (2012), together with magnetostratigraphic information, which is correlated with our log (Table 1).

2.2 Sopelana

The upper Maastrichtian of the Sopelana section in the Vizcaya province of Northern Spain is characterized by a number of large faults, but the lower Maastrichtian is not disturbed and displays a very regular alternation of limestones and marl beds, without the occurrence of turbidites. We refer to the Sopelana 1 section along the Atxabiribil-Arriatera swimming beach, distinguished from the thinner Sopelana 2 section further west (Ward, 1988; Ward et al., 1991). The section was studied for planktonic foraminifera and calcareous nannoplankton by Lamolda et al. (1983). Mary et al. (1991) provided more planktonic foraminifera data and a magnetostratigraphy, and the potential acquisition of a chemical remagnetization signal, particularly by the marl horizons, was discussed by Moreau et al. (1994). The ammonite faunas from Sopelana and the sections of Zumaia, Bidart and Hendaye have been described by Ward and Kennedy (1993). The distribution and shell stable isotope ratios of inoceramids at Sopelana have been studied in detail (Elorza and García-Garmilla, 1998; Gómez-Alday et al., 2004; Gómez –Alday et al., 2008). Intervals at Sopelana were included in studies on $CaCO_3$ and stable isotope variations by Alvarez-Llano et al. (2006), Santander et al. (2007) Domínguez et al. (2007) and Jiménez Berrocoso et al. (2012). The tectonic setting of the Sopelana section has been described by Rodríguez et al. (2008).

3. Material and methods

3.1 Lithostratigraphy and geophysical properties

The Lower Maastrichtian limestone-marl alternations of the Sopelana section were logged and sampled by hammer at a resolution of approximately eight samples per limestone-marl couplet, with an average sampling space of 8 cm. Magnetic susceptibility was measured on the surface of rock fragments in the petrophysical laboratory of the IAMC-CNR in Naples (Italy) with a Bartington MS2E point sensor to measure low-field magnetic susceptibility (MS) (Figs. 3 and 4). As the values were generally low, all samples were measured twice, and each measurement was alternated with blanks. The total light reflectance (L*, in %) of all samples was measured in the same laboratory with a Konica Minolta Spectrophotometer CM 2002 on the surface of the rock fragments (Figs. 3 and 4). All measurements were repeated and directly averaged by the instrument, which records the percentage of reflected energy (RSC) at 31 wavelengths in 10-nm steps, over the visible spectrum from 400 to 700 nm. Cycles 156 to 185 in the Zumaia section have been correlated bed-to-bed to the Sopelana section (Batenburg et al., 2012/Chapter 2) (Fig. 2). The Sopelana and Zumaia datasets were combined at depth level 135.47 m in cycle 169 located in the lowermost 405-kyr minimum at Zumaia and in the uppermost 405-kyr minimum at Sopelana (see 5.1).

Figure 1: Overview photograph and stratigraphic log of the Sopelana section, with cycle numbers indicated. See figure 3 for legend. Please note that due to merging of photographs, the distance between promontories, behind the people and behind the concrete reinforcement, is smaller than in reality, while the cliff wall is unaffected.

3.2 Spectral analysis

Spectral analysis of the geophysical data records was performed with Redfit38, which is particularly suited for unevenly spaced paleoclimatic time series (Schulz and Mudelsee, 2002). Wavelet analyses were applied with a Matlab script (Grinsted et al., 2004) and band-pass filters with AnalySeries (Paillard et al., 1996), centred at the periodicities obtained from the Redfit38 analyses, and typically with a broad bandwidth of approximately 1/4 of the periodicity (details in results section). Spectral analyses were performed on the Sopelana data and on the combined Zumaia/Sopelana datasets.

3.3 Astronomical target curve

The recently published astronomical solution La2010 pushed the reliability of full eccentricity back to 50 Ma (Laskar et al., 2011a). The new La2011 solutions, adjusted to the INPOP10a ephemeris (Fienga et al., 2011), further extend this reliability to ~54 Ma (Westerhold et al., 2012). Four solutions were generated, with slight differences in the initial positions of the planets and the asteroids, to evaluate the solution's stability. Beyond 60 Ma, Earth's eccentricity cannot be precisely calculated, and only the stable 405-kyr cycle can be used for astronomical tuning (Laskar et al., 2011b). The 405-kyr minima as identified in the succession have been tuned to successive 405-kyr minima filtered from the (nominal) La2011 solution (Laskar et al., 2011b) (bandwidth 300-623 kyr).

3.4 Biostratigraphy

37 samples from cycles 173 to 251 of the Sopelana section were investigated for calcareous nannofossil biostratigraphy and processed following the procedure described in Thibault et al. (2012b). This results in an average sample resolution of ca 50 kyr for the studied interval, with three additional samples in cycles 157, 159 and 161 (Table 1). Semi-quantitative counts were performed on key and other potential additional stratigraphic markers at a magnification of ×1600 (×100 oil

objective with a ×1.6 additional lens). Preservation of nannofossils ranges from poor (P) to very poor (VP) in the Sopelana section and this affects the overall abundance of identifiable specimens which is generally low. Counts were determined in the following fashion: a species was determined as few (F) if one specimen or more could be observed in every 10 fields of view, rare (R) if, on average, only one specimen could be observed in 11 to 50 fields, very rare (VR) if, on average, only one specimen could be observed in 51 to 100 fields, and single (S) if only one specimen was observed over a total of 200 fields of view. The biozonation of Burnett et al. (1998) was applied. Calcareous nannofossil species considered in this paper followed taxonomic concepts of Perch-Nielsen (1985) and Young and Bown (1997). Bibliographic references for the determined taxa are given in Perch-Nielsen (1985) and Bown (1998).
For planktonic foraminifer biostratigraphy, the results reported here are published in Batenburg et al. (2012)/Chapter 2 and Pérez-Rodriguez et al. (2012).

3.5 Magnetostratigraphy

Oriented cores for paleomagnetic analyses were taken with a gasoline-powered drill in the topmost and lowermost part of the lower Maastrichtian succession (Fig. 2). From each oriented sample level, one specimen was thermally demagnetized in a magnetically shielded furnace using numerous small temperature increments, at 20, 80, 120, 150, 180, 200, 220, 240, 300, 320, 340 and 360°C. For some samples, the thermal demagnetization was continued up to 550°C. The natural remanent magnetization (NRM) was measured on a 2G Enterprise horizontal cryogenic magnetometer equipped with DC SQUIDS (noise level 3 x 10^{-12} Am^2) at the Paleomagnetic Laboratory Fort Hoofddijk, the Netherlands. The directions of the NRM components were calculated by principal component analysis (Kirschvink, 1980; Zijderveld, 1967). Mean directions were determined for the individual sections using standard Fisher statistics. The 58° tilt helped to distinguish primary (pre-tilt) from secondary (post-tilt) components and to recognise the present-day field overprint (Dec./Inc.; 359/58).

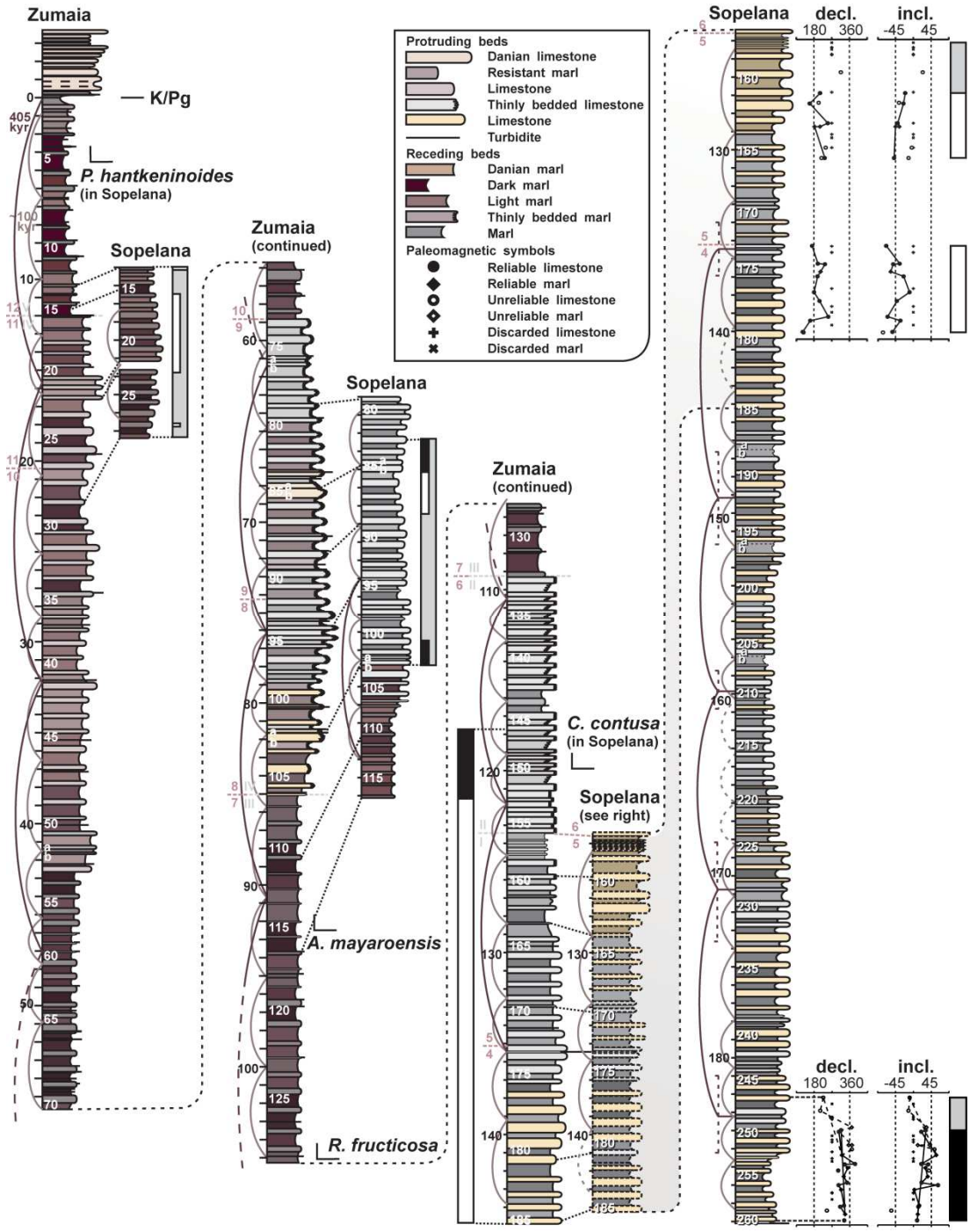

Figure 2: Stratigraphic logs of the Zumaia and Sopelana sections with key biostratigraphic events and magnetostratigraphy from this study. Grey roman numerals indicate the intervals identified by Ward et al. (1991) and lilac numbers the units of Wiedmann (1988). The half circles in deep purple indicate the 405-kyr eccentricity minima, the lighter half circles indicate the 100-kyr bundling. White numbers are cycle numbers.

4. Results

4.1 Lithostratigraphy and geophysical properties

In the lower Maastrichtian of the Sopelana section, hemipelagic limestone marl alternations, on a scale of 50-60 cm per couplet, display variations in the colour and thickness of the marls, albeit less strong than at Zumaia, and variations in the induration and thickness of the limestones. Intervals of distinct variations alternate with poorly expressed limestone-marl couplets, forming bundles of five couplets, and groups of 18 to 20, bounded by particularly poorly expressed marls (Fig. 2). The interval from cycle 212 to 224 has a remarkably constant expression of the limestone-marl couplets and lacks signs of bundling or grouping. A total of 107 couplets has been identified at Sopelana, including three couplets with very poorly expressed marls that have been marked with “a” and “b” (Figs. 1 and 2).
The magnetic susceptibility record (Fig. 3) displays variations that reflect the alternations in the lithology on the scale of the limestone-marl couplets and on a longer scale of ~19 couplets. Values are relatively low (2.5 to 15.5 SI) and short variations over 40-70 cm depth are typically around 5 SI. The amplitude of these variations shows a pattern of gradual increase and decrease on a scale of ~12 m. The reflectance record, varying between 47 and 65%, also follows the lithological pattern, and mostly displays gradual variations in average values with some variation in amplitude. Combining the Sopelana and Zumaia datasets at 135.47 m does not introduce a shift in values; however, the Zumaia datasets show a larger range of variability.

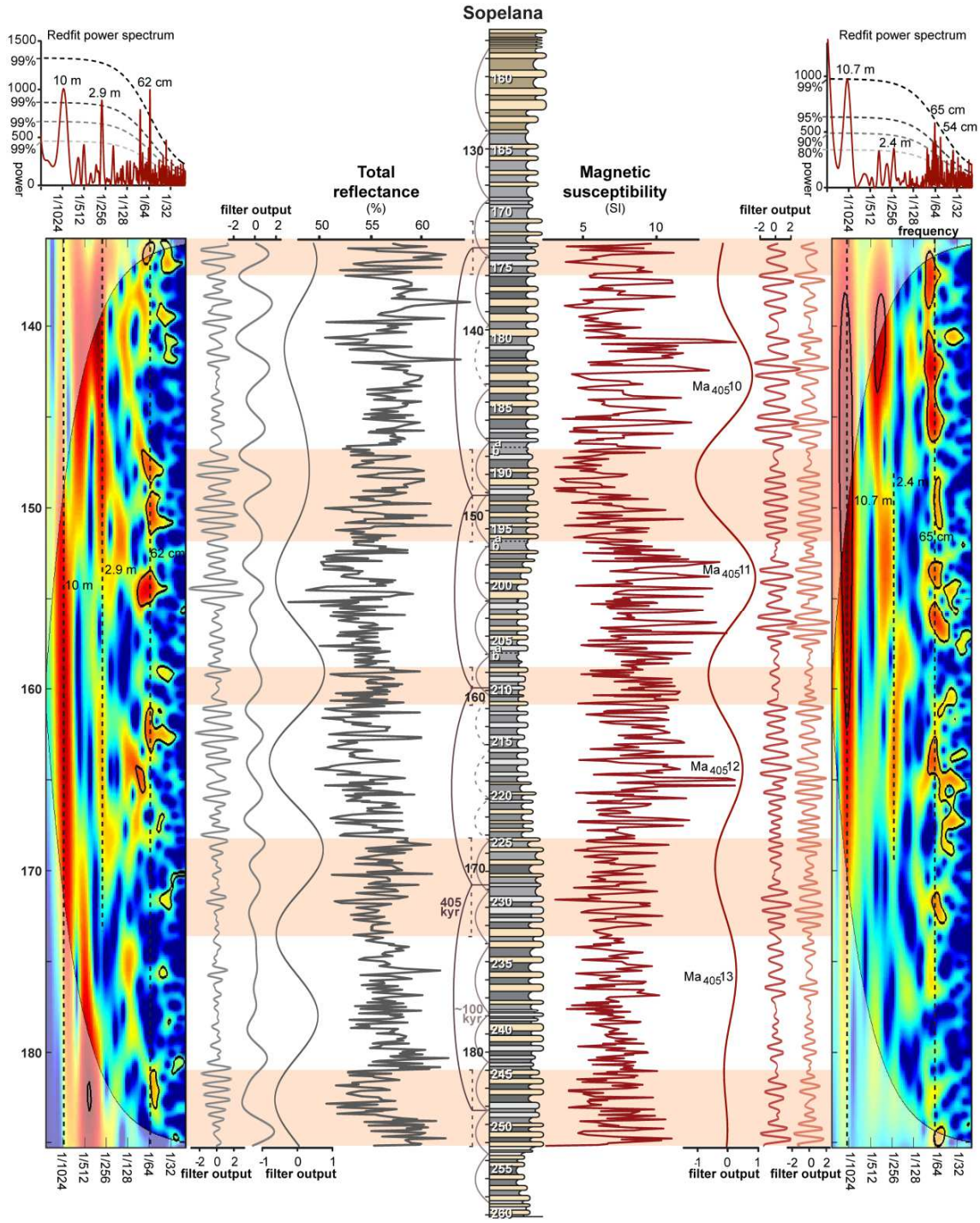

Figure 3: Stratigraphic log of the Sopelana section with total reflectance L on the left and magnetic susceptibility on the right. The data are flanked by their band-pass filters, wavelet analyses and Redfit power spectra. The band-pass filters of reflectance are centred at 10, 2.9 and 0.62 m (in dark grey, middle grey and light grey, with bandwidths 7.7-14.3, 2.0- 5.0, 0.45-1.0 m, respectively) and the filters for magnetic susceptibility are centred at 10.7, 2.4 and 0.65 m (in dark red, red and orange, with bandwidths 8.1-15.8, 1.8- 3.8, and 0.47-1.06 m, respectively). The pink*

bands indicate the stratigraphic levels that are identified as 405-kyr minima, with the black Ma_{405}numbers indicating the 405 eccentricity cycles following the nomenclature of Husson et al. (2011).

4.2 Spectral analysis

Spectral analysis by Redfit 38 of the magnetic susceptibility record of Sopelana shows main periodicities of 10.7 m and 65 and 54 cm (95% confidence level), 82 cm (90% confidence level) and 2.4 m (80% confidence level). The wavelet analysis displays the presence of the periodicities throughout the section, although especially in the upper two thirds, and shows a temporary shift to slightly shorter periodicities between 156 and 168 m depth, mostly around the 2.4 m periodicity and in the 50-60 cm periodicity band, indicating slightly lower sedimentation rates, which is in agreement with a decreased thickness of the beds. The 65 cm filtered component (bandwidth 47-106 cm) shows variations in amplitude on a depth scale of 2 to 3 m, which are also reflected in the 2.4 m filtered component (bandwidth 1.8-3.8 m). The 10.5 m filtered component (bandwidth 8.1-15.8 m) has five minima and four maxima.

The combined magnetic susceptibility record (Fig. 4) of Sopelana and Zumaia reveals main periodicities in the Redfit power spectrum of 17 and 12 m (95 % confidence level) and ~72 cm. The wavelet diagram shows that the longer periodicity ~17 m is mostly present in the upper half of the record, down to 110 m in Zumaia, and the 12 m periodicity in the lower half of the record, which coincides with a shift in bedding thickness in Zumaia and the generally thinner bedding at Sopelana. The wavelet spectrum shows the presence of periodicities slightly longer than 72 cm in the upper half of the data, from Zumaia, and slightly shorter than 72 cm in the lower part, from Sopelana. Outputs of band-pass filters, centred at 17 m (bandwidth 12-29 m) and 12 m (bandwidth 8.5-20 m) periodicities, show the presence of 13 cycles throughout the combined datasets.

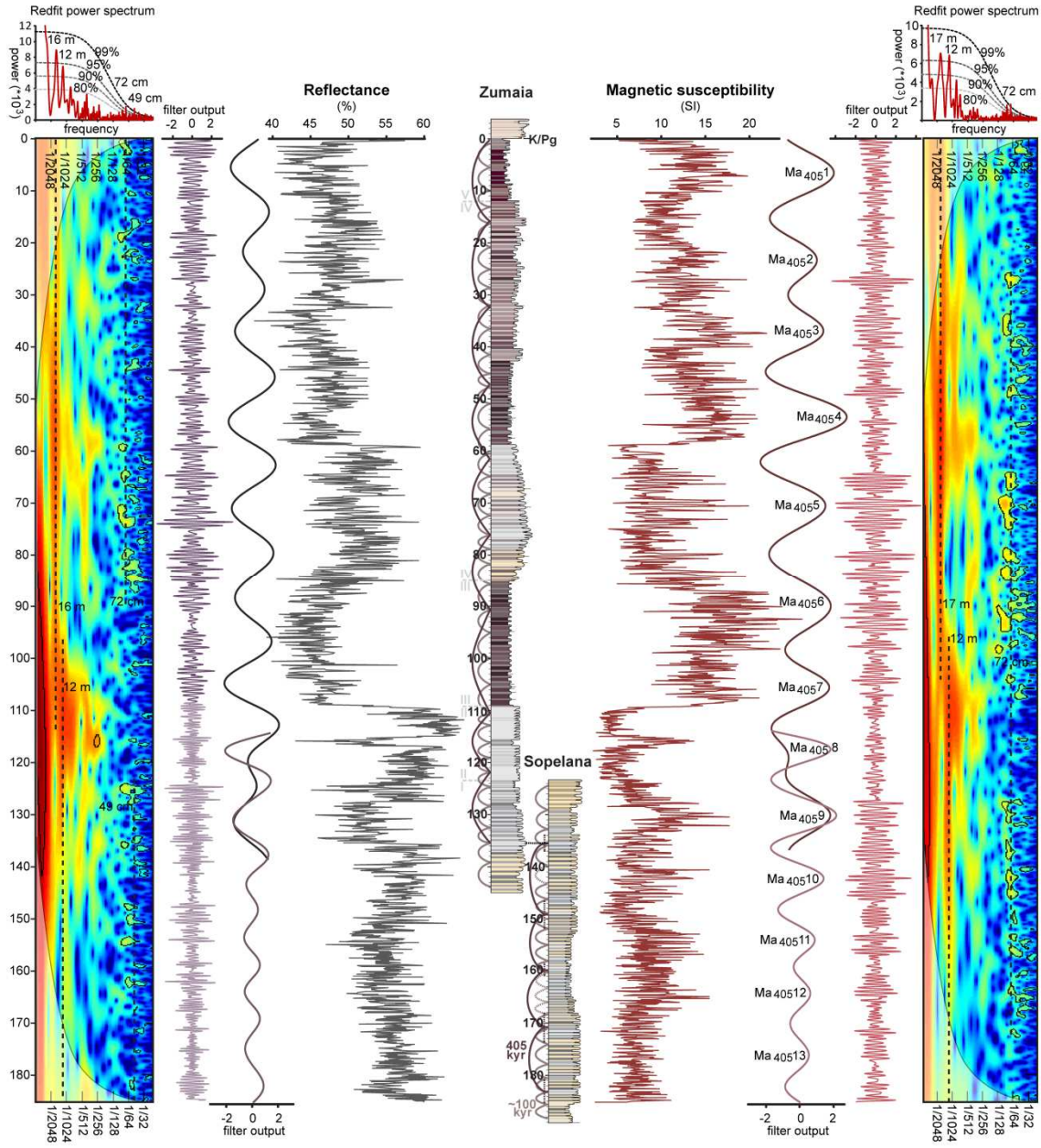

Figure 4: Stratigraphic logs of the Zumaia and Sopelana sections with total reflectance L on the left and magnetic susceptibility on the right, connected at a depth of 135.47 m. The data are flanked by their band-pass filters, wavelet analyses and Redfit power spectra. The band-pass filters of reflectance are centred at 16 m (dark grey, top), 12 m (grey-purple, base) and at 72 cm (purple, top), and 49 cm (lilac, base) (bandwidths of 12-29, 8.5-20 and 0.53-1.1 m respectively). The band-pass filters of magnetic susceptibility are centred at 17 m (dark red, top), 12 m (pink, base) and at 72 cm (red) (bandwidths of 12-24, 8.8-19 and 0.50-1.3 m respectively). The black Ma_{405}numbers indicate the 405 eccentricity cycles following the nomenclature of Husson et al. (2011).*

The reflectance record of Sopelana has its main periodicities at 62 cm (99% confidence level), at 10 and 2.9 m and at 85 cm (95% confidence level). The wavelet diagram shows the influence of the 2.9 and 10 m periodicity throughout the section, and the presence of the 2.9 m periodicity mostly in the upper half of the section. The output of the band-pass filtered centred at 10 m (bandwidth 7.7-14.3 m) shows five maxima and minima, and the 62 cm band-pass filtered component (bandwidth 45-102 cm) shows some bundling on a scale of approximately 3 m. The 2.9 m band-pass filtered component (bandwidth 2.0-5.0 m) shows approximately 17 maxima.

Redfit analysis of the reflectance data from the Zumaia and the Sopelana sections combined displays periodicities at 16 and 12 m (95% and 90% confidence level, respectively). The wavelet diagram displays a transitional interval around 110 m, where the main periodicity changes from a 12 m (below) to a 16 m periodicity (upwards). Other important periodicities are around 72 cm and 49 cm, with the 72 cm periodicity mostly visible in the upper half of the wavelet analyses, and the 49 cm periodicity in the lower part of the diagram. This agrees with a change in sedimentation rate at Zumaia and the generally thicker beds at Zumaia compared to Sopelana. The band-pass filtered components centred at 16 (bandwidth 12-24 m) and 12 m (bandwidth 8.8-19 m) display 13 cycles throughout the combined reflectance dataset.

4.3 Calcareous nannofossil biostratigraphy

For the part of the section of Zumaia investigated for cyclostratigraphy, we correlated the lithological log of Pérez-Rodriguez et al. (2012) (Table 1) to ours by recognition of the large scale lithological intervals originally defined by Wiedman (1988) and Ward et al. (1991)(Fig. 2). Semiquantitative data are not directly comparable between Pérez-Rodriguez et al. (2012) and this study. Nannofossils were observed at 1250x magnification in Pérez-Rodriguez et al. (2012) and at 1600x here. Among the species considered here, none of them was recorded as common, e.g. corresponding to 1-10 specimens per field of view (fov). The category

Frequent/Few (F) is estimated in a similar fashion between the two studies, corresponding to 1 specimen per 2 to 20 fov. Pérez-Rodriguez et al. (2012) considered only one subsequent category, rare (R) for 1 specimen per >20 fov whereas in this study, we considered three following categories, rare (R), very rare (VR) and single (S) (Table 1). Although the categories are different, combination of our results with those of Pérez-Rodriguez et al. (2012) highlights the ranges of key biostratigraphic taxa (Table 1).

A number of species identified in the lower part of the Zumaia section, which corresponds to the upper part of Sopelana, were not found in this study. *Acuturris scotus* was found in only one sample, and *Arkhangelskiella maastrichtiana* and *Eiffelithus eximius* are absent. The first occurrence (FO) of *A. maastrichtiana* in Zumaia is was recorded at 49.91 m (Pérez-Rodríguez et al., 2012) which corresponds to a composite depth of 137.29 m in our study (Precession cycle number 176, 69.69 Ma). Nannofossil bio-events such as the last occurrence (LO) of *A. scotus*, *Broinsonia parca constricta*, *Cribrocorona echinus*, *Reinhardtites levis*, *Tranolithus orionatus* and *Zeugrhabdotus bicrescenticus* cannot be compared between the work of Pérez-Rodriguez et al. (2012) and this study because the interval below 145 m at Zumaia (42.2 m in the scale of Perez-Rodriguez et al., (2012) is highly turbiditic, which prevents correlation to Sopelana. *Uniplanarius trifidus* was not found in Sopelana and those identified for the Zumaia section were considered as highly questionable(Pérez-Rodríguez et al., 2012).

The applied biozonation (Table 1) should be considered here as a tentative interpretation from a record that bears large uncertainties. The top of zones UC17 and UC18 are respectively defined by the last occurrences of *T. orionatus* and *R. levis* which both have very inconsistent records across their ranges and when present are at best rare(Table 1).

Section and references	Precession cycle nr	Height (m, Pérez-rodriguez et al. 2012)	Composite depth (cm)	Age (Myr)	*Acutturris scotus*	*Bronsonia parca constricta*	*Calculites obscurus*	*Ceratolithoides aculeus*	*Ceratolithoides indiensis*	*Ceratolithoides kamptneri*	*Cribrocorona echinus*	*Lithraphidites quadratus*	*Micula murus*	*Micula prinsii*	*Petrarhabdus vietus*	*Reinhardtites levis*	*Tranolithus orionatus*	*Watznaueria manivitiae* s.l.	*Zeugrhabdotus bicrescentticus*	Preservation	Bio-events	UC Zones
Zumaia (Perez-Rodriguez et al. 2012)	1	K/Pg 0-0.3	0.00	65.97					R			F	R					F		VP-M		UC20d^{TP}
	2	189.76	0.60	65.98								R	F	R				R		VP-M		
	3	188.5	1.72	66.01					R			F	F					F		VP-M	Base *M. prinsii*	
	4	188.1	2.08	66.02					R			F	F	R				F		VP-M		
	6	185.9	4.05	66.05								F	F					F		VP-M		UC20c^{TP}
	7	183.92	5.82	66.09					R			F	R					F		VP-M		
	10	181.15	8.29	66.15						R		F	R					F		VP-M	Base *C. kamptneri*	
	11	180.3	9.05	66.17								F	R					F		VP-M		UC20b^{TP}
	17	175.9	13.09	66.29								F	F					F		VP-M	Base *M. murus*	
	24	170.9	18.03	66.44								F						R		VP-M		UC20a^{TP}
	37	159.8	28.99	66.72								R						F		VP-M		
	50	148.8	39.86	66.97								F						F		VP-M		
	61	140.8	47.76	67.22					R			R						F		VP-M		
	72	130.54	57.89	67.19				R				R						R		VP-M		
	85b	119.69	68.61	67.47								F						R		VP-M		
	97	110.42	77.77	68.04								R						F		VP-M		
	110	99.8	88.24	68.33	R	R			R									F	R	P-M		
	122	89	98.84	68.56					R									F		VP-M		
	123	87.8	100.02	68.59					R									R		P-M		
	125	86.6	101.20	68.61														F		VP-P		
	128	83.1	104.64	68.68								F						R		VP-M		
	131	79.55	108.12	68.74											R			R		P-M	Top *P. vietus*	
	131	78.8	108.86	68.75								F			R			F		P-M		
	138	74.81	112.78	68.89	?			R	R			R			R			F	R	VP-M		
	142	72.62	114.93	68.97					F			R						R		VP-M		
	143	71.75	115.78	69.00								?						R		VP-P	Base *L. quadratus*	

	144	70.94	116.58	69.02				R	R		F			F		VP-M		
Sopelana (this study)	157	-	124.08	69.27						S				F		VP	Top *C. echinus*	UC19
	159	-	125.40	69.31										F		VP		
	161	-	127.23	69.35					VR		R	R		F		VP	**Top *R. levis***	
	173	-	135.43	69.61								VR		R		VP		
	175	-	136.67	69.65							S	VR		F		VP	Base *A. maastrichtiana* at Zumaia	
	177	-	138.14	69.69					VR					F		VP-P		
	179	-	139.80	69.73						S				F		VP		
	181	-	141.31	69.77										R		VP		
	183	-	142.94	69.82								S		F		VP-P		
	185	-	144.42	69.86				VR						F		VP-P		
	187	-	145.81	69.90				VR	S	VR				F		VP-P		UC18
	189	-	147.36	69.96				S	S					F		VP		
	191	-	148.78	70.01										F		VP		
	194	-	150.49	70.06				VR	S					F		VP		
	196	-	151.96	70.12										F		VP		
	198	-	153.03	70.17				R	S					F	VR	VP-P	Top *Z. bicrescenticus*	
	201	-	154.88	70.22										R		VP		
	203	-	156.30	70.27				VR	VR					F	VR	VP-P		
	206	-	157.85	70.32			R		R				R	R		VP	**Top *T. orionatus***	
	209	-	159.61	70.40			R	S	S	VR		VR		F	R	VP-P		
	212	-	160.95	70.47			VR		S	VR				F		VP-P		
	214	-	162.31	70.51			S		VR	VR		R		F	VR	VP-P		
	216	-	163.66	70.55						S		S		F	R	VP-P		
	219	-	165.33	70.61			VR		VR					R	S	VP		
	222	-	166.98	70.67								VR		VR		VP		
	225	-	168.52	70.73			R							R		VP		
	227	-	169.82	70.77			R		S			VR		VR	R	VP		UC17
	229	-	171.22	70.81			F	VR				S		R	S	VP-P		
	232	-	172.99	70.87			R			R		VR		F		VP-P		
	234	-	174.39	70.91			R			VR	S	VR		R		VP		
	236	-	176.03	70.96			R			VR		S		F	VR	VP-P		
	238	-	177.47	71.00			F					R		R	VR	VP-P		
	240	-	178.92	71.04	VR		F	VR	R		VR	R	R	F	VR	P		
	243	-	180.50	71.10			F			VR		R		F		VP-P		
	246	-	181.88	71.17			R				VR	VR	S	F	S	VP		
	248	-	183.25	71.21		S	F		S	S		R	S	F	S	VP-P	**Top *B. parca constrica***	UC16
	251	-	184.84	71.27		R	R	S			S	R		R	VR	VP-P		

Table 1: Semiquantitative distribution range chart of selected calcareous nannofossil taxa in the Zumaia and Sopelana sections. F, few; R, rare, VR, very rare; S, single (see methods for details). Species having biostratigraphical significance are highlighted in pale grey. Dark grey indicates occurrences interpreted as reworked. Modified from Pérez-Rodriguez et al. (2012) for results on the Zumaia section.

4.4 Magnetostratigraphy

The demagnetization data of the lower Maastrichtian at Sopelana are of limited quality, but the resulting magnetostratigraphy is relatively straightforward.
In all samples, a randomly oriented viscous component is first removed between 20 and 80°C. Upon further heating a second component is removed, in general up to 200/220°C. The direction of the second component is random in all samples. Heating up to 360°C did not yield reliable directions for all samples as many samples displayed a randomly oriented increase of natural remanent magnetization (NRM) intensity starting from 300°C (Supplementary figure 2). Post-depositional processes might have affected the paleomagnetic signal as has been described by Moreau et al. (1994).When the demagnetization revealed only one component and the NRM intensities at 220°C are extremely high (above 0.2 A/m; similar to suggestions of Moreau et al. (1994), we consider these directions as being related to the process of re-magnetization and therefore unreliable. These samples are mainly from the marly lithology, which agrees with the findings of Moreau et al. (1994). Some samples could be heated up to 550°C (Supplementary figure 2), and the resultant direction of this third component did not differ from the direction yielded between 200/220° and 300-360°C. Equal area projections (Supplementary figure 2) reveal a slight non-antipodality of the normal and reverse directions, but the data do not pass the reversal test. The slight non-antipodality is most likely related to the weak NRM intensities, which make it difficult to isolate the primary component from an overprint component, related to overlapping blocking temperature of the magnetic carrier. The characteristic remanent magnetization (ChRM) directions of the third component of the logged lower Maastrichtian section (Batenburg et al., 2012/Chapter 2)(Fig. 2)., yielded reverse polarity, from

cycle 161-166, and 173-180. Above cycle 161, the quality of the demagnetization data is too poor to yield any reliable polarity. New results show that the lowermost part of the section, from cycle 249 to 260, has stable normal polarity, whereas cycle 247-248 yielded only unreliable and uncertain directions. In particular, the inclination in this interval is too shallow to support a stable normal polarity.

5. Cyclostratigraphy and Astronomical tuning

5.1 Cyclostratigraphy

The observed hierarchy of the limestone-marl alternations at both the Zumaia and Sopelana sections, where they are grouped in bundles of five and groups of 18-20, is a strong indication that eccentricity-modulated precession is the underlying cause of the sedimentary cyclicity. Intervals with maximal difference between lithologies, represent the maximal precessional amplitude within eccentricity maxima, which is the same phase relation as inferred by Dinarès-Turell (2003), Kuiper et al. (2008), Westerhold et al. (2008), Hilgen et al. (2010) and Batenburg et al. (2012)/Chapter 2 for the Paleocene and Maastrichtian of the Zumaia section. To obtain an orbitally tuned chronology, only the 405-kyr period of eccentricity provides a stable and reliable tuning target, which would correspond to the ~17 m periodicity in the upper two thirds of the Zumaia section, and the 10-12 m periodicity in the lower part of the Zumaia section and the whole of the Sopelana section. Time series analyses and lithological observations allow to identify the position of consecutive 405-kyr minima in more detail:

$Ma_{405}9$: The position of the topmost 405-kyr minimum, the base of cycle $Ma_{405}9$, can be reliably obtained from correlation to Zumaia from cycle 157 to 185 (Fig. 2, and Batenburg et al., 2012/Chapter 2), and is characterized by two limestone-marl alternations in which the lithologies are very similar, indicating a reduced amplitude of the underlying forcing mechanism. Specifically, the limestones of cycles 173 and 174 are not prominent and the marl in between, of cycle 173, is particularly thin

and light in colour. Upwards from cycle 171 and downwards from cycle 175, the marls are again darker and thicker. The interval of cycles 172 to175 is characterized by low values of magnetic susceptibility, and a minimum in its 10.7 m filtered component.

Ma_{405}10: Downwards, from cycle 176 to 187, limestones and marls are distinct and cycles are thick, corresponding to a 405-kyr maximum. The interval from cycle 188 to 196 is bounded by marls in which slightly more carbonate rich, but hardly distinguishable, layers occur. These probably represent the very poorly developed limestone-part of a cycle, and have been marked “a” and “b” in the log (Fig. 2). These cycles are likely to have been deposited in the ~ 100-kyr minima of eccentricity within a 405-kyr minimum. In the middle of this interval, the marl of cycle 191 is very thin and light in colour and the limestone of cycle 192 is not prominent. This interval is likely to represent the 405-kyr minimum at the base of cycle Ma_{405}10, which spans 19 cycles and a potential additional cycle marked with “a” and “b”. The minimum interpreted from the lithology coincides with low values, decreased variability, and a minimum in the 10.7 m filtered component of magnetic susceptibility.

Ma_{405}11: Cycles 197 to 205 below consist of distinct limestone-marl alternations. Cycle 206 again has a lighter and more resistant level within the marl, marked with “a” and “b”, likely to represent a 100-kyr minimum close to a 405-kyr minimum. Cycles 206 and 211 have very poorly developed limestones, which are relatively thin and not prominent. Cycles 207 and 212 have the most prominent limestones in this interval and have the lowest values of magnetic susceptibility. This interval is interpreted as the 405-kyr minimum at the base of Ma_{405}11, and coincides with a minimum in the 10.7 m filtered component of magnetic susceptibility.

Ma_{405}12: Cycles 212 to 224 display a very regular alternation of relatively thin limestones and marls in which no bundling can be observed. However, values of magnetic susceptibility are high and variations large, indicative of a 405-kyr maximum of eccentricity. The absence of bundling may be the expression of a

longer term minimum in eccentricity which reduces the amplitude of the ~100 kyr cycles. Downwards, cycles 225 to 233 form the uppermost part of a promontory on the beach. The resistance of the beds likely reflects a slightly higher carbonate content. Some bundling can be observed with a relatively dark marl in cycle 227 and in cycles 230 to 233, bounded by intervals with lighter marls. The limestone of cycle 229 is thin and not prominent, and is bounded by light-coloured marls. The limestone of cycle 230 has very low values of magnetic susceptibility. The interval of cycles 225 to 133 coincides with a minimum in the 10.7 m filtered component of magnetic susceptibility and is likely to span the 405-kyr minimum at the base of cycle $Ma_{405}12$.

$Ma_{405}13$: Cycles 234-244 show distinct limestone-marl alternations with variation in the thickness and colour of the marls. Cycles 234, 238 and 243 in particular have very thin and light-coloured marls, reflecting a bundling of limestone-marl alternations in groups of five. Cycles 245 to 252 form the lowermost part of the promontory on the beach, with relatively little difference among cycles, except in the middle of this interval. The marl of cycle 248 is thin and light, and the bounding limestones of cycles number 248 and 249 are not as prominent as those of neighbouring cycles. The interval coincides with low values of magnetic susceptibility and is interpreted as the 405-kyr minimum of cycle $Ma_{405}13$.

5.2 Age model

An astronomical age model was constructed by correlating the identified 405-kyr minima in the Sopelana section to successively older minima in the filtered 405-kyr cycle from the new La2011 solution (Laskar et al. 2011b) (band-pass filter centred at 405 kyr, bandwidth from 298 to 615 kyr), linked to the tuning of the 405-kyr cyclicity in the Zumaia section (Batenburg et al., 2012/Chapter 2). Using the astronomical tie-points, time series were generated for the combined Zumaia/Sopelana datasets, on which time series analysis was performed (Supplementary figure 2). The Redfit power spectra of reflectance and magnetic susceptibility, respectively, show dominant periodicities of 415 and 409 kyr, but

these are likely (partly) introduced by the tuning. Other important periodicities are 23.6 and 22.3 kyr (magnetic susceptibility, 99% confidence level) and 17.9 kyr (reflectance, 95% confidence level). The wavelet diagram shows a relatively constant behaviour of the major periodicities throughout the sections, with potentially some expression of the ~100 kyr periodicity.

Ages were assigned to biostratigraphic events based on the 405-kyr tuning, the number of precessional beds between consecutive 405-kyr minima and the position of the event with respect to the precessional cyclicity (Tables 1 and 2). The uncertainty estimate is based on the uncertainty in the position of the event, uncertainty in the correlation, the uncertainty in the cyclostratigraphic interpretation (20.8 kyr) and the astronomical tuning (taken here as 23 kyr, the maximal difference detected between 405-kyr minima in between the variants of the La2011 solutions).

6. Discussion

6.1 Biostratigraphy

The succession of calcareous nannofossil and planktic foraminiferal bio-horizons (Fig. 6, Table 2) is similar to other records from low-latitude, tropical sites (Gardin et al., 2012, and references therein; Voigt et al., 2012). Comparison of the ages of bio-events and associated bio-zonal boundaries obtained from cyclostratigraphic studies points to diachronism of nannofossil and planktonic foraminifer events (and biozones) across a wide range of sites (Fig. 7). Among all studies for which biostratigraphic data are available, only two provide ages of calcareous plankton bio-horizons which are calibrated to the most recent late Campanian–Maastrichtian time scale (ODP Site 762C, Exmouth Plateau, Indian Ocean, Thibault et al., 2012b, and the Gubbio area, central Italy, Gardin et al., 2012). A slight discrepancy of 0.03 Myr for biostratigraphic events within magnetochron C29r between these studies and our results is accounted for because these authors considered the K-Pg boundary to have an age of 66 Myr instead of the 65.97 Myr used in our study.

Stratigraphic events (magnetochron boundaries, Planktic foraminifers and calcareous nannofossils)		Height (m, Perez-Rodriguez et al. 2012)	Composite depth (m, this study)	Section and references for the Basque country	Precession cycle nr	Age (Myr)	Average age and uncertainty for the Basque country (Myr)	Average age and uncertainty for the Gubbio area (Myr, Gardin et al., 2012)	Average age and uncertainty for ODP762C, Indian Ocean (Myr, Thibault et al., 2012b)
Top C31r (mag.)	Top	-	121.09	Zumaia (Batenburg et al., 2012)	152	69.18	69.19±0.08	-	69.220±0.070
	Bottom	-	121.95		153	69.21			
Top C32n1n (mag.)	Top	-	182.88	Sopelana (this study)	248	71.19	71.22±0.09	-	71.400±0.080
	Bottom	-	183.96		250	71.23			
FO *Plummerita hantkeninoides* (PF)	Top	-	3.60	Sopelana (Batenburg et al., 2012)	5	66.05	66.06±0.08	66.118±0.017	-
	Bottom	-	4.57		6	66.07			
FO *Pseudoguembelina hariaensis* (PF)	Top	170.90	18.03	Zumaia (Perez-Rodriguez et al. 2012)	24	66.44	66.46±0.12	-	-
	Bottom	168.40	20.50		27	66.49			
LO *Archaeoglobigerina cretacea* (PF)	Top	157.00	31.76	Zumaia (Perez-Rodriguez et al. 2012)	41	66.77	66.84±0.16	-	-
	Bottom	150.90	37.78		48	66.92			
LO *Globotruncana bulloides* (PF)	Top	150.90	37.78	Zumaia (Perez-Rodriguez et al. 2012)	48	66.92	66.99±0.16	-	-
	Bottom	145.32	43.29		54	67.07			
LO *Contusotruncana plummerae* (PF)	Top	126.32	62.06	Zumaia (Perez-Rodriguez et al. 2012)	77	67.59	67.63±0.13	-	-
	Bottom	123.20	65.14		81	67.67			
FO *Rugoglobigerina scotti* (PF)	Top	111.75	76.46	Zumaia (Perez-Rodriguez et al. 2012)	95	68.00	68.07±0.16	-	-
	Bottom	107.10	81.05		102	68.13			
LO *Contusotruncana fornicata* (PF)	Top	103.00	85.10	Zumaia (Perez-Rodriguez et al. 2012)	107	68.26	68.29±0.12	-	-
	Bottom	99.80	88.24		110	68.33			
LO *Globotruncana linneiana* (PF)	Top	99.80	88.24	Zumaia (Perez-Rodriguez et al. 2012)	110	68.33	68.35±0.12	-	70.130±0.140
	Bottom	97.60	90.40		113	68.38			
LO *Globotruncana ventricosa* (PF)	Top	99.80	88.24	Zumaia (Perez-Rodriguez et al. 2012)	110	68.33	68.35±0.12	-	-
	Bottom	97.60	90.40		113	68.38			
FO *Abathomphalus mayaroensis* (PF)	Top	87.80	100.02	Zumaia (Perez-Rodriguez et al. 2012)	123	68.59	68.60±0.10	69.296±0.107	69.920±0.150
	Bottom	86.60	101.20		125	68.61			
FO *Abathomphalus mayaroensis* (PF)	Top	-	92.40	Zumaia (Batenburg et al., 2012)	115	68.42	68.43±0.08	69.296±0.107	69.920±0.150
	Bottom	-	93.28		116	68.44			
FO *Globotruncanita conica* (PF)	Top	79.55	108.12	Zumaia (Perez-Rodriguez et al. 2012)	131	68.74	68.75±0.09	-	-
	Bottom	78.80	108.86		131	68.75			
FO *Racemiguembelina fructicosa* (PF)	Top	78.80	108.86	Zumaia (Perez-Rodriguez et al. 2012)	131	68.75	68.87±0.21	70.137±0.133	67.660±0.220
	Bottom	71.81	115.72		143	68.99			
FO *Racemiguembelina fructicosa* (PF)	Top	-	105.00	Zumaia (Batenburg et al., 2012)	128	68.69	68.70±0.16	70.137±0.133	67.660±0.220
	Bottom	-	106.03		129	68.71			

LO *Contusotruncana morozovae* (PF)	Top	71.81	115.72	Zumaia (Perez-Rodriguez et al. 2012)	143	68.99	69.07±0.17	-	-
	Bottom	67.30	120.15		151	69.15			
FO *Planoglobulina acervulinoides* (PF)	Top	58.80	128.40	Zumaia (Perez-Rodriguez et al. 2012)	164	69.42	69.50±0.17	73.119±0.459	68.360±0.080
	Bottom	52.80	134.40		172	69.58			
FO *Contusotruncana contusa* (PF)	Top	52.80	134.40	Zumaia (Perez-Rodriguez et al. 2012)	172	69.58	69.64±0.16	70.259±0.051	67.660±0.220
	Bottom	47.90	139.30		178	69.71			
FO *Contusotruncana contusa* (PF)	Top	-	119.90	Sopelana (Batenburg et al., 2012)	150	69.14	69.15±0.17	70.259±0.051	67.660±0.220
	Bottom	-	120.48		151	69.16			
FO *Racemiguembelina powelli* (PF)	Top	52.80	134.40	Zumaia (Perez-Rodriguez et al. 2012)	172	69.58	69.64±0.16	-	68.180±0.180
	Bottom	47.90	139.30		178	69.71			
FO *Micula prinsii* (CN)	Top	188.10	1.72	Zumaia (Perez-Rodriguez et al. 2012)	3	66.01	66.02±0.09	66.296±0.077	66.390±0.070
	Bottom	185.90	2.08		4	66.02			
FO *Ceratolithoides kamptneri* (CN)	Top	181.15	8.29	Zumaia (Perez-Rodriguez et al. 2012)	10	66.15	66.16±0.10	-	66.980±0.100
	Bottom	180.30	9.05		11	66.17			
FO *Micula murus* (CN)	Top	175.90	13.09	Zumaia (Perez-Rodriguez et al. 2012)	17	66.29	66.37±0.16	67.919±0.125	67.330±0.070
	Bottom	170.90	18.03		24	66.44			
LO *Petrarhabdus vietus* (CN)	Top	83.10	104.64	Zumaia (Perez-Rodriguez et al. 2012)	128	68.68	68.71±0.12	-	67.790±0.060
	Bottom	79.55	108.12		131	68.74			
FO *Lithraphidites quadratus* (CN)	Top	72.62	114.93	Zumaia (Perez-Rodriguez et al. 2012)	142	68.97	69.00±0.11	69.131±0.067	67.790±0.060
	Bottom	70.94	116.58		144	69.02			
LO *Cribrocorona echinus* (CN)	Top	70.94	116.58	Sopelana (this study)	144	69.02	69.15±0.19	-	-
	Bottom	-	124.08		157	69.27			
LO *Reinhardtites levis* (CN)	Top	-	125.40	Sopelana (this study)	159	69.31	69.33±0.09	70.154±0.047	69.750±0.150
	Bottom	-	127.23		161	69.35			
FO *Arhkangelskiella maastrichtiana* (CN)	Top	49.91	137.29	Zumaia (Perez-Rodriguez et al. 2012)	176	69.69	69.78±0.28	70.590±0.483	-
	Bottom	40.21	~146.99		~187	~69.88			
LO *Zeugrhabdotus bicrescenticus* (CN)	Top	-	151.96	Sopelana (this study)	196	70.12	70.15±0.09	-	69.750±0.150
	Bottom	-	153.03		198	70.17			
LO *Tranolithus orionatus* (CN)	Top	-	156.30	Sopelana (this study)	203	70.27	70.30±0.09	70.723±0.107	69.560±0.070
	Bottom	-	157.85		206	70.32			
LO *Eiffelithus eximius* (CN)	Top	22.21	~162.00	Zumaia (Perez-Rodriguez et al. 2012)	-	~70.5	70.55±0.20	75.601±0.399	73.900±0.090
	Bottom	25.30	~165.00		-	~70.6			
LO *Broinsonia parca constricta* (CN)	Top	-	181.88	Sopelana (this study)	246	71.17	71.19±0.09	71.004±0.287	69.480±0.100
	Bottom	-	183.25		248	71.21			

Table 2: Top and Bottom heights (or depths), and estimated ages of significant stratigraphic events recorded in the Zumaia and Sopelana sections compared to the Gubbio area, Italy and the Exmouth Plateau, Indian Ocean. Mag., magnetic reversal boundary; PF , planktic foraminifers; CN, calcareous nannofossils. Reported uncertainties are the sum of the uncertainty in the stratigraphic position (difference in top and bottom height), the uncertainty in the cyclostratigraphic interpretation (taken as two precessional cycles, 43.6 kyr), the uncertainty in the astronomical solution (taken as 23 kyr, the maximal differences in the position of the 405 kyr minima between the La2011 astronomical solutions) and, for the data of Pérez-Rodriguez (2012), an additional uncertainty of one precessional cycle (21.8 kyr) for the correlation.

Comparison of our results with the Gubbio area and Site 762C further reinforces diachronism as a major feature of the upper Campanian–Maastrichtian interval (Table 2). Of the 13 bio-horizons in common between Zumaia/Sopelana and the Gubbio area, 9 of them point to much younger ages in the Basque country (Table 2). These discrepancies are much above the given ranges of uncertainties and in some cases account for up to 3.6 Myr (FO of *Planoglobulina acervulinoides*). With respect to the key planktic foraminifer and nannofossil biostratigraphic markers used for biozonation, discrepancies between the Basque country and the Gubbio area vary between a reasonable amount of 136 kyr (FO of *Lithraphidites quadratus*) and ca 1.5 Myr for the FOs of *Racemiguembelina fructicosa* and *Micula murus* (Table 2). Discrepancies between the Basque country and the Indian Ocean are generally even more pronounced (Table 2). Although correlation between Sopelana and Zumaia is imprecise below 145 m, it is possible to propose a linear estimation for the age of the LO of *Eiffelithus eximius* documented by Pérez-Rodriguez et al. (2012). This estimate points to the largest discrepancy with a very late age of 70.55±0.05 Ma for the Basque country as compared to 73.90±0.05 in the Indian Ocean and 75.60±0.40 in the Gubbio area (Table 2). However, this stratigraphic interval is turbiditic at Zumaia so these specimens of *E. eximius* may be reworked. Overall, the observed diachronism may result from different sources of error. Different taxonomic concepts and the existence of intermediate evolutionary forms

in planktonic foraminifers can be, for instance, invoked to explain discrepant ages for the FOs of *Abathomphalus mayaroensis*, *Racemiguembelina fructicosa* and *Contusotruncana contusa* between Pérez-Rodriguez et al. (2012) and our study of the Zumaia and Sopelana sections (Table 2). In this study, such a source of error accounts for less than 500 kyr. Taxonomy is much less problematic for the key nannofossil biostratigraphic markers and is unlikely to account for the observed discrepancy. However, preservation might also play a role, especially for the calcareous nannofossil bio-horizons at Zumaia and Sopelana because the assemblage is generally poorly to very poorly preserved. Nevertheless, it is likely that these discrepancies are partly the result of true migration patterns across latitudes and different oceanic basins, controlled by the high climate variability of the late Campanian–Maastrichtian interval. Strongly diachronic succession and ages of late Campanian–Maastrichtian calcareous plankton bio-horizons have already been interpreted as the expression of climatically induced migration patterns between Tethyan, Transitional and Austral provinces (Huber and Watkins 1992; Nifuku et al. 2009; Thibault et al. 2010; Thibault et al. 2012b). This potential mechanism must be acknowledged, thoroughly assessed and quantified in the Late Cretaceous because many studies use calcareous plankton biochronology to build their age-models.

6.2 Magnetostratigraphy

The upper part of the lower Maastrichtian interval of the Sopelana section has reversed polarity. The magnetic reversal boundary C31r/C31n has been reliably detected slightly higher in the stratigraphy in cycles 152/153 at Zumaia ((Batenburg et al., 2012/Chapter 2; Pérez-Rodríguez et al., 2012). In the lowermost part of the section, normal polarity can be reliably detected, with uncertain polarity from cycles 247 to 249. The whole section was studied previously by Mary et al. (1991), who found reverse polarity until 59 m downwards from the C31r/n boundary, which would correspond approximately to a depth of 181 m, around cycle 245. The samples from the limestones of cycles 247 and 248 may represent reverse polarity, and the reversal is interpreted to be within cycles 248-249, although the exact

position could be slightly higher in the stratigraphy. The reversal has been assigned an age of 71.22 +/- 0.09 Ma (table 2), the uncertainty being based on the uncertainty in the stratigraphic position, in the cyclostratigraphic interpretation, and in the astronomical target curve.

The normal polarity in the lowermost part of the section likely represents C32n1n, the short normal polarity interval above the main normal polarity subchron C32n2n, which near its top contains the Campanian/Maastrichtian boundary.
The magnetostratigraphy from Zumaia and Sopelana compares well to the recently published chronologies of Husson et al. (2011) and Thibault et al. (2012b) (Figs. 5, 7 and Table 3). The base of C29r, which was obtained by correlation with Westerhold et al. (2008), at 66.31 ± 0.09 Ma, falls between the ages from these studies, at 66.3 ± 0.07 and 66.376 Ma, respectively. The total amount of time between the K/Pg boundary and the C31n/C31r reversal as reported by Husson et al. (2011) and Batenburg et al. (2012)/Chapter 2 is identical at 3.22 Myr. The position of C31n/C31r is in the middle of the stratigraphic range established by Pérez-Rodriguez et al. (2012). The total amount of time between the K/Pg boundary and the reversal C31r/C32n1n at Zumaia and Sopelana of 5.26 Myr is slightly less than the 5.4 Myr reported by Husson et al. (2011). The orbital estimate for this time-span by Husson et al. (2011), is based mostly on the grey level variations in Hole 762C, which show a strong presence of the 405-kyr period of eccentricity. However, obliquity cycle variability in the 405-kyr cycle spanning the C31r/C32n1n transition, cycle $Ma_{405}14$, seems to obscure the influence of the 100-kyr cycle of eccentricity (Husson et al., 2011), and there is a small uncertainty in the exact stratigraphic position of this transition. These factors may have contributed to a slightly longer estimate of the duration of Chron C31r by Husson et al. (2011)(Fig. 5).

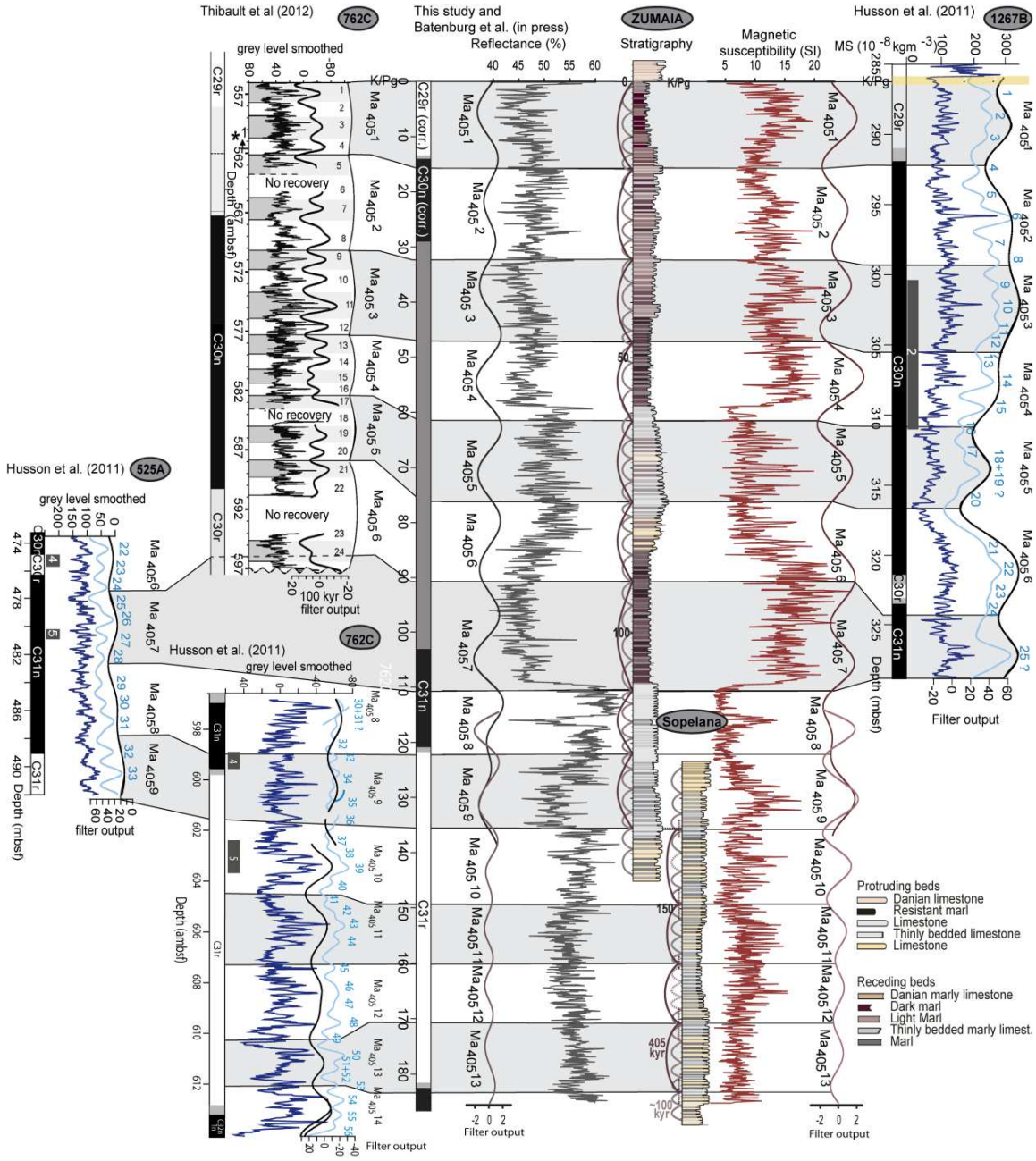

Figure 5: Comparison of Maastrichtian astrochronologies, with grey bands indicating the identified 405-kyr cycles, numbered $Ma_{405}1$, $Ma_{405}2$, ... , from the K/Pg boundary downwards, following Husson et al. (2011). From left to right the cyclostratigraphic interpretation of Husson et al. (2011) of the grey level data of Hole 525A and Hole 762C, with their ~100 kyr and 405 kyr band-pass filters; the cyclostratigraphic framework of Thibault et al. (2012b) of the grey level data of Hole

762C; the magnetostratigraphy, 16 and 12 m band-pass filters (bandwidths 12-29 and 8.5-20 m) of reflectance, the reflectance data, the stratigraphic column, the magnetic susceptibility data and the 17 and 12 m band-pass filters of magnetic susceptibility (bandwidths of 12-24 and 8.8-19m) of Zumaia and Sopelana (this study and Batenburg et al., 2012/Chapter 2); the cyclostratigraphic interpretation of the magnetic susceptibility data of Hole 1267B by Husson et al. (2011).

	Batenburg et al. (2012)	Pérez-Rodriguez et al. (2012)	This study	Thibault et al. (2012b)	Husson et al. (2011)	Cande & Kent (1995)	Herbert (1995[1], 1999)
	Zumaia	**Zumaia**	**Sopelana**	**ODP Hole 762C**	**ODP 1267B, 762C, DSDP 525A**	**Magnetic anomaly profiles**	**DSDP 357, 516F, 525A, 527-529**
K/Pg boundary	65.97 ± 0.02	65.97 ± 0.02	65.97 ± 0.02	66	66 ± 0.07	65	65.97[2]
Mag.strat.							
C29r/C30n	66.31 ± 0.09			66.376	66.3 ± 0.07	65.578	66.347 ± 21[1]
C30n/C30r				68.165	68.2 ± 0.07	67.61	68.047
C30r/C31n				68.338*	68.32 ± 0.07	67.735	68.152
C31n/C31r	69.19 ± 0.08	69.22 ± 0.21			69.22 ± 0.07	68.737	69.077
C31r/C32n1n			71.22 ± 0.09		71.4 ± 0.08	71.071	

Table 3: Comparison of Maastrichtian magnetostratigraphies. [1] Age of C29r/C30n from Herbert (1995), other boundaries from Herbert et al. (1999); [2] A K/Pg boundary age of 65.97 Ma was assigned for comparison.

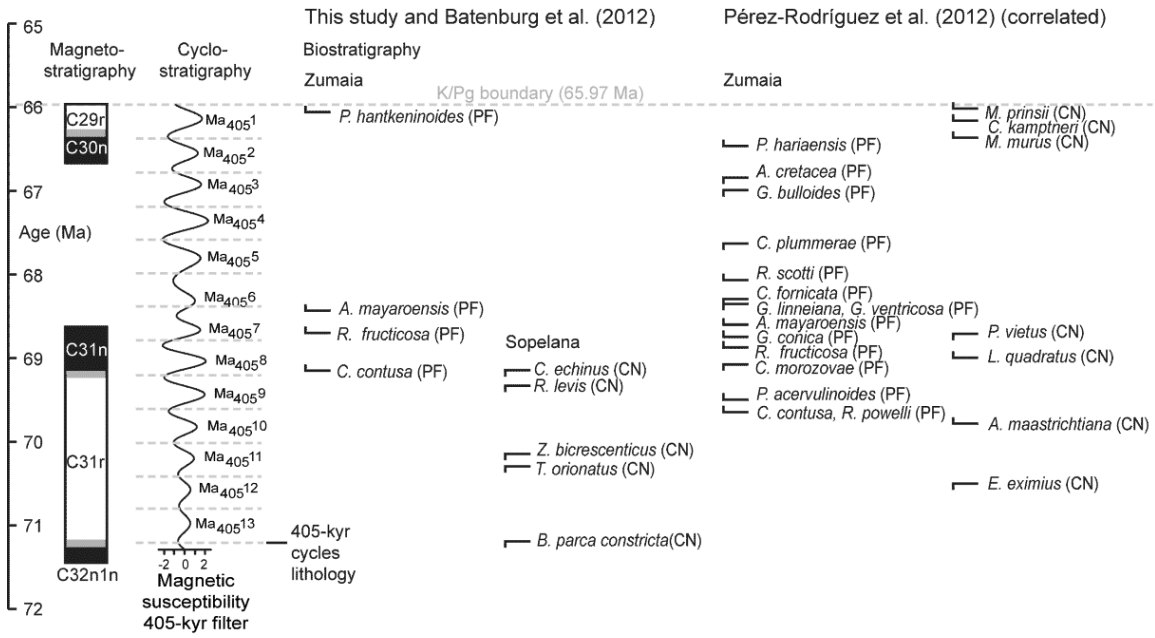

Figure 6: Cyclostratigraphy and tuned ages of biostratigraphic and magnetostratigraphic events, as obtained in this study, Batenburg et al. (2012)/Chapter 2 and by correlation with Pérez-Rodriguez et al. (2012).

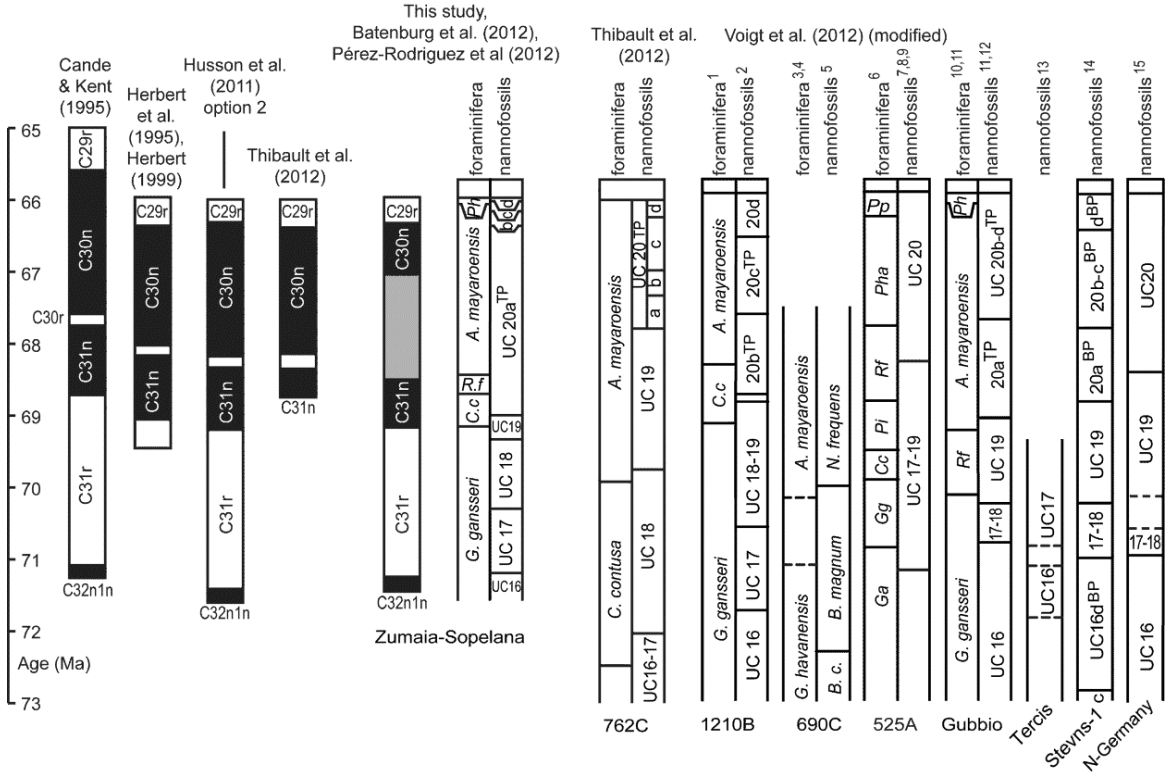

Figure 7: Maastrichtian time scales with magneto-, bio- and chemostratigraphic events according to Cande and Kent (1995), Herbert et al. (1995), Herbert (1999), option 2 of Husson et al. (2011), Thibault et al. (2012b), Batenburg et al. (2012)/Chapter 2, Pérez-Rodríguez et al. (2012), and the summary of biozones based on correlation of carbon isotope stratigraphies by Voigt et al. (2012), with [1]Bralower et al. (2002); [2]Lees and Bown (2005); [3]Huber (1990); [4]Huber (1992); [5]Pospichal and Wise (1990); [6]Li and Keller (1998); [7]Manivit (1984); [8]Henriksson (1993); [9]Thibault and Gardin (2007); [10]Premoli-Silva and Sliter (1995); [11]Gardin et al. (2012); [12]Monechi and Thierstein (1985); [13]Gardin et al. (2001); [14]Thibault et al. (2012a); [15]Burnett (1990). For Herbert et al. (1995) and Herbert (1999), who only report durations, a K/Pg-boundary age of 65.97 Ma has been assigned for comparison.

6.3 Orbital pacing

The Zumaia section shows strong variability in the expression of the marls, which reflect the amplitude modulation of precession by eccentricity, likely caused by variations in clay supply by run-off (Batenburg et al., 2012/Chapter 2; Mount and Ward, 1986). An enhanced seasonal contrast (on the northern hemisphere) during precession minima at times of eccentricity maxima may have led to an intensified hydrological cycle, leading to deposition of thicker, darker marls. The Zumaia section shows a strong influence of terrigenous input, and was likely closer to the source of clastic sediment than the Sopelana section, which is corroborated by the frequent occurrence of turbidites at Zumaia, and the substantial changes in sedimentation rate. In contrast, the marls in the Sopelana section vary less in expression than at Zumaia, whereas the carbonates vary more strongly in thickness and degree of weathering, displaying the combined influence of variations in productivity and clay input (dilution). As the marls correspond to precessional minima, it is logical to assume that limestones reflect precession maxima. The increased productivity may be due either to an increased input from nutrients through the enhanced hydrological cycle during the preceding precession

minimum, or to an input of nutrients from eolian dust during periods of a weakened hydrological cycle during precession maxima. Whereas the phase relationship with eccentricity is clear, the phase relation with precession and the proposed climatic mechanism underlying the rhythmic sedimentation requires further testing, for instance through elemental analysis and climate modelling of orbital extremes, using Late Cretaceous boundary conditions. The records are dominated by eccentricity-modulated precession and do not display an evident expression of ~41 kyr obliquity, indicating that regional climate was controlled by lower latitude insolation.

A potential influence of a 1.2 Myr cycle can be observed in the upper Maastrichtian of Zumaia and Sopelana, with strong shifts in lithologies from predominantly carbonates to predominantly marls. These shifts, at a ~50 m scale, or approximately 60 cycles apart (counting cycles marked with “a” and “b”), are likely due to changes in relative sea level (Batenburg et al., 2012/Chapter 2). In the lower Maastrichtian of Sopelana, no such shift in lithology can be observed. In cycle 191, which is 60 cycles below the lowermost shift in Zumaia in cycle 132 (counting cycles marked with “a” and “b”), the overall clay and carbonate content of the limestone-marl alternations does not change noticeably. However, the potential influence of a longer-term periodicity might be reflected in the varying strength of the ~100-kyr periodicity through the Sopelana section. A reduced amplitude of the ~100- kyr cycle can be observed in the interval from cycle 212 to 224, ~90 cycles below the lowermost shift in Zumaia. This could be the expression of a long-term eccentricity minimum as the expression of the 100-kyr cycle is minimal in such a minimum because the different ~100-kyr eccentricity components cancel each other out. If the potential 1.2 Myr cyclicity is indeed present throughout the succession, the weakening of the ~100-kyr cycle occurs in the opposite phase of the 1.2 Myr cyclicity as compared to the lithological shifts in the Zumaia section (Batenburg et al., 2012/Chapter 2). Unfortunately, comparison of the expression of this very long period eccentricity cycle with the La2011 eccentricity is not possible as this cycle is not reliable in the solution further back in time than ~54 Ma (Westerhold et al., 2012).

7. Conclusions

In summary, the astronomically tuned time-scale for Zumaia and Sopelana is in good agreement with previously published astronomic time-scales by Herbert (1999), Husson et al. (2011) and Thibault et al. (2012b). Minor refinements include a slightly younger and more tightly constrained age for the C31r/C32n1n chron boundary compared to the astronomically tuned age suggested by Husson et al. (2011), which is used in The Geologic Time Scale 2012 (Ogg and Hinnov, 2012). The astronomical tunings demonstrate that, while the reported durations of magnetostratigraphic chrons are consistent, several biostratigraphic events are not coeval on a global scale, which may be due to true diachroneity, or alternatively to migration patterns and/or misidentification and/or preservational factors. This emphasises the importance of establishing integrated stratigraphies with independent constraints on correlation, which can successfully be achieved by carbon isotope stratigraphy and magnetostratigraphy. The close agreement between astronomical tunings is a confirmation that the Maastrichtian time-scale is now consistent and stable. However, to securely anchor the Mesozoic time-scale further intercalibration with radiometric dating techniques is required to solve the problem of the age of the K/Pg boundary.

Appendix B. Supplementary information Chapter 2

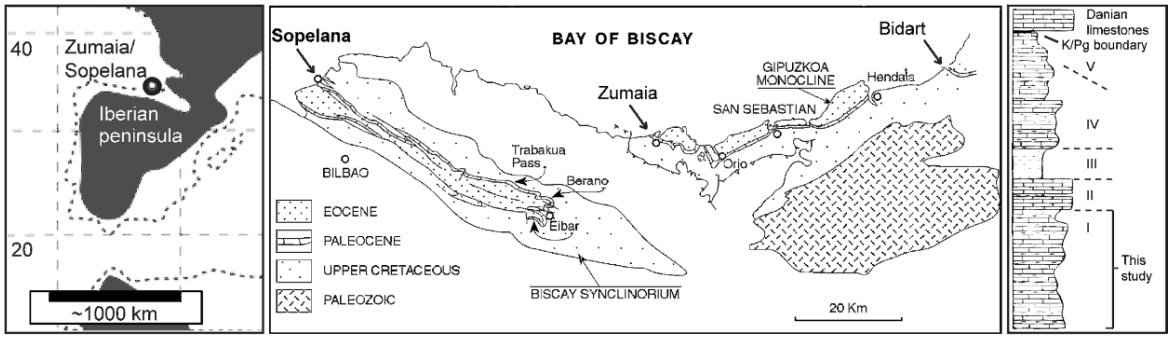

Supplementary figure 1: Paleogeographic setting (Gómez –Alday et al., 2008), simplified geologic map of the study area, from Pujalte et al. (1998) and schematic stratigraphic log from Ward et al. (1991).

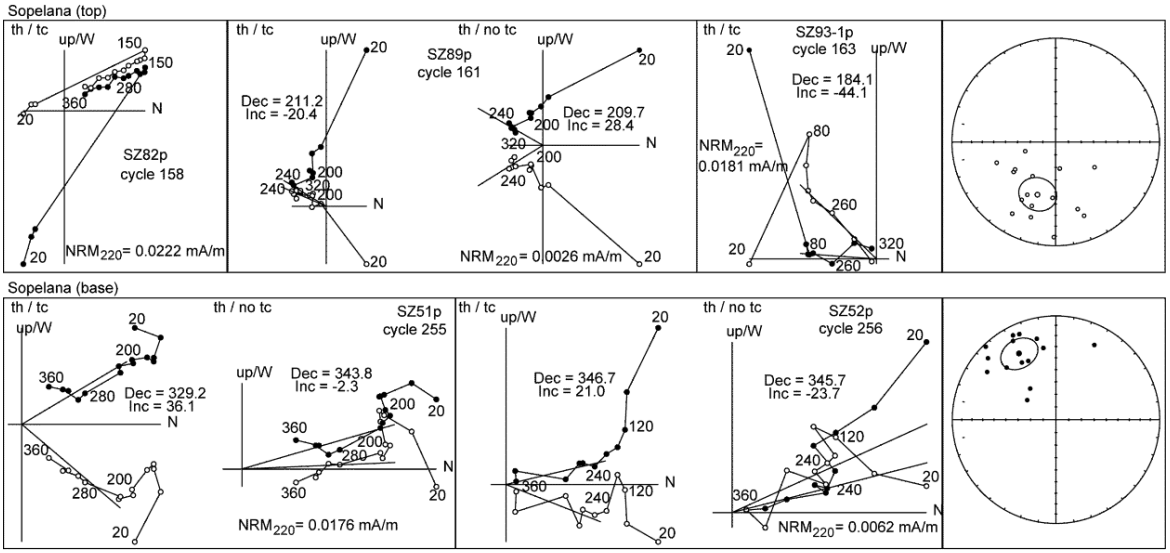

Supplementary Figure 2: Examples of Zijderveld diagrams and equal area projections for the paleomagnetic results of the Sopelana section.

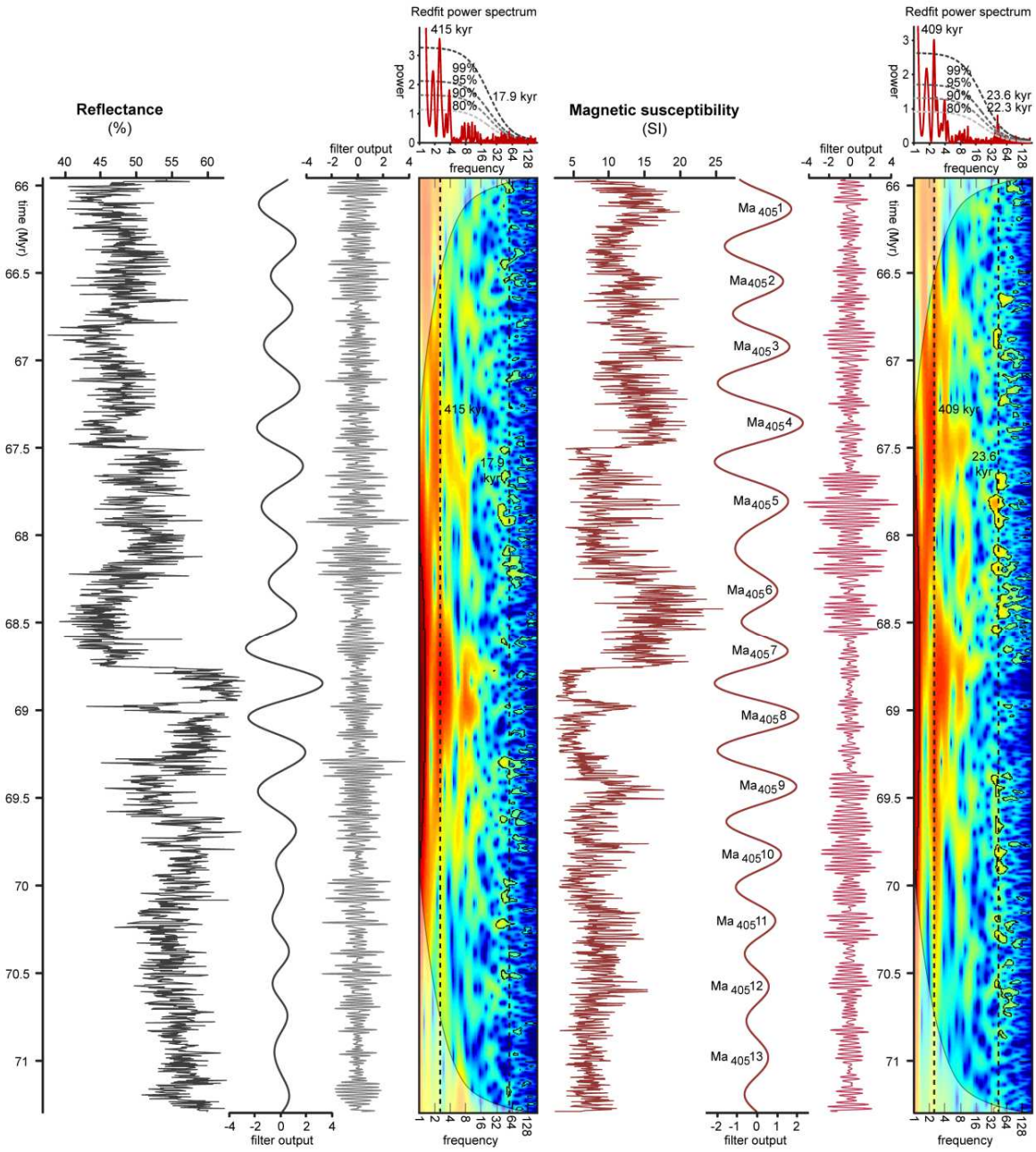

Supplementary figure 3: The reflectance (L*) and magnetic susceptibility (MS) data series in the time domain, with their 415, 17.9, 409 and 23.6 kyr band-pass filters (in dark grey, light grey, dark red and pink, with band-widths of 311-621, 13.4-27.2, 308-609, 17.8-35.3 kyr, respectively), wavelet analyses and Redfit spectra. The 405 eccentricity cycles (black Ma405no.s) follow the nomenclature of Husson et al. (2011).

Chapter 4. Orbitally tuned carbon isotope stratigraphy for the Maastrichtian from Zumaia and Sopelana (Basque Country, N-Spain) – new insights from global correlation

In collaboration with: Silke Voigt, Nicolas Thibault, Mario Sprovieri, Andy Gale, Frits Hilgen

Abstract

An orbitally tuned bulk carbonate carbon isotope curve is presented from the Maastrichtian Zumaia and Sopelana sections in the Basque country, N-Spain, with a high resolution and a remarkable amplitude of variation. Strong oscillations in $\delta^{13}C$ seem regularly paced by the 405-kyr periodicity of eccentricity modulated precession. Additionally, sharp negative shifts associated with falls in sea-level occur at regular intervals of ~1.2 Myr. We present a new global correlation of carbon isotope stratigraphies with an astronomically tuned age model based on the cyclostratigraphy of Zumaia and Sopelana and site 762C (Exmouth Plateau). The exclusion of short magnetic polarity chrons from the age model greatly reduces variations in sedimentation rates. The Late Campanian/Maastrichtian carbon isotope correlation scheme allows for a detailed comparison of different paleo-environmental settings. Although the carbon isotope curves display distinctly different values and intensities of variations, a series of trends and excursions can be observed across the different depositional settings. Notably, the mid-Maastrichtian event is expressed in most records as two positive peaks with maximal $\delta^{13}C$ values in the Maastrichtian, separated by a pronounced negative excursion, and displaying oscillations on a 405-kyr scale. We propose that the 405-kyr cycle of eccentricity, and potentially longer periodicities, paced the latest Cretaceous carbon cycle.

1. Introduction

Increasingly, carbon isotopes are being used to correlate and date Late Cretaceous successions, and to understand paleoclimatic trends. Carbon isotope stratigraphies are being generated for the late Campanian and Maastrichtian, and used as a reliable correlation tool (Jung et al., 2012; Thibault et al., 2012a, 2012b; Voigt et al., 2012, 2010). Such correlations are a welcome improvement of existing chronologies, as magnetostratigraphic data are only sparsely available for the Campanian and Maastrichtian, and planktonic foraminifera and calcareous nannoplankton are affected by increased provinciality due to ongoing Late Cretaceous cooling (e.g. Thibault et al., 2012b), following the extreme mid-Cretaceous greenhouse warmth (Barrera and Savin, 1999; Clarke and Jenkyns, 1999; Friedrich et al., 2012; Huber et al., 1995; Jenkyns et al., 1994). The gradual cooling was punctuated by a distinct cooling event during the Campanian-Maastrichtian transition (Barrera et al., 1997; Li and Keller, 1998) and periods of intermittent warming (Bralower et al., 2002; Frank and Arthur, 1999; Li and Keller, 1998; Sheldon et al., 2010). To understand the impact of climatic variations on the carbon cycle in the latest Cretaceous, carbon isotope records from different oceanographic settings need to be compared and tied to the astronomically tuned time scale.

Here we present a global correlation of the recently established integrated stratigraphy of the Zumaia and Sopelana sections (Basque country, N-Spain) with new d13C data from the Sopelana section. The detailed cyclostratigraphic framework of the Basque sections provides orbitally tuned ages of calcareous nannofossil, planktonic foraminifera and magnetostratigraphic events. The high resolution and remarkable amplitude of $\delta^{13}C$ variations allows for a detailed comparison with existing carbon isotope stratigraphies.

2. Geologic setting and sections

The Zumaia and Sopelana sections in the Basque country, N-Spain, contain rhythmically bedded hemipelagic limestone-marl alternations of Late Cretaceous to Eocene age. The Zumaia section is a reference section for the Cretaceous/Paleogene (K/Pg) boundary and together, the Sopelana and Zumaia sections span most of the Maastrichtian. Low resolution carbon isotope data have been presented for the upper Maastrichtian and Danian of the Zumaia section (Margolis et al., 1987), and for an interval spanning the lower to upper Maastrichtian transition in Zumaia and Sopelana (Paul and Lamolda, 2007). After cyclostratigraphic efforts around the K/Pg boundary (Ten Kate and Sprenger, 1993) and in the Paleocene (Dinarès-Turell et al., 2003; Kuiper et al., 2008), a cyclostratigraphic framework for the Maastrichtian at Zumaia was obtained recently, with tuned ages for bio- and magnetostratigraphic events (Batenburg et al., 2012/Chapter 2). The astronomical tuning is being extended downwards with new calcareous nannofossil and magnetostratigraphic data from the Sopelana section (Chapter 3). Additional biostratigraphic data for the Zumaia section were obtained from Pérez-Rodríguez et al. (2012).

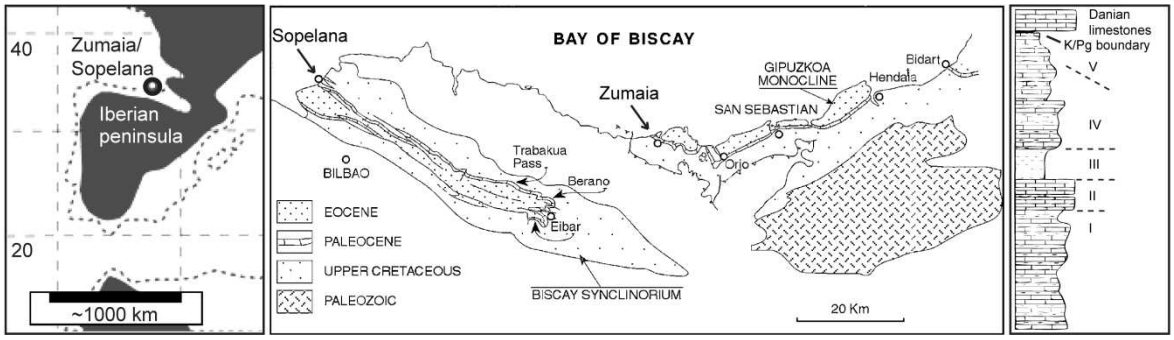

Figure 1: Paleogeographic setting (Gómez –Alday et al., 2008), geological map (Pujalte et al., 1998) and schematised stratigraphy after Ward et al (1991).

3. Methodology

For bulk carbonate stable carbon isotope analyses, two samples were selected per couplet, one from the carbonate-rich, and one from the marly part of the cycle, in Zumaia and Sopelana. Additional samples were selected in a resolution of approximately eight samples per cycle for selected intervals of the two sections; between 0 and 6 m, and between 15.5 and 25.7 m in the upper part of the Zumaia section, and in the lower part of the Sopelana section between 174 and 180.8 m. From the samples, a small amount of powder was obtained with a small handheld 2 mm drill for most samples and for the selected intervals with a micro-mill. The powders were heated to 400°C to remove organic components. Analyses were performed in the geochemistry laboratory at the IAMC-CNR (Naples, Italy) with an automated continuous flow carbonate preparation GasBenchII device and a ThermoElectron Delta Plus XP mass spectrometer. Acidification of samples was performed at 50°C. Samples were calibrated to Vienna Pee Belemnite using an internal standard (Carrara Marble with $\delta^{13}C$ = 2.43 ‰VPDB) and NBS19. The precision/repeatability of $\delta^{13}C$ measurements was estimated to be better than 0.14 ‰. All isotope data are reported in per mil (‰) relative to the VPDB standard. Measurements with extremely negative values for $\delta^{13}C$ were repeated. Five outliers from the Zumaia record outside a 9-point moving average ±2σ were excluded.
To identify potential periodicities in the datasets, time series analyses were applied in with the programme Redfit, which is particularly applicable to unevenly-spaced data-sets (Schulz and Mudelsee, 2002). Also, a script for wavelet analysis (Grinsted et al., 2004) was applied in the programme Matlab to examine the datasets, as well as a band-pass filter in the programme AnalySeries (Paillard et al., 1996).

4. Results

A cross-plot of all carbon and oxygen isotope values does not seem to show significant trends or differences amongst the Danian and Maastrichtian data from Zumaia or amongst the Maastrichtian data from Zumaia and Sopelana (Fig 3.). However, cross-plots of the separate intervals may indicate a slight degree of co-variance, particularly for the Danian interval. The carbon isotope curve of the Zumaia and Sopelana sections shows an overall decline through the Maastrichtian, with maximum values of 2.2 ‰ around 120m, and minimal values around 0.2 ‰ below the k/Pg boundary (Fig. 4). The record displays marked variability on two depth scales. The lower half of the curve is dominated by a very long variation on a scale of approximately 43m, and the upper half of the curve is strongly dominated by a variability on a scale of ~17 m. Values can vary by as much as one permil over a 43 or a 16 m cycle. The presence of these periodicities is confirmed by the Redfit and wavelet analyses.

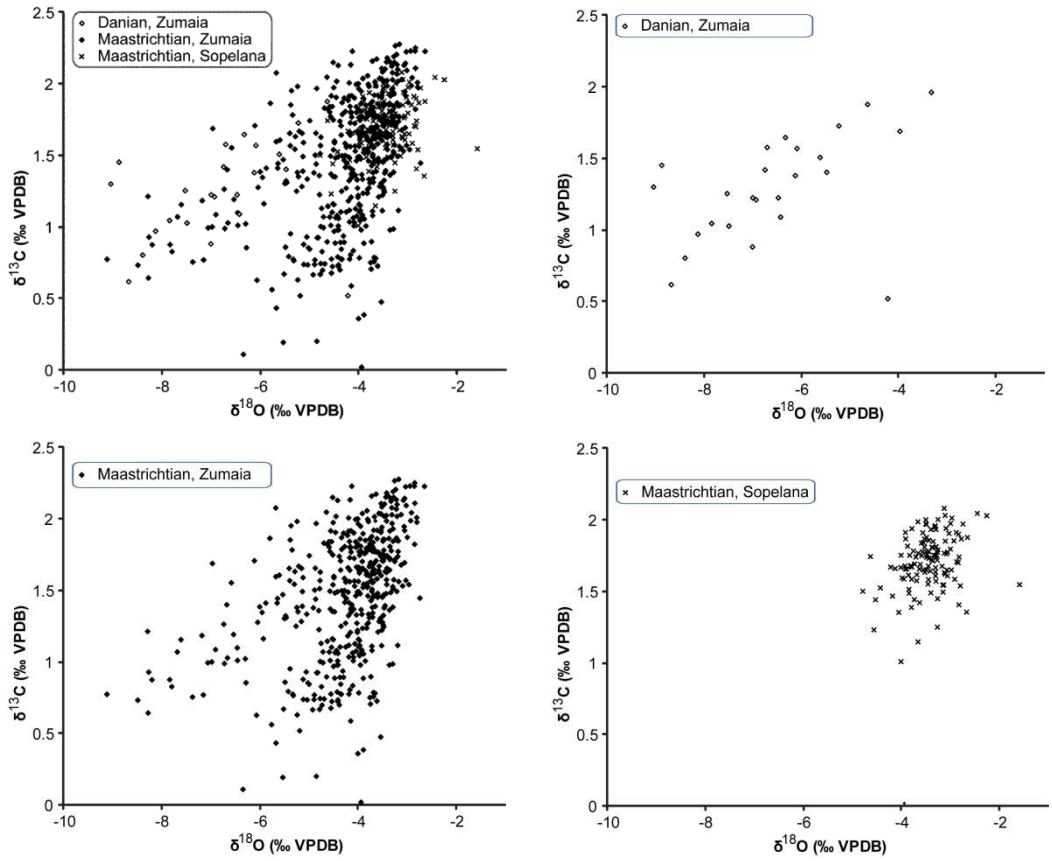

Figure 2: Cross-plots of bulk carbonate carbon and oxygen isotope data of the lowermost Danian and the Maastrichtian of Zumaia and Sopelana.

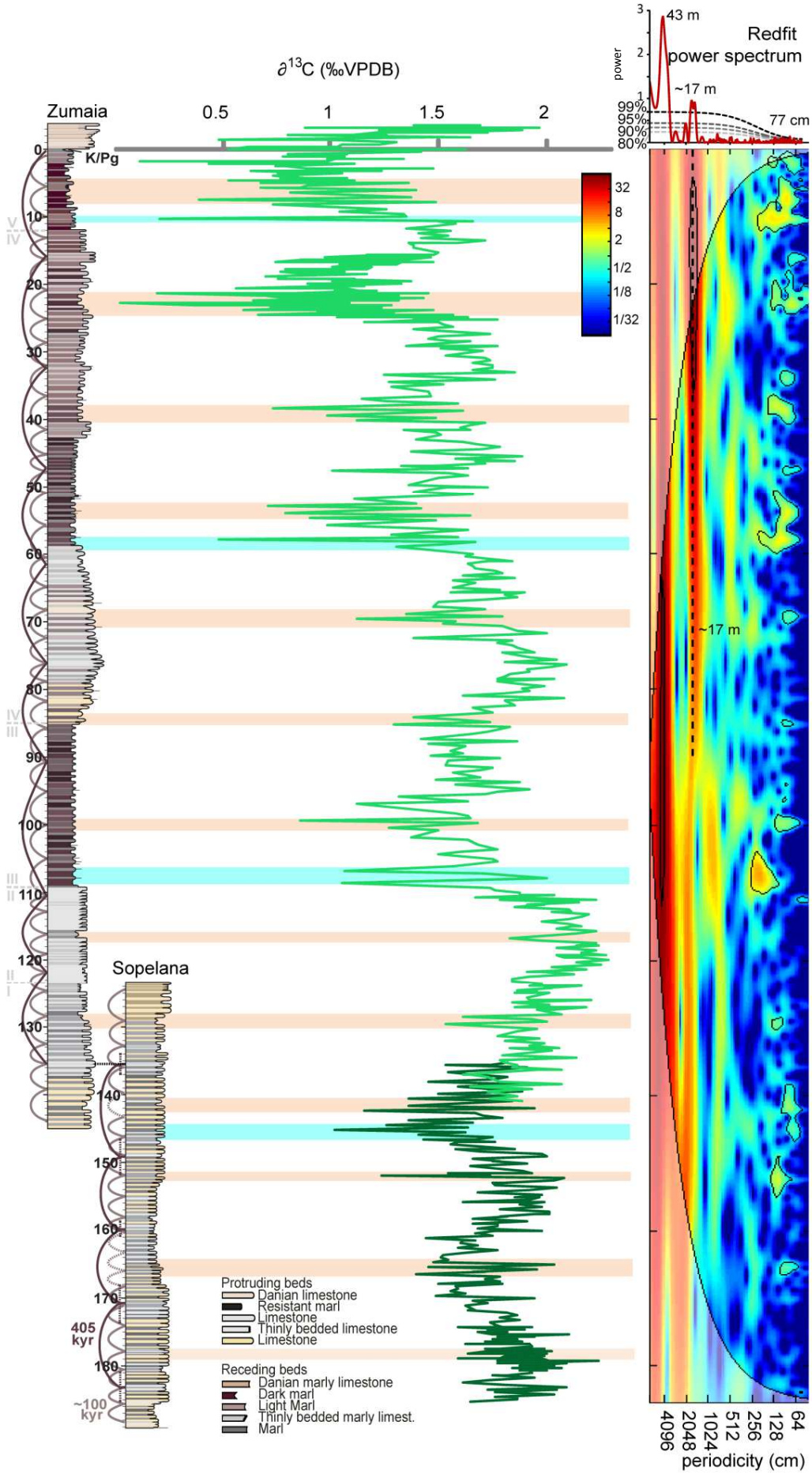
Redfit
power spectrum
43 m
~17 m
77 cm
power
99%
95%
90%
80%
∂13C (‰VPDB)
0.5
1
1.5
2
Zumaia
K/Pg
32
8
2
1/2
1/8
1/32
~17 m
Sopelana
405 kyr
~100 kyr
Protruding beds
Danian limestone
Resistant marl
Limestone
Thinly bedded limestone
Limestone
Receding beds
Danian marly limestone
Dark marl
Light Marl
Thinly bedded marly limest.
Marl
4096
2048
1024
512
256
128
64
periodicity (cm)

Figure 3: Carbon isotope values of the Maastrichtian and lowermost Danian part of the Zumaia and Sopelana sections, with logged limestone marl couplets and cyclostratigraphic interpretation to the left, and Redfit power spectrum and the outcome of wavelet analysis on the right. Pink bands indicate the minima in $\delta^{13}C$ at a regular pacing of ~17m in Zumaia and ~10 m at Sopelana. Blue bands indicate negative shifts in $\delta^{13}C$, which are coincident with lithological shifts in the Zumaia section.

The data were plotted on the age model of Batenburg et al. (2012)/Chapter 2 and Chapter 3, which is based on orbital tuning of the lithological variations in Zumaia and Sopelana to the La2011 solution (Fig 4.). A periodicity around 1.1 Myr is present throughout the record, in the wavelet diagram, and a periodicity around 420 kyr mostly in the upper two thirds of the record. A band-pass filter centred at 405 kyr (bandwidth 333 to 623 kyr) allows for comparison with the filtered 405-kyr periodicity from the magnetic susceptibility record (in black).

Figure 4 (next page): Magnetostratigraphy, planktonic foraminifera biostratigraphy, calcareous nannoplankton biostratigraphy and carbon isotope stratigraphy from the Zumaia and Sopelana sections in the time domain. The age model is based on the astronomical tuning of the lithology and the geophysical data records (Batenburg et al., 2012/Chapter 2; Chapter 3), of which the band-pass filtered 405-kyr component of magnetic susceptibility is displayed in black. Blue dashed lines indicate the levels of negative shifts on a 1.2 Myr scale, the green line shows the extracted 405-kyr component of the carbon isotope record (bandwidth 333 to 623 kyr). Black Ma_{405} numbers indicate the number of 405-kyr cycles from the K/Pg boundary downwards, following Husson et al. (2011). The Redfit power spectrum and wavelet analysis of the combined carbon isotope data of the Zumaia and Sopelana sections are displayed on the right.

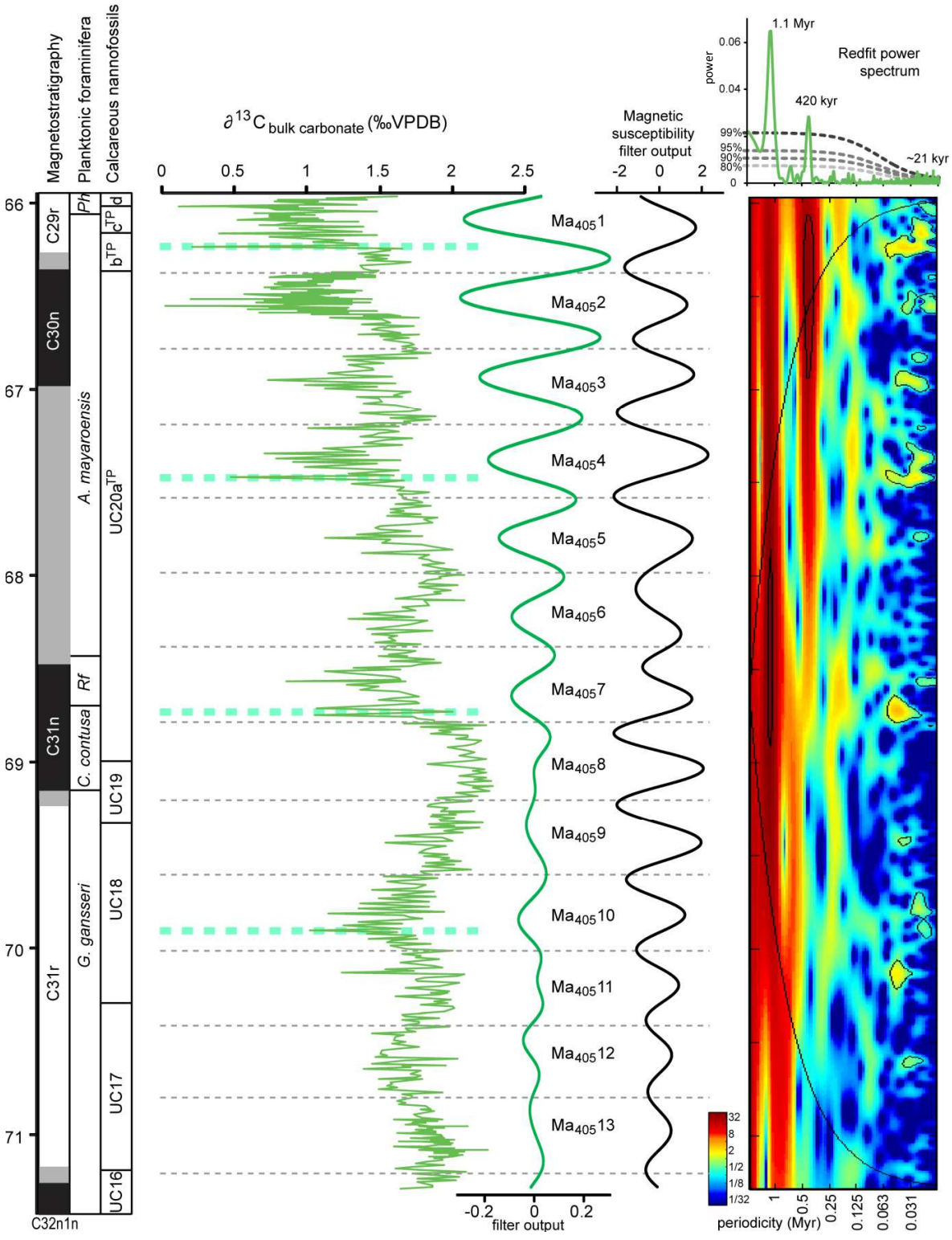

Figure 4 (for caption see previous page)

5 Correlation

5.1 Late Campanian/Maastrichtian carbon isotope correlation

The carbon isotope profile of the Zumaia and Sopelana sections is correlated to the carbon isotope data of ten Campanian-Maastrichtian successions, following recent correlation efforts by Voigt et al. (2012) and Thibault et al. (2012b). Voigt et al. (2012) presented a detailed and extensive correlation of carbon isotope stratigraphies of Maastrichtian and Late Campanian successions, which has been largely followed here. To avoid large changes in sedimentation rate and discrepancies in magnetostratigraphic datum levels, we have applied less tie-points for correlation (Table 1) and construction of the age-model. The correlation to the Zumaia-Sopelana curve provides a detailed and accurate age-model for the Maastrichtian. For the Late Campanian, and the Campanian-Maastrichtian boundary interval, ages form the astronomical tuning of Husson et al. (2011) were applied, following the approach of Thibault et al (2012b).

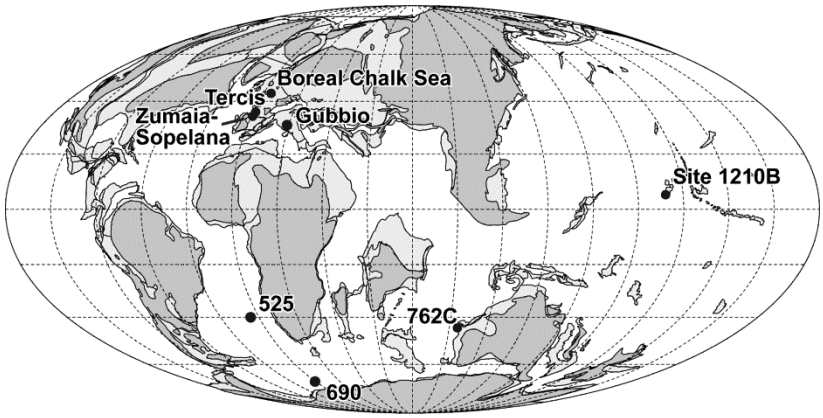

Figure 5: Paleogeographic map of the early Maastrichtian (70 Ma) with the localities used in this study (after Hay et al., 1999).

5.2 Correlated sections

Trunch borehole and Norfolk coast

A Cenomanian-Lowermost Maastrichtian high resolution carbon and oxygen isotope stratigraphy was obtained from the Trunch borehole in north-eastern Norfolk (Jarvis et al., 2006, 2002). The existing carbon isotope stratigraphy of the nearby Norfolk coast cliffs by Jenkyns et al. (Jenkyns et al., 1994) was recently improved and included in a global correlation scheme by Voigt et al. (2012). Belemnites from the Norfolk coast were studied by Schultz (1979), and calcareous nannofossils from the Trunch borehole were reported by Burnett (1990) and updated by Voigt et al. (2012) to reflect the zonation of Burnett et al. (1998).

Stevns-1

The Stevns-1 core, drilled off the coastal cliff of Stevns Klimt in Denmark, spans 450 m of chalk from the Upper Campanian to the lower Danian (Stemmerik et al., 2006). Very high resolution carbon isotope data of bulk carbonate were obtained by Schovsbo et al. (2008) and Thibault et al. (2012a), and included in the global correlation scheme of Voigt et al. (2012). The core was studied for nannofossil biostratigraphy by Sheldon et al. (2008), and Thibault et al. (2012a).

Tercis

An abandoned quarry at Tercis les Bains in south west France, has been proposed as the Global Stratotype Section and Point (GSSP) of the Campanian-Maastrichtian stage boundary (Odin and Lamaurelle, 2001; Odin, 2001) and was ratified in 2002, defined as the arithmetic mean of nine biostratigraphic datum levels. A high resolution bulk carbonate carbon isotope stratigraphy is presented by Voigt et al. (2012), which allows for worldwide correlation of the base of the Maastrichtian stage. Following Voigt et al. (2012), the ammonite stratigraphy was provided by Küchler and Odin (2001), the inoceramid data by Walaszczyk (2002) and the calcareous nannofossil data by Gardin et al, (2001).

N-Germany

The Lägerdorf-Kronsmoor and Hemmoor sections in northern Germany together span the Coniacian to Maastrichtian and form the reference sections for the German white chalk. The Maastrichtian bulk carbonate $\delta^{13}C$ curve of Hemmoor(Stenvall, 1997), and the Coniacian-lower Maastrichtian bulk carbonate carbon isotope stratigraphy of Lägerdorf-Kronsmoor (Voigt and Schönfeld, 2010) provide a near-continuous record of the last 20 Myr of Cretaceous boreal chalk deposition. Calcareous nannofossil data from Burnett (1990) and macrofossils from Schulz et al. (1984) were assembled in the correlation scheme of Voigt et al. (2012).

1210B

An upper Campanian-Maastrichtian high-resolution bulk carbonate carbon-isotope record was obtained from ODP Hole 1210B on Shatsky Rise, in the tropical Pacific (Jung et al., 2012). The distinct variations allow for detailed correlation and comparison of carbon isotope records across the Campanian-Maastrichtian Boundary (Voigt et al., 2012). Planktonic foraminifera were reported by Bralower et al.(2002) and Petrizzo et al.(2011), and calcareous nannoplankton by Lees and Bown (2005).

Gubbio

The Campanian-Maastrichtian succession of the Bottaccione Gorge and along the Contessa Highway, both near Gubbio, Italy, serve as a reference section for the Tethyan Realm (Gardin et al., 2012). Detailed stratigraphic and magnetostratigraphic studies were performed at Bottaccione by Arthur and Fischer (1977), Lowrie and Alvarez (1977)and Channell et al. (1978) and at Contessa by Lowrie et al. (1982), Chauris et al. (1998) and Gardin et al (2012). Planktonic foraminifera and calcareous nannofossil data were provided by Premoli Silva and Sliter (1995), Monechi and Thierstein (1985) and Gardin et al. (2012). New bulk carbonate $\delta^{13}C$ data of both sections, and as a composite record for Gubbio, were presented by Voigt et al (2012).

525A

Maastrichtian sediments were recovered from DSDP Hole 525A on the Walvis Ridge in the South Atlantic (Moore and Rabinowitz, 1984), with a planktonic foraminifera biostratigraphy by Li and Keller (1998), calcareous nannoplankton data from Manivit (1984), Henriksson (1993) and Thibault and Gardin (2007), and paleomagnetic data from Chave (1984). Carbon isotope data from benthic foraminifera are provided by Li and Keller (1998) and Friedrich et al. (2009).

690C

For the Upper Campanian-Maastrichtian sediments from ODP Hole 690C on Maud Rise in the Weddell Sea (Barker et al., 1990), planktonic foraminfera and calcareous nannoplankton stratigraphies were provided by Barrera and Huber (1990), Huber (1990) and Pospichal and Wise (1990), and magnetostratigraphy by Hamilton (1990). A high resolution carbon isotope stratigraphy was established by Friedrich et al. (2009).

762C

DSDP Hole 762C was incorporated in the astronomical tuning of the Maastrichtian by Husson et al. (2011), who refined the original magnetostratigraphy from Galbrun (1992).Recently, the astronomical tuning of 762C was extended and a $\delta^{13}C$ curve was presented by Thibault et al. (2012b), who correlated it worldwide. This curve was not correlated with tie-points, but plotted on its own age scale based on astronomical tuning by Husson et al. (2011) and Thibault et al. (2012b). A calcareous nannofossil zonation was established by Bralower and Siesser (1992), and refined by Thibault et al. (2012b), and planktonic foraminifera were studied by Wonders (1992) and Zepeda (1998).

Tie-points	
1	K/Pg boundary
2	Prominent $\delta^{13}C$ minimum close to the base of C29r (tie-point 2 in Voigt et al., 2012)
3	Negative $\delta^{13}C$ -excursion within C30n, bounded by maxima of Maastrichtian $\delta^{13}C$ values
4	$\delta^{13}C$ minimum within C31r, inflection to long-term Maastrichtian $\delta^{13}C$ rise (tie-point 6 in Voigt et al., 2012)
5	base of $\delta^{13}C$ maximum near the base of C31r (tie-point 7 in Voigt et al., 2012)
6	$\delta^{13}C$ minimum near the top of C32n2n (tie-point 8 in Voigt et al., 2012)
7	$\delta^{13}C$ maximum in C32n2n
8	$\delta^{13}C$ minimum in C32r1r (tie-point 10 in Voigt et al., 2012)
9	top of pronounced $\delta^{13}C$ minimum in C33n (tie-point 11 in Voigt et al., 2012)
10	base of $\delta^{13}C$ minimum in C33n (tie-point 12 in Voigt et al., 2012)

Table 1: Description of the tie-points used for carbon isotope correlation

5.3 Age model

The age model for the correlation of the data records to the Zumaia-Sopelana record is based on the ages of tie-points 1 to 5, as obtained from orbital tuning of the lithological and geophysical data of the Basque sections to the La2011 astronomical target curve (Batenburg et al., 2012/ Chapter 2; Chapter 3; Laskar et al., 2011b). Below the level of tie-point 5, the data records were correlated to the Gubbio composite curve as presented by Voigt et al. (2012), with ages for selected magnetic reversals, C32n2n/C32n1r, C32r1r/C32n2n, C32r2r/C32r1n, C33n/C32r2r, as determined by Husson et al. (2011). For this interval, ages were obtained by astronomical tuning of geophysical data from ODP hole 762C (Exmouth Plateau, Indian Ocean), for which new $\delta^{13}C$ data, an extended astronomical tuning and a global correlation were recently presented by Thibault et al. (2012b).

The duration between the base of C29r and the Cretaceous/Paleogene boundary of 0.34 ± 0.09 Myr at Zumaia, as obtained through correlation with IODP Sites 1262 and 1267 (Westerhold et al., 2008), is in good agreement with the duration of 0.3 ± 0.02 Myr obtained by astronomical tuning of IODP Hole 1267B by Husson et al (2011) and the duration of 0.397 ± 0.22 Myr by tuning of ODP Hole 762C (Thibault

et al., 2012b). Also, the duration between C31r/C31n and the K/Pg boundary is in good agreement between Zumaia-Sopelana, at 3.22 Myr, and the tuning of Husson et al. (2011), with a duration of 3.22 Myr, based on geophysical data of IODP Hole 1267B and DSDP Hole 525A.

However, there are discrepancies in the ages and positions of several magnetic reversals amongst sites. C30r was not reliably identified at Zumaia (Batenburg et al., 2012/Chapter 2) and appears much higher in the stratigraphy at the Bottaccione and Contessa sections, of which the composite, Gubbio, is considered a reference section for the Tethyan realm (Gardin et al., 2012). The base of C31r is found to be slightly younger, at 71.22 Ma, in the astronomical tuning of Zumaia and Sopelana (Chapter 3) than in the tuning of Husson et al (2011), at 71.4 Ma. Also, the ratio of the thickness of C32n1n and C32n1r seems different at Gubbio (Gardin et al., 2012) than at 762C (Thibault et al., 2012b), and C32r1n seems relatively thick at 762 (Thibault et al., 2012b) compared with Gubbio (Gardin et al., 2012). For this reason, these reversals were not incorporated in the age model for the tie-points used in this correlation.

5.4 Biostratigraphy

For the mid- to upper-Maastrichtian, the exclusion of Chron C30r in Gubbio from the age model, leads to changes in the length of biozones of Stevns-1, N-Germany, 525A and Gubbio as compared to Voigt et al. (2012). These changes have affected these records in similar ways, most notably by shifting ages of mid-Maastrichtian bio-events to younger values. Originally, a comparison of ages of bio-events with Zumaia and Sopelana to the compilation of Voigt et al. (2012), showed that, of the thirteen bio-events identified at Zumaia-Sopelana and Gubbio, nine were considerably younger in the Basque sections (Chapter 3). With the alternative age-model presented here, the ages of biostratigraphic events between tie-points 2 and 4 change for the correlated sections of Stevns-1, N-Germany, 1210B and Gubbio. For the Gubbio section, new calculates ages are presented in table 2. The ages indicate a slightly better agreement between Zumaia-Sopelana and Gubbio in the calcareous nannofossil and planktonic foraminifera biozonations. However, as the

age models of Stevns-1, N-Germany and 1210B change similarly, existing diachroneity between these sites remains.

For a detailed review of the biostratigraphic events in the Late Campanian and around the Campanian-Maastrichtian boundary, we refer to Voigt et al. (2012) and Thibault et al. (2012b), as our age-model and correlation have not caused substantial changes in the ages of biozones for these intervals.

	Average age and uncertainty (Myr)		
Planktic foraminifer and calcareous nannofossil events	**Basque country (Chapter 3)**	**Gubbio area (Gardin et al., 2012)**	**762C, Indian Ocean (Thibault et al., 2012)**
FO *Plummerita hantkeninoides* (PF)	66.059±0.075	66.12±0.01	-
FO *Abathomphalus mayaroensis* (PF)	68.432±0.079	69.30±0.05	69.920±0.150
FO *Racemiguembelina fructicosa* (PF)	68.872±0.210	70.20±0.11	67.660±0.220
FO *Planoglobulina acervulinoides* (PF)	69.496±0.167	73.57±0.07	68.360±0.080
FO *Contusotruncana contusa* (PF)	69.151±0.166	70.39±0.05	67.660±0.220
FO *Micula prinsii* (CN)	66.016±0.093	66.31±0.06	66.390±0.070
FO *Micula murus* (CN)	66.365±0.163	67.13±0.11	67.330±0.070
FO *Lithraphidites quadratus* (CN)	68.995±0.113	69.06±0.08	67.790±0.060
LO *Reinhardtites levis* (CN)	69.330±0.087	70.31±0.11	69.750±0.150
LO *Tranolithus orionatus* (CN)	70.295±0.092	70.75±0.0.04	69.560±0.070
LO *Broinsonia parca constricta* (CN)	71.190±0.087	70.83±0.04	69.480±0.100
LO *Eiffelithus eximius* (CN)	70.550±0.200	75.52	73.900±0.090

Table 2: Ages of planktic foraminifer and calcareous nannofossil events for the Basque country (Batenburg et al., in prep.), Gubbio (Gardin et al., 2012) and 762C (Thibault et al, 2012b) with adjusted ages for Gubbio based on the presented global carbon isotope correlation.

Campanian
Maastrichtian
Zumaia-Sopelana
Gubbio
Norfolk coast
Trunch
Stevns-1
Tercis
N-Germany
KPgE
MME
CMBE
LCE
Zumaia-Sopelana
Stevns-1
N-Germany
Gubbio
Tercis
Trunch & Norfolk coast
all scales: δ13C ‰ VPDB
magnetostrat.
foraminifera
nannofossils
ammonmites
belemnites
macrofossils

Fig 6: Correlation of the bulk carbonate $\delta^{13}C$ records from the European successions of: the Norfolk coast (Voigt et al., 2012) and the Trunch borehole (Jarvis et al., 2002; Jenkyns et al., 1994) in the United Kingdom; Zumaia (Batenburg et al., 2012) and Sopelana (this study) in the Basque country, N-Spain; the Stevns-1 borehole in Denmark (Thibault et al., 2012a); Tercis, SW France (Voigt et al., 2012); Lägerdorf, Kronsmoor and Hemmoor, N-Germany (Voigt et al., 2010); and Gubbio, Italy (Voigt et al., 2012). Grey areas indicate the carbon isotope events as identified by Voigt et al. (2012): the late Campanian Event (LCE), the Campanian-Maastrichtian Boundary Event (CMBE), the mid-Maastrichtian Event (MME) and the Cretaceous/Paleogene Event (KPgE). Pink bands indicate the carbon isotope minima identified approximately every 405-kyr in the Zumaia-Sopelana record. Similarly, the blue dashed lines pinpoint the negative shift on a 1.2 Myr scale. Dashed lines with numbers indicate the tie-points used for correlation. The age model is based on the tuning of the Zumaia-Sopelana record (Batenburg et al., 2012; in prep) and selected paleomagnetic reversals at Gubbio (see text) as identified by Arthur and Fischer (1977) and Gardin et al. (2012), with astronomically tuned ages from Husson et al. (2011). Planktonic foraminifera and calcareous annofssil data for Zumaia and Sopelana are from Batenburg et al. (2012; in prep) and Peréz-Rodríguez et al. (2012).For Gubbio, planktonic foraminifera data were provided by Gardin et al. (2012), Premoli-Silva and Sliter (1995), and calcareous nannofossil data by Gardin et al. (2012) and Monechi and Thierstein (1985). The belemnite zonation of the Norfolk coast section is from Schulz (1979) and the nannofossil zones for the Trunch borehole are from Burnett (1990). For Stevns-1, nannofossil data are from Thibault et al. (2012a). Ammonite data for Tercis are from Küchler and Odin (2001), inoceramid data are from Walaszczyk et al. (2002), and nannofossils from Gardin et al. (2001). Nannofossil data from N-Germany are provided by Burnett et al. (1990), and the macrofossil zonation is from Schulz et al. (1984).

Campanian
Maastrichtian
Zumaia-Sopelana
1210B
Gubbio
525A
690C
762C
magnetostrat.
foraminifera
nannofossils
KPgE
MME
CMBE
LCE
Exmouth Plateau Event
all scales: δ13C ‰ VPDB

Fig 7: Global correlation of bulk carbonate $\delta^{13}C$ records from Zumaia and Sopelana, Basque country, N-Spain (Batenburg et al., 2012; this study), ODP Hole 1210B, Shatsky Rise, tropical Pacific (Jung et al., 2012), Gubbio, Italy (Voigt et al., 2012) and ODP Hole 762C, Exmouth Plateau, Indian Ocean (2012b), and benthic foraminiferal $\delta^{13}C$ records from DSDP Hole 525A,Walvis Ridge, South Atlantic (Friedrich et al., 2009; Li and Keller, 1998) and ODP Hole 690C, Maud Rise, Weddel Sea (Friedrich et al., 2009). Grey areas indicate the carbon isotope events as identified by Voigt et al. (2012): the late Campanian Event (LCE), the Campanian-Maastrichtian Boundary Event (CMBE), the mid-Maastrichtian Event (MME) and the Cretaceous/Paleogene Event (KPgE). Pink band indicate the carbon isotope minima identified approximately every 405-kyr in the Zumaia-Sopelana record. Similarly, the blue dashed lines pinpoint the negative shift on a 1.2 Myr scale. Dashed lines with numbers indicate the tie-points used for correlation of the records from Zumaia-Sopelana, 1210B,and Gubbio. The records from Hole 525A and 690C are tied in with their paleomagnetic reversal data (Chave, 1984; Hamilton, 1990). The age model for Zumaia-Sopelana, Site 1210B, Gubbio, Hole 525A and Hole 690C is based on the tuning of the Zumaia-Sopelana record (Batenburg et al., 2012; in prep) and selected paleomagnetic reversals at Gubbio (see text) as identified by Arthur and Fischer (1977) and Gardin et al. (2012), with astronomically tuned ages from Husson et al. (2011). The age model for Hole 762C is provided by tuning of the geophysical data from this site by Husson et al. (2011) and Thibault et al. (2012b). Planktonic foraminifera and calcareous annofssil data for Zumaia and Sopelana are from Batenburg et al. (2012; in prep) and Peréz-Rodríguez et al. (2012). For 1210B, the calcareous nannofossil data from Lees and Bown (2005) were used, as well as the planktonic foraminifer data from Bralower et al. (2002). For Gubbio, planktonic foraminifera data were provided by Gardin et al. (2012), Premoli-Silva and Sliter (1995), and calcareous nannofossil data by Gardin et al. (2012) and Monechi and Thierstein (1985). Nannofossils from Hole 525A were studied by Manivit (1984), Henriksson (1993) and Thibault and Gardin (2007), and planktonic foraminifera by Li and Keller (1998). For Hole 690C, planktonic foraminfera and calcareous nannoplankton stratigraphies were provided by Barrera and Huber (1990), Huber (1990) and Pospichal and Wise (1990). Magnetostratigraphy from Hole 762C is from

Galbrun (1992) and Husson et al. (2011), calcareous nannofossils from Bralower and Siesser (1992) and Thibault et al. (2012b), and planktonic foraminifera from Wonders (1992) and Zepeda (1998).

5.5 Characteristics of the Late Campanian/Maastrichtian carbon isotope curves

The general pattern of the selected $\delta^{13}C$ records displays a gradual decrease through the Upper Campanian, with a strong decrease around the Campanian-Maastrichtian Boundary. $\delta^{13}C$ values increase to a Mid-Maastrichtian plateau, fall during the end Maastrichtian and hit particularly low levels before the Cretaceous-Paleogene Boundary. The different $\delta^{13}C$ records have hugely varying expressions of this general pattern, and in the intensity of the variations. The carbon isotope curve from Hemmoor seems to reflect very gradual, long-term variations in $\delta^{13}C$. In contrast the Zumaia-Sopelana section, Stevns-1, site 1210B and Gubbio show very distinct shorter-term variations. The Zumaia-Sopelana record displays a stronger general decreasing trend towards the K/Pg boundary then most other records, with the possible exception of Stevns-1 and N-Germany.

Late Campanian Event (LCE)

A marked negative carbon isotope excursion around ~75 Ma, within C33n, termed the Late Campanian Event (LCE) can be recognised in the data from the Trunch borehole (with an excursion of 0.4‰), Tercis (0.8‰), N-Germany (0.4‰) and Gubbio (0.3‰) (Voigt et al., 2012). It is less strongly expressed at Site 1210B (Jung et al., 2012; Voigt et al., 2012), and potentially reflected as a negative shift of 0.2‰ at Site 762C (Thibault et al., 2012b).

Upper Campanian interval between the LCE and the CMBE

Above the LCE, the carbon isotope values from the boreal realm and Tercis remain relatively stable, whereas the Gubbio,1210B and 762C curves display a marked rise in $\delta^{13}C$. A negative shift around 74 Ma, within C32r1r, acts as a tie-point in our correlation (tie-point 8 in Table 1, corresponding to tie-point 10 in Voigt et al., 2012). The Gubbio and 762c records show a decline around 73.3 Ma, within C32n2n, termed C1- by Thibault et al. (2012b).

Campanian-Maastrichtian Boundary Event (CMBE)

The Campanian Maastrichtian boundary interval is marked by a negative excursion $\delta^{13}C$ in both shelf sea and open ocean settings (as summarised in Voigt et al., 2012). The magnitude of the excursion can vary from 0.3 – 0.4‰ (Tercis, Gubbio, 1210B and 762C) to 1‰ at Kronsmoor, Norfolk, Stevns-1, 690C and 525A. Voigt et al. (2012) recognised five positive oscillations within the Campanian-Maastrichtian Boundary Event, of which the lowermost maximum termed CMB-1, which acts as our tie-point 7, corresponds to the base of the CMBa event recognised by Thibault et al. (2012a, 2012b). Near the top of C32n2n, $\delta^{13}C$ values reach a distinct minimum in the Stevns-1, Tercis, N-Germany, Gubbio and Hole 762C curves, which is our tie-point 6, tie-point 8 in Voigt et al. (2012), and the CMBc event in Thibault et al. (2012b). The Campanian-Maastrichtian boundary, as defined at Tercis, is located within the $\delta^{13}C$ decrease of the CMBE, marked by a negative shift below the minimum of tie-point 6 (Figures 6 and 7) (Thibault et al., 2012b; Voigt et al., 2012). Values rise towards a maximum near the base of C31r in the records of the Norfolk coast, Stevns-1, Tercis, 1210B, Gubbio, 525A, and 762C, termed CMBE4 and M1+ by Voigt et al. (2012) and Thibault et al. (2012b), respectively. The inflection towards this maximum is used as tie-point 5 in this study, and tie-point 7 in Voigt et al. (2012). A negative excursion, marking the top of the CMBE in Voigt et al., and termed the M1- by Thibault et al., acts as our tie-point 4 (tiepoint 6 in Voigt et al., 2012) and can be recognised in the Zumaia-Sopelana record, Stevns-1, N-Germany, Gubbio, and Hole 762C.

Lower-mid Maastrichtian

From the minimum at tie-point 4 upwards, all selected records show an increase towards maximum values in the mid-Maastrichtian around 69 Ma. This rise is punctuated by a strong negative shift at Sopelana around 69.8 Ma, of about 0.8‰. This shift is not reflected so strongly in the other records. There is a slight excursion in the record of Gubbio, 1210B, and negative values between M2+ and M3+ in 762C (Thibault et al., 2012b).

Mid-Maastrichtian Event

The base of the mid-Maastrichtian event (MME) as defined by Voigt et al (2012) is characterised by a sharp positive shift in $\delta^{13}C$ values near the base of C31n (tie-point 5 in Voigt et al., 2012) in the Zumaia-Sopelana record, the Stevns-1 record, the data from Gubbio, from 1210B, and possibly 762C (shift M3+ of Thibault et al., 2012b). The mid-Maastrichtian event is expressed in most records as two positive peaks with maximal $\delta^{13}C$ values in the Maastrichtian, separated by a pronounced negative excursion. This negative inflection around 68.6 Ma, our tie-point 3, is expressed in all records with data for this interval. The Zumaia-Sopelana record shows the largest shift of 1‰, whereas the other records, Stevns-1, N-Germany, Gubbio and 1210B, show an excursion of 0.3-0.4‰. After this negative excursion, values rise towards a second maximum, with a 405-kyr scale oscillation in the Zumaia-Sopelana, Stevns-1, and 1210B records. This maximum has been used by Voigt et al. (2012) as tie-point 4, but has been lined up slightly differently here, following changes in the age-model. At the top of the mid-Maastrichtian event, values shift to more negative values around 67.9 Ma.

Interval between the MME and the K/Pg boundary

The expression of the carbon isotope records for the interval between the MME and the K/Pg boundary is highly variable amongst the different records. Values show an overall decrease, with four 405-kyr scale maxima in the Zumaia-Sopelana and Stevns-1 curves, and potentially in the Hemmoor data. The lowermost two maxima likely correspond to the pronounced peak in $\delta^{13}C$ values in 1210B and 762C, identified as the Exmouth plateau event by Thibault et al. (2012b) around

67.5 Ma. The third maximum can be recognised in Gubbio, 1210B and at 762C, as M4+ (Thibault et al., 2012b). At 66.5 Ma, near the base of C29r, a strong negative excursion occurs in the Zumaia-Sopelana record (approximately -1.2‰), the Stevns-1 record (approximately -0.5‰), the Hemmoor data (approximately -0.3 ‰), the 11210B curve (approximately -0.5‰), the Gubbio curve (approximately -0.4‰), and the 762C curve (approximately -0.3‰), and is used as our second tie-point. The maximum in $\delta^{13}C$ values just below the K/Pg boundary, which is the fourth maximum above the MME in the Zumaia- and Stevns-1 records, is well expressed in Gubbio and potentially in the Hemmoor data. The latter record has a slight uncertainty in correlation, as the section does not reach the K/Pg boundary. Above this maximum, a negative shift occurs at Zumaia, Stevns-1 and Gubbio, to values similar as the previous minimum, before rising towards the K/Pg boundary. This rise in $\delta^{13}C$ values also occurs at Site 525A and at 762C, termed M5+ by Thibault et al. (2012b).

6. Discussion

6.1 Carbon isotopes as climatic markers

Previous studies indicate that bulk carbonate carbon isotope curves can be used as a powerful and reliable correlation and dating tool (Gale et al., 1993; Jenkyns et al., 1994). Although the absolute values and the amplitude of variations amongst sites are markedly different, the records have a similar pattern of $\delta^{13}C$ variations, which is supported by (selected) magnetostratigraphic data, by the identification of the K/Pg boundary and largely by the biostratigraphies.

Diagenesis is more likely to affect oxygen isotopes rations than $\delta^{13}C$ (Schrag et al., 1995), and indeed the oxygen isotopes of the Zumaia and Sopelana sections do not seem to display trends and are therefore not shown here. A cross-plot of carbon and oxygen isotope values does not completely exclude covariance, but the good correspondence with other available $\delta^{13}C$ records leads us to suggest that the carbon isotope record reflects original fluctuations of the carbon cycle.

6.2 Orbital pacing

6.2.1 The 405-kyr periodicity of eccentricity

The Zumaia-Sopelana record displays a very prominent cyclicity on a 420-kyr scale, with values varying by 0.5-1 ‰ within a cycle, which likely reflects the influence of the 405-kyr periodicity of eccentricity-modulated precession. Minima in $\delta^{13}C$ data typically coincide with dark and thick marls within intervals of limestone-marl alternations. These limestone-marl alternations likely reflect dilution cycles driven by eccentricity-modulated precession, which influences the intensity of the hydrological cycle and the input of siliciclastic material to the basin (Batenburg et al., 2012)(Batenburg et al. in prep.). A high seasonal contrast could intensify monsoon and lead to more marl deposition and increased input of ^{12}C-rich dissolved inorganic carbon to the basin. Consecutive 405-kyr minima in the $\delta^{13}C$ data, as identified in the record from Zumaia and Sopelana, have been indicated with pink bars. These minima can often be recognised in the other sections, in particular in the records of Stevns-1, 1210B and Gubbio. However, the expression of these cycles at Zumaia is much stronger, which might be caused by the restricted nature of the Basque basin as this was a narrow inter-plate trough (Pujalte et al., 1995).

6.2.2 Origin of the 1.2-Myr periodicity

A distinct feature of the carbon isotope record from Zumaia and Sopelana is the occurrence of a 1.1 Myr periodicity (Fig. 5), similar to the periodicity of ~1.2 Myr in the geophysical data records (Batenburg et al., 2012)(Batenburg et al., in prep). The periodicity is expressed in the carbon isotope record as pronounced negative shifts, on the order of 1‰, indicated with blue (dashed) lines (Figs. 4, 5, 6 and 7). These shifts coincide with changes in the lithology in the Zumaia section from carbonate-rich to marly sediments, at 109 and 59m, and to a lesser degree at 12m (Fig. 4). These lithological shifts occur slightly after the identified 405-kyr minima in the lithology, magnetic susceptibility and reflectance records and are coincident with

major negative shifts in $\delta^{13}C$ and reflectance, and positive shifts in magnetic susceptibility. These lithological changes have been interpreted as facies changes from carbonate rich High Stand Systems Tract deposits to marly Low Stand Fan deposits (Pujalte et al., 1995), indicating a fast drop in relative sea level, which could have caused erosion of organic rich shelf material and increased availability of ^{12}C. Eustatic sea-level fall has been suggested a a controlling mechanism of negative carbon isotope excursions in the Campanian (Jarvis et al., 2006, 2002). Alternatively, these shifts might be caused by variation in the hydrological cycle, similar to the 405-kyr oscillations. At Sopelana, there are no comparable lithological shifts, however, an interval of reduced amplitude of the 100-kyr periodicity of eccentricity from 161to 168 m may indicate the influence of a longer periodicity, specifically the expression of the opposite extreme of the 1.2 Myr cycle (Batenburg et al., in prep.). Although the records are rather short for detection of this periodicity, it deserves consideration as it may represent an orbital imprint. We would like to present several hypotheses that require further testing:

1) A 1.2 Myr periodicity is present in obliquity, which can act as a driving force on glaciations and sea level (Lourens and Hilgen, 1997; Shackleton et al., 1999). However, we do not find a strong imprint of the short obliquity cycle, which should have a duration of approximately 41 kyr, which may reduce the likelihood of this explanation.

2) The long-term periodicity of eccentricity has been 2.4 Myr for at least the past 50 Myr (Laskar et al. 2011) but it may have switched to a shorter periodicity of 1.2 Myr in the past due to the chaotic evolution of the solar system. This could be investigated with long datasets, preferably with independent age control, to identify or refute the existence of a 2.4 Myr forcing for this time interval.

3) Another option could be a reinforcement of the 405-kyr cycle every three cycles, possibly caused by an underlying climatic or tectonic trend. This could be supported by the occurrence of the $\delta^{13}C$ shifts and the sharp lithological transitions closely above the expression of the minima of the 405-kyr periodicity of eccentricity-modulated precession in the lithological and geophysical data records.

4) Finally, the observed shifts and proposed sea-level changes may be caused by tectonic pulses in the Basque basin. However, these pulses would have

had to be very regular and do not explain the interval of reduced amplitude of the 100-kyr periodicity at Sopelana.

In contrast to the 405-kyr periodicity, the shifts on a 1.2 Myr scale cannot be clearly recognised in the other curves. The proposed sea level fall and/or hydrological changes could have been either local phenomena, which would explain the lack of expression in the records of shallow-shelf settings in the boreal chalk sea, or they could have had an exceptionally strong expression in the Basque basin due to its restricted nature. However, although the 1.2 Myr shifts are not expressed in the other records, there are some indications for oscillations on a 1.2 Myr scale, for example the 1210B and the Gubbio record shows two such variations from 70.7 to 73.2. The 1.2-Myr shifts from Zumaia do seem to coincide with long-term minima in the records, especially in the Gubbio record. Also, the Gubbio records displays potential 2.4 Myr oscillations, namely from LCE to base CMBE, between the top of the CMBE to the MME, and from the MME to KPgE. However such observations remain speculative due to the uncertainties in the age model and the limited duration of the record.

7. Summary

The extended high-resolution carbon isotope record for the Zumaia and Sopelana sections in the Basque country, northern Spain displays regular variations with remarkable amplitude which provide a good basis for global correlation. These variations are paced by the 405-kyr periodicity of eccentricity and negative shifts seem to occur at regular intervals of 1.2 Myr. The orbitally tuned curve from Zumaia and Sopelana provides improved age control for trends and excursions, such as the mid Maastrichtian Event (MME). The omission of relatively short magnetic chrons from the age model reduces large changes in sedimentation rate. The resultant correlation shows the influence of the 405-kyr periodicity across sites and the potential influence of longer periodicities. We hypothesise that the 1.2 Myr cycle might represent an orbital forcing mechanism acting on sea level and/or hydrological patterns.

Chapter 5. The origin of Maastrichtian and Danian limestone-marl alternations at Zumaia and Sopelana, Basque Country, N-Spain

In collaboration with: Frits Hilgen, Mario Sprovieri, Andrew S. Gale

Abstract

Although the limestone-marl couplets of the Zumaia and Sopelana section along the Bay of Biscay, N-Spain, have been used for astronomical tuning, the exact origins of the rhythmic sedimentation and in particular the phase relationship with precession have not been fully understood. Here we present a critical assessment of the thickness variations through the Maastrichtian succession, as well as high resolution elemental, geophysical and stable isotope data of selected intervals of Danian and early and late Maastrichtian age. The observed variations in thickness, mostly in the marly component of the limestone-marl couplets, display the periodicities of eccentricity-modulated precession. Elemental analysis by XRF reveals the contribution of siliciclastic material as the main factor in determining the thickness of the beds and the limestone-marl couplets. As thickness of the beds is primarily determined by terrigenous supply of siliciclastic material, the limestone-marl alternations represent dilution cycles. The Danian interval at Zumaia and the lower Maastrichtian interval at Sopelana display additional variability in productivity as a control on limestone sedimentation. Both terrigenous input and biological productivity may have been controlled by eccentricity-modulated precession through its influence on the hydrological cycle. A high seasonal contrast on the northern hemisphere during precession minima at times of maximum eccentricity may have led to an intensification of the hydrological cycle, thereby increasing run-off and siliciclastic supply, whereas a low seasonal contrast, or the long-term absence of seasonal extremes, may have been characterised by dry conditions, with increased dust input to the basin and a higher productivity, as indicated by the elemental ratios of Ti/Al, Zr/Al and Ba/Al.

1 Introduction

1.1 Rhythmic limestone-marl alternations

Late Cretaceous cyclic limestone-marl alternations are frequently studied for cyclostratigraphy and astronomical tuning. However, before such applications, the suitability of rhythmic successions needs to be assessed, to ascertain the primary origin of the rhythmicity and exclude a large contribution of post-depositional processes such as diagenetic unmixing (Westphal et al., 2010). We present a detailed and high resolution study of selected intervals in the Zumaia and Sopelana sections, of early Maastrichtian, late Maastrichtian, and Danian age. These intervals have been included in several cyclostratigraphic studies (Batenburg et al., 2012; Dinarès-Turell et al., 2003; Kuiper et al., 2008; ten Kate and Sprenger, 1993; Westerhold et al., 2008), and were likely formed in similar depositional settings, yet display marked differences in appearance. By unravelling the contributions of terrestrial input versus biogenic productivity and dissolution (Einsele, 1982), we aim to better understand the underlying causes of rhythmic marl-limestone deposition in the late Cretaceous-early Paleogene of the Basque-Cantabric basin.

1.2 Geological setting and sections

The Zumaia and Sopelana sections contain hemipelagic limestones and marls, deposited in the flysch trough of the Basque-Cantabric basin. This basin was a deep and narrow trough along the European-Iberian plate boundary, formed during the opening of the Bay of Biscay. It was surrounded by shallow shelf areas to the north and south and likely received siliciclastic material from the east (Mathey, 1988; Mount and Ward, 1986; Pujalte et al., 1998; Rat, 1988). The Sopelana and Zumaia sections have been uplifted in Eocene times as parts of the Biscay synclinorium and in the Gipuzkoa monocline, respectively (Pujalte et al., 1998).

The coastal cliffs of Zumaia with hemipelagic limestones, marls and intercalated turbidites, have been the subject of many paleoclimatic, magnetostratigraphic, biostratigraphic and cyclostratigraphic studies (Herm, 1965; Percival and Fischer,

1977; Lamolda, 1990; Ward et al., 1991; Ward and Kennedy, 1993; ten Kate and Sprenger, 1993; Pujalte et al., 1998; Dinarès-Turell et al., 2003; Elorza and García-Garmilla, 1998; Gómez –Alday et al., 2008; Kuiper et al., 2008; Pérez-Rodríguez et al., 2012). The Global Stratotype Sections and Points for the bases of the Thanetian and Selandian stages of the Paleocene are formally defined in the Zumaia section (Schmitz et al., 2011). The section is one of the reference sections for the K/Pg-boundary interval (Molina et al., 2009; Pujalte et al., 1995; Smit and ten Kate, 1982) and the tuned Danian part of the succession plays an important role in the discussion on the age of the K/Pg boundary (Dinarès-Turell et al., 2003; Hilgen et al., 2010; Kuiper et al., 2008; Westerhold et al., 2012, 2008).

The Sopelana section located further west, near Bilbao, displays a very regular succession of alternating hemipelagic limestones and marls, without turbidites , and has been studied for ammonites, inoceramids, planktonic foraminifera, calcareous nannofossils and magnetostratigraphy (Elorza and García-Garmilla, 1998; Gómez – Alday et al., 2008; Gómez-Alday et al., 2004; Lamolda et al., 1983; Mary et al., 1991; Moreau et al., 1994; Ward and Kennedy, 1993; Ward, 1988; Ward et al., 1991). Intervals at Sopelana were included in studies on thickness, $CaCO_3$ and stable isotope variations by Alvarez-Llano et al. (2006), Santander et al. (2007) Domínguez et al. (2007) and Jiménez Berrocoso et al. (2012).

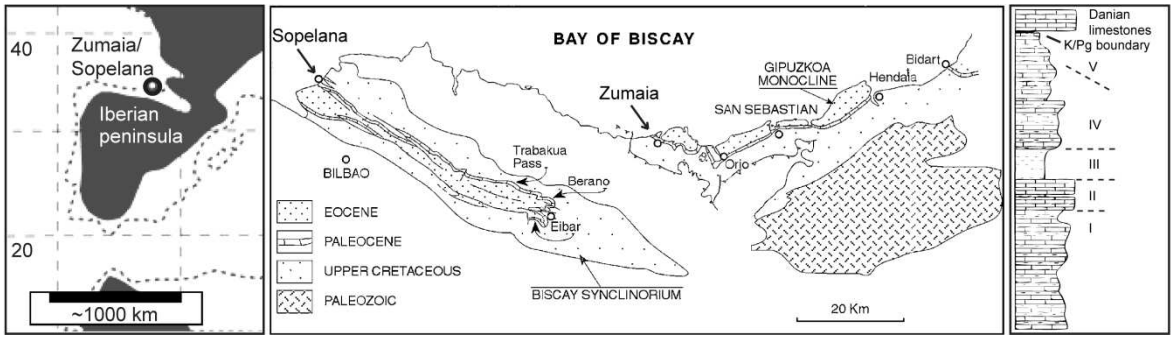

Figure 1: Paleogeographic setting (Gómez –Alday et al., 2008), geological map (Pujalte et al., 1998) and schematised stratigraphy after Ward et al (1991).

1.3 Lithological cycles

The stratigraphy of the Maastrichtian part of the Zumaia section is characterised by lithological variation on several scales. A hierarchy of four cycles can be distinguished, of which three have previously been identified by Mount and Ward (1986). On the largest scale, intervals of dark-coloured marls and marly limestones alternate with intervals composed of light-coloured limestones and marls, with alternations having a thickness of approximately 49 m. Within this first-order cyclicity, second order cycles occur with a thickness of 16-19 m, in which intervals of darker and lighter coloured marls alternate. In addition to the cycles described by Mount and Ward (1986), a bundling of basic cycles occurs on a scale of approximately 4 m, with variations mostly in the thickness and colour of the marl component of the limestone-marl alternations. The smallest scale basic cycle is composed of the alternation of individual limestone and marl beds with an average thickness of 77 cm, from hereon called couplets. Mount and Ward (1986) have interpreted the different cyclicities as the product of superimposed periodicities, and analysed these by calculating the clay/carbonate ratio. This enabled them to identify threshold values for the deposition of limestone and for the deposition of limestone-dominated stratal packages, dependent on shifts in the running average of this ratio.

Whereas the variation between couplets in the Maastrichtian of the Zumaia section occurs predominantly in the marls, the nearby Sopelana section displays variability in the expression of both marls and limestones, which overall is less pronounced than at Zumaia. Intervals in which both lithologies are markedly different, with dark marls and indurated limestones, alternate with intervals in which the difference between lithologies are less notable, with light-coloured marls and thin and less indurated limestones. These variations, which are superimposed on the individual limestone-marl alternations, occur on a scale of approximately three meters (five couplets) and twelve meters (18 to 20 couplets).

The Danian part of the Zumaia section directly above the Cretaceous/Paleogene (K/Pg) is dominated by very indurated limestones with thin marls being infrequently intercalated. This has been ascribed to a starvation of siliciclastic influx from the

western Pyrenees, due to relative tectonic quiescence of the hinterland (Pujalte et al., 1998). Despite the sparse occurrence of marls, different modes of cyclicity can be observed, with bundling on a scale of five couplets, and grouping of these bundles in groups of four (or ~20 individual couplets) (Dinarès-Turell et al., 2003; Kuiper et al., 2008). The siliciclastic sediment starvation has led to a rather variable appearance of couplets and bundles, with extremely low siliciclastic input resulting in so-called crowded bundles, in which marly layers are not developed (Pujalte et al., 1998). Further upward in the stratigraphy, the amount and thickness of marly layers increases, although the thickness of the couplets remains smaller than in the Maastrichtian part of the succession.

The hierarchical stacking pattern at Zumaia and Sopelana with a ratio of 1: 5: 20 has been interpreted to represent the ratios of the periods of eccentricity modulated precession (21.8: ~100: 405 kyr). Couplets with the most pronounced difference between their marl and limestone component likely represent eccentricity maxima, and this phase relation allows for the astronomical tuning to the stable 405-kyr eccentricity cycle (Batenburg et al., 2012; Kuiper et al., 2008; ten Kate and Sprenger, 1993; Westerhold et al., 2008).

As a mechanism for variations in lithologies and thicknesses, we hypothesise that variations in eccentricity-modulated precession may have driven the intensity of the hydrological cycle, controlling runoff and siliciclastic supply. An increased seasonal contrast may have amplified the land-sea temperature contrast, leading to increased run-off and deposition of thicker marls. In contrast, climate with a low seasonal contrast or long-term absence of seasonal extremes may have been characterised by dryer conditions, which could enhance dust deposition, and increase carbonate productivity.

2. Methology

2.1 Bed thickness

Maastrichtian sediments of the Zumaia and Sopelana sections have been logged in detail, and sampled for geophysical properties and stable isotope data, to obtain a cyclostratigraphic framework and an orbitally tuned carbon isotope stratigraphy for correlation in the Maastrichtian (Batenburg et al., 2012, in prep.) (Fig. 2). As an assessment of whether the observed variations in thickness were indeed formed in response to orbital forcing, we present an analysis of bed thickness in both the depth and the time domain (Fig. 3). The thickness of the beds is used as proxy value to allow for time series analyses. In this way, variation in distance between bed boundaries, which in essence is variation in frequency in the depth domain, gets translated into variation in amplitude. For this exercise, turbidites were subtracted as their occurrence is not related to the depositional mechanisms of limestones and marls (Mount and Ward, 1986; ten Kate and Sprenger, 1993). An age model has been assigned to the data, based on the identification of 405-kyr minima in the lithological and geophysical data records (Batenburg et al., 2012, in prep.) followed by tuning to the 405-kyr eccentricity component of the latest astronomical solution La2011 (Laskar et al., 2011). Spectral analysis of the bed thickness records was performed with Redfit38 (Schulz and Mudelsee, 2002), wavelet analysis was applied with a Matlab script (Grinsted et al., 2004) and band-pass filtering with AnalySeries (Paillard et al., 1996), centred at the main periods obtained from the Redfit38 analyses. The thicknesses of marl beds, limestone beds and cycles are plotted against cycle number in Figure 4, in order to investigate the relative importance of thickness changes in the different lithologies on cycle thickness.

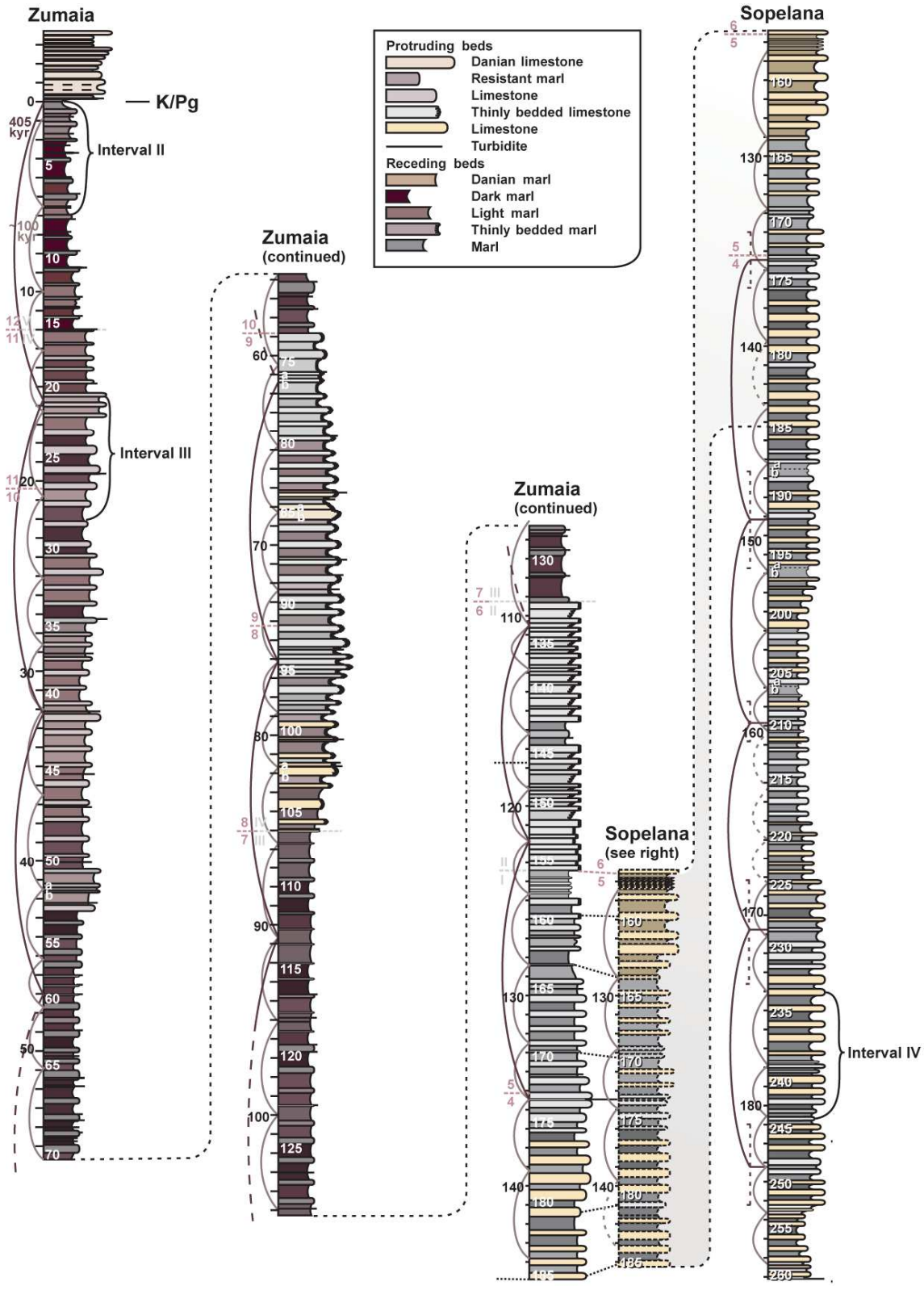

Figure 2: Stratigraphic log of the studied Maastrichtian succession of the Zumaia and Sopelana sections, with selected intervals II to IV indicated. Grey roman numerals indicate the intervals identified by Ward et al. (1991) and lilac numbers

the units of Wiedmann (1988). The half circles in deep purple indicate the 405-kyr eccentricity minima, the lighter half circles indicate the 100-kyr bundling. White numbers are cycle numbers.

2.2 Analyses of selected intervals

Four intervals of the Sopelana and Zumaia sections have been studied in detail for elemental analyses, stable isotope ratios and the geophysical properties of magnetic susceptibility (MS), total reflectance (L*) and redness (a*) (Fig. 2). Interval I (Fig. 5) is located in the Danian part of the Zumaia section and crops out in a cove in the Punta Aitzgorri headland, below the chapel of Saint Telmo. The interval contains 10 limestone-marl alternations, which show variations in marl thickness and colour likely representing ~100 kyr bundling. Interval II is located in the red-purplish marly interval just below the K/Pg boundary (Fig. 6) and spans a ~100 kyr bundle (Batenburg et al., 2012). This interval has been included in a study of trace element compositions around the K/Pg boundary (Smit and Ten Kate, 1982). Interval III, stratigraphically approximately 20 m below, displays regularly alternating limestones and marls, with the poorly developed marls of cycle 21 representing a 405-kyr minimum which forms a small promontory (Batenburg et al., 2012) (Fig. 7). Interval IV is selected in the lowermost part of the Sopelana section, in a promontory on the Atxabiribil-Arriatera swimming beach (Fig. 7). This interval of 10 limestone-marl couplets spans two ~100 kyr cycles within a 405-kyr maximum (Batenburg et al., in prep.). The interval contains two couplets that were previously investigated for $CaCO_3$ content and stable isotope ratios by Jiménez-Berrocoso et al. (2012), and is located within an interval of 55 limestone-marl couplets studied for thickness and $CaCO_3$ content by Alvarez-Llano et al. (2006). Samples with a resolution of 5-10 samples per couplet were powdered in a micromill and approximately 7 grams of powder were pressed in pellets for X-Ray Fluorescence (XRF) at the School of Science at the University of Greenwich, United Kingdom, for the analysis of major and minor elements.

For the geophysical properties and the stable carbon and oxygen isotope ratios of bulk carbonate, analyses were performed at the IAMC-CNR (Naples, Italy), as reported in Batenburg et al. (2012).

2.3 Paleo-environmental proxies

The relative contribution of elements to the sedimentary rhythms, together with the stable isotope ratios, thickness variations and geophysical properties, can be used to better understand the climatic mechanisms underlying sedimentation. The first indicator is whether the variations in thickness of the cycles are primarily determined by variations in thickness of the limestone or variations in thickness of the marly part of the couplet. Secondly, the relative contribution of calcium versus the siliciclastic input provides an indication of the relative importance of clay input versus carbonate productivity. Of the range of elements obtained by XRF analysis, we focus on the Ti/Al, K/Al, Zr/Al, Ba/Al, P/Al, Co/Al, Ni/Al, Zn/Al and Mo/Al ratios, to unravel the various processes involved.

The Ti/Al and Zr/Al ratios are proxies for grain size and commonly used as tools to distinguish between wind-blown dust, rich in Ti and Zr, and riverine contributions of siliciclastic material, rich in Al (Calvert and Pedersen, 2007; Spears and Kanaris-Sotiriou, 1976; Beckmann et al., 2005). Dust may act as a fertiliser of marine productivity by providing elements such as Fe to the marine environment (Martin, 1990). Barite can be used as a proxy for marine productivity (Dehairs et al., 1992). Although the exact pathways of barite formation are not entirely understood, the formation is possibly linked to micro-environments with decaying organic matter (Chow and Goldberg, 1960). Besides barite, detrital influx is a major source of Ba, so that normalisation to Al is required. The Ba/Al ratio is commonly used as a proxy for export productivity (Calvert, 1983; Shimmield, 1992). The amount of phosphorous and the P/Al ratio can be used as an indicator of original organic matter deposition (as summarised in Calvert and Pedersen, 2007).The K/Al ratio may reflect the relative abundance of clay mineral species, as they have different elemental compositions, which can be used to reconstruct changes in terrestrial climate(Beckmann et al., 2005). At lowest precipitation rates, more

montmorillonite will be formed and major cations will be retained, vermiculite and illite are formed under intermediate conditions, and kaolinite and halloysite, with the greatest loss of cations, are formed when leaching intensities are highest (Singer, 1980). For example, kaolinite, which is rich in Al, forms in soils in warm and humid conditions, whereas feldspar, relatively poor in Al, only survives soil forming processes in drier conditions. However, the K/Al ratio may also respond to changes in the source of the siliciclastic material, as a result of changes in drainage area. Cu, Ni, and Zn are redox-sensitive elements, insoluble in anoxic conditions (Brumsack, 1989). They can be derived from detrital input, for which can be corrected by normalization to Al, they can be enriched in the sediment below anoxic water masses or they may be added by diffusion of dissolved metals from oxygenated waters into the subsurface anoxic horizons (Calvert and Pedersen, 1993). Mo is a redox-sensitive element, but can be enriched in sediments below both oxic and anoxic water masses. Mo enrichment is controlled by the presence of sulphide, which may occur in euxinic conditions in the water column, but also in the subsurface of near-shore sediments in the presence of decomposing organic matter (Calvert and Pedersen, 2007; Helz et al., 1996). Variations in the stable oxygen isotope ratio $\delta^{18}O$ of bulk carbonate are likely to reflect variations in temperature and salinity, and potentially ice volume, although the presence of ice in the latest Cretaceous is debated (Bornemann et al., 2008; Miller et al., 2003). The $\delta^{18}O$ values should be interpreted with great care, as they may have been affected by diagenesis (Jiménez Berrocoso et al., 2012). Meteoric water, with low $\delta^{18}O$ values, may have affected $\delta^{18}O$ in porous lithologies. The stable carbon isotope ratio, $\delta^{13}C$, of bulk carbonate, is generally less likely to suffer from diagenetic overprinting and may reveal climatic variation on different time scales. The $\delta^{13}C$ record throughout the Zumaia section shows a strong influence of the 405-kyr periodicity of eccentricity modulated precession. High values of $\delta^{13}C$ occur shortly after eccentricity minima, which may reflect a reduced input of the lighter isotope ^{12}C by rivers (Batenburg et al., 2012). On shorter time-scales, $\delta^{13}C$ of the bulk carbonate may increase in response to enhanced productivity as organisms preferentially incorporate the lighter isotope ^{12}C, thus leaving the water relatively enriched in ^{13}C. The stable isotope composition of the carbonate is likely to reflect the conditions in

surface waters, as the main source of carbonate is provided by calcareous nannofossils and planktonic foraminifera (Gómez-Alday et al., 2004). Magnetic susceptibility (MS) and total colour reflectance (L*) vary in response to the siliciclastic content of the sediments, and a* is a measure of the redness.

3. Results

3.1 Bed thickness

The thickness record (Fig. 3) clearly shows the influence of a 17 m periodicity in the upper two thirds of the record, and a 12 m periodicity in the lower part of the record. Other periods are found around 49 m, 4.2 and 2.8 m, and between 80 cm to 1 m, but the latter likely corresponds to the individual beds and can therefore not be resolved with the resolution of the bed-thickness record, which has, in essence, only two values per cycle.

The 4.2 and 2.8 m, and 17 and 12 m periodicities likely correspond to the observed bundling of five and 18-20 couplets, which likely represent the ~100 kyr and 405-kyr eccentricity cycles, respectively. The 49 m periodicity may reflect the potential influence of a 1.2 Myr cycle. Time series analyses in the time domain reveal main periodicities around 1.2 Myr, around 400 kyr, which might be partly introduced by the tuning, around 115 kyr, 38 kyr and around 19-25 kyr. These shortest periodicities may reflect the influence of precession and potentially obliquity, however, the resolution of the bed thickness record is not sufficient for reliable detection.

In the Maastrichtian interval at Zumaia, the thickness variations of the cycles (Fig. 4) are strongly determined by the thickness of the marl beds. Marl and limestone bed thicknesses vary in opposite phase, with for example very thin limestone beds in intervals with thick marls. In the Danian interval at Zumaia and the Maastrichtian at Sopelana, variations in marl thickness and limestone thickness are more in concert, but the shape of the cycle thickness curve closely reflects that of the marl thickness.

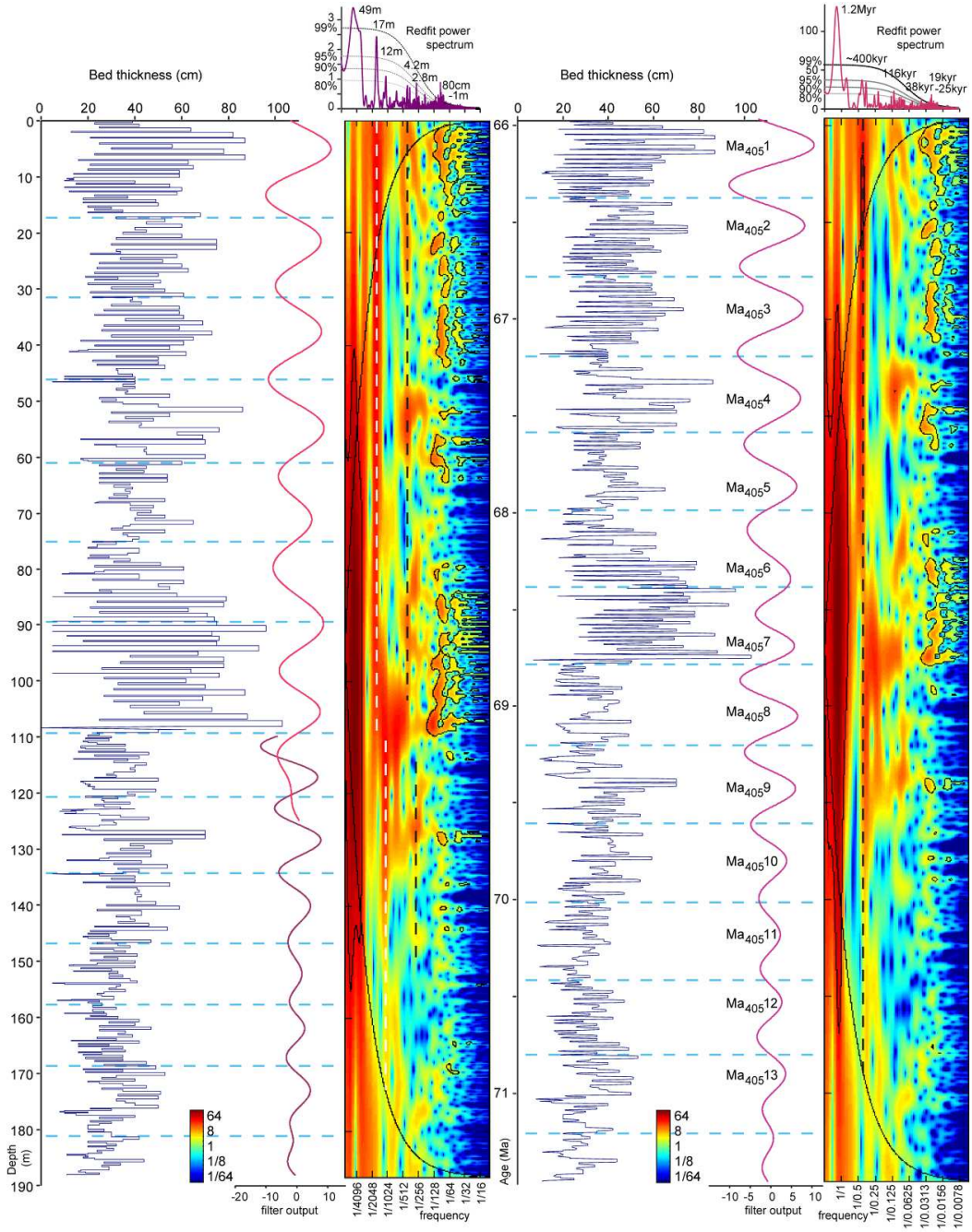

Figure 3: Bed thickness and its time series analyses in the depth (left) and time domain (right), flanked by their band pass filters centred at 17 m (upper two thirds of the record, bandwidth 12 to 29 m) and 12 m (lower interval, bandwidth 8.5 to 20 m) and 405 kyr (bandwidth 300-623 kyr). Main periodicities around 49, 17, 12, 4.2 and 2.8 m and around 80 cm to 1 m (left) and around 1.2 Myr, 400 kyr, 115 kyr, 38 kyr and 19-25 kyr can be observed in the Redfit analysis (top) and wavelet analyses. Blue dashed lines indicate the position of identified 405-kyr minima in the lithology and geophysical data records (Batenburg et al., 2012, in prep.), with black cycle numbers (Ma_{405}) following Husson et al. (2011).

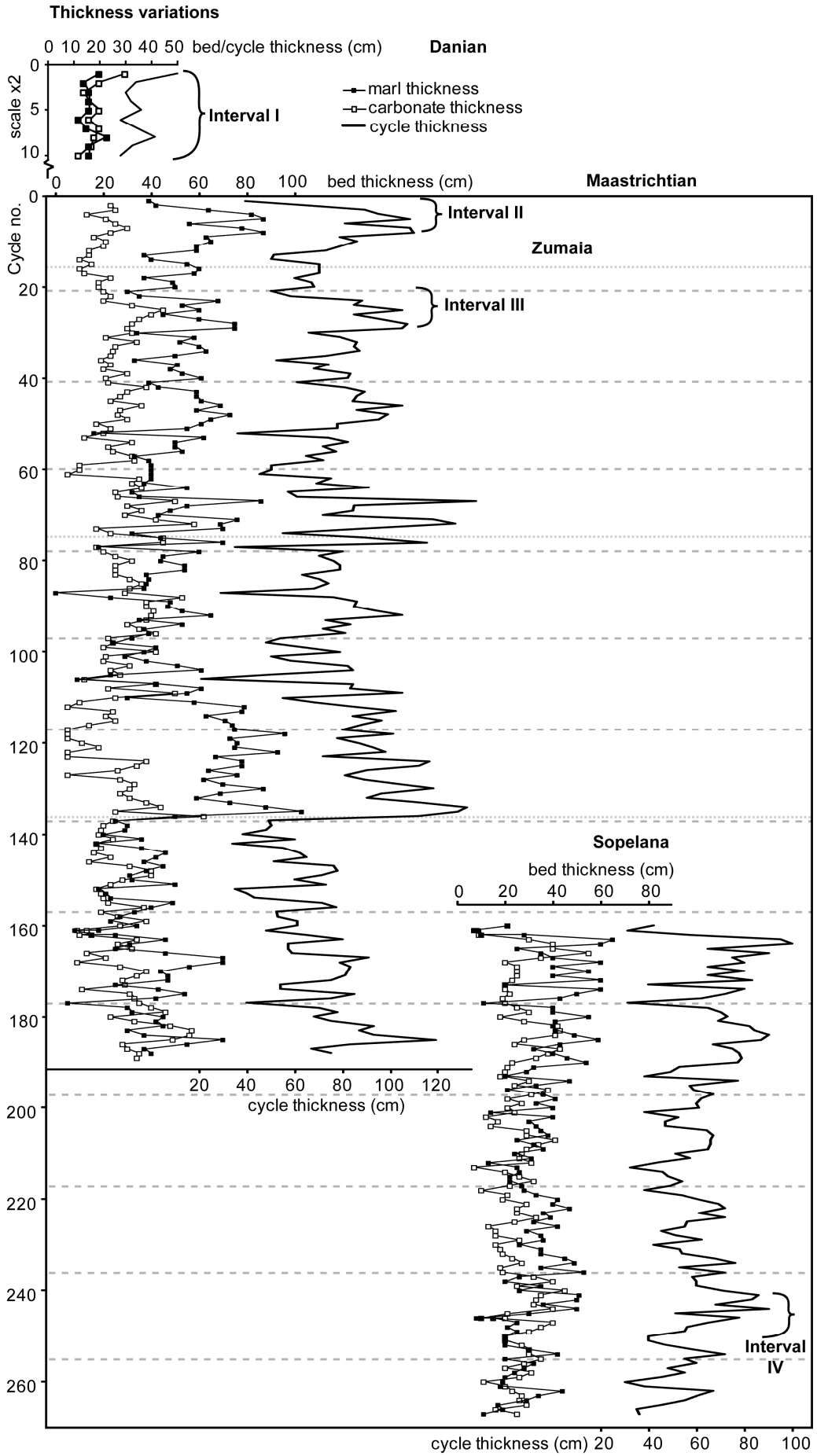
Thickness variations
0 10 20 30 40 50 bed/cycle thickness (cm)
Danian
scale x2
0
5
10
Interval I
marl thickness
carbonate thickness
cycle thickness
0 20 40 60 80 100 bed thickness (cm)
Maastrichtian
Cycle no.
0
20
40
60
80
100
120
140
160
180
200
220
240
260
Interval II
Zumaia
Interval III
Sopelana
bed thickness (cm)
0 20 40 60 80
20 40 60 80 100 120
cycle thickness (cm)
Interval IV
cycle thickness (cm) 20 40 60 80 100

Figure 4: Thickness variations of the limestone (white squares) and marl beds (black squares) and cycles (black line) in the Zumaia and Sopelana sections, with the selected intervals indicated. Cycle numbers are slightly shifted from those in figure 2, as "a" and "b" cycles are included in the numbering. Dashed lines indicate the 405-kyr minima in the cyclostratigraphic interpretation (large dashes) and the shifts from carbonate-rich to marl-dominated intervals occurring approximately every 1.2 Myr (small dashes).

3.2 Selected intervals

3.2.1 Interval I

The selected Danian interval of the Zumaia section displays a regular alternation of marls and limestones (Fig. 5). The thickness of the cycles is relatively constant, around 35 cm, but the relative proportions of the limestone and marl beds varies, with thicker limestones bounded by thinner marls and vice versa. Only near the base of the selected interval (from 0 to 1 m), the thickness of the dark marls contributes to thicker cycles. The main component of the sediment is calcium (44% CaO, or $3.1 * 10^5$ ppm Ca), followed by silica (18% SiO_2, or $8.5 * 10^4$ ppm Si) and aluminium (4% Al_2O_3, or $2.0 * 10^4$ ppm Al). The SiO_2 and Al_2O_3 records mirror the CaO record, which follows the weathering profile of the lithology, with high values of CaO at indurated limestone levels. The Ti/Al and Ba/Al ratios generally display the same cyclic pattern as CaO, with higher values in limestones than in marls, with a peak at 1.3 m, especially in Ti/Al, and a peak in Ba/Al at 2.8 m. Zr/Al shows a peak at 1.3 m. Lowest values of K/Al occur in ~100 kyr eccentricity maxima and highest values in eccentricity minima, although the pattern is scattered. Phosphorous (not shown) was too low to be reliably detected. Ni/Al, Zn/Al, Mo, Al, and Cu/Al show a pattern of relative enrichment in limestones with respect to marls, with a peak in Zn/Al and Mo/Al at 1.3 m, and a peak in Cu/Al at 2.6 m. Values of $\delta^{18}O$ seem to be higher in limestones than in marls, although there is some scatter in the values. $\delta^{13}C$ displays a general increasing trend, with lower values in the marls than in the limestones.

3.2.2 Interval II

The interval just below the K/Pg boundary in Zumaia contains very red to purple marls and marly limestones (Fig 6.). The thickness of the marly limestones is rather constant, while the thickness and colour of the marl beds is more variable and determines the variations in cycle thickness (Fig. 4). The main components of the sediment are silica (34% SiO_2, or 1.6 * 10^5ppm Si) and calcium (23% CaO, or 1.6 * 10^5 ppm Ca), followed by aluminium (10% Al_2O_3, or 5.3 * 10^4 ppm Al). SiO_2 and Al_2O_3 show a pattern of high values in the marls, and low values in the marly limestones, opposite to CaO. The Ti/Al, Zr/Al, K/Al, Ba/Al, Ni/Al, Zn/Al, Mo/Al, and Cu/Al values are highest and very variable just below the K/Pg boundary level. Further down Ti/Al and Zr/Al display higher values in marls and lower values in marly limestones, with a peak at 5.4 m, and K/Al displays lower values in marls and higher values in marly limestones. Ba/Al, Ni/Al and Zn/Al do not show a very clear pattern. Phosphorous (not shown) was too low to be reliably detected. Mo/Al has lowest values in a dark marl around 2.9 m and in a lighter marl around 5.5 m, and higher values in a limestone at 5m and in the more carbonate-rich interval below the K/Pg boundary. Cu/Al shows slightly higher values in the limestones than in the marls, particularly at 2 m. The $\delta^{18}O$ data show much scatter, with as much as 4‰ variations between adjacent samples. $\delta^{13}C$ shows an overall increase towards the K/Pg boundary. Magnetic susceptibility (MS) reveals a decrease, and total reflectance (L*) an increase. a*, which is a measure of the redness of the sediments, decreases near the K/Pg boundary, where the sediments have a more greenish grey colour. The geophysical stable isotope data do not clearly reflect the marl/marly limestone alternations.

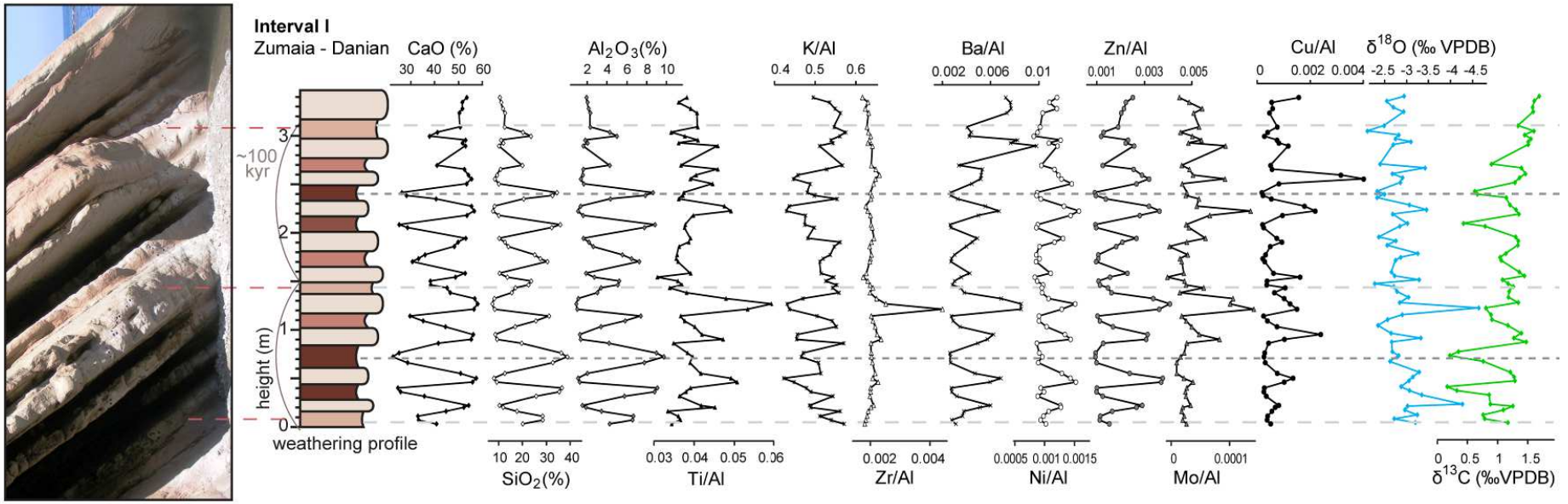

Figure 5: The selected Danian interval of the Zumaia section in a cove in the Punta Aitzgorri headland, with elemental, stable isotope and geophysical data. Light grey dashed lines indicate the ~100 kyr minima as identified in the lithology, dark grey dashed lines indicate levels of ~100 kyr maxima.

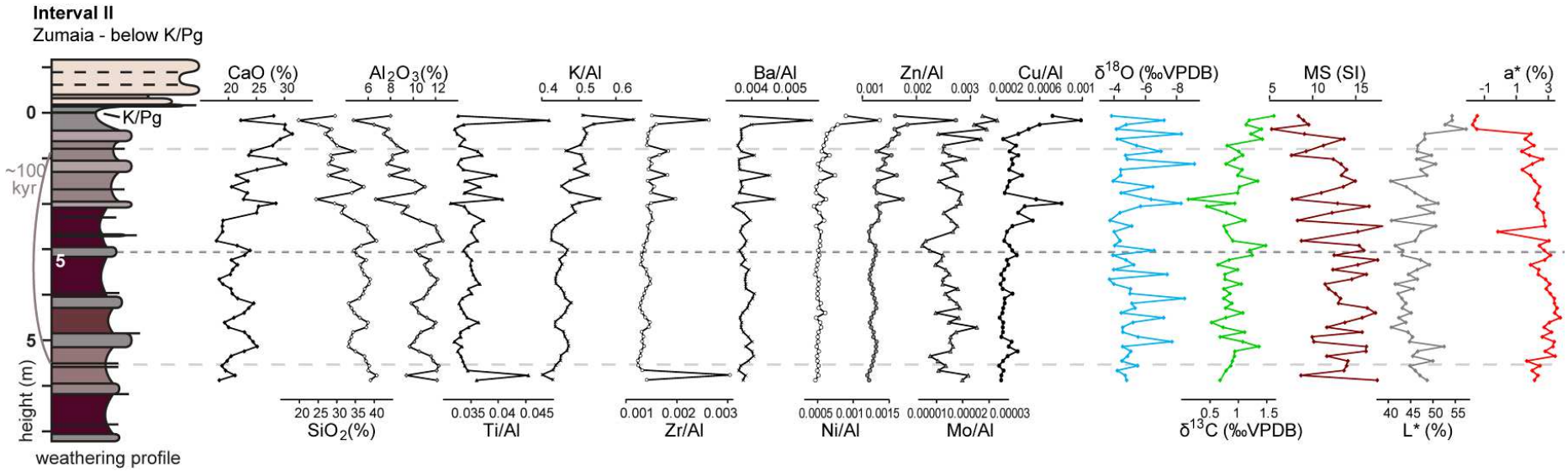

Figure 6: The interval in Zumaia just below the K/Pg boundary, with elemental, stable isotope and geophysical data. Light grey dashed lines indicate the ~100 kyr minima as identified in the lithology, dark grey dashed lines indicate levels of ~100 kyr maxima.

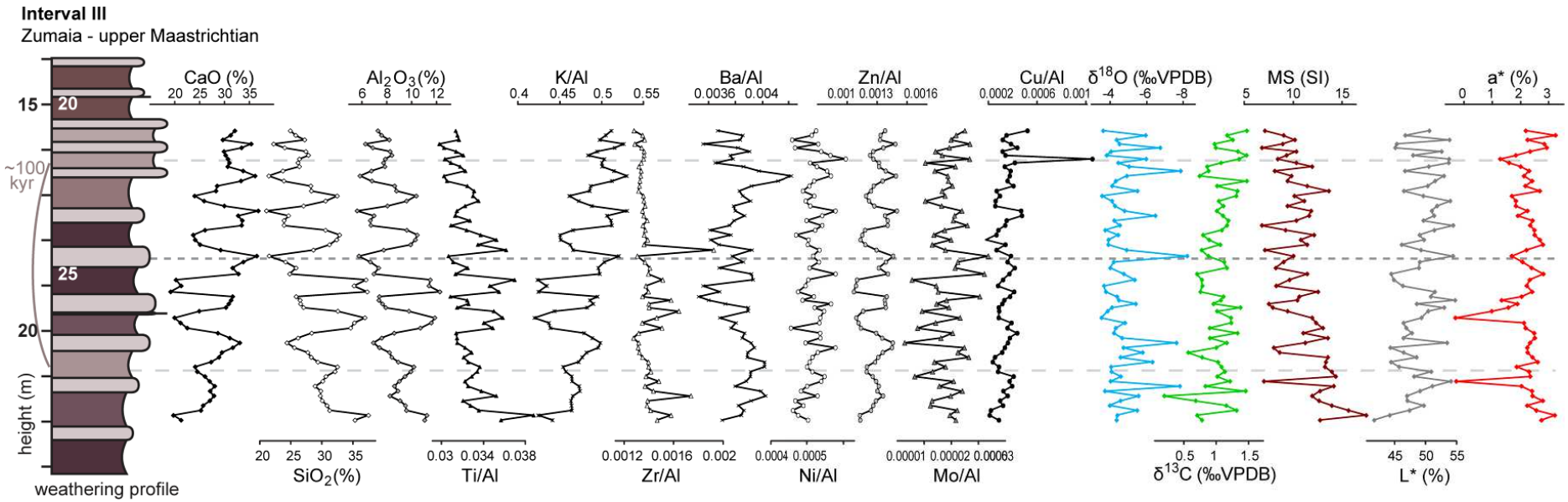

Figure 7: The upper Maastrichtian interval in Zumaia, in the second 405-kyr cycle, with elemental, stable isotope and geophysical data. Light grey dashed lines indicate the ~100 kyr minima as identified in the lithology, dark grey dashed lines indicate levels of ~100 kyr maxima.

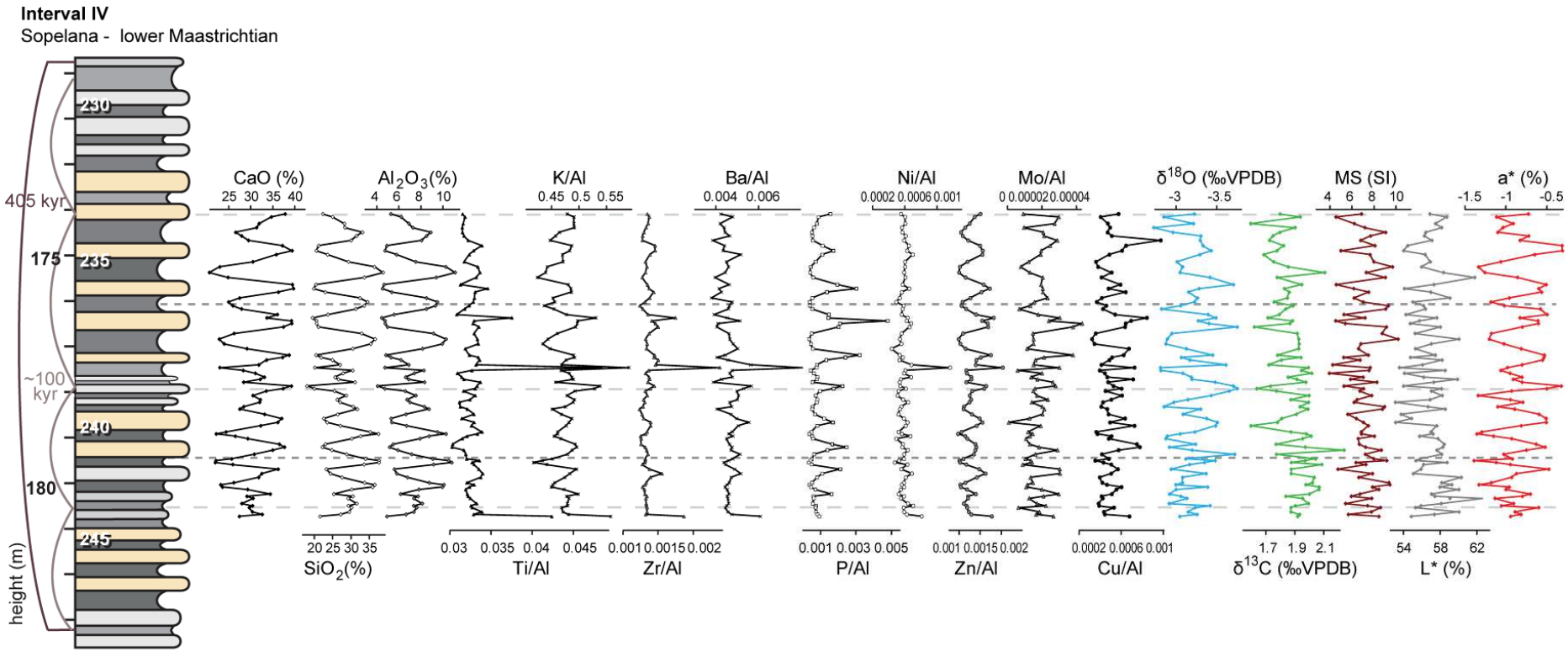

Figure 8: the lowermost 405-kyr cycle at Sopelana with interval IV, with elemental, stable isotope and geophysical data. Light grey dashed lines indicate the ~100 kyr minima as identified in the lithology, dark grey dashed lines indicate levels of ~100 kyr maxima.

3.2.3 Interval III

This interval shows a very regular alternation of limestones and marls, with clear variation in the darkness and thickness of the marls, which determines the thickness of the couplets (Figs. 4 and 7). The average concentration of CaO is 27%, or 1.9 * 10^5 ppm Ca, the average concentration of SiO_2 is 30%, or 1.4 * 10^5 ppm Si, and the average concentration of Al_2O_3 is 9%, or 4.8 * 10^4 ppm Al. The calcium content of the sediment increases towards the top of the interval. SiO_2, Al_2O_3, Ti/Al, and to some extent Zr/Al, display high values in the marls and low values in the limestones, while CaO and K/Al, show high values in the limestones. The Ba/Al ratio shows lowest values in the dark marls of cycle 24 and 25, and high values in cycle 22 and 23, and in cycle 27 and 28, near the ~100 kyr minima. Phosphorous (not shown) was too low to be reliably detected. The Ni/Al, Zn/Al, Mo/Al and Cu/Al ratios seem to be higher in the limestones than in the marls, although the pattern is slightly obscured by scatter. The $\delta^{18}O$ and a* records do not show a pattern, and $\delta^{13}C$ and reflectance (L*) values reveal an increase towards the top of the interval. Although the lithological alternations are not clearly reflected in the data, lowest values of $\delta^{13}C$ and reflectance (L*) and highest values of magnetic susceptibility (MS) occur in the marls and high values of $\delta^{13}C$ and reflectance (L*) and low vales of MS in the limestones.

3.2.4 Interval IV

The selected interval in the lower part of the Sopelana section shows a rhythmically bedded succession, with variations in thickness amongst both the marls and the limestones (Figs. 4 and 8). The most abundant element is calcium (31% CaO, or 2.2 * 10^5 ppm Ca), followed by silica (28% SiO_2, or 1.3 * 10^5 ppm Si) and aluminium (7% Al_2O_3, or 3.8 * 10^4 ppm Al). Ti/Al, Zr/Al, K/Al and Ba/Al show a peak at 177.5 m, which is likely due to a anomalously low value of Al. Beneath this peak, the pattern in Ti/Al is unclear, but in the upper half of the selected interval highest Ti/Al values seem to occur in the limestones and lowest values in the marls, a pattern which Zr/Al and K/Al values reveal throughout the interval. Ba/Al has lowest values in the

marls, and highest in the limestones, especially in the lower half of the interval. The interval in Sopelana is the only interval in which P/Al could be measured reliably, showing a clear cyclicity, with peaks in the limestone beds. The Ni/Al, Zn/Al, Mo/Al and Cu/Al ratios seem to be higher in the limestones than in the marls, although the records display some scatter. $\delta^{18}O$ shows a pattern of low values in the limestones and higher values in the marls. $\delta^{13}C$ does not show a clear pattern throughout, but in cycles 237 to 240 values seem lowest in the limestones . The geophysical data records of magnetic susceptibility and reflectance do not show an obvious pattern, while a*displays a very regular oscillation, with higher values in the limestones and lower values in the marls.

4. Discussion

4.1 Thickness variations

The bed thickness record displays the full range of periodicities of eccentricity-modulated precession. Maximal thickness variation between successive beds, coinciding with the maximal difference in lithologies, likely represents the maximal amplitude of the forcing, in case we assume a similar duration for the individual limestone-marl couplets. This allows to interpret these intervals as eccentricity maxima (Batenburg et al., 2012; Kuiper et al., 2008). The thickness record is very suitable as an additional cyclostratigraphic tool, especially for intervals where the variability of geophysical proxy records is relatively low, such as in the Sopelana section. In the lowermost part of that section, an additional 405-kyr cycle seems to be detected by the band-pass filter output (Fig. 3), which could be partly explained by the slightly longer length of the thickness record in comparison with the geophysical data records, and possibly by a reduced reliability of the filter output near the base of the section. With the determination of the influence of orbital forcing on the thickness record and the phase relationship with eccentricity, the direct cause of the thickness variations of the beds and couplets can be investigated.

4.2 Paleo-environmental interpretation

4.2.1 Interval I

The Danian interval shows relatively low contributions of silica and aluminium, and an average contribution of calcium that is twice as high as the average concentration in Interval II. This is in agreement with the generally much thinner cycles and siliciclastic sediment starvation of the basin during the Danian (Pujalte et al., 1998). The thickness variations suggest a combined influence of siliciclastic supply and productivity, except near the base of the interval, where clay input was dominant in determining cycle thickness. The Ti/Al and Zr/Al ratios indicate a higher dust input during ~100 kyr eccentricity maxima, specifically in the limestone beds, which may have spurred productivity, as suggested by coincident variations in Ba/Al. The variations in the redox sensitive elements Ni, Zn, Mo and Cu, corrected for their detrital influx by normalization to Al, indicate less oxic conditions in the sediment during limestone deposition. Reduced oxygenation may have occurred within the sediment subsurface as a result of organic matter degradation, resulting from increased productivity during limestone deposition. On a ~100-kyr time scale, lowest K/Al ratios, reflecting warm and wet conditions, occur during eccentricity maxima, and highest values of K/Al during eccentricity minima. The pattern of $\delta^{18}O$ might indicate warmer conditions during limestone deposition. Higher $\delta^{13}C$ values in limestones could indicate depletion of ^{12}C by increased productivity, especially during eccentricity minima.

Together, these observations suggest that activity of the hydrological cycle was amplified during eccentricity maxima, with more siliciclastic supply via run-off, and reduced during eccentricity minima. Within these eccentricity minima, limestone levels were deposited during driest conditions, with higher productivity possibly spurred by increased dust input. Levels of increased dust input and productivity can occur in the periods of lowest seasonal contrast (for the northern hemisphere precession maxima within eccentricity maxima) and in periods of prolonged absence of seasonal extremes during eccentricity minima.

4.2.2 Interval II

The selected interval just below the K/Pg boundary has the highest siliciclastic fraction of the intervals studied, and the lowest content of calcium. Bed thickness variations indicate that variations in siliciclastic supply were the main factor controlling the formation of the lithological alternations. The large riverine input required to deposit these sediments may have been the main factor in determining the concentrations of Ti and Ba, besides productivity and dust supply. The higher values of Ba/Al and Ti/Al in the marls may indicate a larger grain size of the deposited siliciclastic material. K/Al point to wet and warm conditions during marl deposition, and drier conditions during marly limestone formation. Of the redox sensitive elements, the Cu/Al and Mo/Al ratios suggest slightly less oxic conditions in the sediment during limestone deposition, but overall, the patterns of the redox sensitive elements are rather stable, except for the interval below the K/Pg boundary, which is probably related to the impact layer (Smit and Ten Kate, 1982). The high variability of $\delta^{18}O$ suggests that diagenetic overprinting played a role, especially in the limestone beds. Sediments are more carbonate-rich in cycles 2 and 3, which reflect a ~100-kyr eccentricity minimum near the top of the interval. This is also reflected in the geophysical data records. $\delta^{13}C$ values also rise towards the minimum of the 405-kyr eccentricity cycle, which spans the K/Pg boundary interval (Batenburg et al., 2012; Kuiper et al., 2008; ten Kate and Sprenger, 1993; Westerhold et al., 2008). A reduced hydrological cycle during eccentricity minima, would have led to less runoff and hence a decreased input of siliciclastics and ^{12}C into the basin. These observations support the hypothesis that the intensity of the hydrological cycle, controlled by eccentricity-modulated precession, was the primary forcing factor of the observed lithological cyclicity.

4.2.3 Interval III

The interval in the second 405-kyr cycle below the K/Pg boundary at Zumaia is characterised by a high siliciclastic contribution, albeit smaller than in Interval II, and the cycle thickness is mostly determined by the input of siliciclastic material. High values of Ti/Al and Zr/Al in the marls may indicate a larger grain size of the deposited terrigenous material. The redox sensitive elements point towards less oxic conditions in the sediment during limestone deposition, which could result from increased organic matter deposition. The Ba/Al ratio shows a gradual pattern across the interval, with higher values in the ~100 kyr eccentricity minima and lower values in the ~100 kyr maximum. This may indicate that the amount of productivity varied across these cycles, and was maximal when seasonal extremes were less pronounced, similar to the Danian interval (Interval I). K/Al reveals a pattern of high values in limestones and low values in marls, indicating wet conditions with more leaching during times of marl deposition, as in Interval II. The $\delta^{18}O$ values, which reach highest and most variable values in limestones, may be affected by diagenesis. The $\delta^{13}C$ values might either reflect a reduced input of ^{12}C-rich dissolved inorganic carbon or an increased productivity towards the top of the interval, or both. Taken together, the proxy data suggest a similar mechanism of formation as for interval I, albeit with a smaller siliciclastic input, and potentially more variability in productivity.

4.2.4 Interval IV

The selected interval near the base of the Sopelana section has a higher calcium content than the Maastrichtian intervals of Zumaia (intervals II and III) and variations in thickness of the cycles is determined by variations in thickness of both limestones and marls, which is in agreement with earlier findings (Alvarez-Llano et al., 2006). This suggests that the lithological alternations represent an interplay between clay input and carbonate productivity. Throughout the interval, Zr/Al ratios indicate a potentially higher dust input during limestone deposition, which is

corroborated by Ti/Al in the upper half of the interval. In accordance with this, K/Al ratios seem to display a similar pattern as in the Maastrichtian intervals at Zumaia, with higher values in limestones, indicating drier conditions during deposition. Ba values mostly seem to vary simultaneously with aluminium content, but in the lower half of the interval, Ba/Al ratios reveal some additional variability, suggesting higher productivity in the limestone levels. This is confirmed by the P/Al ratios, which indicate more organic matter deposition in limestone levels than in marls. A higher amount of organic matter may have caused less oxygenated conditions within the sediment, as observed in the redox sensitive element ratios. This suggests that the limestone levels represent periods of increased productivity, coincident with increased dust input, and higher temperatures, as indicated by $\delta^{18}O$. In this interval, $\delta^{18}O$ does not display much scatter and likely reflects primary oxygen isotope variations. The pattern is in very close agreement with the extremely high resolution measurements of 1 sample per 2 cm performed by Jiménez-Berrocoso et al. (2012). The $\delta^{13}C$, magnetic susceptibility and total reflectance do not display a clear pattern. However, the redness indicator a* closely follows the lithological alternations and could provide an additional proxy for cyclostratigraphic analysis.

4.3 Orbital forcing and paleoclimate

Hydrology was the most important driving factor for the observed sedimentary cyclicity, as variations in thickness are most pronounced in the marl-rich component of the limestone-marl couplets, while limestones remain more constant in thickness and induration. This suggests that the lithological variations are primarily influenced by the amount of siliciclastic supply, which likely reflects the impact of eccentricity-modulated precession on the hydrological cycle, with more continental runoff linked to high seasonal contrast during precession minima, especially at times of eccentricity maxima. This is in agreement with the findings of Mount and Ward (1986), who used the occurrence of turbidites, assuming they are unrelated to limestone or marl deposition, as an independent control on sedimentation rates.

Turbidites are spaced further apart in marl-rich intervals than in limestone-dominated intervals, indicating an increased sedimentation rate during marl-dominated deposition. As consequence, the limestone-marl alternations can be classified as dilution cycles, formed primarily by variations in siliciclastic supply. In particular, red marly intervals, such as the one studied just below the K/Pg boundary, show a dominant influence of siliciclastic supply. However, both the Danian interval at Zumaia and the lower Maastrichtian interval at Sopelana, and to some extent the interval ~20 m below the K/Pg boundary at Zumaia, reveal the additional influence of productivity on the lithological alternations. Limestones were deposited during dry conditions, with a higher productivity driven by increased dust input, and display higher $\delta^{18}O$ values, potentially indicating warmer conditions.

A third scenario, in which limestone-marl alternations are the result of dissolution, can be excluded. The depositional setting was relatively shallow at ~1500 m (as summarised in Pujalte et al., 1998), and therefore well above the levels of pressure-controlled dissolution,. Moreover, there are no indications for dissolution hardgrounds, or dissolution of pelagic and benthic organisms (Mount and Ward, 1986). It is likely that the basin was well oxygenated at all times, and that slight enrichments of redox sensitive elements may have occurred within the sediment as a result of organic matter degradation at times of limestone deposition. As the redox sensitive element enrichments do not occur during maximum siliciclastic input into the basin resulting from runoff, it can be concluded that episodes of increased hydrological activity did not lead to stratification and anoxia. The deeper waters of the narrow Basque-Cantabric Basin were always relatively well oxygenated during the deposition of the sedimentary succession.
The differences amongst the selected intervals mostly represent shifts in the importance of siliciclastic input and productivity, but the overall mode of sedimentation and the phase relationship with eccentricity-modulated precession seem to remain constant. The large scale alternations of limestone-dominated and marl-dominated intervals have been interpreted to reflect different sea level regimes (Pujalte et al., 1995). The reddish purple marls of Interval II were likely

deposited as part of a lowstand fan, and the other intervals during Transgressive or High Stand Systems Tracts (Alvarez-Llano et al., 2006; Pujalte et al., 1998, 1995), yet the inferred sea level variations do not represent substantial changes in the mode of sedimentation (Alvarez-Llano et al., 2006; Mount and Ward, 1986). However, after the K/Pg boundary, the siliciclastic input to the basin was greatly reduced, possibly indicating a change in the intensity of the hydrological cycle. Also, the response of the carbon cycle to the orbital forcing may have changed, as the oscillations in $\delta^{13}C$ in the Danian interval reflect the influence of the precessional cycle more strongly than the $\delta^{13}C$ variations in the Maastrichtian intervals.

The small scale lithological alternations of limestones and marls may represent a shift of climate zones, for example, the alternating influence of the temperate and arid belt (Jiménez Berrocoso et al., 2012). General circular models (GCMs) in combination with climate proxy data suggest that Late Cretaceous precipitation patterns in the subtropics may have been sensitive to orbital forcing, in particular to eccentricity-modulated precession (Barron et al., 1985; Beckmann et al., 2005; Flögel et al., 2008; Oglesby and Park, 1989; Park and Oglesby, 1991). For example, variations of the African monsoon intensity during the Late Cretaceous were likely driven by precession, with high fluvial discharge during maximum seasonal contrast (Beckmann et al., 2005). The influence of different orbital configurations were tested in GCM simulations by Floegel and Wagner (2006), which suggest an influence of insolation changes at 25–55°S on the intensity of the African Monsoon, through variation of pressure systems and variation in the magnitude and direction of surface winds. The existence of cross-latitudinal teleconnections during parts of the precessional cycle implies a reduced role of the tropics as drivers of Late Cretaceous climate. Closer to the Basque region, the northern margin of the Tethys ocean may have been sensitive to variations in seasonality, with increased seasonality leading to a stronger land-ocean contrast and intense winter precipitation (Barron et al., 1985). The high precipitation over the continental margin in this model simulation is not monsoonal in character but due to the changing position of mid-latitude storm tracks (Barron et al., 1985). In general, high ocean temperatures during the Late Cretaceous would have led to high levels of

precipitation (Oglesby and Park, 1989; Sellwood and Valdes, 2006). With a paleolatitude of the Zumaia and Sopelana section during the Maastrichtian between 30° and 35 °N (Hay et al., 1999), the sections would likely have been near the northern edge of the Hadley cell on the northern hemisphere, characterised by sinking dry air. GCM studies indicate an expansion of the Hadley cell during the Late Cretaceous, with a poleward shift of the sub-tropical high pressure belt to latitudes between 31° and 37°N (Hasegawa et al., 2012). We hypothesize that the Basque-Cantabric basin would have been very sensitive to seasonal shifts of the Inter Tropical Convergence Zone (ITCZ). Additionally, variations in pressure systems and wind patterns may have influenced the amount of precipitation on land-masses surrounding the Basque-Cantabric basin, leading to the variations in siliciclastic supply responsible for the limestone-marl rhythms at Zumaia and Sopelana.

Chapter 6. Summary and conclusions

The Zumaia and Sopelana sections in the Basque country in northern Spain provide a unique opportunity to improve our understanding of Late Cretaceous climate and the Maastrichtian time scale. The coastal cliffs contain limestones and marls that were originally deposited in a hemipelagic setting. The alternating lithologies reflect the periodicities of the Earth's orbital parameters of eccentricity and precession, with a maximal difference in lithologies representing the maximal amplitude of the forcing mechanism. Specifically, alternations of dark and thick marls with indurated limestones were formed in response to a large precessional amplitude during eccentricity maxima.

The recognition of the ratio of the periodicities of eccentricity-modulated precession allowed for reliably detecting the influence of the 405-kyr periodicity of eccentricity, which is stable over long time scales. Tuning to astronomical target curves provided a refinement of the Geologic Time Scale for the Maastrichtian. Nine 405-kyr cycles were detected at Zumaia, and correlation to Sopelana enabled to extend this cyclostratigraphic framework to a total of thirteen 405-kyr cycles, spanning a total of 5.3 Myr. The cyclostratigraphic interpretation, based on the lithological alternations, was confirmed by time series analysis of high resolution climatically sensitive records; the geophysical properties colour reflectance and magnetic susceptibility, and the stable carbon isotope ratios of bulk carbonate. Magnetostratigraphic and biostratigraphic data were obtained so that the orbital tuning can be applied globally. The change from normal polarity in magnetochron C32n1n to the reversed polarity of C31r, which took place shortly after the Campanian-Maastrichtian transition, was detected near the base of the Sopelana section. In the Zumaia section, the C31r/C31n reversal was reliably detected, and the position of the base of C29r was established by correlation. New planktonic foraminifer data were obtained for the Zumaia section and samples from the Sopelana section were studied for calcareous nannoplankton bio-events. These results were combined with existing biostratigraphic data and reveal considerable diachroneity for the studied Maastrichtian interval.

In addition, the carbon isotope stratigraphy of the Basque sections reveals a strong influence of the 405-kyr cycle of eccentricity-modulated precession on the carbon cycle. An increased hydrological cycle may have carried more of the lighter isotope of carbon to the basin. Additionally, negative shifts occur approximately every 1.2 Myr, coinciding with marked lithological changes at Zumaia, which have been interpreted as relative falls in sea level. The large amplitude of variation and the high resolution of the orbitally tuned carbon isotope curve allow for a detailed global correlation to late Campanian-Maastrichtian carbon isotope stratigraphies. Although there is much variation in carbon isotope curves amongst sections, a series of trends and excursions can be observed across different paleo-environmental settings. The age model indicates less variation in sedimentation rates than previous correlation efforts. The correlation reveals that the late Campanian/ Maastrichtian carbon cycle was strongly influenced by the 405-kyr periodicity of eccentricity and potentially paced by longer periodicities.

Finally, to understand the paleoclimatic and paleo-environmental causes of the rhythmic limestone-marl alternations, the thickness of the individual limestone and marl beds has been analysed throughout the Maastrichtian part of the Zumaia and Sopelana sections. Also, several intervals were selected in the Upper Maastrichtian and the Danian of the Zumaia section, and in the lower Maastrichtian of the Sopelana section. These intervals have been analysed in a high resolution for variations in elements, stable isotope ratios, and geophysical properties. These data revealed that the marl-rich part of the limestone-marl couplets was formed during maximal seasonal contrast, for the northern hemisphere during precession minima, which amplified hydrological activity and caused more runoff, carrying siliciclastic material, to the Basque-Cantabric basin. This basin was a deep, narrow trough between the Iberian and the European plate. Due to its restricted nature, it was sensitive to local and regional climatic variations. Periods of low seasonal contrast or long-term avoidance of seasonal extremes were characterised by dry conditions, with an increased dust deposition which spurred biological productivity. The terrigenous siliciclastic input was the dominant control on sedimentation rates, classifying the limestone-marl alternations as dilution cycles.

Future outlook

To fully anchor the astronomically tuned Maastrichtian time scale, and thereby enable the development of an absolute geologic time scale for the Mesozoic, the age of the Cretaceous/ Paleogene boundary needs to be resolved. This is expected to occur swiftly, by the ongoing intercalibration of radiometric and astronomical dating techniques, and potentially by the continuous detection of orbital periodicities throughout the entire Cenozoic. However, it is likely that the Late Cretaceous cannot be fully resolved by astronomical tuning efforts. For example, there is a scarcity of Campanian cyclic successions and cyclostratigraphic studies. For older successions, independent age control can be obtained from radiometric dating techniques, but the cumulative error of these techniques and the astronomical solution may inhibit the development of an anchored astronomical time scale for the Late Cretaceous. Despite a potential limit to astronomical tuning, cyclostratigraphy may still provide a valuable tool for establishing durations. Also, the recognition of long-term periodicities further back in time may shed light on the chaotic behaviour of the solar system. Additionally, long term cyclicities in the carbon cycle may point to internal feedback mechanism of Late Cretaceous climate. The ongoing development of detailed carbon isotope stratigraphies from different oceanographic settings is expected to greatly improve our understanding of the Late Cretaceous carbon cycle.

Acknowledgements

I am very grateful to my colleagues, friends and family for their help and support. You helped me feel at home in strange countries and you did not forget about me while I was far away.

First of all, my thanks go to Frits Hilgen, Mario Sprovieri and Andy Gale. While I was finishing my master's studies in Utrecht, Frits allowed me to join the first year's fieldwork in Spain as a junior (baby) staff member together with Desiree. On the way there, he showed us the Zumaia section and he was the only one to keep his socks dry when visiting the Cretaceous/Paleogene boundary. Thank you Frits, for sharing your stratigraphic insight and for your inspiration! I want to thank Mario for being an oceanographic mastermind and for keeping me out of bureaucratic trouble. You made me discover Italy, and I will always feel a bit homesick. Andy, thank you for introducing me to all the fascinating field geology and to some delicious mushrooms.

In the field, the help of Janja de Jonge, Agnes van Loevezijn, Christian Zeeden, Mattia Vallefuoco, Fabrizio Lirer, Jan Smit, Alessandro Montanari and Rodolfo Coccioni was indispensible. Xabier Orue-Etxebarria, Estibaliz Apellániz, Nicolas Thibault, Myriam Boussaha have gone out of their way to help with the biostratigraphy of the successions. I would also like to thank Silja Hüsing for her help with interpreting the paleomagnetic results, and Juan Ignacio Baceta for taking additional samples. I thank David Wray for being so kind to run our samples for XRF analysis. Thanks to Michele Iavarone for his help with the stable isotope analysis, and to Silke Voigt for helping with the correlation. Nicola Pelosi lent a hand with the statistical analysis of the records and Jacques Laskar kindly allowed us to use his latest, partly unpublished results. I would also like to thank Simone Galeotti, Domenico Rio, David Loydell and Jim Hendry for their kind and constructive comments.

Vorrei ringraziare i miei colleghi e amici Napoletani, per farmi sentire a casa e per la pazienza quando stavo imparando l'italiano. Grazie Antonio e Ananda e la piccola Thea, Mattia e Stella, Barbara, Roberto, Ciccio, Miscia e sopratutto Luciana, per condividere un po della vostra vita con me.

I thank my colleagues within the GTSnext project, Jon and Ben, Christian, Anne, Leah, Ariadna, Tiffany, Jörn, Joe and Diana, for the motivation, and Klaudia for all your organising efforts.

I am very grateful to all the wonderful extraordinary people at the department in Portsmouth. I sincerely thank Sarah B., Sarah P., Mark, Richard, Graeme, Emilie and all the postgrad students for sharing so many great experiences.

Ik wil graag mijn vrienden Gijs, Willem, Desiree, en Sanne bedanken dat jullie me overal op zijn komen zoeken, en ook op afstand altijd betrokken zijn. Diederik, bedankt voor je wijsheid, hulp en geduld, en dat je in mijn leven bent. Ik ben mijn ouders, Loek en Geertje, en mijn zus, Anneke, heel dankbaar voor al hun steun. Bedankt dat jullie er altijd voor me zijn en ik hoop dat ik meer tijd met jullie door kan brengen in de toekomst.

References

Adhémar, J., 1842. Révolutions de la mer, deluges periodiques. Carilian-Goeury et V. Dalmont, Paris.

Alvarez, W., Alvarez, L. W., Asaro, F. & Michel, H. V. 1982. Current status of the impact theory for the Terminal Cretaceous extinction. Geol. Soc. Am. spec. Pap. 190: 305-315.

Alvarez-Llano, I., Baguer, A., Martinez López de Sabando, M., Mugica, J., Pérez-García, J.R., Unanue, L., Elorza, J., 2006. Variaciones de espesor y de contenido en CaCO3 en los pares marga-caliza del Maastrichtiense inferior en Sopelana (Arco Vasco). Geogazeta 39, 131–134.

Apellaniz, E., Baceta, J.I., Bernaola-Bilbao, G., Núñez-Betelu, K., Orue-Etxebarria, X., Payros, A., Pujalte, V., Robin E. & Rocchia R. 1997. Analysis of uppermost Cretaceous-lowermost Tertiary hemipelagic successions in the Basque Country (Western Pyrenees): evidence for a sudden extinction of more than half planktic foraminifer species at the K/T boundary. Bulletin de la Societé Géologique de France 168(6): 783-793.

Arthur, M.A., Fischer, A.G., 1977. Upper Cretaceous-Paleocene magnetic stratigraphy at Gubbio, Italy.I. Lithostratigraphy and sedimentology. GSA Bulletin 88, 367–371.

Barker, P.F., Kennett, J.P., And the Shipboard Scientific Party, 1990. Proceedings of the Ocean Drilling program, Scientific Results, 113. Ocean Drilling Program, College Station, TX.

Barrera, E., Huber, B.T., 1990. Evolution of Antarctic Waters during the Maestrichtian: Foraminifer Oxygen and Carbon Isotope Ratios, Leg 113. Barker, P. F., Kenett, J. P., and the Shipboard Scientific Party. Proceedings of the Ocean Drilling Program, Scientific Results 113, 813–827.

Barrera, E., Savin, S.M., 1999. Evolution of late Campanian-Maastrichtian marine climates and oceans, in: Barrera, E.J., and Johnson, C. C. (Eds.). Evolution of the Cretaceous Ocean-Climate System, Geological Society of America Special Paper. pp. 245–282.

Barrera, E., Savin, S.M., Thomas, E., Jones, C.E., 1997. Evidence for thermohaline-circulation reversals controlled by sea-level change in the latest Cretaceous. Geology 25, 715.

Barron, E.J., Arthur, M.A., Kauffman, E.G., 1985. Cretaceous rhythmic bedding sequences: a plausible link between orbital variations and climate. Earth and Planetary Science Letters 72, 327–340.

Batenburg, S.J., Sprovieri, M., Gale, A.S., Hilgen, F.J., Hüsing, S., Laskar, J., Liebrand, D., Lirer, F., Orue-Etxebarria, X., Pelosi, N., Smit, J., 2012. Cyclostratigraphy and astronomical tuning of the Late Maastrichtian at Zumaia (Basque country, Northern Spain). Earth and Planetary Science Letters 359–360, 264–278.

Beckmann, B., Flögel, S., Hofmann, P., Schulz, M., Wagner, T., 2005. Orbital forcing of Cretaceous river discharge in tropical Africa and ocean response. Nature 437, 241–244.

Berger, A., 1978. Long-Term Variations of Caloric Insolation Resulting from the Earth's Orbital Elements. Quaternary Research 9, 139–167.
Berger, A., Loutre, M.F., 1994. Astronomical Forcing through Geological Time, in: De Boer, P.L., Smith, D.G. (Eds.), Orbital Forcing and Cyclic Sequences., Special Publication 19, International Association of Sedimentologists. Blackwell Scientific, Oxford, pp. 15–24.
Bornemann, A., Norris, R.D., Friedrich, O., Beckmann, B., Schouten, S., Damste, J.S.S., Vogel, J., Hofmann, P., Wagner, T., 2008. Isotopic Evidence for Glaciation During the Cretaceous Supergreenhouse. Science 319, 189–192.
Bouligand, C., Dyment, J., Gallet, Y., Hulot, G., 2006. Geomagnetic field variations between chrons 33r and 19r (83-41 Ma) from sea-surface magnetic anomaly profiles. Earth and Planetary Science Letters 250, 541–560.
Bown, P., 1998. Calcareous Nannofossil Biostratigraphy, British Micropalaeontological Society Publication Series. Chapman and Hall; Kluwer Academic, London.
Bralower, T.J., Premoli Silva, I., Malone, M.J., And the Shipboard Scientific Party, 2002. Site 1210B. Proceedings of the Ocean Drilling Program, Preliminary Reports 198, 1–89.
Bralower, T.J., Siesser, W.G., 1992. Cretaceous Calcareous Nannofossil Biostratigraphy of Sites 761, 762, and 763, Exmouth and Wombat Plateaus, Northwest Australia. Proceedings of the Ocean Drilling Program, Scientific Results 122, 529–556.
Brumsack, H.-J., 1989. Geochemistry of recent TOC-rich sediments from the Gulf of California and the Black Sea. Geologische Rundschau 78, 851–882.
Burnett, J.A., 1990. A new nannofossil zonation scheme for the boreal Campanian. INA newsletter 12, 67–70.
Burnett, J.A., Gallagher, M.J., Hampton, M.J., 1998. Upper Cretaceous, in: P.R. Bown (Ed.), Calcareous Nannofossil Biostratigraphy, British Micropalaeontological Society Series. Chapman & Hall/Kluwer Academic Publishers, London, pp. 132–199.
Calvert, S.., Pedersen, T.., 1993. Geochemistry of Recent oxic and anoxic marine sediments: Implications for the geological record. Marine Geology 113, 67–88.
Calvert, S.E., 1983. Geochemistry of pleistocene sapropels and associated sediments from the eastern mediterranean. Oceanologica Acta 6, 255–267.
Calvert, S.E., Pedersen, T.F., 2007. Elemental Proxies for Palaeoclimatic and Palaeoceanographic Variability in Marine Sediments: Interpretation and Application, in: Developments in Marine Geology.
Cande, S.C., Kent, D.V., 1992. A New Geomagnetic Polarity Time Scale for the Late Cretaceous and Cenozoic. Journal of Geophysical Research 97, 13917–13951.
Cande, S.C., Kent, D.V., 1995. Revised calibration of the geomagnetic polarity time scale for the Late Cretaceous and Cenozoic. Journal of Geophysical Research 100, 6093–6095.
Channell, J.E.T., Lowrie, W., Medizza, F., Alvarez, W., 1978. Palaeomagnetism and tectonics in Umbria, Italy. Earth and Planetary Science Letters 39, 199–210.

Chauris, H., LeRousseau, J., Beaudoin, B., Propson, S., Montanari, A., 1998. Inoceramid extinction in the Gubbio basin (northeastern Apennines of Italy) and relations with mid-Maastrichtian environmental changes. Palaeogeography, Palaeoclimatology, Palaeoecology 139, 177–193.

Chave, A.D., 1984. Lower Paleocene-Upper Cretaceous Magnetostratigraphy, Sites 525, 527, 528, and 529, Deep Sea Drilling Project Leg 74, in: Moore, T. C., Jr., Rabinowitz, P. D., Et Al., Initial Reports of the Deep Sea Drilling Project. pp. 525–532.

Chow, T.J., Goldberg, E.D., 1960. On the marine geochemistry of barium. Geochimica et Cosmochimica Acta 20, 192–198.

Clarke, L.J., Jenkyns, H.C., 1999. New oxygen isotope evidence for long-term Cretaceous climatic change in the Southern Hemisphere. Geology 27, 699–702.

Croll, J., 1864. On the physical cause of the change of climate during geological epochs. Philosophical Magazine Series 4 28, 121–137.

Dehairs, F., Baeyens, W., Goeyens, L., 1992. Accumulation of Suspended Barite at Mesopelagic Depths and Export Production in the Southern Ocean. Science 258, 1332–1335.

Dinarès-Turell, J., Baceta, J.I., Pujalte, V., Orue-Etxebarria, X., Bernaola, G., Lorito, S., 2003. Untangling the Palaeocene climatic rhythm: an astronomically calibrated Early Palaeocene magnetostratigraphy and biostratigraphy at Zumaia (Basque basin, northern Spain). Earth and Planetary Science Letters 216, 483–500.

Domínguez, E., Echeberria, J., Gómez-Urtasun, I., Ibisate, R., Martínez-García, B., Elorza, J., 2007. Espesores y contenido de CaCO3 en los pares marga-caliza del Daniense (Sopelana, Arco Vasco). Geogazeta 41:, 67–70.

Einsele, G., 1982. Limestone-Marl Cycles (Periodites): Diagnosis, Significance, Causes — a Review, in: Einsele, P.D.G., Seilacher, P.D.A. (Eds.), Cyclic and Event Stratification. Springer Berlin Heidelberg, pp. 8–53.

Elorza, J., García-Garmilla, F., 1998. Palaeoenvironmental implications and diagenesis of inoceramid shlls (Bivalvia) in the mid-Maastrichtian beds of the Sopelana, Zumaya and Bidart sections (coast of the Bay of Biscay, Basque Country). Palaeogeography, Palaeoclimatology, Palaeoecology 141, 303–328.

Emiliani, C., 1955. Pleistocene temperatures. The Journal of Geology 63, 538–578.

Fienga, A., Laskar, J., Kuchynka, P., Manche, H., Desvignes, G., Gastineau, M., Cognard, I., Theureau, G., 2011. The INPOP10a planetary ephemeris and its applications in fundamental physics. Celestial Mechanics and Dynamical Astronomy 111, 363–385.

Fiet, N., Beaudoin, B., Parize, O., 2001. Lithostratigraphic analysis of Milankovitch cyclicity in pelagic Albian deposits of central Italy: implications for the duration of the stage and substages. Cretaceous Research 22, 265–275.

Fischer, A.G., Hilgen, F.J., Garrison, R.E., 2009. Mediterranean contributions to cyclostratigraphy and astrochronology. Sedimentology 56, 63–94.

Flögel, S., Beckmann, B., Hofmann, P., Bornemann, A., Westerhold, T., Norris, R.D., Dullo, C., Wagner, T., 2008. Evolution of tropical watersheds and continental hydrology during the Late Cretaceous greenhouse; impact on marine carbon

burial and possible implications for the future. Earth and Planetary Science Letters 274, 1–13.
Floegel, S., Wagner, T., 2006. Insolation-control on the Late Cretaceous hydrological cycle and tropical African climate—global climate modelling linked to marine climate records. Palaeogeography, Palaeoclimatology, Palaeoecology 235, 288–304.
Frank, T.D., Arthur, M.A., 1999. Tectonic forcings of Maastrichtian ocean-climate evolution. Paleoceanography 14, 103–117.
Friedrich, O., Herrle, J.O., Kößler, P., Hemleben, C., 2004. Early Maastrichtian stable isotopes: changing deep water sources in the North Atlantic? Palaeogeography, Palaeoclimatology, Palaeoecology 211, 171–184.
Friedrich, O., Herrle, J.O., Wilson, P.A., Cooper, M.J., Erbacher, J., Hemleben, C., 2009. Early Maastrichtian carbon cycle perturbation and cooling event: Implications from the South Atlantic Ocean. Paleoceanography 24.
Friedrich, O., Norris, R.D., Erbacher, J., 2012. Evolution of middle to Late Cretaceous oceans--A 55 m.y. record of Earth's temperature and carbon cycle. Geology 40, 107–110.
Galbrun, B., 1992. Magnetostratigraphy of Upper Cretaceous and Lower Tertiary Sediments, Sites 761 and 762, Exmouth Plateau, Northwest Australia. Proceedings of the Ocean Drilling Program, Scientific Results 122, 699–716.
Galbrun, B., Gardin, S., 2004. New chronostratigraphy of the Cretaceous-Paleogene boundary interval at Bidart (France). Earth and Planetary Science Letters 224, 19–32.
Gale, A.S., Jenkyns, H.C., Kennedy, W.J., Corfield, R.M., 1993. Chemostratigraphy versus biostratigraphy: data from around the Cenomanian/Turonian boundary. Journal of the Geological Society, London 150, 29–32.
Gale, A.S., Young, J.R., Shackleton, N.J., Crowhurst, S.J., Wray, D.S., 1999. Orbital tuning of Cenomanian marly chalk successions: towards a Milankovitch time-scale for the Late Cretaceous. Philosophical Transactions Royal Society London A 357, 1815–1829.
Gardin, S., Galbrun, B., Thibault, N., Coccioni, R., Silva, I.P., 2012. Bio-magnetochronology for the upper Campanian - Maastrichtian from the Gubbio area, Italy: new results from the Contessa Highway and Bottaccione sections. Newsletters on Stratigraphy.
Gardin, S., Odin, G.S., Bonnemaison, M., Melinte, M., Monechi, S., Von Salis, K., 2001. Results of the cooperative study on the calcereous nannofossils across the Campanian-Maastrichtian boundary at Tercis les Bains (Landes, France), in: Gilles S. Odin (Ed.), Odin, G.S. (ed.). The Campanian-Maastrichtian Stage Boundary - Characterization at Tercis Les Bains (France) and Correlation with Europe and Other Continents., Developments in Palaeontology and Stratigraphy. Elsevier, pp. 293–309.
Gilbert, G.K., 1895. Sedimentary measurement of Cretaceous time. The Journal of Geology 3, 121–127.
Gómez –Alday, J.J., Zuluaga, M.C., Elorza, J., 2008. 87Sr/86Sr ratios in inoceramids (Bivalvia) and carbonate matrix as indicators of differential diagenesis during burial. Early Maastrichtian Bay of Biscay sections (Spain and France). Potential use for chemostratigraphy? Cretaceous Research 29, 563–576.

Gómez-Alday, J.J., López, G., Elorza, J., 2004. Evidence of climatic cooling at the Early/Late Maastrichtian boundary from inoceramid distribution and isotopes: Sopelana sections, Basque Country, Spain. Cretaceous Research 25, 649–668.

Gradstein, F.M., Ogg, J.., Smith, A.G., 2004. A Geologic Time Scale 2004. Cambridge University Press, New York.

Grinsted, A., Moore, J.C., Jevrejeva, S., 2004. Application of the cross wavelet transform and wavelet coherence to geophysical time series. Nonlinear Processes in Geophysics 11, 561–566.

H.Z., Sprenger, A., 1993. Orbital cyclicities above and below the Cretaceous/Paleogene boundary at Zumaya (N Spain), Agost and Relleu (SE Spain). Sedimentary Geology 87, 69–101.

Hamilton, N.P.F., 1990. Mesozoic Magnetostratigraphy of Maud Rise, Antarctica, in: Barker, P. F., Kennett, J. P., and the Shipboard Scientific Party. Proceedings of the Ocean Drilling Program: Scientific Results. pp. 255–260.

Hasegawa, T., Crampton, J.S., Schiøler, P., Field, B., Fukushi, K., Kakizaki, Y., 2012. Carbon isotope stratigraphy and depositional oxia through Cenomanian/Turonian boundary sequences (Upper Cretaceous) in New Zealand. Cretaceous Research.

Hay, W.W., DeConto, R.M., Wold, C.N., Wilson, K.M., Voigt, S., Schulz, M., Wold, A.R., Dullo, W.C., Ronov, A.B., Balukhovsky, A.N., Soding, E., 1999. Alternative global Cretaceous paleogeography, in: Barrera, E., Johnson, C. C. (Eds.),Evolution of the Cretaceous Ocean-climate System, Geological Society of America Special Paper. Boulder, pp. 1–47.

Helz, G.R., Miller, C.V., Charnock, J.M., Mosselmans, J.F.W., Pattrick, R.A.D., Garner, C.D., Vaughan, D.J., 1996. Mechanism of molybdenum removal from the sea and its concentration in black shales: EXAFS evidence. Geochimica et Cosmochimica Acta 60, 3631–3642.

Henriksson, A.S., 1993. Biochronology of the terminal Cretaceous calcareous nannofossil Zone of Micula prinsii. Cretaceous Research 14, 59–68.

Herbert, T., 1992. Paleomagnetic calibration of Milankovitch cyclicity in Lower Cretaceous sediments. Earth and Planetary Science Letters 112, 15–28.

Herbert, T., 1999. Toward a composite orbital chronology for the Late Cretaceous and Early Palaeocene GPTS. Philosophical Transactions Royal Society London A 357, 1891–1905.

Herbert, T.D., D'Hondt, S.L., 1990. Precessional climate cyclicity in late Cretaceous-early Tertiary marine sediments: a high resolution chronometer of Cretaceous-Tertiary boundary events. Earth and Planetary Science Letters 99, 263–275.

Herbert, T.D., Fischer, A.G., 1986. Milankovitch climatic origin of mid-Cretaceous black shale rhythms in central Italy. Nature 321, 739–743.

Herbert, T.D., Premoli Silva, I., Erba, E., Fischer, A.G., 1995. Orbital chronology of Cretaceous-Paleocene marine sediments., in: Berggren, W.A., Kent, D.V. Aubry, M.-P., Hardenbol, J. (Eds) Geochronology Time Scales and Global Stratigraphic Correlation, SEPM Special Publication. pp. 81–92.

Herm, D., 1965. Mikropaläontologisch-stratigraphische Untersuchungen im Kreideflysch zwischen Deva und Zumaya (Prov. Guipuzcoa, Nordspanien). Zeitschrift der Deutschen Geologischen Gesellschaft 115, 277–342.

Hilgen, F.J., Aziz, H.A., Krijgsman, W., Langereis, C.G., Lourens, L.J., Meulenkamp, J.E., Raffi, I., Steenbrink, J., Turco, E., Vugt, N. van, Wijbrans, J.R., Zachariasse, W.J., 1999. Present status of the astronomical (polarity) time-scale for the Mediterranean Late Neogene. Phil. Trans. R. Soc. Lond. A 357, 1931–1947.

Hilgen, F.J., Kuiper, K.F., Lourens, L.J., 2010. Evaluation of the astronomical time scale for the Paleocene and earliest Eocene. Earth and Planetary Science Letters 300, 139–151.

Hinnov, L.A., 2000. New Perspectives on Orbitally Forced Stratigraphy. Annual Review of Earth and Planetary Sciences 419–75.

Hinnov, L.A., Ogg, J.., 2007. Cyclostratigraphy and the Astronomical Time Scale. Stratigraphy 4, 239–251.

Holbourn, A., Kuhnt, W., Schulz, M., Flores, J.A., Andersen, N., 2007. Orbitally-paced climate evolution during the middle Miocene. Earth and Planetary Science Letters 261, 534–550.

Huber, B.T., 1990. Maestrichtian planktonic foraminifer biostratigraphy of the Maud Rise (Weddel Sea, Antarctica): ODP Leg 113 Holes 698B and 690C, in: Barker, P. F., Kennet, P. J. Et Al., Proceedings of the Ocean Drilling Program, Scientific Results. pp. 489–513.

Huber, B.T., 1992. Upper cretaceous planktic foraminiferal biozonation for the austra realm. Marine Micropaleontology 20, 107–128.

Huber, B.T., Hodell, D.A., Hamilton, C.P., 1995. Middle–Late Cretaceous climate of the southern high latitudes: Stable isotopic evidence for minimal equator-to-pole thermal gradients. Geological Society of America Bulletin 107, 1164–1191.

Huber, B.T., Watkins, D.K., 1992. Biogeography of Campanian-Maastrichtian calcareous plankton in the region of the Southern Ocean: Paleogeographic and paleoclimatic implications, in: Kennett, J.P., Warnke, D.A. (Eds.), The Antarctic Paleoenvironment: A Perspective on Global Change, American Geophysical Union, Antarctic Research Series. American Geophysical Union, Washington, pp. 31–60.

Husson, D., Galbrun, B., Laskar, J., Hinnov, L.A., Thibault, N., Gardin, S., Locklair, R.E., 2011. Astronomical calibration of the Maastrichtian (Late Cretaceous). Earth and Planetary Science Letters 305, 328–340.

Jarvis, I., Gale, A.S., Jenkyns, H.C., Pearce, M.A., 2006. Secular variation in Late Cretaceous carbon isotopes: a new δ13C carbonate reference curve for the Cenomanian–Campanian (99.6–70.6 Ma). Geol. Mag. 143, 561–608.

Jarvis, I., Mabrouk, A., Moody, R.T.., De Cabrera, S., 2002. Late Cretaceous (Campanian) carbon isotope events, sea-level change and correlation of the Tethyan and Boreal realms. Palaeogeography, Palaeoclimatology, Palaeoecology 188, 215–248.

Jenkyns, H.C., Gale, A.S., Corfield, R.M., 1994. Carbon-and oxygen-isotope stratigraphy of the English Chalk and Italian Scaglia and its paleoclimatic significance. Geological Magazine 131, 1–1.

Jiménez Berrocoso, Á., Elorza, J., MacLeod, K.G., 2012. Proximate environmental forcing in fine-scale geochemical records of calcareous couples (Upper Cretaceous and Palaeocene of the Basque-Cantabrian Basin, eastern North Atlantic). Sedimentary Geology.

Jung, C., Voigt, S., Friedrich, O., 2012. High-resolution carbon-isotope stratigraphy across the Campanian–Maastrichtian boundary at Shatsky Rise (tropical Pacific). Cretaceous Research 37, 177–185.

Kirschvink, J.L., 1980. The least-square line and plane and the analysis of paleomagnetic data. Geophysical Journal International 62, 699–718.

Küchler, T., Odin, G.S., 2001. Upper Campanian-Maastrichtian ammonites (Nostoceratidae, Diplomoceratidae) from tercis les bains (landes, France), in: The Odin, G. S. (ed.). Gampanian-Maastrichtian Stage Boundary - Characterization at Tercis Les Bains (France) and Correlation with Europe and Other Continents., Developments in Palaeontology and Stratigraphy. pp. 500–528.

Kuiper, K.F., Deino, A., Hilgen, F.J., Krijgsman, W., Renne, P.R., Wijbrans, J.R., 2008. Synchronizing Rock Clocks of Earth History. Science 320, 500–504.

Lamolda, M.A., 1990. The Cretaceous-Tertiary boundary crisis at Zumaya (Northern Spain). Micropaleontological data, in: Kauffman, E.G. and O.H. Walliser, Eds. Extinction Events in Earth History, Lecture Notes in Earth Sciences. Springer Verlag, Leiden, pp. 393–399.

Lamolda, M.A., Orue-Etxebarria, X., Proto-Decima, F., 1983. The Cretaceous-Tertiary boundary in Sopelana (Biscay, Basque Country). Zitteliana 10, 663–670.

Laskar, J., Fienga, A., Gastineau, M., Manche, H., 2011a. La2010: A new orbital solution for the long term motion of the Earth. Astronomy and Astrophysics 532, A89.

Laskar, J., Gastineau, M., Delisle, J.-B., Farrés, A., Fienga, A., 2011. Strong chaos induced by close encounters with Ceres and Vesta. Astronomy and Astrophysics 532, L4.

Laskar, J., Joutel, F., Boudin, F., 1993. Orbital, precessional and insolation quantities for the Earth from -20 myr to +10 myr. Astronomy and Astrophysics 270, 522–533.

Laskar, J., Robutel, P., Joutel, F., Gastineau, M., Correia, A.C.M., Levrard, B., 2004. A long-term numerical solution for the insolation quantities of the Earth. Astronomy and Astrophysics 428, 261–285.

Lees, J.A., Bown, P.R., 2005. Upper Cretaceous calcareous nannofossil biostratigraphy, ODP Leg 198 (Shatsky Rise, northwest Pacific ocean), in: Bralower, T.J., Premoli-Silva, I., Malone, M.J., Proceedings of the Ocean Drilling Program, Scientific Results. College Station, TX, pp. 1–60.

Li, L., Keller, G., 1998. Abrupt deep-sea warming at the end of the Cretaceous. Geology 26, 995.

Li, L., Keller, G., 1998. Maastrichtian climate, productivity and faunal turnovers in planktic foraminifera in South Atlantic DSDP sites 525A and 21. Marine Micropaleontology 33, 55–86.

Lourens, L.J., Hilgen, F.J., 1997. Long-periodic variations in the earth's obliquity and their relation to third-order eustatic cycles and late Neogene glaciations. Quaternary International 40, 43–52.

Lourens, L.J., Hilgen, F.J., Shackleton, N.J., Laskar, J., Wilson, D., 2004. The Neogene Period, in: Gradstein, F., Ogg, J.G., Smith, A.G. (Eds.), A Geologic Time Scale 2004. Cambridge University Press, Cambridge, pp. 409–440.

Lourens, L.J., Sluijs, A., Kroon, D., Zachos, J.C., Thomas, E., Röhl, U., Bowles, J., Raffi, I., 2005. Astronomical pacing of late Palaeocene to early Eocene global warming events. Nature 435, 1083–1087.

Lowrie, W., Alvarez, W., 1977. Upper Cretaceous-Paleocene magnetic stratigraphy at Gubbio, Italy. III. Upper Cretaceous magnetic stratigraphy. GSA Bulletin 88, 374–377.

Lowrie, W., Alvarez, W., Napoleone, G., Perch-Nielsen, K., Premoli Silva, I., Toumarkine, M., 1982. Paleogene magnetic stratigraphy in Umbrian pelagic carbonate rocks: The Contessa sections, Gubbio. Geological Society of America Bulletin 93, 414–432.

Manivit, H., 1984. Paleogene and Upper Cretaceous calcareous nannofossils from Deep Sea Drilling Program Leg 74, in: Moore, T. C., Jr., Rabinowitz, P. D., Et Al., Initial Reports of the Deep Sea Drilling Program. pp. 475–499.

Margolis, S.V., Mount, J.F., Doehne, E., Showers, W., Ward, P., 1987. The Cretaceous/Tertiary boundary carbon and oxygen isotope stratigraphy, diagenesis, and paleoceanography at Zumaya, Spain. Paleoceanography 2, 361–377.

Martin, J.H., 1990. Glacial-interglacial CO2 change: The Iron Hypothesis. Paleoceanography 5, 1–13.

Mary, C., Moreau, M.-G., Orue-Etxebarria, X., Apellaniz, E., Courtillot, V., 1991. Biostratigraphy and magnetostratigraphy of the Cretaceous/Tertiary Sopelana section (Basque country). Earth and Planetary Science Letters 106, 133–150.

Mathey, B., 1988. The Paleogeographical evolution of the Basco-Cantabrian domain during the Upper Cretaceous, in: M. Lamolda (ed.) Field Excursion of the K/T Boundary at Zumaya and Biarritz, Paleontologica Et Evoluto: Exstinctionis Phoenomina, III,. Universidad de Pais Vasco, Bilbao, Leioa (Vizcaya), pp. 142–147.

Milanković, M., 1941. Kanon der Erdbestrahlung und seine Anwendung auf das Eiszeitenproblem. Mihaila Ćurčića.

Miller, K.G., Sugarman, P.J., Browning, J.V., Kominz, M.A., Hernández, J.C., Olsson, R.K., Wright, J.D., Feigenson, M.D., Van Sickel, W., 2003. Late Cretaceous chronology of large, rapid sea-level changes: Glacioeustasy during the greenhouse world. Geology 31, 585.

Miller, K.G., Wright, J.D., Browning, J.V., 2005. Visions of ice sheets in a greenhouse world. Marine Geology 217, 215–231.

Molina, E., Alegret, L., Arenillas, I., Arz, J.A., Gallala, N., Grajales-Nishimura, J.M., Murillo-Muñetón, G., Zaghbib-Turki, D., 2009. The Global Boundary Stratotype Section and Point for the base of the Danian Stage (Paleocene, Paleogene, “Tertiary”, Cenozoic): auxiliary sections and correlation. Episodes 32, 84–95.

Monechi, S., Thierstein, H.R., 1985. Late Cretaceous-Eocene nannofossil and magnetostratigraphic correlations near Gubbio, Italy. Marine Micropaleontology 9, 419–440.

Moore, T.C., Jr., Rabinowitz, P.D., 1984. Site 525, in: Moore, T. C., Jr., Rabinowitz, P. D. Et Al., Initial Reports of the Deep Sea Drilling Project. pp. 525–532.
Moreau, M.-G., Cojan, I., Ory, J., 1994. Mechanisms of remanent magnetization acquisition in marl and limestone alternations. Case study: Upper Cretaceous (Chron 31-30), Sopelana, Basque Country. Earth and Planetary Science Letters 123, 15–37.
Mount, J., Ward, P., 1986. Origin of limestone/marl alterations in the upper Maastrichtian of Zumaya, Spain. Journal of Sedimentary Research 56, 228–236.
Mount, J.F., Margolis, S.V., Showers, W., Ward, P., Doehne, E., 1986. Carbon and Oxygen Isotope Stratigraphy of the Upper Maastrichtian, Zumaya, Spain: A Record of Oceanographic and Biologic Changes at the End of the Cretaceous Period. PALAIOS 1, 87–92.
Mount, J.F., Ward, P., 1986. Origin of Limestone/Marl Alternations in the Upper Maastrichtian of Zumaya, Spain. SEPM Journal of Sedimentary Research Vol. 56.
Nifuku, K., Kodama, K., Shigeta, Y., Naruse, H., 2009. Faunal turnover at the end of the Cretaceous in the North Pacific region: Implications from combined magnetostratigraphy and biostratigraphy of the Maastrichtian Senpohshi Formation in the eastern Hokkaido Island, northern Japan. Palaeogeography, Palaeoclimatology, Palaeoecology 271, 84–95.
Odin, G.S., 2001. The Gampanian-Maastrichtian Stage Boundary - characterization at Tercis les Bains (France) and correlation with Europe and other continents., Developments in palaeontology and stratigraphy. Elsevier.
Odin, G.S., Lamaurelle, M.A., 2001. The global Campanian-Maastrichtian stage boundary. Episodes 24, 229–238.
Ogg, J.., Ogg, G., Gradstein, F.M., 2008. The Concise Geologic Time Scale. Cambridge University Press, Cambridge.
Ogg, J.G., Hinnov, L.A., 2012. Cretaceous, in: Gradstein, F., Ogg, J.G., Schmitz, M. and Ogg, G. (Eds.), The Geologic Time Scale 2012. Elsevier.
Oglesby, R., Park, J., 1989. The effect of precessional Insolation Changes on Cretaceous Climate and Cyclic Sedimentation. Journal of Geophysical Research 94, 14793–14816.
Paillard, D., Labeyrie, L., Yiou, P., 1996. Macintosh program performs time-series analysis. Eos transactions American Geophysical Union 77, 379–397.
Pälike, H., Frazier, J., Zachos, J.C., 2006. Extended orbitally forced palaeoclimatic records from the equatorial Atlantic Ceara Rise. Quaternary Science Reviews 25, 3138–3149.
Pälike, H., Hilgen, F., 2008. Correspondence. Rock clock synchronization. Nature Geoscience 1, 282.
Pälike, H., Norris, R.D., Herrle, J.O., Wilson, P.A., Coxall, H.K., Lear, C.H., Shackleton, N.J., Tripati, A.K., Wade, B.S., 2006. The Heartbeat of the Oligocene Climate System. Science 314, 1894–1898.
Pälike, H., Shackleton, N.J., Röhl, U., 2001. Astronomical forcing in Late Eocene marine sediments. Earth and Planetary Science Letters 193, 589–602.

Park, J., Oglesby, R.J., 1991. Milankovitch rhythms in the Cretaceous: A GCM modelling study. Palaeogeography, Palaeoclimatology, Palaeoecology 90, 329–355.
Paul, C.R.C., Lamolda, M.A., 2007. Carbon and oxygen stable isotopes in the Maastrichtian of the Basque Country, N. Spain. Cretaceous Research 28, 812–820.
Perch-Nielsen, K., 1985. Mesozoic calcareous nannofossils, in: Bolli, H.M., Et Al. (Eds.) Plankton Stratigraphy. Cambridge University Press, pp. 329–426.
Percival, S.F., Fischer, A.G., 1977. Changes in Calcareous nannoplankton in the Cretaceous-Tertiary biotic crisis at Zumaya, Spain. Evolutionary Theory 2, 1–35.
Pérez-Rodríguez, I., Lees, J.A., Larrasoaña, J.C., Arz, J.A., Arenillas, I., 2012. Planktonic foraminiferal and calcareous nannofossil biostratigraphy and magnetostratigraphy of the uppermost Campanian and Maastrichtian at Zumaia, northern Spain. Cretaceous Research 37, 100–126.
Petrizzo, M.R., Falzoni, F., Silva, I.P., 2011. Identification of the base of the lower-to-middle Campanian Globotruncana ventricosa Zone: Comments on reliability and global correlations. Cretaceous Research 32, 387–405.
Pospichal, J.J., Wise, S.W., 1990. Maestrichtian calcareous nannofossil biostratigraphy of the Maud Rise (ODP Leg 113 Sites 689 and 690, Weddel Sea, in: Barker, P. F., Kennet, P. J. Et Al., Proceedings of the Ocean Drilling Program, Scientific Results. pp. 465–487.
Premoli Silva, I., Sliter, W., 1995. Cretaceous planktonic Foraminiferal stratigraphy and evolutionary trends from the Bottaccione section, Gubbio, Italy. Paleontographia Italica 82, 1–89.
Pujalte, V., Baceta, J.I., Dinarès-Turell, J., Orue-etxebarria, X., Parés, J.M., Payros, A., 1995. Biostratigraphic and magnetostratigraphic intercalibration of latest Cretaceous and Paleocene depositional sequences from the deep-water Basque basin, western Pyrenees, Spain. Earth and Planetary Science Letters 136, 17–30.
Pujalte, V., Baceta, J.I., Orue-Etxebarria, X., Payros, A., 1998. Paleocene Strata of the Basque Country, Western Pyrenees, Northern Spain: Facies, and Sequence Development in a Deep-water Starved Basin, in: Mesozoic and Cenozoic Sequence Stratigraphy of European Basins, SEPM Special Publication. pp. 311–328.
Pujalte, V., Robles, S., Orue-Etxebarria, X., Baceta, J.I., Payros, A., Larruzea, I.F., 2000. Uppermost Cretaceous-Middle Eocene strata of the Basque-Cantabrian Region and western Pyrenees: a sequence stratigraphic perspective. Revista de la Sociedad Geológica de España 13, 191–211.
Rat, P., 1988. The Basque-Cantabrian basin between the Iberian and European plates, some facts but still many problems. Revista de la Sociedad Geológica de España 1, 327–348.
Rivera, T.A., Storey, M., Zeeden, C., Hilgen, F.J., Kuiper, K., 2011. A refined astronomically calibrated 40Ar/39Ar age for Fish Canyon sanidine. Earth and Planetary Science Letters 311, 420–426.
Rodríguez, L., Esteban, J.J., Vegas, N., Cuevas, J., 2008. Tectónica de inversión en la Playa de Sopelana (Arco Vasco, Pirineos occidentales). Geogaceta 45, 23–26.

Röhl, U., Norris, R.D., Ogg, J.G., 2003. Cyclostratigraphy of upper Paleocene and lower Eocene sediments at Blake Nose Site 1051 (western North Atlantic). Geological Society of America Special Papers 369, 567–588.

Santander, J., Sopelana, A., Ramírez-Rodríguez, J.A., García-Peregrina, I., Castaños, J., Díez-López, A., Perdigón, O., Elorza, J., 2007. Contenidos de CaCO3 en los pares marga-caliza del Maastrichtiense y Daniense en Sopelana, Arco Vasco: facies grises frente a facies rojas. Geogaceta 43, 95–98.

Schmitz, B., Pujalte, V., Molina, E., Monechi, S., Orue-Etxebarria, X., Speijer, R.P., Alegret, L., Apellaniz, E., Arenillas, I., Aubry, M.P., Baceta, J.I., Berggren, W.A., Bernaola, G., Caballero, F., Clemmensen, A., Dinarès-Turell, J., Dupuis, C., Heilmann-Clausen, C., Orús, A.H., Knox, R., Martín-Rubio, M., Ortiz, S., Payros, A., Petrizzo, M.R., von Salis, K., Sprong, J., Steurbaut, E., Thomsen, E., 2011. The Global Stratotype Sections and Points for the bases of the Selandian (Middle Paleocene) and Thanetian (Upper Paleocene) stages at Zumaia, Spain. Episodes 34, 220–243.

Schovsbo, N.H., Rasmussen, S.L., Sheldon, E., Stemmerik, L., 2008. Correlation of carbon isotope events in Danish Upper Cretaceous chalk. Geological Survey of Denmark and Greenland Bulletin 15, 13–16.

Schrag, D.P., DePaolo, D.J., Richter, F.M., 1995. Reconstructing past sea surface temperatures: Correcting for diagenesis of bulk marine carbonate. Geochimica et Cosmochimica Acta 59, 2265–2278.

Schulz, M., Mudelsee, M., 2002. REDFIT: estimatingred-noise spectra directly from unevenly spaced paleoclimatic time series. Computers & Geosciences 28, 421–426.

Schulz, M.-G., 1979. Morphometrisch-variationsstatistische Untersuchungen zur Phylogenie der Belemniten-Gattung Belemnella im Untermaastricht NW-Europas. Geologisches Jahrbuch A47, 3–157.

Schulz, M.G., Ernst, G., Ernst, H., Schmid, F., 1984. Coniacian to Maastrichtian stage boundaries in the standard section for the Upper Cretaceous white chalk of NW Germany (L\ägerdorf-Kronsmoor-Hemmoor): Definitions and proposals. Bulletin of the Geological Society of Denmark 33, 203–215.

Sellwood, B.W., Valdes, P.J., 2006. Mesozoic climates: General circulation models and the rock record. Sedimentary Geology 190, 269–287.

Shackleton, N.J., Crowhurst, S.J., Weedon, G.P., Laskar, J., 1999. Astronomical Calibration of Oligocene-Miocene Time. Philosophical Transactions: Mathematical, Physical and Engineering Sciences 357, 1907–1929.

Sheldon, E., 2008. Upper Campanian - Maastrichtian calcareous nannofossil biostratigraphy of the Stevns-1 borehole, Denmark. Journal of Nannoplankton Research 30, 39–49.

Sheldon, E., Ineson, J., Bown, P., 2010. Late Maastrichtian warming in the Boreal Realm: Calcareous nannofossil evidence from Denmark. Palaeogeography, Palaeoclimatology, Palaeoecology 295, 55–75.

Shimmield, G.B., 1992. Can sediment geochemistry record changes in coastal upwelling palaeoproductivity? Evidence from northwest Africa and the Arabian Sea. Geological Society, London, Special Publications 64, 29–46.

Singer, A., 1980. The paleoclimatic interpretation of clay minerals in soils and weathering profiles. Earth-Science Reviews 15, 303–326.

Smit, J., Ten Kate, W.G.H.Z., 1982. Trace-element Patterns at the Cretaceous-Tertiary Boundary-Consequences of a Large Impact. Cretaceous Research 3, 307–332.

Spears, D.., Kanaris-Sotiriou, R., 1976. Titanium in some Carboniferous sediments from Great Britain. Geochimica et Cosmochimica Acta 40, 345–351.

Sprovieri, M., Coccioni, R., Lirer, F., Pelosi, N., Lozar, F., 2006. Orbital tuning of a lower Cretaceous composite record (Maiolica Formation, central Italy). Paleoceanography 21, PA4212.

Stemmerik, L., Surlyk, F., Klitten, K., Rasmussen, S.L., Schovsbo, N., 2006. Shallow core drilling of the Upper Cretaceous chalk at Stevns Klint, Denmark. Geological Survey of Denmark and Greenland, Bulletin 10, 13–16.

Stenvall, O., 1997. Stable isotopic (δ13C, δ18O) records through the Maastrichtian at 1041 Henmoor, NW Germany: implications for regional-global correlations, Göteborg University Publication.

Ten Kate, W.G.H.Z., Sprenger, A., 1993. Orbital cyclicities above and below the Cretaceous/Paleogene boundary at Zumaya (N Spain), Agost and Relleu (SE Spain). Sedimentary Geology 87, 69–101.

Thibault, N., Gardin, S., 2007. The late Maastrichtian nannofossil record of climate change in the South Atlantic DSDP Hole 525A. Marine Micropaleontology 65, 163–184.

Thibault, N., Gardin, S., Galbrun, B., 2010. Latitudinal migration of calcareous nannofossil Micula murus in the Maastrichtian: Implications for global climate change. Geology 38, 203–206.

Thibault, N., Harlou, R., Schovsbo, N., Schiøler, P., Minoletti, F., Galbrun, B., Lauridsen, B.W., Sheldon, E., Stemmerik, L., Surlyk, F., 2012a. Upper Campanian–Maastrichtian nannofossil biostratigraphy and high-resolution carbon-isotope stratigraphy of the Danish Basin: Towards a standard δ13C curve for the Boreal Realm. Cretaceous Research 33, 72–90.

Thibault, N., Husson, D., Harlou, R., Gardin, S., Galbrun, B., Huret, E., Minoletti, F., 2012b. Astronomical calibration of upper Campanian–Maastrichtian carbon isotope events and calcareous plankton biostratigraphy in the Indian Ocean (ODP Hole 762C): Implication for the age of the Campanian–Maastrichtian boundary. Palaeogeography, Palaeoclimatology, Palaeoecology 337-338, 52–71.

Varadi, F., Runnegar, B., Ghil, M., 2003. Long-Term Integrations of Planetary Orbits. The Astrophysical Journal 592, 620–630.

Voigt, S., Friedrich, O., Norris, R.D., Schönfeld, J., 2010. Campanian – Maastrichtian carbon isotope stratigraphy: shelf-ocean correlation between the European shelf sea and the tropical Pacific Ocean. Newsletters on Stratigraphy 44, 52–72.

Voigt, S., Gale, A.S., Jung, C., Jenkyns, H.C., 2012. Global correlation of Upper Campanian – Maastrichtian successions using carbon-isotope stratigraphy: development of a new Maastrichtian timescale. Newsletters on Stratigraphy 45, 25–53.

Voigt, S., Schönfeld, J., 2010. Cyclostratigraphy of the reference section for the Cretaceous white chalk of northern Germany, Lägerdorf-Kronsmoor: A late

Campanian-early Maastrichtian orbital time scale. Palaeogeography, Palaeoclimatology, Palaeoecology.
Walaszczyk, I., Odin, G.S., D'Hondt, A.V., 2002. Inoceramids from the Upper Campanian and Lower Maastrichtian of the Tercis section (SW France), the Global Stratotype Section and Point for the Campanian-Maastrichtian boundary; taxonomy, biostratigraphy and correlation potential. Acta Geologica Polonica 52, 269–305.
Ward, P.D., 1988. Maastrichtian ammonite and inoceramid ranges from Bay of Biscay Cretaceous-Tertiary boundary sections. Revista Española de Paleontología n.° Extraordinario, Palaeontology and Evolution: Extinction Events, 119–126.
Ward, P.D., Kennedy, W.J., 1993. Maastrichtian Ammonites from the Biscay Region (France, Spain). Memoir (The Paleontological Society) 34, 1–58.
Ward, P.D., Kennedy, W.J., MacLeod, K.G., Mount, J.F., 1991. Ammonite and inoceramid bivalve extinction patterns in Cretaceous/Tertiary boundary sections of the Biscay region (southwestern France, northern Spain). Geology 19, 1181–1184.
Westerhold, T., Röhl, U., 2009. High resolution cyclostratigraphy of the early Eocene – new insights into the origin of the Cenozoic cooling trend. Climate of the Past Discussions 5, 495–534.
Westerhold, T., Röhl, U., Donner, B., McCarren, H.K., Zachos, J.C., 2011. A complete high-resolution Paleocene benthic stable isotope record for the central Pacific (ODP Site 1209). Paleoceanography 26, 2216.
Westerhold, T., Röhl, U., Laskar, J., 2012. Time scale controversy: Accurate orbital calibration of the early Paleogene. Geochemistry Geophysics Geosystems 13, Q06015.
Westerhold, T., Röhl, U., Raffi, I., Fornaciari, E., Monechi, S., Reale, V., Bowles, J., Evans, H.F., 2008. Astronomical calibration of the Paleocene time. Palaeogeography, Palaeoclimatology, Palaeoecology 257, 377–403.
Westphal, H., Hilgen, F., Munnecke, A., 2010. An assessment of the suitability of individual rhythmic carbonate successions for astrochronological application. Earth-Science Reviews 99, 19–30.
Wiedmann, J., 1988. The K/T boundary section of Zumaya, Giúzcoa, in: M. Lamolda (ed.) Field Excursion of the K/T Boundary at Zumaya and Biarritz, Paleontologica Et Evoluto: Exstinctionis Phoenomina, III,. Universidad de Pais Vasco, Bilbao, Leioa (Vizcaya), pp. 148–152.
Wonders, A.A.H., 1992. Cretaceous Planktonic Foraminiferal Biostratigraphy, Leg 122, Exmouth Plateau, Australia. Proceedings of the Ocean Drilling Program, Scientific Results 122, 587–600.
Young, J.R., Bown, P., 1997. Higher classification of calcareous nannofossils. Journal of Nannoplankton Research 19, 15–20.
Zepeda, M.A., 1998. Planktonic foraminiferal diversity, equitability and biostratigraphy of the uppermost Campanian–Maastrichtian, ODP Leg 122, Hole 762C, Exmouth Plateau, NW Australia, eastern Indian Ocean. Cretaceous Research 19, 117–152.

Zijderveld, J.D.A., 1967. A.C. demagnetization of rocks: analysis and results, in: Runcon, S.K., Ed., Developments in Solid Earth Geosciences Methods in Paleomagnetism. Elsevier Publishing Company, Amsterdam.

Appendix C. Geophysical data of the Zumaia and Sopelana sections

Zumaia

Depth	Age	MS	L*
5	65.968	8.3	54.2
15	65.971	8.9	54.3
24	65.973	9.5	52.7
34	65.976	5.2	57.4
45	65.979	9.0	48.2
56	65.982	13.6	48.1
71	65.985	11.2	46.6
83	65.989	9.2	46.5
92	65.991	7.5	49.6
101	65.993	12.4	46.3
111	65.996	13.3	50.6
124	65.999	13.9	47.2
136	66.002	13.3	48.6
149	66.006	14.9	40.5
162	66.009	13.5	44.0
175	66.013	11.0	45.9
189	66.016	7.6	48.4
198	66.019	12.9	51.1
205	66.020	16.5	46.6
219	66.024	12.2	50.2
236	66.028	8.2	40.7
249	66.032	18.1	50.6
261	66.035	15.2	47.3
281	66.040	8.7	46.0
292	66.043	15.4	41.5
302	66.046	15.9	43.2
313	66.048	12.5	43.1
324	66.051	17.5	47.2
334	66.054	15.2	49.2
345	66.057	12.3	46.5
355	66.059	16.2	44.5
366	66.062	14.5	46.5
377	66.065	11.4	41.5
387	66.068	11.8	45.6
398	66.070	12.6	42.2
409	66.073	13.2	43.0
419	66.076	13.0	44.0
430	66.079	16.3	43.1
440	66.081	17.3	45.1
451	66.084	15.7	42.3
462	66.087	13.7	43.9
472	66.090	11.6	40.7
483	66.093	15.7	44.4
494	66.095	9.9	45.4
504	66.098	10.1	44.7
515	66.101	16.2	52.4
525	66.104	16.2	46.5
536	66.106	11.6	45.4
547	66.109	14.1	49.9
557	66.112	13.9	44.8
568	66.115	13.6	46.0
579	66.117	8.6	47.1
589	66.120	17.5	48.7
601	66.123	13.8	46.8
612	66.126	12.8	50.5
624	66.129	12.5	45.3
635	66.132	16.2	45.1
646	66.135	17.8	40.3
657	66.138	16.9	45.2
668	66.141	18.5	43.3
679	66.144	17.1	46.7
690	66.146	15.6	46.5
701	66.149	18.2	46.7
710	66.152	19.8	47.6
718	66.154	15.4	48.2
728	66.156	13.2	46.9
741	66.160	12.3	41.4
754	66.163	11.9	49.9
766	66.166	12.6	42.1
779	66.169	14.2	46.6
790	66.172	11.9	50.6
801	66.175	11.0	43.9
813	66.178	16.7	47.8
826	66.182	16.9	45.2
839	66.185	14.4	47.8
852	66.188	14.1	47.9
865	66.192	14.2	51.4
880	66.196	11.1	46.6
890	66.198	18.0	51.4
902	66.202	12.0	47.3
917	66.205	11.7	45.3
932	66.209	14.1	44.3
947	66.213	10.8	45.8
961	66.217	14.8	48.0
975	66.220	12.0	46.1
990	66.224	14.5	46.6
1005	66.228	16.8	42.7
1020	66.232	11.4	43.3
1029	66.235	10.6	50.1
1034	66.236	8.2	45.4
1039	66.237	11.8	46.0
1043	66.238	8.3	41.2
1047	66.239	11.0	47.7
1050	66.240	10.7	47.7
1054	66.241	12.3	44.1
1059	66.242	12.4	47.8
1064	66.243	13.2	43.8
1068	66.245	12.1	41.1
1072	66.246	10.0	43.9
1076	66.247	10.0	45.6
1083	66.248	10.3	51.6
1093	66.251	13.3	47.5
1103	66.254	10.7	51.2
1113	66.256	9.8	45.7
1123	66.259	10.8	43.8
1132	66.261	10.4	48.9
1139	66.263	13.4	47.4
1149	66.265	12.8	49.7
1160	66.268	13.5	48.9
1171	66.271	11.8	47.5
1182	66.274	13.0	51.3
1193	66.277	12.7	47.5
1201	66.279	7.6	
1206	66.280	7.7	45.3
1214	66.283	11.7	49.9
1226	66.286	11.8	47.5
1238	66.289	12.5	49.2
1250	66.292	9.4	47.6
1262	66.295	8.0	52.0
1271	66.297	11.6	50.2
1277	66.299	8.1	49.2
1287	66.302	9.0	51.2
1302	66.305	10.0	48.6
1316	66.309	10.2	45.5
1331	66.313	12.5	50.8
1344	66.316	8.2	49.3
1355	66.319	12.1	49.8
1366	66.322	10.2	47.7
1375	66.324	9.1	49.0
1384	66.327	11.4	49.9
1393	66.329	10.6	47.2
1403	66.331	9.6	47.1
1412	66.334	8.5	48.9
1421	66.336	10.7	52.9
1431	66.339	10.5	46.8
1441	66.341	8.7	47.7
1450	66.344	14.4	48.4
1460	66.346	10.4	47.1
1470	66.349	10.8	45.2
1479	66.351	8.2	46.5
1488	66.354	11.8	48.0
1498	66.356	12.1	48.4
1508	66.359	12.2	49.7
1518	66.362	13.9	47.6
1528	66.364	9.9	48.3
1538	66.367	7.3	47.0
1548	66.369	7.5	42.9
1558	66.372	7.1	50.5
1568	66.375	9.0	46.6
1578	66.377	10.2	53.8
1587	66.379	8.9	45.3
1595	66.381	6.8	45.0
1604	66.383	10.3	52.5
1612	66.385	9.3	47.9
1620	66.387	8.4	53.7
1629	66.389	10.3	53.7
1637	66.391	11.9	50.5
1647	66.394	8.1	46.6
1658	66.396	9.8	52.9
1669	66.399	9.4	51.5
1680	66.402	11.4	50.3
1691	66.405	13.6	46.4
1702	66.407	10.1	49.6
1713	66.410	11.1	53.9
1724	66.413	9.4	51.8
1734	66.415	11.8	50.9
1745	66.418	11.6	51.3
1756	66.421	10.3	49.6
1766	66.423	6.8	54.4
1777	66.426	9.2	51.3
1787	66.428	12.1	49.0
1798	66.431	10.8	49.7

1809	66.434	11.4	46.1	2448	66.591	13.0	46.8	3175	66.769	10.0	52.4
1821	66.437	7.1	49.2	2457	66.593	15.3	46.0	3185	66.772	12.0	42.7
1834	66.440	10.0	54.4	2466	66.595	10.6	51.2	3195	66.774	10.1	47.8
1847	66.443	9.0	49.0	2477	66.598	12.1	49.2	3204	66.777	15.1	49.3
1860	66.446	8.2	48.9	2488	66.601	10.6	51.5	3219	66.780	10.9	47.9
1873	66.449	11.4	44.4	2499	66.603	12.3	49.7	3234	66.784	6.9	55.7
1886	66.453	9.6	44.8	2509	66.606	10.8	46.7	3253	66.789	10.1	47.3
1899	66.456	8.3	46.3	2520	66.609	9.0	47.6	3267	66.794	8.8	48.2
1912	66.459	12.5	51.4	2531	66.611	11.5	48.9	3278	66.797	10.7	47.7
1923	66.462	10.6	50.8	2542	66.614	12.2	49.5	3289	66.800	13.2	43.6
1931	66.464	10.4	54.7	2550	66.616	10.5	47.3	3300	66.803	11.8	41.8
1939	66.466	7.5	48.5	2556	66.617	7.2	52.2	3310	66.805	10.4	47.0
1947	66.468	7.9	52.9	2563	66.619	8.0	52.7	3320	66.808	10.6	45.6
1955	66.470	9.4	50.4	2569	66.620	8.3	42.1	3330	66.811	14.6	39.4
1970	66.473	11.9	49.3	2580	66.623	12.7	49.3	3342	66.814	13.9	44.2
1981	66.476	12.3	46.4	2595	66.627	13.3	47.0	3357	66.819	14.0	44.8
1992	66.479	13.0	46.8	2610	66.630	13.4	46.2	3372	66.823	15.7	45.0
2003	66.482	11.0	47.7	2625	66.634	14.2	48.5	3387	66.827	14.8	42.6
2014	66.484	13.5	46.4	2636	66.637	13.5	52.7	3399	66.830	11.6	47.8
2025	66.487	11.2	53.4	2644	66.639	11.6	47.3	3408	66.833	11.7	43.0
2035	66.489	8.0	44.2	2652	66.641	9.4	51.9	3417	66.835	14.7	44.6
2046	66.492	8.6	46.4	2664	66.644	11.4	49.8	3429	66.838	15.9	45.1
2057	66.495	13.5	48.5	2680	66.648	12.4	46.4	3444	66.843	18.1	44.8
2067	66.497	13.3	44.4	2695	66.652	19.7	50.5	3459	66.847	17.0	45.4
2078	66.500	13.2	45.7	2711	66.655	8.7	57.2	3474	66.851	13.6	46.3
2088	66.502	13.9	50.8	2732	66.661	6.6	50.4	3485	66.854	11.5	49.6
2099	66.505	14.3	48.1	2741	66.663	11.0	54.8	3493	66.856	10.6	37.6
2109	66.508	7.0	54.0	2752	66.666	15.1	50.8	3500	66.858	12.4	46.2
2120	66.510	14.1	51.0	2765	66.669	16.4	52.3	3513	66.862	13.9	45.4
2131	66.513	12.7	49.0	2777	66.672	12.3	46.6	3530	66.866	17.4	44.5
2141	66.515	11.9	46.9	2790	66.675	11.1	46.9	3547	66.871	15.0	42.8
2152	66.518	12.6	47.0	2801	66.677	9.7	46.6	3564	66.876	16.7	47.1
2163	66.521	13.9	49.7	2810	66.680	13.6	48.8	3578	66.880	11.8	46.5
2174	66.523	15.6	47.3	2821	66.682	16.1	46.5	3590	66.883	10.2	39.8
2184	66.526	17.4	44.1	2832	66.685	13.4	48.1	3602	66.887	16.9	42.9
2195	66.529	12.7	41.6	2843	66.688	12.1	49.2	3615	66.890	17.9	42.9
2206	66.531	12.9	47.9	2852	66.690	17.0	50.0	3629	66.894	15.0	41.6
2217	66.534	14.5	48.9	2860	66.692	8.3	47.7	3643	66.898	14.6	46.3
2229	66.537	16.4	50.4	2867	66.694	12.2	49.7	3656	66.902	17.2	42.6
2240	66.540	12.8	48.4	2880	66.697	12.9	47.9	3670	66.906	11.9	44.4
2252	66.543	14.8	49.4	2897	66.701	14.8	49.0	3684	66.909	14.1	47.6
2264	66.545	12.1	45.4	2917	66.706	17.7	45.3	3697	66.913	14.1	46.1
2275	66.548	11.8	44.1	2930	66.709	11.6	47.5	3710	66.917	19.2	43.7
2287	66.551	10.8	51.5	2940	66.712	12.7	46.3	3722	66.920	21.0	42.9
2299	66.554	11.1	52.6	2951	66.714	14.4	45.1	3735	66.923	21.9	44.5
2310	66.557	14.1	48.4	2963	66.717	9.8	46.3	3747	66.927	16.0	48.6
2320	66.559	12.0	48.7	2975	66.720	10.5	43.6	3759	66.930	16.1	46.2
2328	66.561	11.3	47.5	2987	66.723	14.3	46.9	3769	66.933	17.9	47.4
2337	66.563	14.6	51.2	3001	66.727	13.7	44.7	3778	66.936	14.3	48.4
2345	66.565	16.4	43.5	3016	66.730	10.4	48.0	3787	66.938	15.5	46.3
2353	66.567	16.5	52.6	3030	66.734	15.0	46.4	3798	66.941	15.9	45.5
2361	66.569	8.9	40.9	3043	66.737	14.4	49.5	3813	66.945	18.5	45.2
2370	66.572	16.0	42.8	3056	66.740	16.0	42.9	3828	66.949	15.7	44.5
2378	66.574	13.3	45.6	3069	66.743	10.7	46.5	3843	66.954	9.1	46.0
2386	66.576	11.7	49.3	3081	66.746	11.4	48.9	3858	66.958	15.0	46.7
2395	66.578	9.9	48.0	3092	66.749	13.5	46.2	3870	66.961	17.7	45.0
2404	66.580	12.5	51.1	3105	66.752	11.9	49.2	3880	66.964	11.5	42.1
2413	66.582	15.0	46.2	3120	66.756	12.0	48.3	3890	66.967	14.6	47.8
2422	66.584	11.8	44.5	3135	66.760	10.4	50.1	3902	66.970	16.2	46.0
2430	66.586	12.7	49.4	3150	66.763	10.6	47.3	3915	66.974	16.6	48.0
2439	66.589	14.3	48.1	3164	66.767	9.8	50.0	3928	66.977	16.3	48.5

3941	66.981	20.0	44.1	4605	67.165	12.4	52.5	5219	67.328	12.6	47.3
3954	66.984	11.4	42.8	4610	67.167	12.0	44.2	5238	67.333	17.9	47.9
3963	66.987	11.5	46.4	4616	67.169	9.2	46.6	5255	67.337	16.1	47.3
3972	66.989	16.6	41.4	4624	67.171	15.1	46.0	5270	67.341	16.5	43.3
3986	66.993	16.4	40.7	4632	67.173	19.6	47.7	5283	67.344	16.0	44.6
4002	66.998	20.3	45.1	4640	67.175	14.8	47.3	5294	67.347	20.6	42.4
4018	67.002	8.8	49.6	4648	67.177	14.8	45.3	5305	67.350	16.2	44.7
4034	67.007	13.5	44.0	4657	67.180	9.5	52.4	5316	67.353	15.1	47.2
4046	67.010	11.1	48.4	4666	67.182	15.1	47.3	5327	67.356	17.9	44.0
4054	67.012	8.1	47.5	4674	67.185	15.8	48.5	5341	67.360	15.7	44.6
4061	67.014	9.0	47.7	4682	67.187	19.5	47.9	5360	67.365	17.7	42.6
4072	67.017	11.9	51.0	4690	67.189	11.7	48.3	5372	67.368	13.6	45.5
4086	67.021	8.6	46.4	4698	67.191	12.7	47.6	5379	67.369	18.5	44.7
4099	67.025	10.4	47.5	4705	67.193	10.9	45.8	5385	67.371	20.8	45.0
4113	67.029	14.7	44.9	4712	67.195	15.0	49.3	5391	67.373	15.6	42.7
4125	67.032	10.5	47.9	4722	67.198	14.4	43.2	5398	67.374	17.5	46.0
4135	67.035	10.7	46.8	4732	67.200	15.8	48.7	5410	67.378	17.2	46.3
4143	67.037	13.7	45.0	4742	67.203	14.2	48.0	5426	67.382	12.9	46.9
4148	67.038	14.6	45.9	4758	67.207	12.6	52.6	5441	67.386	16.1	44.2
4153	67.040	11.5	47.9	4769	67.210	13.0	46.4	5453	67.389	15.4	47.1
4159	67.042	9.4	45.3	4781	67.213	11.3	51.2	5462	67.391	15.9	41.4
4165	67.043	9.0	42.6	4787	67.215	14.9	47.3	5470	67.393	17.5	45.8
4175	67.046	9.2	48.8	4797	67.217	14.1	50.0	5477	67.395	19.9	43.1
4188	67.049	13.0	45.2	4807	67.220	21.0	45.7	5484	67.397	15.9	47.8
4201	67.053	9.5	47.9	4817	67.223	16.3	44.4	5490	67.399	7.9	48.3
4214	67.057	11.7	50.7	4827	67.225	13.6	48.1	5500	67.401	11.1	48.7
4228	67.061	11.6	47.4	4838	67.228	13.9	46.8	5514	67.405	15.7	44.9
4241	67.064	10.5	51.2	4849	67.231	11.7	45.3	5528	67.409	13.1	45.0
4257	67.069	8.1	50.6	4859	67.233	14.8	45.6	5540	67.412	11.3	48.2
4271	67.073	10.4	46.2	4868	67.236	18.0	46.7	5551	67.415	17.0	45.8
4284	67.076	13.1	44.9	4877	67.238	15.3	49.0	5562	67.417	17.1	45.4
4296	67.080	12.4	52.5	4886	67.241	14.5	49.7	5573	67.420	18.5	44.9
4309	67.083	18.3	47.4	4897	67.243	11.8	48.1	5584	67.423	17.5	43.5
4319	67.086	7.9	51.3	4909	67.247	8.1	52.5	5595	67.426	16.7	46.3
4326	67.088	14.2	45.3	4921	67.250	11.8	50.1	5606	67.429	15.5	49.3
4333	67.090	10.9	45.7	4933	67.253	16.1	46.7	5621	67.433	16.2	48.6
4343	67.093	14.9	51.3	4944	67.256	18.2	47.2	5640	67.438	17.3	51.6
4356	67.096	10.6	48.0	4955	67.259	17.2	46.6	5659	67.443	11.9	44.4
4368	67.100	17.0	48.4	4966	67.261	13.5	44.6	5674	67.447	19.3	45.7
4381	67.103	9.2	42.1	4977	67.264	19.5	46.9	5684	67.449	19.1	51.3
4391	67.106	7.8	48.2	4986	67.267	16.2	51.8	5694	67.452	17.5	47.4
4399	67.108	8.4	52.7	4995	67.269	11.4	52.6	5704	67.455	18.7	46.9
4407	67.110	12.8	47.6	5003	67.271	15.2	45.2	5714	67.457	18.3	44.5
4418	67.113	14.1	44.5	5011	67.273	13.5	48.3	5724	67.460	19.4	48.4
4431	67.117	11.7	41.0	5019	67.275	18.3	48.6	5734	67.462	14.9	43.9
4444	67.121	12.9	45.2	5028	67.278	14.0	46.3	5742	67.464	16.9	43.5
4457	67.124	17.1	47.1	5036	67.280	15.6	51.2	5748	67.466	15.1	48.5
4469	67.128	12.0	49.8	5044	67.282	14.6	47.1	5754	67.468	12.8	46.6
4480	67.131	11.6	49.4	5053	67.284	12.9	50.9	5764	67.470	17.9	43.7
4491	67.134	12.5	48.1	5062	67.287	14.4	50.4	5778	67.474	14.1	40.6
4500	67.136	12.4	49.1	5070	67.289	12.3	50.2	5792	67.478	14.9	45.2
4508	67.139	11.9	48.8	5079	67.291	17.0	46.2	5806	67.481	16.2	45.3
4517	67.141	16.0	48.1	5088	67.293	14.4	42.7	5820	67.485	11.9	42.0
4525	67.143	10.9	48.8	5097	67.296	13.9	50.3	5833	67.488	11.7	46.7
4537	67.147	8.9	50.9	5109	67.299	18.9	48.5	5844	67.491	11.3	47.7
4554	67.151	11.5	48.9	5126	67.303	15.1	49.8	5853	67.494	10.9	50.4
4567	67.155	14.0	47.8	5143	67.308	12.8	47.2	5860	67.495	13.1	42.5
4577	67.158	12.1	49.4	5156	67.311	16.0	50.6	5866	67.497	12.1	47.1
4587	67.161	15.0	44.7	5166	67.314	15.8	48.8	5872	67.499	11.2	48.9
4595	67.163	18.5	48.0	5175	67.316	12.4	45.3	5879	67.500	7.5	49.5
4600	67.164	13.6	48.0	5200	67.323	16.8	47.1	5888	67.503	4.0	50.5

5899	67.505	6.8	52.6	6584	67.693	7.3	50.5	7258	67.885	7.0	56.9
5910	67.508	7.3	57.2	6594	67.696	7.8	45.2	7271	67.889	7.9	48.1
5921	67.511	5.5	59.4	6604	67.699	11.9	52.3	7284	67.893	8.3	54.9
5934	67.515	6.0	54.8	6614	67.702	12.9	50.1	7297	67.896	9.5	51.3
5949	67.519	5.7	51.6	6623	67.705	10.7	47.8	7307	67.899	15.9	49.5
5964	67.522	5.3	51.6	6633	67.707	17.3	46.8	7314	67.901	12.2	46.7
5979	67.526	6.3	51.6	6643	67.710	8.7	53.0	7321	67.903	17.5	48.1
5994	67.530	6.1	54.8	6652	67.713	7.2	52.7	7328	67.905	8.1	45.6
6009	67.534	5.4	54.3	6661	67.715	6.0	54.9	7335	67.907	13.1	49.5
6023	67.538	8.4	54.5	6670	67.718	6.5	55.6	7343	67.909	5.7	54.3
6037	67.542	10.0	48.3	6679	67.720	10.9	53.5	7353	67.912	6.7	53.3
6051	67.545	10.3	52.5	6688	67.723	11.2	50.6	7363	67.915	9.1	59.3
6065	67.549	10.3	50.2	6698	67.726	11.9	51.8	7373	67.918	13.2	47.0
6079	67.553	5.6	49.9	6707	67.729	9.2	49.4	7384	67.921	12.7	47.7
6093	67.556	6.7	52.4	6716	67.731	6.8	56.1	7395	67.924	10.9	44.4
6107	67.560	7.3	53.2	6725	67.734	5.9	56.5	7405	67.927	13.4	46.2
6120	67.563	7.3	47.0	6734	67.736	7.4	52.6	7416	67.930	8.0	54.4
6134	67.567	4.4	54.3	6743	67.739	6.7	48.4	7427	67.933	7.9	48.8
6149	67.571	8.3	51.7	6752	67.741	8.8	55.2	7439	67.937	6.6	50.8
6164	67.575	10.0	55.9	6761	67.744	10.4	51.6	7450	67.940	10.2	45.2
6179	67.579	7.4	55.0	6771	67.747	11.3	51.4	7461	67.943	10.2	45.7
6194	67.583	10.2	50.5	6780	67.749	11.3	50.2	7470	67.945	14.1	46.9
6205	67.586	8.2	56.0	6793	67.753	8.8	51.7	7479	67.948	9.6	53.8
6214	67.588	8.3	51.2	6810	67.758	7.8	54.3	7488	67.951	8.4	48.0
6222	67.590	9.2	46.1	6826	67.762	8.3	53.9	7496	67.953	8.4	51.3
6232	67.593	7.5	56.3	6842	67.767	8.3	55.3	7504	67.955	4.0	51.3
6243	67.596	9.0	47.8	6859	67.772	6.9	57.4	7517	67.959	5.3	52.0
6254	67.600	10.1	52.6	6871	67.775	7.6	49.2	7530	67.963	8.8	52.1
6265	67.603	9.3	55.6	6880	67.778	10.4	49.2	7540	67.965	5.8	49.7
6276	67.606	6.8	53.3	6888	67.780	9.5	49.1	7548	67.968	6.4	49.1
6287	67.609	8.3	54.7	6897	67.782	7.2	45.9	7556	67.970	10.8	55.1
6298	67.612	9.1	49.5	6906	67.785	6.5	50.8	7564	67.972	5.7	52.5
6309	67.615	9.6	52.0	6916	67.788	11.2	51.5	7572	67.975	9.7	47.9
6320	67.618	9.5	53.6	6925	67.791	9.0	50.5	7580	67.977	7.1	50.4
6331	67.621	6.3	53.6	6936	67.794	15.1	47.6	7587	67.979	7.6	52.1
6342	67.624	11.8	48.9	6948	67.797	17.1	45.5	7594	67.981	6.1	53.5
6351	67.627	7.4	57.1	6960	67.800	14.8	51.1	7602	67.983	7.4	51.5
6360	67.630	8.2	55.1	6972	67.804	15.3	50.0	7610	67.985	10.7	51.1
6368	67.632	9.8	50.1	6983	67.807	7.1	48.6	7618	67.988	11.3	50.4
6377	67.635	8.6	51.4	6992	67.810	4.6	46.1	7626	67.990	7.8	49.5
6388	67.638	8.7	49.0	7002	67.812	8.5	48.5	7634	67.992	8.3	55.1
6399	67.641	6.3	52.2	7011	67.815	7.7	50.9	7642	67.994	8.6	52.7
6410	67.644	13.4	50.3	7022	67.818	10.7	46.6	7650	67.996	7.0	52.1
6421	67.647	5.7	51.1	7034	67.821	16.1	44.9	7658	67.999	7.4	56.0
6430	67.650	9.0	53.8	7045	67.825	15.3	47.9	7666	68.001	7.5	56.7
6439	67.652	5.4	48.1	7057	67.828	19.9	47.1	7674	68.003	8.9	53.6
6447	67.654	9.0	45.4	7068	67.831	8.1	54.0	7681	68.005	7.2	54.1
6456	67.657	11.9	46.0	7079	67.834	6.0	52.9	7688	68.007	7.3	52.1
6467	67.660	12.0	44.1	7089	67.837	6.3	50.8	7695	68.009	5.3	56.7
6478	67.663	16.1	47.1	7100	67.840	10.1	48.5	7702	68.011	8.8	52.1
6489	67.666	13.5	49.7	7112	67.844	9.4	50.6	7711	68.013	12.7	50.7
6500	67.669	6.4	55.4	7125	67.847	11.6	46.8	7719	68.015	9.7	52.0
6509	67.672	8.6	51.2	7138	67.851	16.0	44.1	7727	68.017	11.2	52.8
6518	67.675	4.5	46.9	7151	67.855	8.3	51.2	7736	68.020	11.5	56.6
6526	67.677	8.1	50.5	7165	67.859	9.5	54.0	7745	68.022	5.8	55.0
6534	67.679	9.1	46.1	7178	67.862	6.6	52.4	7756	68.025	8.8	48.9
6541	67.681	9.0	51.0	7191	67.866	6.0	51.0	7766	68.028	8.5	55.0
6549	67.684	14.7	47.9	7205	67.870	6.9	48.3	7777	68.031	7.6	56.5
6557	67.686	12.8	44.8	7218	67.874	9.4	50.3	7787	68.034	6.8	51.7
6564	67.688	9.3	48.3	7232	67.878	10.1	50.6	7796	68.036	7.9	54.2
6573	67.690	6.9	52.8	7245	67.881	8.2	51.3	7805	68.039	8.4	53.5

7814	68.041	8.9	55.0	8381	68.196	13.7	46.9	8994	68.364	20.0	49.0
7823	68.043	6.7	50.2	8393	68.199	14.4	50.4	9004	68.366	23.7	45.6
7830	68.045	5.4	50.1	8404	68.202	14.8	45.2	9015	68.369	13.6	45.8
7837	68.047	6.6	49.5	8415	68.205	19.5	45.2	9023	68.371	13.6	47.6
7844	68.049	8.6	52.7	8426	68.208	17.2	43.5	9031	68.374	18.3	49.2
7851	68.051	6.3	49.1	8437	68.211	15.2	46.6	9044	68.377	22.1	49.0
7858	68.053	5.4	51.3	8445	68.214	9.5	52.8	9056	68.381	19.7	44.6
7865	68.055	10.1	50.2	8451	68.215	11.6	53.2	9069	68.384	13.4	46.9
7872	68.057	7.0	51.9	8458	68.217	8.2	53.9	9081	68.386	16.6	46.9
7879	68.059	9.2	52.9	8464	68.219	9.9	51.0	9094	68.389	8.0	47.9
7886	68.061	7.7	56.4	8471	68.221	11.2	48.2	9103	68.391	17.3	47.9
7893	68.063	8.5	51.8	8479	68.223	16.6	40.6	9111	68.392	13.7	45.6
7900	68.065	12.8	49.2	8486	68.225	11.0	45.5	9123	68.395	14.5	47.8
7908	68.067	12.3	52.6	8494	68.227	14.5	52.2	9135	68.397	20.2	42.3
7916	68.069	7.9	51.5	8503	68.229	11.7	57.3	9147	68.400	19.8	46.6
7923	68.071	7.4	48.8	8512	68.232	8.4	46.5	9159	68.402	15.9	40.8
7932	68.073	8.0	49.0	8520	68.234	9.8	49.4	9171	68.404	15.8	43.7
7943	68.076	7.2	55.5	8529	68.236	8.9	51.3	9195	68.409	18.5	42.6
7953	68.079	6.7	53.8	8537	68.239	8.2	47.6	9195	68.409		42.4
7963	68.082	9.2	52.9	8545	68.241	13.7	51.1	9202	68.411	18.2	43.7
7973	68.085	10.1	47.5	8554	68.243	12.2	49.2	9205	68.411	11.2	47.0
7984	68.087	16.9	50.6	8562	68.246	13.4	46.3	9212	68.413		41.5
7994	68.090	16.0	47.7	8569	68.247	5.0	53.1	9224	68.415	11.1	43.6
8004	68.093	11.8	54.9	8577	68.250	17.0	46.8	9236	68.418	21.4	47.9
8013	68.096	8.7	55.0	8588	68.253	13.5	46.6	9249	68.420	26.0	44.1
8021	68.098	6.8	56.5	8599	68.256	14.3	44.8	9261	68.423	16.2	46.6
8029	68.100	6.4	51.2	8611	68.259	16.2	50.0	9273	68.425	23.1	43.5
8039	68.103	8.8	52.1	8622	68.262	12.5	48.9	9282	68.427	16.0	48.3
8051	68.106	10.1	50.3	8633	68.265	12.2	43.7	9287	68.428	19.1	41.6
8064	68.109	15.3	48.9	8644	68.268	9.2	46.5	9296	68.430	19.5	46.1
8076	68.113	13.7	52.4	8656	68.271	13.8	48.1	9309	68.432	15.4	46.5
8088	68.116	8.4	52.0	8668	68.275	11.8	51.5	9322	68.435	18.1	42.6
8097	68.119	5.7	56.8	8680	68.278	11.0	51.0	9334	68.438	22.5	45.4
8104	68.120	7.3	55.3	8691	68.281	14.1	43.1	9347	68.440	23.0	45.0
8111	68.122	5.4	59.2	8702	68.284	13.7	46.8	9360	68.443	20.0	42.6
8118	68.124	7.2	53.9	8713	68.287	18.9	48.4	9371	68.445	16.5	44.7
8125	68.126	11.6	50.2	8724	68.290	20.8	47.3	9380	68.447	17.7	48.5
8133	68.128	11.3	51.2	8735	68.293	22.0	47.9	9390	68.449	12.0	40.4
8140	68.130	7.7	52.7	8746	68.296	14.9	47.6	9403	68.452	15.3	48.9
8153	68.134	7.8	56.6	8757	68.299	13.7	52.3	9415	68.454	14.3	45.2
8171	68.139	7.6	52.5	8768	68.302	22.1	50.0	9428	68.457	22.0	44.6
8180	68.141	10.7	51.0	8778	68.305	17.8	46.3	9440	68.459	23.3	46.9
8189	68.144	7.1	48.4	8789	68.308	17.9	45.4	9453	68.462	17.5	46.7
8198	68.146	7.6	55.7	8799	68.310	17.4	42.3	9462	68.463	18.8	41.6
8207	68.149	10.1	55.8	8810	68.313	15.6	46.7	9472	68.466	14.2	45.3
8216	68.151	6.0	50.6	8820	68.316	14.5	46.8	9488	68.469	17.2	43.5
8225	68.153	9.2	49.0	8831	68.319	19.7	47.9	9503	68.472	12.2	47.6
8233	68.156	12.8	47.6	8842	68.322	18.0	45.0	9519	68.475	16.1	40.8
8241	68.158	11.1	46.0	8855	68.326	14.1	48.1	9535	68.478	19.5	46.3
8250	68.160	8.8	51.1	8867	68.329	18.7	43.9	9550	68.482	12.1	46.0
8258	68.162	5.7	54.9	8879	68.332	20.3	43.8	9559	68.483	14.8	45.7
8265	68.164	6.4	55.0	8891	68.335	17.1	44.8	9562	68.484	16.0	45.1
8272	68.166	10.0	55.6	8902	68.339	14.4	42.4	9569	68.485	21.1	46.9
8282	68.169	10.1	45.4	8914	68.342	21.8	42.1	9580	68.488	11.5	43.3
8294	68.172	10.9	46.2	8926	68.345	20.7	46.1	9591	68.490	20.3	39.3
8307	68.176	13.9	46.5	8936	68.348	13.6	47.2	9602	68.492	13.5	48.6
8319	68.179	16.3	48.0	8943	68.350	15.0	48.6	9613	68.494	15.6	40.8
8331	68.182	18.5	45.3	8951	68.352	10.8	50.1	9624	68.497	19.2	44.5
8343	68.186	9.1	49.7	8962	68.355	12.6	48.5	9636	68.499	13.4	48.3
8356	68.189	6.4	50.8	8972	68.358	19.0	45.4	9649	68.502	17.1	46.2
8368	68.193	12.0	45.1	8983	68.361	14.0	44.7	9662	68.504	16.2	45.4

9675	68.507	22.1	46.7	10419	68.658	13.8	46.0	11137	68.818	3.1	57.8
9688	68.509	17.1	41.0	10430	68.660	9.3	51.7	11147	68.821	3.8	56.4
9701	68.512	15.6	47.7	10444	68.663	16.6	46.9	11156	68.825	5.8	61.5
9714	68.515	17.4	44.0	10459	68.666	14.9	45.4	11163	68.828	4.4	55.9
9727	68.517	17.2	43.6	10472	68.669	15.7	47.6	11168	68.829	3.2	60.6
9740	68.520	20.1	46.9	10482	68.671	15.6	48.8	11172	68.831	5.2	64.1
9752	68.522	16.0	41.7	10492	68.673	8.9	45.5	11177	68.832	3.8	62.0
9763	68.525	11.1	45.1	10502	68.675	13.0	50.5	11184	68.835	3.8	65.2
9774	68.527	16.2	49.1	10512	68.677	14.2	48.7	11194	68.839	3.9	62.2
9788	68.530	19.3	48.6	10522	68.679	16.0	51.1	11202	68.842	4.9	62.1
9803	68.533	20.4	46.2	10537	68.682	13.7	48.6	11208	68.844	5.0	63.4
9819	68.536	23.5	42.5	10556	68.686	17.0	46.3	11214	68.846	3.5	60.8
9835	68.539	17.1	46.8	10572	68.689	18.5	46.4	11220	68.848	4.3	62.8
9850	68.542	16.3	44.0	10587	68.692	12.1	49.3	11228	68.851	3.5	61.5
9862	68.545	12.9	46.5	10599	68.695	20.7	47.3	11237	68.854	3.9	61.6
9871	68.547	16.7	44.3	10611	68.697	16.7	48.3	11246	68.858	4.4	60.5
9880	68.548	12.3	47.2	10622	68.699	16.1	45.8	11255	68.861	5.5	63.1
9889	68.550	9.0	48.1	10634	68.702	13.5	47.6	11261	68.863	4.3	59.8
9900	68.553	12.6	48.1	10648	68.705	14.9	48.0	11265	68.865	5.2	62.2
9911	68.555	14.5	47.9	10663	68.708	13.4	48.2	11270	68.866	3.5	63.4
9921	68.557	13.6	47.0	10678	68.711	10.5	50.2	11274	68.868	5.3	58.1
9932	68.559	14.1	44.6	10692	68.714	13.9	43.6	11280	68.870	5.3	60.2
9943	68.561	17.4	45.7	10707	68.717	19.1	46.6	11289	68.873	4.3	56.5
9951	68.563	18.0	42.6	10722	68.720	15.5	46.0	11298	68.877	4.0	64.4
9959	68.565	14.3	45.7	10736	68.723	11.8	46.1	11307	68.880	4.5	59.0
9972	68.567	14.8	46.3	10751	68.726	21.1	47.3	11317	68.884	3.6	58.9
9985	68.570	13.7	45.5	10766	68.729	16.8	45.6	11326	68.887	4.1	62.3
9997	68.572	14.3	44.8	10780	68.731	15.3	47.1	11335	68.890	3.9	60.5
10010	68.575	13.3	45.9	10793	68.734	18.7	43.9	11344	68.893	4.0	62.7
10023	68.578	13.8	45.4	10808	68.737	18.6	47.0	11352	68.896	5.2	64.8
10036	68.580	16.8	46.9	10825	68.741	17.1	45.9	11360	68.899	6.8	64.0
10049	68.583	12.3	39.9	10842	68.744	16.1	44.9	11369	68.903	3.5	61.5
10062	68.586	15.2	47.4	10859	68.747	17.0	45.0	11378	68.906	4.9	61.6
10075	68.588	13.2	45.1	10876	68.751	14.6	47.9	11387	68.909	4.1	63.6
10087	68.591	17.5	48.1	10893	68.754	13.4	45.9	11396	68.913	4.1	62.3
10099	68.593	11.0	47.6	10907	68.757	14.7	53.2	11405	68.916	4.1	62.0
10112	68.596	18.7	46.4	10916	68.759	12.3	51.8	11414	68.919	4.2	63.1
10124	68.598	9.4	56.3	10925	68.761	11.8	55.3	11422	68.922	2.8	64.5
10135	68.600	14.1	41.2	10936	68.763	6.2	55.8	11429	68.925	2.6	62.7
10146	68.602	14.5	44.4	10947	68.765	6.4	55.4	11440	68.929	4.1	61.0
10158	68.605	18.5	45.1	10958	68.768	8.0	60.1	11454	68.934	4.5	63.2
10172	68.608	13.4	45.1	10970	68.770	6.7	62.1	11468	68.939	4.9	64.1
10186	68.611	17.8	42.7	10983	68.773	6.0	60.9	11479	68.943	7.1	62.6
10200	68.614	13.3	42.1	10995	68.775	4.9	58.6	11486	68.945	7.5	64.0
10214	68.616	16.6	46.9	11008	68.778	3.9	60.7	11492	68.948	2.9	62.4
10229	68.619	18.4	47.0	11018	68.780	7.2	60.0	11498	68.950	6.5	59.0
10244	68.623	15.4	50.8	11026	68.781	3.6	59.5	11504	68.952	5.1	59.9
10260	68.626	11.9	43.6	11034	68.783	7.3	55.3	11511	68.954	8.7	59.3
10277	68.629	15.2	42.1	11042	68.785	5.7	57.7	11517	68.957	9.3	59.1
10294	68.633	15.2	43.9	11051	68.786	4.5	55.1	11523	68.959	6.7	57.4
10307	68.635	13.0	46.0	11059	68.789	3.2	58.0	11534	68.963	11.4	52.4
10316	68.637	16.0	42.1	11066	68.792	3.5	62.3	11549	68.969	8.4	55.8
10326	68.639	15.3	41.7	11073	68.795	3.4	52.5	11562	68.973	5.1	53.6
10335	68.641	10.7	46.2	11080	68.797	4.0	61.3	11571	68.976	13.1	48.1
10345	68.643	15.8	46.2	11088	68.800	4.2	60.4	11580	68.980	10.6	50.1
10354	68.645	11.9	46.6	11098	68.804	6.0	61.8	11589	68.983	13.7	43.0
10363	68.647	12.3	44.3	11108	68.807	4.8	56.8	11598	68.986	8.0	52.9
10373	68.649	16.5	41.8	11115	68.810	4.2	62.3	11607	68.990	10.7	50.5
10384	68.651	18.4	44.2	11120	68.812	5.0	64.3	11617	68.993	12.7	53.1
10396	68.653	15.6	44.7	11125	68.813	3.0	61.3	11627	68.997	11.9	53.3
10407	68.656	10.9	46.3	11130	68.815	3.2	58.9	11637	69.001	9.1	50.6

11647	69.004	10.3	48.4	12166	69.194	6.2	54.9	12608	69.328	4.1	54.0
11656	69.008	9.1	56.2	12175	69.197	5.3	60.3	12615	69.330	5.9	53.2
11666	69.011	6.2	54.5	12186	69.201	3.0	55.4	12623	69.332	8.9	57.7
11675	69.015	8.5	51.8	12197	69.205	4.3	59.9	12630	69.334	6.1	62.6
11685	69.018	5.1	58.4	12205	69.208	3.2	54.9	12637	69.336	7.0	56.5
11695	69.022	6.2	62.3	12212	69.209	3.4	58.7	12643	69.338	6.5	56.8
11705	69.025	8.2	61.2	12218	69.211	5.7	61.3	12649	69.340	7.9	58.6
11715	69.029	9.5	61.6	12225	69.213	4.9	59.5	12656	69.342	6.3	59.2
11725	69.033	3.7	62.3	12231	69.215	5.0	55.2	12663	69.344	5.7	53.4
11736	69.037	5.2	59.7	12238	69.217	6.7	57.8	12672	69.347	11.1	55.7
11746	69.040	6.4	60.6	12245	69.219	5.1	58.1	12680	69.349	8.1	56.1
11756	69.044	4.1	62.8	12252	69.221	6.2	60.2	12687	69.351	7.3	56.3
11765	69.047	2.3	57.9	12260	69.224	5.6	60.3	12694	69.353	7.7	60.3
11774	69.051	6.0	59.2	12269	69.227	6.2	60.6	12700	69.355	6.7	55.9
11783	69.054	4.0	57.5	12279	69.229	3.1	58.8	12706	69.357	5.9	58.4
11791	69.057	4.6	60.5	12288	69.232	4.2	61.4	12713	69.359	6.5	56.5
11799	69.060	3.6	60.4	12297	69.235	3.0	62.5	12720	69.361	11.0	56.3
11807	69.063	3.8	57.3	12305	69.237	3.5	55.8	12729	69.364	6.2	55.4
11815	69.066	7.4	59.5	12312	69.239	3.1	53.7	12738	69.366	6.1	60.4
11823	69.068	5.1	56.9	12321	69.242	4.9	59.7	12746	69.369	6.2	62.5
11830	69.071	5.5	58.2	12330	69.245	6.5	58.5	12751	69.370	6.5	60.7
11840	69.075	5.5	55.8	12339	69.247	7.9	55.7	12756	69.372	6.4	52.9
11853	69.079	8.0	58.4	12347	69.250	5.1	58.3	12761	69.373	6.5	52.8
11865	69.084	3.1	56.9	12364	69.255	7.5	56.8	12770	69.376	12.4	51.3
11878	69.089	3.8	54.5	12373	69.258	5.2	56.0	12782	69.379	14.2	49.2
11887	69.092	6.1	60.3	12379	69.259	5.8	55.1	12793	69.383	11.4	53.4
11893	69.094	7.2	58.5	12382	69.260	6.5	58.3	12805	69.386	6.7	52.7
11898	69.096	6.2	59.4	12385	69.261	5.6	54.2	12817	69.390	5.4	52.9
11904	69.098	6.6	57.9	12389	69.262	6.6	56.1	12828	69.393	9.8	50.7
11910	69.100	6.7	56.8	12395	69.264	5.9	57.1	12839	69.396	3.9	52.8
11916	69.103	5.1	60.4	12401	69.266	10.0	52.6	12849	69.399	8.0	48.2
11922	69.105	4.2	59.7	12406	69.267	7.1	57.6	12861	69.403	8.4	55.6
11929	69.107	3.8	60.2	12411	69.269	9.6	54.0	12872	69.406	11.1	49.2
11935	69.109	2.6	57.5	12415	69.270	6.8	55.5	12884	69.410	13.1	51.3
11942	69.112	5.2	61.2	12419	69.271	5.7	61.2	12896	69.413	8.9	49.3
11949	69.114	6.9	57.6	12423	69.272	7.9	54.0	12907	69.417	9.6	50.8
11956	69.117	5.2	55.2	12428	69.274	9.2	53.6	12916	69.420	12.1	53.9
11962	69.119	5.5	60.4	12433	69.275	8.3	59.3	12923	69.422	10.4	52.7
11969	69.122	7.4	59.8	12438	69.277	4.3	58.2	12930	69.424	9.4	51.9
11976	69.124	5.7	61.7	12443	69.278	7.8	56.6	12937	69.426	9.6	50.6
11983	69.127	5.2	53.9	12448	69.280	9.7	47.1	12947	69.429	9.9	52.0
11991	69.130	4.5	55.7	12453	69.281	6.0	54.6	12961	69.433	15.5	55.2
11998	69.133	5.0	59.0	12458	69.283	6.1	53.5	12976	69.437	15.8	52.4
12006	69.135	3.5	60.5	12463	69.284	6.3	54.1	12990	69.442	13.0	53.3
12013	69.138	5.4	58.6	12468	69.286	8.6	51.3	13002	69.445	13.0	50.0
12020	69.141	6.0	58.9	12474	69.288	5.4	49.0	13011	69.448	9.9	45.7
12029	69.144	4.0	60.8	12481	69.290	4.6	52.8	13021	69.451	14.1	48.3
12039	69.147	3.4	55.3	12487	69.292	4.2	55.8	13030	69.454	14.5	52.0
12049	69.151	3.4	60.5	12494	69.294	6.5	59.5	13041	69.457	17.7	51.0
12058	69.155	5.5	63.1	12503	69.296	6.8	60.4	13052	69.460	13.3	49.9
12068	69.158	5.4	59.3	12511	69.299	5.1	56.1	13063	69.463	9.7	50.6
12078	69.162	2.9	58.6	12520	69.301	8.3	51.3	13074	69.466	14.1	54.2
12087	69.165	3.7	59.3	12530	69.304	8.2	45.1	13083	69.469	8.9	58.3
12096	69.168	4.8	56.5	12541	69.308	5.5	51.4	13092	69.472	6.6	53.8
12105	69.172	3.9	61.2	12553	69.311	7.0	52.6	13100	69.474	11.5	48.7
12115	69.175	3.3	59.2	12564	69.315	6.4	49.5	13109	69.477	10.4	53.4
12125	69.179	5.3	60.3	12573	69.317	5.7	56.2	13119	69.480	11.7	54.6
12135	69.183	4.4	59.9	12580	69.319	8.8	59.6	13131	69.483	12.3	52.9
12145	69.186	5.9	57.8	12586	69.321	7.2	58.8	13142	69.487	9.8	54.9
12153	69.189	4.8	57.8	12593	69.323	7.3	57.7	13154	69.490	12.4	51.1
12160	69.192	5.3	58.9	12600	69.325	4.9	53.9	13164	69.493	9.5	51.9

13171	69.495	8.8	52.9
13178	69.497	6.9	51.2
13185	69.500	9.5	52.3
13194	69.502	12.7	50.9
13206	69.506	17.7	51.6
13217	69.509	9.8	48.8
13229	69.513	10.9	50.6
13239	69.516	10.5	52.9
13246	69.518	10.6	53.3
13253	69.520	7.4	54.9
13260	69.522	11.8	50.5
13268	69.525	8.9	52.4
13277	69.527	9.6	52.3
13285	69.529	8.4	53.7
13292	69.532	8.7	58.5
13297	69.533	5.5	52.2
13305	69.536	12.3	53.8
13316	69.539	11.2	50.9
13327	69.542	7.4	48.2
13338	69.545	7.9	53.9
13347	69.548	7.6	54.0
13355	69.550	4.6	53.9
13362	69.553	6.6	55.2
13370	69.555	7.8	54.1
13381	69.558	7.4	54.4
13395	69.562	7.9	53.2
13408	69.566	9.4	50.6
13422	69.570	4.7	50.7
13435	69.574	6.7	53.5
13448	69.578	6.3	45.9
13461	69.582	4.4	47.1
13472	69.585	10.3	53.7
13483	69.588	8.9	50.2
13493	69.592	11.1	52.8
13504	69.595	10.5	48.6
13513	69.598	7.5	56.3
13522	69.600	7.0	55.9
13531	69.603	6.3	55.2
13540	69.605	7.6	51.7
13547	69.608	6.0	49.3
13553	69.609	6.2	50.9
13561	69.611	12.4	54.8
13569	69.613	7.7	52.1
13577	69.615	8.5	53.5
13585	69.617	10.7	50.6
13594	69.620	12.4	53.6
13604	69.622	9.8	54.1
13614	69.625	9.1	51.9
13625	69.627	7.6	46.9
13636	69.630	8.4	53.1
13648	69.633	8.0	47.3
13659	69.636	9.4	50.7
13669	69.639	10.8	46.3
13677	69.641	8.8	50.3
13685	69.643	9.7	47.6
13693	69.645	5.8	48.4
13701	69.647	7.7	59.2
13709	69.649	10.1	52.4
13716	69.651	9.8	54.3
13726	69.653	11.0	44.8
13737	69.656	12.1	51.4
13748	69.659	8.2	48.3
13759	69.662	7.6	51.3
13771	69.664	5.1	52.8
13782	69.667	6.4	56.5
13793	69.670	9.3	49.8
13805	69.673	9.5	45.0
13819	69.677	12.0	57.3
13833	69.680	10.6	53.1
13846	69.684	3.2	59.1
13858	69.687	6.4	59.6
13870	69.690	7.6	51.3
13882	69.693	5.8	52.0
13894	69.696	13.4	55.6
13905	69.698	11.2	55.7
13916	69.701	8.6	56.3
13927	69.704	8.2	47.3
13940	69.707	6.0	46.8
13954	69.711	6.1	51.5
13969	69.715	7.3	50.4
13983	69.718	9.9	52.9
13995	69.721	9.2	55.8
14005	69.724	9.6	55.4
14015	69.726	6.4	59.5
14027	69.729	7.9	57.7
14041	69.733	7.5	56.3
14055	69.737	9.1	54.0
14069	69.740	9.4	55.5
14081	69.743	9.0	49.5
14090	69.745	6.4	52.9
14099	69.748	10.9	46.8
14108	69.750	13.1	53.6

Sopelana

Depth (cm)	Age (Ma)	MS (SI)	L* (%)
13524	69.601	9.6	57.3
13531	69.603	7.3	58.1
13538	69.605	3.9	60.4
13543	69.606	5.9	58.8
13547	69.608	9.2	57.9
13550	69.609	8.1	53.0
13556	69.610	4.8	55.5
13565	69.613	7.0	55.6
13573	69.615	11.2	60.6
13584	69.619	6.9	62.3
13597	69.623	5.7	59.2
13610	69.627	6.0	61.9
13622	69.630	3.9	55.4
13632	69.633	5.8	53.4
13642	69.636	7.7	54.5
13654	69.640	9.1	61.9
13667	69.644	8.7	52.1
13680	69.648	9.7	59.0
13690	69.651	5.8	57.4
13696	69.653	5.9	55.8
13702	69.654	5.5	52.7
13712	69.657	5.6	55.1
13726	69.662	11.1	58.1
13739	69.666	11.1	59.0
13753	69.670	6.4	59.0
13764	69.673	6.1	57.7
13771	69.675	7.1	57.3
13778	69.677	4.9	60.4
13785	69.679	7.9	58.7
13793	69.682	7.6	58.4
13803	69.685	7.4	57.7
13814	69.688	11.3	58.3
13824	69.691	9.0	57.2
13834	69.694	5.1	61.6
13845	69.698	5.7	64.7
13855	69.701	5.2	61.6
13866	69.704	3.8	59.2
13876	69.707	4.6	58.4
13886	69.710	9.2	58.0
13896	69.713	7.3	57.4
13906	69.716	6.6	56.0
13916	69.719	5.7	55.8
13927	69.723	4.8	57.5
13938	69.726	6.0	62.1
13949	69.729	5.2	57.1
13959	69.732	6.2	50.7
13969	69.735	7.6	58.9
13980	69.738	5.2	56.8
13990	69.741	8.9	57.6
14000	69.745	5.1	55.7
14010	69.748	6.4	58.5
14021	69.751	7.4	54.9
14031	69.754	7.9	53.9
14042	69.757	5.2	50.6
14054	69.761	13.2	54.8
14067	69.765	15.5	54.4
14079	69.768	6.3	51.6
14089	69.771	11.5	56.9
14096	69.773	10.9	59.0
14103	69.776	8.1	53.8
14110	69.778	11.4	53.0
14119	69.780	6.8	56.4
14131	69.784	11.8	56.7
14143	69.788	10.4	57.8
14154	69.791	11.2	59.0
14166	69.795	8.7	63.7
14175	69.797	7.0	59.0
14181	69.799	5.4	53.3
14187	69.801	7.7	56.5
14193	69.803	5.5	58.1
14201	69.805	11.1	58.9
14212	69.809	12.7	56.2
14223	69.812	13.6	58.5
14234	69.815	8.4	58.3
14244	69.818	4.3	58.7
14255	69.822	4.7	60.1
14266	69.825	5.1	59.9
14277	69.828	5.6	59.8
14286	69.831	8.2	59.0
14294	69.833	8.3	58.3
14302	69.836	9.1	58.3
14310	69.838	6.3	59.9
14319	69.841	4.7	57.1
14328	69.844	5.4	54.7
14338	69.847	7.7	59.1
14347	69.850	7.7	57.2

14357	69.852	7.8	54.8	14856	70.003	6.2	58.3	15286	70.159	14.3	50.2
14367	69.855	8.5	56.5	14864	70.006	6.3	58.5	15294	70.162	13.0	50.4
14377	69.858	11.7	57.4	14871	70.008	7.2	58.6	15303	70.165	11.9	50.5
14387	69.862	5.4	55.4	14878	70.010	3.1	56.2	15311	70.168	10.3	52.4
14396	69.864	6.4	60.0	14885	70.012	4.5	57.4	15319	70.171	8.6	53.3
14404	69.867	6.5	58.1	14893	70.014	3.2	54.3	15326	70.173	8.7	50.5
14413	69.869	6.3	58.6	14900	70.017	5.4	58.5	15333	70.176	6.9	54.3
14421	69.872	6.8	58.4	14908	70.020	5.4	57.9	15340	70.179	8.2	53.9
14431	69.875	8.8	57.7	14917	70.023	8.2	57.1	15348	70.182	11.4	53.8
14442	69.878	10.6	55.1	14926	70.026	6.1	53.2	15357	70.185	11.5	52.6
14454	69.882	8.7	57.6	14935	70.029	9.4	55.3	15366	70.188	13.6	52.2
14465	69.885	7.1	54.4	14944	70.033	5.6	54.0	15375	70.191	10.2	53.8
14474	69.888	7.5	59.1	14951	70.035	5.0	56.9	15383	70.194	8.3	57.4
14480	69.890	4.5	55.2	14956	70.037	4.2	56.4	15390	70.197	7.3	55.0
14485	69.891	6.9	58.4	14961	70.039	7.0	60.9	15397	70.200	7.9	57.2
14491	69.893	3.6	54.4	14966	70.041	6.4	56.4	15404	70.202	8.4	55.6
14501	69.896	10.1	56.9	14974	70.044	7.7	54.6	15413	70.205	4.5	56.5
14514	69.900	12.4	59.8	14984	70.048	7.9	50.7	15422	70.209	9.1	50.8
14528	69.904	8.9	58.4	14995	70.052	10.6	53.2	15432	70.212	13.8	49.6
14541	69.908	4.4	57.4	15005	70.055	7.3	53.3	15441	70.216	8.0	48.8
14551	69.911	4.4	55.7	15013	70.058	4.8	55.3	15450	70.219	7.3	57.4
14556	69.913	6.0	60.1	15020	70.061	5.8	56.6	15458	70.222	7.1	59.2
14561	69.914	4.1	55.0	15027	70.063	7.6	60.5	15467	70.225	8.6	57.6
14566	69.916	5.5	54.8	15034	70.066	6.8	56.4	15475	70.228	13.2	56.8
14573	69.918	11.2	57.2	15041	70.069	4.6	59.2	15483	70.231	7.8	53.2
14581	69.920	7.7	57.5	15049	70.072	11.8	54.5	15488	70.233	8.1	55.4
14589	69.923	7.8	57.0	15058	70.075	7.5	54.5	15491	70.234	7.2	56.1
14597	69.925	7.8	58.2	15066	70.078	6.1	52.6	15495	70.235	8.2	52.6
14604	69.927	6.0	58.3	15073	70.080	6.8	58.2	15500	70.237	6.6	50.3
14609	69.928	6.4	57.1	15078	70.082	5.3	58.5	15504	70.239	7.8	47.0
14614	69.930	4.8	57.2	15083	70.084	3.8	62.9	15507	70.240	9.8	53.8
14619	69.931	4.9	57.9	15088	70.086	5.9	55.4	15510	70.241	10.0	53.5
14626	69.934	4.5	55.9	15096	70.089	9.5	55.0	15516	70.243	5.6	53.1
14636	69.937	7.3	57.5	15106	70.093	7.3	51.7	15525	70.246	9.5	50.2
14645	69.940	7.4	52.7	15116	70.096	9.4	54.3	15533	70.250	6.7	56.6
14653	69.942	10.3	53.1	15126	70.100	6.1	53.1	15542	70.253	6.9	52.1
14659	69.944	7.1	52.3	15134	70.103	5.7	54.7	15550	70.256	13.2	55.5
14665	69.946	5.7	54.9	15140	70.105	5.3	57.4	15558	70.259	12.7	54.6
14671	69.947	4.7	53.1	15146	70.107	4.4	53.2	15566	70.262	10.7	51.5
14678	69.949	9.2	54.8	15152	70.109	6.5	55.9	15574	70.265	7.4	52.6
14685	69.951	6.7	55.3	15157	70.111	6.8	54.9	15582	70.267	8.3	58.3
14692	69.954	6.0	53.1	15162	70.113	8.5	55.7	15589	70.270	8.0	51.1
14699	69.956	5.5	58.8	15167	70.115	9.0	53.4	15596	70.273	8.5	53.0
14707	69.958	3.7	57.7	15171	70.116	8.6	55.2	15603	70.275	7.1	53.9
14714	69.960	6.7	57.3	15175	70.118	5.3	53.8	15612	70.278	9.5	52.0
14724	69.963	5.2	54.3	15179	70.119	6.4	53.5	15621	70.282	14.1	53.7
14736	69.967	4.4	55.2	15186	70.122	7.1	53.4	15630	70.285	13.6	55.3
14747	69.970	6.3	53.4	15196	70.126	9.7	56.5	15639	70.288	10.5	55.6
14759	69.974	3.1	53.3	15206	70.129	6.2	56.0	15646	70.291	8.2	54.0
14768	69.977	5.9	59.1	15216	70.133	11.2	58.6	15653	70.294	6.2	54.1
14774	69.978	5.7	59.7	15223	70.136	7.1	51.8	15660	70.296	6.7	57.2
14780	69.980	4.8	60.2	15227	70.137	8.7	55.7	15667	70.299	9.7	54.9
14786	69.982	5.8	59.3	15232	70.139	8.9	58.6	15673	70.301	6.8	54.0
14793	69.984	6.4	55.8	15236	70.140	5.0	56.5	15679	70.303	13.2	52.1
14801	69.987	8.0	55.6	15243	70.143	9.2	51.7	15685	70.305	14.8	55.7
14810	69.989	7.6	53.8	15253	70.147	11.6	50.5	15691	70.308	7.6	52.0
14818	69.992	5.7	56.6	15263	70.150	7.2	54.7	15697	70.310	7.0	51.8
14826	69.994	3.5	60.2	15270	70.153	12.2	50.8	15704	70.312	7.5	55.7
14833	69.996	3.8	60.2	15273	70.154	8.5	53.9	15710	70.315	7.9	54.6
14841	69.999	3.9	59.6	15277	70.155	8.9	56.0	15717	70.317	7.2	53.7
14849	70.001	6.1	58.8	15280	70.157	5.7	53.0	15724	70.320	5.4	54.2

15732	70.322	12.5	55.9	16123	70.464	10.7	59.7	16596	70.632	12.1	53.8
15739	70.325	9.3	53.3	16128	70.466	6.6	55.1	16603	70.634	7.8	53.2
15747	70.328	4.9	53.3	16133	70.468	5.2	53.3	16609	70.636	7.6	52.8
15755	70.331	5.5	50.0	16140	70.471	6.9	55.9	16613	70.638	6.0	54.8
15763	70.334	9.3	55.8	16151	70.474	10.1	50.4	16617	70.639	7.0	54.2
15770	70.337	9.4	56.0	16161	70.478	10.9	52.3	16621	70.640	5.4	56.5
15778	70.340	6.5	52.0	16172	70.482	6.2	52.4	16627	70.643	9.6	57.5
15785	70.342	7.7	56.8	16181	70.485	7.1	55.0	16636	70.646	9.3	56.1
15792	70.345	12.3	55.5	16188	70.487	8.4	53.4	16645	70.649	8.3	57.9
15797	70.346	11.1	54.5	16195	70.490	10.6	54.9	16654	70.652	7.0	54.8
15800	70.348	7.2	54.1	16202	70.492	8.4	56.9	16661	70.655	5.9	55.1
15806	70.350	8.4	53.5	16211	70.496	10.0	56.6	16668	70.657	7.9	54.7
15815	70.353	10.1	55.3	16221	70.499	10.5	56.7	16674	70.659	8.2	58.0
15823	70.356	11.1	55.0	16231	70.503	10.9	52.7	16681	70.662	6.2	54.8
15830	70.358	8.8	53.5	16241	70.506	9.6	51.1	16689	70.664	6.1	53.2
15835	70.360	9.2	54.6	16249	70.509	7.5	53.5	16698	70.667	7.2	51.9
15840	70.362	7.7	56.8	16255	70.511	9.7	60.0	16707	70.671	10.6	51.2
15845	70.364	8.4	53.6	16262	70.513	7.9	59.9	16716	70.674	12.3	53.8
15851	70.366	10.9	55.5	16268	70.516	9.9	58.8	16723	70.676	4.8	58.1
15860	70.370	7.7	54.8	16277	70.519	11.6	52.0	16728	70.678	4.7	54.2
15869	70.373	8.6	53.5	16289	70.523	11.9	53.7	16733	70.680	6.2	51.7
15876	70.376	8.4	57.3	16300	70.527	7.1	52.4	16740	70.683	9.9	54.7
15883	70.378	9.1	57.0	16312	70.531	8.8	50.9	16749	70.686	11.8	55.6
15889	70.380	5.5	57.7	16321	70.534	5.5	52.0	16758	70.689	7.4	55.3
15896	70.383	6.4	59.8	16327	70.537	7.4	54.6	16765	70.691	7.4	57.7
15902	70.385	8.5	57.1	16334	70.539	9.7	55.2	16771	70.693	5.4	58.2
15907	70.387	4.9	51.2	16340	70.541	10.5	53.5	16777	70.696	7.2	56.0
15913	70.389	8.2	51.8	16348	70.544	8.9	53.0	16784	70.698	7.2	57.1
15918	70.391	5.7	52.2	16357	70.547	7.6	53.4	16793	70.701	7.8	52.5
15925	70.394	7.5	56.4	16366	70.550	13.9	53.0	16802	70.704	8.5	52.1
15933	70.397	11.0	57.3	16375	70.553	8.0	53.9	16811	70.707	6.6	57.0
15941	70.399	8.9	55.0	16383	70.556	4.7	56.4	16817	70.710	8.5	58.6
15949	70.402	7.1	54.7	16391	70.559	6.6	57.8	16822	70.711	7.1	58.4
15956	70.405	11.1	55.5	16400	70.562	7.6	54.5	16827	70.713	5.4	58.5
15961	70.407	9.9	54.8	16408	70.565	10.8	52.2	16832	70.715	5.2	58.5
15967	70.409	8.9	58.1	16417	70.568	10.5	51.2	16840	70.718	5.9	57.7
15972	70.411	9.5	56.4	16427	70.572	11.0	51.1	16852	70.722	10.8	60.9
15978	70.413	11.3	57.7	16436	70.575	11.6	49.7	16863	70.726	7.0	57.0
15983	70.415	8.1	54.8	16446	70.579	9.4	52.3	16872	70.729	5.3	54.6
15989	70.417	9.1	55.2	16454	70.581	10.4	53.9	16878	70.731	5.3	59.0
15994	70.419	7.7	56.6	16460	70.583	6.9	53.8	16883	70.733	4.5	58.0
16000	70.421	10.2	55.4	16466	70.586	5.8	51.8	16889	70.735	5.9	54.9
16007	70.423	11.6	56.9	16472	70.588	8.8	54.8	16898	70.738	10.1	58.3
16014	70.426	11.5	51.6	16479	70.590	9.7	57.5	16909	70.742	6.2	56.1
16021	70.428	11.3	56.6	16487	70.593	14.9	58.3	16920	70.746	5.1	54.9
16026	70.430	5.8	52.3	16495	70.596	15.4	55.0	16931	70.750	7.4	53.6
16029	70.431	10.3	55.1	16503	70.599	8.9	55.3	16940	70.753	7.0	57.1
16032	70.432	7.1	54.0	16509	70.601	7.4	53.0	16947	70.756	5.8	55.8
16038	70.434	9.9	54.9	16514	70.602	9.9	56.6	16954	70.758	7.2	58.1
16045	70.437	10.0	53.4	16518	70.604	10.0	54.1	16961	70.760	6.9	53.5
16052	70.439	11.5	56.6	16524	70.606	15.4	50.6	16970	70.764	10.0	57.1
16059	70.442	10.0	51.1	16533	70.609	10.4	54.1	16982	70.768	8.1	57.6
16065	70.444	6.1	58.2	16541	70.612	8.8	55.0	16995	70.772	7.7	58.1
16070	70.446	4.7	56.9	16549	70.615	7.7	52.3	17007	70.777	5.7	54.7
16075	70.447	7.9	54.2	16558	70.618	10.0	56.2	17016	70.780	9.1	60.9
16080	70.449	9.0	52.8	16564	70.620	4.5	58.1	17022	70.782	7.1	51.3
16087	70.452	10.7	56.3	16568	70.622	5.0	57.5	17028	70.784	5.3	55.1
16095	70.455	10.9	52.5	16572	70.623	5.6	53.6	17035	70.787	6.1	56.5
16104	70.458	10.5	50.6	16576	70.624	8.4	59.3	17044	70.790	6.6	56.8
16112	70.460	6.7	51.7	16582	70.626	7.3	52.6	17053	70.793	5.6	56.9
16118	70.463	6.4	53.3	16589	70.629	10.8	54.1	17062	70.796	9.3	55.5

17069	70.799	7.5	54.9	17672	70.995	8.7	55.2	18131	71.145	8.8	53.1
17076	70.801	7.3	59.6	17684	70.999	10.2	60.0	18136	71.146	8.3	55.2
17082	70.803	7.5	57.2	17694	71.003	6.8	57.0	18141	71.148	8.5	55.4
17090	70.806	4.4	54.5	17705	71.006	6.6	55.3	18152	71.152	4.6	57.1
17101	70.809	8.2	57.4	17719	71.011	7.5	57.5	18157	71.154	6.6	57.8
17112	70.813	10.0	57.6	17724	71.012	5.2	54.7	18164	71.156	5.0	54.6
17122	70.816	7.9	53.7	17730	71.014	6.7	58.2	18170	71.158	7.6	53.3
17133	70.820	5.4	55.9	17741	71.018	4.2	56.0	18181	71.161	9.1	53.8
17142	70.823	5.5	58.7	17747	71.020	7.7	53.5	18188	71.163	7.0	51.7
17150	70.825	6.2	57.7	17753	71.022	7.5	58.5	18193	71.165	8.7	54.4
17158	70.828	3.1	54.8	17759	71.024	3.9	54.1	18199	71.167	8.0	56.1
17166	70.830	6.2	51.6	17768	71.027	7.0	56.2	18212	71.171	4.1	56.9
17174	70.833	9.6	52.3	17772	71.028	5.9	59.9	18218	71.173	4.1	54.1
17183	70.836	8.9	57.0	17779	71.030	8.3	57.3	18224	71.175	6.4	53.1
17192	70.839	9.6	55.9	17787	71.033	5.3	54.0	18231	71.177	5.0	52.7
17202	70.842	7.7	53.7	17793	71.035	7.0	58.1	18244	71.182	5.8	54.2
17216	70.847	5.4	55.8	17798	71.036	6.7	57.0	18252	71.184	9.8	55.8
17226	70.850	4.9	55.6	17808	71.040	7.8	58.2	18259	71.187	5.5	56.1
17240	70.855	9.2	53.1	17817	71.043	6.5	56.9	18266	71.189	6.7	56.1
17246	70.856	10.4	54.5	17823	71.044	6.2	53.1	18272	71.191	5.4	57.4
17250	70.858	7.2	56.3	17833	71.048	9.0	56.7	18286	71.195	5.6	50.8
17262	70.862	7.2	55.6	17838	71.049	8.8	58.5	18292	71.197	6.2	55.7
17269	70.864	5.9	53.4	17849	71.053	5.6	53.7	18300	71.200	4.5	52.4
17274	70.866	5.5	53.9	17858	71.056	6.4	54.8	18308	71.203	4.1	51.8
17288	70.870	8.9	56.8	17867	71.059	7.0	53.1	18317	71.206	9.8	57.5
17299	70.874	9.7	55.3	17874	71.061	7.5	57.6	18321	71.207	7.5	56.8
17309	70.877	7.4	55.2	17888	71.066	6.8	57.0	18325	71.208	6.3	54.6
17327	70.883	5.8	55.1	17892	71.067	6.9	57.2	18329	71.210	8.9	56.2
17340	70.887	5.9	57.1	17897	71.069	8.0	55.7	18341	71.215	8.2	51.8
17353	70.891	7.0	53.4	17903	71.071	6.6	57.7	18347	71.218	6.1	55.6
17367	70.896	6.2	56.3	17915	71.075	6.7	58.4	18354	71.220	9.9	55.9
17374	70.898	7.7	55.6	17921	71.077	7.2	58.3	18368	71.226	6.6	58.1
17381	70.900	7.2	54.6	17928	71.079	8.7	57.6	18374	71.229	10.6	59.6
17394	70.905	7.8	55.7	17937	71.082	7.2	58.1	18379	71.231	8.5	57.2
17401	70.907	5.8	57.2	17947	71.085	8.0	55.8	18383	71.233	4.9	61.4
17409	70.910	6.9	56.9	17951	71.086	9.2	55.3	18388	71.235	5.9	54.5
17416	70.912	4.5	58.7	17955	71.088	6.4	58.7	18397	71.238	6.5	58.5
17430	70.917	6.2	57.5	17959	71.089	7.3	56.2	18402	71.241	7.0	60.2
17439	70.919	7.2	58.1	17970	71.092	4.7	55.9	18406	71.242	7.5	54.9
17450	70.923	9.1	56.4	17979	71.096	7.9	55.0	18410	71.244	6.1	58.8
17458	70.925	7.7	56.3	17988	71.098	6.6	60.3	18419	71.248	8.3	60.6
17467	70.929	6.8	57.1	17999	71.102	9.4	58.1	18423	71.249	10.5	58.6
17479	70.932	8.1	54.4	18004	71.103	9.4	59.2	18428	71.251	9.1	60.0
17490	70.936	5.0	54.0	18009	71.105	7.9	57.9	18432	71.253	8.5	58.8
17499	70.939	7.6	56.3	18014	71.107	8.4	60.0	18437	71.255	5.0	55.2
17514	70.944	8.0	56.9	18024	71.110	6.7	57.0	18448	71.260	4.7	60.3
17526	70.948	9.7	56.0	18029	71.112	5.9	57.4	18456	71.263	5.3	59.8
17538	70.952	7.3	58.3	18034	71.113	7.8	62.6	18465	71.267	7.2	56.2
17549	70.955	9.0	61.8	18045	71.117	5.4	58.1	18478	71.273	11.0	62.3
17564	70.960	4.6	57.3	18050	71.119	7.4	55.9	18484	71.275	7.7	58.9
17573	70.963	6.2	54.1	18054	71.120	8.6	55.3	18490	71.278	10.3	58.5
17581	70.966	7.5	56.9	18063	71.123	7.8	60.0	18502	71.282	6.8	58.9
17594	70.970	6.2	59.0	18069	71.125	5.7	57.4	18507	71.285	6.7	60.0
17603	70.973	7.0	55.0	18073	71.126	8.4	54.8	18512	71.287	6.0	59.8
17611	70.975	9.3	56.2	18084	71.130	7.8	61.8	18518	71.289	2.5	55.4
17618	70.978	9.1	56.4	18089	71.131	8.4	58.0				
17630	70.982	5.3	54.2	18094	71.133	7.6	60.7				
17637	70.984	7.2	57.6	18105	71.136	10.0	54.5				
17644	70.986	4.5	55.7	18110	71.138	6.7	52.8				
17650	70.988	5.4	54.7	18115	71.140	7.3	52.9				
17657	70.991	9.1	58.0	18120	71.141	5.8	57.0				

Appendix D. Stable carbon isotope data of bulk carbonate

Zumaia

Depth (cm)	Age (Ma)	δ13C (‰VPDB)
-362		1.5726
-350		1.6928
-338		1.3829
-326		1.4066
-317		0.8845
-307		1.9649
-297		1.5104
-288		1.2281
-277		1.5800
-267		1.8809
-255		1.4233
-244		1.7305
-233		1.2141
-219		1.0927
-203		1.2578
-190		0.8065
-179		1.6498
-164		1.4552
-140		0.4821
-120		0.9739
-103		1.3033
-75		1.2279
-51		1.0486
-36		1.0304
-25		0.6205
-8		0.5228
5	65.968	1.6227
15	65.971	1.1878
24	65.973	1.1332
34	65.976	1.4031
45	65.979	1.2164
56	65.982	1.4173
71	65.985	0.7966
83	65.989	1.0035
92	65.991	1.0738
101	65.993	0.9288
111	65.996	0.7769
124	65.999	1.0630
136	66.002	0.9826
149	66.006	1.3368
162	66.009	1.0138
175	66.013	0.9819
189	66.016	0.1121
198	66.019	0.9318
205	66.020	0.4364
219	66.024	0.7791
236	66.028	1.1133
249	66.032	0.7411
261	66.035	0.7869
281	66.040	0.8957
292	66.043	1.4771
302	66.046	1.1956
313	66.048	1.2386
324	66.051	0.8304
334	66.054	0.6330
345	66.057	0.9819
355	66.059	0.7580
366	66.062	0.7605
377	66.065	1.0470
387	66.068	0.7382
398	66.070	0.8480
409	66.073	0.7356
419	66.076	0.8816
430	66.079	0.7683
440	66.081	1.0750
451	66.084	0.7729
462	66.087	0.5221
472	66.090	0.7267
483	66.093	1.1057
494	66.095	0.6735
504	66.098	1.0730
515	66.101	1.3579
525	66.104	0.9331
536	66.106	0.9278
547	66.109	0.8901
557	66.112	0.8620
568	66.115	0.7787
589	66.120	0.6718
601	66.123	1.3928
657	66.138	0.8091
710	66.152	1.3733
754	66.163	0.3886
790	66.172	1.4854
839	66.185	0.7375
880	66.196	1.2534
917	66.205	1.0386
961	66.217	1.3378
990	66.224	1.3485
1034	66.236	0.2037
1047	66.239	0.6303
1059	66.242	1.6581
1072	66.246	1.5430
1083	66.248	1.4985
1103	66.254	1.5722
1132	66.261	1.4741
1171	66.271	1.3545
1201	66.279	1.5570
1238	66.289	1.4033
1271	66.297	1.5469
1302	66.305	1.4146
1344	66.316	1.7111
1375	66.324	1.5921
1403	66.331	1.3624
1441	66.341	1.3787
1470	66.349	1.3888
1508	66.359	1.4428
1538	66.367	1.4942
1558	66.372	1.4697
1568	66.375	1.1658
1578	66.377	1.2529
1587	66.379	0.9725
1595	66.381	0.9922
1604	66.383	1.3318
1612	66.385	1.4650
1620	66.387	1.3495
1629	66.389	1.0706
1637	66.391	0.8569
1647	66.394	0.8791
1658	66.396	0.7404
1669	66.399	1.4699
1680	66.402	1.0115
1691	66.405	1.3255
1702	66.407	1.3075
1713	66.410	1.0365
1724	66.413	1.1079
1734	66.415	1.0064
1745	66.418	1.1017
1756	66.421	1.1852
1766	66.423	1.1647
1777	66.426	1.0832
1787	66.428	0.7936
1798	66.431	0.8890
1809	66.434	1.0595
1821	66.437	0.7721
1834	66.440	0.8780
1847	66.443	1.1204
1860	66.446	1.1624
1873	66.449	0.7009
1886	66.453	0.7775
1899	66.456	0.7843
1912	66.459	0.7542
1923	66.462	1.1082
1931	66.464	1.0678
1939	66.466	0.9555
1947	66.468	1.3717
1955	66.470	1.0101
1970	66.473	1.2254
1981	66.476	1.2293
1992	66.479	0.8962
2003	66.482	1.3265
2014	66.484	0.8990
2025	66.487	1.1592
2035	66.489	0.9980
2046	66.492	0.5650
2057	66.495	0.7789
2067	66.497	1.0254
2078	66.500	1.0790
2088	66.502	1.1304
2099	66.505	1.0136
2109	66.508	1.2105
2120	66.510	0.8305
2131	66.513	1.4521
2141	66.515	0.1958
2152	66.518	0.6798
2163	66.521	1.1528
2174	66.523	1.3127
2184	66.526	0.7031
2195	66.529	0.7773
2206	66.531	0.8374
2217	66.534	1.4321
2229	66.537	0.6467
2240	66.540	1.3128

2252	66.543	0.8477	3643	66.898	1.4587	6107	67.560	1.7273
2264	66.545	1.0867	3684	66.909	1.1480	6134	67.567	1.6313
2275	66.548	0.7476	3735	66.923	1.2609	6164	67.575	1.6580
2287	66.551	0.0223	3778	66.936	1.5846	6214	67.588	1.6649
2299	66.554	0.3628	3828	66.949	0.7296	6243	67.596	1.7570
2310	66.557	1.2131	3880	66.964	1.6076	6287	67.609	1.7906
2320	66.559	1.0830	3928	66.977	0.9890	6320	67.618	1.6081
2328	66.561	1.2803	3972	66.989	1.4808	6360	67.630	1.8478
2337	66.563	0.7447	4002	66.998	1.1193	6399	67.641	1.5703
2345	66.565	1.2403	4054	67.012	1.7109	6439	67.652	1.6728
2353	66.567	0.7252	4086	67.021	1.6457	6478	67.663	1.5689
2361	66.569	0.9909	4125	67.032	1.6018	6518	67.675	1.7786
2370	66.572	0.5904	4148	67.038	1.6504	6549	67.684	1.5514
2378	66.574	1.2677	4159	67.042	1.3369	6584	67.693	1.9003
2386	66.576	0.9973	4201	67.053	1.4887	6614	67.702	1.8083
2395	66.578	1.4797	4241	67.064	1.5108	6652	67.713	1.8596
2404	66.580	1.0725	4284	67.076	1.3921	6688	67.723	1.7190
2413	66.582	0.9394	4326	67.088	1.6132	6725	67.734	1.5028
2422	66.584	1.2867	4356	67.096	1.6813	6761	67.744	1.4720
2430	66.586	1.0896	4399	67.108	1.7842	6793	67.753	1.5014
2439	66.589	0.6693	4431	67.117	1.6971	6826	67.762	1.7085
2448	66.591	1.2101	4480	67.131	1.3693	6880	67.778	1.3453
2457	66.593	1.2757	4508	67.139	1.5450	6906	67.785	1.7902
2466	66.595	1.5611	4537	67.147	1.8887	6948	67.797	1.1174
2477	66.598	1.0313	4587	67.161	1.5781	6992	67.810	1.5749
2488	66.601	1.5664	4605	67.165	1.8531	7034	67.821	1.5161
2499	66.603	1.6393	4632	67.173	1.6671	7079	67.834	1.7916
2509	66.606	1.5300	4657	67.180	1.7120	7125	67.847	1.8575
2520	66.609	1.3840	4682	67.187	1.4827	7178	67.862	2.0040
2531	66.611	1.7755	4705	67.193	1.3286	7232	67.878	1.3808
2542	66.614	1.4668	4722	67.198	1.6353	7284	67.893	1.8447
2550	66.616	1.2239	4769	67.210	1.0104	7321	67.903	1.7699
2556	66.617	1.2672	4797	67.217	1.5441	7353	67.912	1.8434
2563	66.619	1.1599	4838	67.228	1.6292	7395	67.924	1.8632
2569	66.620	1.4948	4868	67.236	1.4963	7439	67.937	1.9454
2595	66.627	1.5162	4909	67.247	1.4571	7470	67.945	1.7947
2644	66.639	1.5710	4955	67.259	1.3659	7517	67.959	1.9191
2680	66.648	1.3819	4995	67.269	1.7289	7556	67.970	2.0421
2732	66.661	1.7323	5019	67.275	1.5346	7587	67.979	1.8132
2765	66.669	1.4931	5053	67.284	1.4550	7610	67.985	1.8060
2801	66.677	1.4472	5079	67.291	1.3865	7642	67.994	2.0882
2832	66.685	1.5616	5126	67.303	1.6585	7666	68.001	2.0213
2860	66.692	1.6448	5200	67.323	1.1101	7688	68.007	1.9054
2897	66.701	1.3540	5255	67.337	1.3966	7719	68.015	1.9222
2930	66.709	1.7719	5305	67.350	0.7090	7756	68.025	1.8312
2963	66.717	1.5057	5341	67.360	1.4199	7796	68.036	1.8090
3001	66.727	1.7060	5385	67.371	0.7895	7830	68.045	1.7743
3043	66.737	1.5335	5426	67.382	1.6428	7851	68.051	2.0382
3081	66.746	1.7100	5470	67.393	0.9003	7879	68.059	1.7764
3120	66.756	1.7417	5514	67.405	1.4818	7908	68.067	1.8634
3164	66.767	1.6588	5573	67.420	0.9816	7943	68.076	1.9892
3195	66.774	1.7516	5640	67.438	1.6298	7984	68.087	1.8806
3234	66.784	1.7463	5704	67.455	1.2805	8021	68.098	1.9199
3278	66.797	1.6607	5748	67.466	1.5933	8064	68.109	1.8108
3320	66.808	1.8468	5792	67.478	0.4786	8104	68.120	1.6103
3357	66.819	1.2482	5833	67.488	1.6699	8133	68.128	2.0816
3408	66.833	1.7572	5866	67.497	1.5246	8153	68.134	1.8059
3444	66.843	1.2743	5899	67.505	1.3073	8233	68.156	1.8458
3493	66.856	1.5241	5994	67.530	1.6621	8265	68.164	1.6577
3530	66.866	1.2820	6051	67.545	1.6250	8307	68.176	1.7058
3590	66.883	1.4499	6093	67.556	1.8390	8356	68.189	1.7470

8415	68.205	1.3842	10947	68.765	1.7617	12411	69.269	1.9910
8451	68.215	1.5872	10995	68.775	1.8701	12419	69.271	1.9853
8479	68.223	1.7408	11026	68.781	1.8727	12433	69.275	2.0270
8503	68.229	1.2863	11051	68.786	2.0339	12448	69.280	1.8676
8537	68.239	1.8337	11066	68.792	1.6724	12458	69.283	1.9518
8611	68.259	1.7298	11073	68.795	1.7998	12474	69.288	1.8533
8656	68.271	1.6463	11098	68.804	2.2319	12503	69.296	2.0107
8713	68.287	1.4151	11120	68.812	1.7864	12541	69.308	1.9093
8757	68.299	1.8656	11147	68.821	2.1466	12580	69.319	1.9177
8799	68.310	1.4470	11172	68.831	1.9091	12608	69.328	2.2092
8842	68.322	1.6203	11184	68.835	1.9893	12643	69.338	1.8359
8891	68.335	1.5590	11208	68.844	1.8566	12672	69.347	2.0126
8936	68.348	1.6074	11237	68.854	2.1047	12687	69.351	1.8506
8983	68.361	1.4658	11265	68.865	2.1130	12700	69.355	2.1844
9023	68.371	1.7854	11298	68.877	2.0211	12729	69.364	2.0325
9056	68.381	1.5467	11326	68.887	2.1946	12751	69.370	1.9500
9103	68.391	1.5308	11352	68.896	2.1539	12793	69.383	2.0727
9147	68.400	1.7491	11387	68.909	2.0972	12839	69.396	1.6120
9202	68.411	1.6908	11422	68.922	1.9714	12872	69.406	1.9342
9236	68.418	1.5655	11454	68.934	2.1075	12923	69.422	2.0012
9282	68.427	1.6916	11479	68.943	2.1562	12961	69.433	1.5356
9322	68.435	1.4915	11504	68.952	2.1104	13011	69.448	1.9557
9371	68.445	1.8748	11534	68.963	2.0467	13052	69.460	1.8671
9415	68.454	1.5779	11580	68.980	2.2329	13092	69.472	1.8124
9462	68.463	1.9238	11617	68.993	2.1342	13131	69.483	1.7752
9503	68.472	1.7726	11656	69.008	1.8261	13171	69.495	1.9688
9559	68.483	1.7185	11695	69.022	1.9778	13206	69.506	1.8103
9591	68.490	1.3162	11736	69.037	2.2284	13246	69.518	1.9855
9649	68.502	1.6398	11765	69.047	2.1369	13277	69.527	1.9207
9701	68.512	1.1182	11791	69.057	2.2338	13292	69.532	2.0603
9819	68.536	1.5732	11823	69.068	2.0508	13316	69.539	1.8228
9871	68.547	1.6354	11853	69.079	2.2310	13355	69.550	2.0188
9911	68.555	1.6459	11893	69.094	2.1579	13395	69.562	1.7973
9951	68.563	0.8578	11910	69.100	2.2696	13448	69.578	2.1325
9985	68.570	1.6823	11929	69.107	2.0417	13483	69.588	1.7807
10036	68.580	1.2743	11949	69.114	2.0803	13522	69.600	1.8069
10087	68.591	1.4953	11969	69.122	2.1629	13547	69.608	1.8614
10186	68.611	1.3691	11991	69.130	2.2805	13569	69.613	1.8375
10229	68.619	1.6364	12013	69.138	2.1378	13604	69.622	2.0668
10294	68.633	1.6742	12049	69.151	2.2554	13636	69.630	1.9583
10354	68.645	1.7665	12087	69.165	2.0219	13677	69.641	1.6082
10396	68.653	1.5996	12125	69.179	2.1768	13709	69.649	1.6498
10444	68.663	1.4963	12160	69.192	1.9041	13737	69.656	1.7270
10492	68.673	1.7478	12186	69.201	1.9807	13782	69.667	1.7784
10537	68.682	1.7701	12212	69.209	2.1274	13819	69.677	2.0697
10599	68.695	1.5647	12238	69.217	1.9243	13858	69.687	1.6468
10663	68.708	1.0663	12269	69.227	1.8443	13905	69.698	1.9348
10722	68.720	1.6990	12305	69.237	1.8343	14005	69.724	1.8625
10780	68.731	1.9997	12330	69.245	1.9720	14041	69.733	1.7424
10842	68.744	1.0571	12382	69.260	1.9227	14090	69.745	1.8867
10916	68.759	1.7415	12395	69.264	2.1540	13954	69.711	1.7300

Sopelana

Depth (cm)	Age (Ma)	δ13C (‰ VPDB)
13531	69.603	1.8137
13547	69.608	1.7424
13565	69.613	1.5283
13597	69.623	1.9031
13632	69.633	1.7571
13667	69.644	1.5485
13696	69.653	1.6602
13726	69.662	1.8200
13771	69.675	1.7475
13803	69.685	1.4526
13845	69.698	1.8709
13886	69.710	1.5884
13927	69.723	1.8822
13969	69.735	1.4933
14010	69.748	1.8453
14054	69.761	1.3608
14096	69.773	1.8417
14143	69.788	1.3589
14181	69.799	1.9421
14212	69.809	1.1506
14255	69.822	1.6705
14294	69.833	1.7048
14328	69.844	1.7994
14367	69.855	1.3568
14404	69.867	1.6545
14442	69.878	1.2533
14480	69.890	1.6394
14514	69.900	1.0124
14556	69.913	1.6201
14581	69.920	1.4097
14609	69.928	1.7499
14636	69.937	1.6631
14659	69.944	1.4250
14678	69.949	1.7596
14699	69.956	1.5902
14736	69.967	1.5551
14774	69.978	1.8527
14801	69.987	1.5780
14841	69.999	1.6954
14871	70.008	1.9746
14893	70.014	2.0041
14926	70.026	1.6532
14956	70.037	1.7865
14984	70.048	1.7444
15020	70.061	1.9134
15049	70.072	1.6458
15078	70.082	1.7564
15106	70.093	1.8808
15140	70.105	1.9359
15162	70.113	1.5424
15175	70.118	1.7352
15196	70.126	1.2346
15227	70.137	2.0845
15253	70.147	2.0346
15273	70.154	1.8094
15294	70.162	1.7435
15326	70.173	1.7561
15357	70.185	2.0493
15390	70.197	1.9154
15422	70.209	1.6814
15467	70.225	1.9778
15488	70.233	1.8551
15495	70.235	1.8603
15507	70.240	1.9630
15525	70.246	1.9155
15558	70.259	1.6126
15589	70.270	1.9903
15621	70.282	1.8710
15653	70.294	1.9712
15679	70.303	1.7815
15704	70.312	2.0061
15732	70.322	2.0165
15763	70.334	1.9444
15785	70.342	1.7791
15797	70.346	1.8166
15815	70.353	1.6533
15835	70.360	1.6841
15860	70.370	1.9091
15883	70.378	1.6601
15907	70.387	1.7711
15933	70.397	1.7718
15961	70.407	1.6781
15983	70.415	1.9785
16007	70.423	1.7584
16029	70.431	1.6739
16045	70.437	1.6919
16070	70.446	1.7524
16095	70.455	1.4446
16123	70.464	1.6696
16151	70.474	1.6123
16188	70.487	1.5982
16221	70.499	1.6808
16255	70.511	1.5884
16289	70.523	1.7659
16327	70.537	1.6375
16357	70.547	1.5172
16391	70.559	1.5044
16427	70.572	1.5478
16460	70.583	1.4707
16487	70.593	2.0328
16514	70.602	1.6794
16541	70.612	1.4463
16568	70.622	1.9525
16589	70.629	1.6536
16613	70.638	1.7160
16636	70.646	1.3917
16668	70.657	1.7772
16698	70.667	1.7109
16728	70.678	1.7804
16749	70.686	1.7527
16771	70.693	1.4985
16793	70.701	1.7940
16822	70.711	1.5747
16852	70.722	1.5862
16878	70.731	1.5508
16909	70.742	1.6247
16947	70.756	1.4906
16982	70.768	1.9368
17022	70.782	1.6601
17044	70.790	1.7268
17076	70.801	1.7226
17112	70.813	1.6176
17150	70.825	1.6738
17183	70.836	1.6354
17216	70.847	1.8128
17246	70.856	1.8573
17269	70.864	1.7806
17299	70.874	1.8706
17340	70.887	1.7382
17374	70.898	1.7572
17401	70.907	1.7995
17409	70.910	1.7959
17416	70.912	1.9366
17430	70.917	1.5922
17439	70.919	1.9005
17450	70.923	1.7949
17458	70.925	1.7464
17467	70.929	1.7223
17479	70.932	1.8208
17490	70.936	1.7750
17499	70.939	1.6836
17514	70.944	1.7518
17526	70.948	1.8530
17538	70.952	2.1067
17549	70.955	1.7752
17564	70.960	1.9470
17573	70.963	1.8262
17581	70.966	1.8600
17594	70.970	1.8464
17603	70.973	1.7539
17611	70.975	1.8869
17618	70.978	1.8356
17630	70.982	1.7907
17637	70.984	1.7120
17644	70.986	1.8824
17650	70.988	1.8647
17657	70.991	1.6174
17672	70.995	1.9156
17684	70.999	1.9260
17694	71.003	1.9290
17705	71.006	1.9263
17719	71.011	1.7786
17724	71.012	1.9412
17730	71.014	1.8060
17741	71.018	1.7177
17747	71.020	1.9934
17753	71.022	1.9451
17759	71.024	2.0168
17768	71.027	1.8522
17772	71.028	1.9136
17779	71.030	1.9750
17787	71.033	1.7297
17793	71.035	1.6345
17798	71.036	1.7710
17808	71.040	1.9977
17817	71.043	1.8704
17823	71.044	1.9943
17833	71.048	1.9349

17838	71.049	1.9903
17849	71.053	1.9085
17858	71.056	1.8074
17867	71.059	1.7777
17874	71.061	1.5936
17888	71.066	1.8717
17892	71.067	1.9788
17897	71.069	2.0125
17903	71.071	1.9531
17915	71.075	1.7679
17921	71.077	1.9710
17928	71.079	2.2410
17937	71.082	1.7706
17947	71.085	2.0427
17951	71.086	1.9704
17955	71.088	1.8741
17959	71.089	2.0863
17970	71.092	1.8737
17979	71.096	1.8737
17988	71.098	2.0336
17999	71.102	2.0216
18004	71.103	1.9749
18009	71.105	2.0676
18014	71.107	2.0661
18024	71.110	2.0000
18029	71.112	1.8360
18034	71.113	1.9524
18045	71.117	1.9937
18050	71.119	1.9024
18054	71.120	1.8719
18063	71.123	1.8719
18069	71.125	1.9320
18073	71.126	1.9181
18089	71.131	1.9361
18110	71.138	1.8209
18136	71.146	1.7432
18164	71.156	1.9479
18193	71.165	1.7372
18224	71.175	1.6139
18259	71.187	1.8029
18292	71.197	2.0939
18321	71.207	1.7225
18347	71.218	2.0449
18379	71.231	1.7646
18402	71.241	2.0314
18428	71.251	1.7641
18456	71.263	1.8598
18484	71.275	1.8659
18507	71.285	1.6414

Appendix D. Stable carbon isotope data of bulk carbonate

Zumaia

Depth (cm)	Age (Ma)	δ13C (‰VPDB)
-362		1.5726
-350		1.6928
-338		1.3829
-326		1.4066
-317		0.8845
-307		1.9649
-297		1.5104
-288		1.2281
-277		1.5800
-267		1.8809
-255		1.4233
-244		1.7305
-233		1.2141
-219		1.0927
-203		1.2578
-190		0.8065
-179		1.6498
-164		1.4552
-140		0.4821
-120		0.9739
-103		1.3033
-75		1.2279
-51		1.0486
-36		1.0304
-25		0.6205
-8		0.5228
5	65.968	1.6227
15	65.971	1.1878
24	65.973	1.1332
34	65.976	1.4031
45	65.979	1.2164
56	65.982	1.4173
71	65.985	0.7966
83	65.989	1.0035
92	65.991	1.0738
101	65.993	0.9288
111	65.996	0.7769
124	65.999	1.0630
136	66.002	0.9826
149	66.006	1.3368
162	66.009	1.0138
175	66.013	0.9819
189	66.016	0.1121
198	66.019	0.9318
205	66.020	0.4364
219	66.024	0.7791
236	66.028	1.1133
249	66.032	0.7411
261	66.035	0.7869
281	66.040	0.8957
292	66.043	1.4771
302	66.046	1.1956
313	66.048	1.2386
324	66.051	0.8304
334	66.054	0.6330
345	66.057	0.9819
355	66.059	0.7580
366	66.062	0.7605
377	66.065	1.0470
387	66.068	0.7382
398	66.070	0.8480
409	66.073	0.7356
419	66.076	0.8816
430	66.079	0.7683
440	66.081	1.0750
451	66.084	0.7729
462	66.087	0.5221
472	66.090	0.7267
483	66.093	1.1057
494	66.095	0.6735
504	66.098	1.0730
515	66.101	1.3579
525	66.104	0.9331
536	66.106	0.9278
547	66.109	0.8901
557	66.112	0.8620
568	66.115	0.7787
589	66.120	0.6718
601	66.123	1.3928
657	66.138	0.8091
710	66.152	1.3733
754	66.163	0.3886
790	66.172	1.4854
839	66.185	0.7375
880	66.196	1.2534
917	66.205	1.0386
961	66.217	1.3378
990	66.224	1.3485
1034	66.236	0.2037
1047	66.239	0.6303
1059	66.242	1.6581
1072	66.246	1.5430
1083	66.248	1.4985
1103	66.254	1.5722
1132	66.261	1.4741
1171	66.271	1.3545
1201	66.279	1.5570
1238	66.289	1.4033
1271	66.297	1.5469
1302	66.305	1.4146
1344	66.316	1.7111
1375	66.324	1.5921
1403	66.331	1.3624
1441	66.341	1.3787
1470	66.349	1.3888
1508	66.359	1.4428
1538	66.367	1.4942
1558	66.372	1.4697
1568	66.375	1.1658
1578	66.377	1.2529
1587	66.379	0.9725
1595	66.381	0.9922
1604	66.383	1.3318
1612	66.385	1.4650
1620	66.387	1.3495
1629	66.389	1.0706
1637	66.391	0.8569
1647	66.394	0.8791
1658	66.396	0.7404
1669	66.399	1.4699
1680	66.402	1.0115
1691	66.405	1.3255
1702	66.407	1.3075
1713	66.410	1.0365
1724	66.413	1.1079
1734	66.415	1.0064
1745	66.418	1.1017
1756	66.421	1.1852
1766	66.423	1.1647
1777	66.426	1.0832
1787	66.428	0.7936
1798	66.431	0.8890
1809	66.434	1.0595
1821	66.437	0.7721
1834	66.440	0.8780
1847	66.443	1.1204
1860	66.446	1.1624
1873	66.449	0.7009
1886	66.453	0.7775
1899	66.456	0.7843
1912	66.459	0.7542
1923	66.462	1.1082
1931	66.464	1.0678
1939	66.466	0.9555
1947	66.468	1.3717
1955	66.470	1.0101
1970	66.473	1.2254
1981	66.476	1.2293
1992	66.479	0.8962
2003	66.482	1.3265
2014	66.484	0.8990
2025	66.487	1.1592
2035	66.489	0.9980
2046	66.492	0.5650
2057	66.495	0.7789
2067	66.497	1.0254
2078	66.500	1.0790
2088	66.502	1.1304
2099	66.505	1.0136
2109	66.508	1.2105
2120	66.510	0.8305
2131	66.513	1.4521
2141	66.515	0.1958
2152	66.518	0.6798
2163	66.521	1.1528
2174	66.523	1.3127
2184	66.526	0.7031
2195	66.529	0.7773
2206	66.531	0.8374
2217	66.534	1.4321
2229	66.537	0.6467
2240	66.540	1.3128

2252	66.543	0.8477	3643	66.898	1.4587	6107	67.560	1.7273
2264	66.545	1.0867	3684	66.909	1.1480	6134	67.567	1.6313
2275	66.548	0.7476	3735	66.923	1.2609	6164	67.575	1.6580
2287	66.551	0.0223	3778	66.936	1.5846	6214	67.588	1.6649
2299	66.554	0.3628	3828	66.949	0.7296	6243	67.596	1.7570
2310	66.557	1.2131	3880	66.964	1.6076	6287	67.609	1.7906
2320	66.559	1.0830	3928	66.977	0.9890	6320	67.618	1.6081
2328	66.561	1.2803	3972	66.989	1.4808	6360	67.630	1.8478
2337	66.563	0.7447	4002	66.998	1.1193	6399	67.641	1.5703
2345	66.565	1.2403	4054	67.012	1.7109	6439	67.652	1.6728
2353	66.567	0.7252	4086	67.021	1.6457	6478	67.663	1.5689
2361	66.569	0.9909	4125	67.032	1.6018	6518	67.675	1.7786
2370	66.572	0.5904	4148	67.038	1.6504	6549	67.684	1.5514
2378	66.574	1.2677	4159	67.042	1.3369	6584	67.693	1.9003
2386	66.576	0.9973	4201	67.053	1.4887	6614	67.702	1.8083
2395	66.578	1.4797	4241	67.064	1.5108	6652	67.713	1.8596
2404	66.580	1.0725	4284	67.076	1.3921	6688	67.723	1.7190
2413	66.582	0.9394	4326	67.088	1.6132	6725	67.734	1.5028
2422	66.584	1.2867	4356	67.096	1.6813	6761	67.744	1.4720
2430	66.586	1.0896	4399	67.108	1.7842	6793	67.753	1.5014
2439	66.589	0.6693	4431	67.117	1.6971	6826	67.762	1.7085
2448	66.591	1.2101	4480	67.131	1.3693	6880	67.778	1.3453
2457	66.593	1.2757	4508	67.139	1.5450	6906	67.785	1.7902
2466	66.595	1.5611	4537	67.147	1.8887	6948	67.797	1.1174
2477	66.598	1.0313	4587	67.161	1.5781	6992	67.810	1.5749
2488	66.601	1.5664	4605	67.165	1.8531	7034	67.821	1.5161
2499	66.603	1.6393	4632	67.173	1.6671	7079	67.834	1.7916
2509	66.606	1.5300	4657	67.180	1.7120	7125	67.847	1.8575
2520	66.609	1.3840	4682	67.187	1.4827	7178	67.862	2.0040
2531	66.611	1.7755	4705	67.193	1.3286	7232	67.878	1.3808
2542	66.614	1.4668	4722	67.198	1.6353	7284	67.893	1.8447
2550	66.616	1.2239	4769	67.210	1.0104	7321	67.903	1.7699
2556	66.617	1.2672	4797	67.217	1.5441	7353	67.912	1.8434
2563	66.619	1.1599	4838	67.228	1.6292	7395	67.924	1.8632
2569	66.620	1.4948	4868	67.236	1.4963	7439	67.937	1.9454
2595	66.627	1.5162	4909	67.247	1.4571	7470	67.945	1.7947
2644	66.639	1.5710	4955	67.259	1.3659	7517	67.959	1.9191
2680	66.648	1.3819	4995	67.269	1.7289	7556	67.970	2.0421
2732	66.661	1.7323	5019	67.275	1.5346	7587	67.979	1.8132
2765	66.669	1.4931	5053	67.284	1.4550	7610	67.985	1.8060
2801	66.677	1.4472	5079	67.291	1.3865	7642	67.994	2.0882
2832	66.685	1.5616	5126	67.303	1.6585	7666	68.001	2.0213
2860	66.692	1.6448	5200	67.323	1.1101	7688	68.007	1.9054
2897	66.701	1.3540	5255	67.337	1.3966	7719	68.015	1.9222
2930	66.709	1.7719	5305	67.350	0.7090	7756	68.025	1.8312
2963	66.717	1.5057	5341	67.360	1.4199	7796	68.036	1.8090
3001	66.727	1.7060	5385	67.371	0.7895	7830	68.045	1.7743
3043	66.737	1.5335	5426	67.382	1.6428	7851	68.051	2.0382
3081	66.746	1.7100	5470	67.393	0.9003	7879	68.059	1.7764
3120	66.756	1.7417	5514	67.405	1.4818	7908	68.067	1.8634
3164	66.767	1.6588	5573	67.420	0.9816	7943	68.076	1.9892
3195	66.774	1.7516	5640	67.438	1.6298	7984	68.087	1.8806
3234	66.784	1.7463	5704	67.455	1.2805	8021	68.098	1.9199
3278	66.797	1.6607	5748	67.466	1.5933	8064	68.109	1.8108
3320	66.808	1.8468	5792	67.478	0.4786	8104	68.120	1.6103
3357	66.819	1.2482	5833	67.488	1.6699	8133	68.128	2.0816
3408	66.833	1.7572	5866	67.497	1.5246	8153	68.134	1.8059
3444	66.843	1.2743	5899	67.505	1.3073	8233	68.156	1.8458
3493	66.856	1.5241	5994	67.530	1.6621	8265	68.164	1.6577
3530	66.866	1.2820	6051	67.545	1.6250	8307	68.176	1.7058
3590	66.883	1.4499	6093	67.556	1.8390	8356	68.189	1.7470

8415	68.205	1.3842	10947	68.765	1.7617	12411	69.269	1.9910
8451	68.215	1.5872	10995	68.775	1.8701	12419	69.271	1.9853
8479	68.223	1.7408	11026	68.781	1.8727	12433	69.275	2.0270
8503	68.229	1.2863	11051	68.786	2.0339	12448	69.280	1.8676
8537	68.239	1.8337	11066	68.792	1.6724	12458	69.283	1.9518
8611	68.259	1.7298	11073	68.795	1.7998	12474	69.288	1.8533
8656	68.271	1.6463	11098	68.804	2.2319	12503	69.296	2.0107
8713	68.287	1.4151	11120	68.812	1.7864	12541	69.308	1.9093
8757	68.299	1.8656	11147	68.821	2.1466	12580	69.319	1.9177
8799	68.310	1.4470	11172	68.831	1.9091	12608	69.328	2.2092
8842	68.322	1.6203	11184	68.835	1.9893	12643	69.338	1.8359
8891	68.335	1.5590	11208	68.844	1.8566	12672	69.347	2.0126
8936	68.348	1.6074	11237	68.854	2.1047	12687	69.351	1.8506
8983	68.361	1.4658	11265	68.865	2.1130	12700	69.355	2.1844
9023	68.371	1.7854	11298	68.877	2.0211	12729	69.364	2.0325
9056	68.381	1.5467	11326	68.887	2.1946	12751	69.370	1.9500
9103	68.391	1.5308	11352	68.896	2.1539	12793	69.383	2.0727
9147	68.400	1.7491	11387	68.909	2.0972	12839	69.396	1.6120
9202	68.411	1.6908	11422	68.922	1.9714	12872	69.406	1.9342
9236	68.418	1.5655	11454	68.934	2.1075	12923	69.422	2.0012
9282	68.427	1.6916	11479	68.943	2.1562	12961	69.433	1.5356
9322	68.435	1.4915	11504	68.952	2.1104	13011	69.448	1.9557
9371	68.445	1.8748	11534	68.963	2.0467	13052	69.460	1.8671
9415	68.454	1.5779	11580	68.980	2.2329	13092	69.472	1.8124
9462	68.463	1.9238	11617	68.993	2.1342	13131	69.483	1.7752
9503	68.472	1.7726	11656	69.008	1.8261	13171	69.495	1.9688
9559	68.483	1.7185	11695	69.022	1.9778	13206	69.506	1.8103
9591	68.490	1.3162	11736	69.037	2.2284	13246	69.518	1.9855
9649	68.502	1.6398	11765	69.047	2.1369	13277	69.527	1.9207
9701	68.512	1.1182	11791	69.057	2.2338	13292	69.532	2.0603
9819	68.536	1.5732	11823	69.068	2.0508	13316	69.539	1.8228
9871	68.547	1.6354	11853	69.079	2.2310	13355	69.550	2.0188
9911	68.555	1.6459	11893	69.094	2.1579	13395	69.562	1.7973
9951	68.563	0.8578	11910	69.100	2.2696	13448	69.578	2.1325
9985	68.570	1.6823	11929	69.107	2.0417	13483	69.588	1.7807
10036	68.580	1.2743	11949	69.114	2.0803	13522	69.600	1.8069
10087	68.591	1.4953	11969	69.122	2.1629	13547	69.608	1.8614
10186	68.611	1.3691	11991	69.130	2.2805	13569	69.613	1.8375
10229	68.619	1.6364	12013	69.138	2.1378	13604	69.622	2.0668
10294	68.633	1.6742	12049	69.151	2.2554	13636	69.630	1.9583
10354	68.645	1.7665	12087	69.165	2.0219	13677	69.641	1.6082
10396	68.653	1.5996	12125	69.179	2.1768	13709	69.649	1.6498
10444	68.663	1.4963	12160	69.192	1.9041	13737	69.656	1.7270
10492	68.673	1.7478	12186	69.201	1.9807	13782	69.667	1.7784
10537	68.682	1.7701	12212	69.209	2.1274	13819	69.677	2.0697
10599	68.695	1.5647	12238	69.217	1.9243	13858	69.687	1.6468
10663	68.708	1.0663	12269	69.227	1.8443	13905	69.698	1.9348
10722	68.720	1.6990	12305	69.237	1.8343	14005	69.724	1.8625
10780	68.731	1.9997	12330	69.245	1.9720	14041	69.733	1.7424
10842	68.744	1.0571	12382	69.260	1.9227	14090	69.745	1.8867
10916	68.759	1.7415	12395	69.264	2.1540	13954	69.711	1.7300

Sopelana

Depth (cm)	Age (Ma)	δ13C (‰ VPDB)
13531	69.603	1.8137
13547	69.608	1.7424
13565	69.613	1.5283
13597	69.623	1.9031
13632	69.633	1.7571
13667	69.644	1.5485
13696	69.653	1.6602
13726	69.662	1.8200
13771	69.675	1.7475
13803	69.685	1.4526
13845	69.698	1.8709
13886	69.710	1.5884
13927	69.723	1.8822
13969	69.735	1.4933
14010	69.748	1.8453
14054	69.761	1.3608
14096	69.773	1.8417
14143	69.788	1.3589
14181	69.799	1.9421
14212	69.809	1.1506
14255	69.822	1.6705
14294	69.833	1.7048
14328	69.844	1.7994
14367	69.855	1.3568
14404	69.867	1.6545
14442	69.878	1.2533
14480	69.890	1.6394
14514	69.900	1.0124
14556	69.913	1.6201
14581	69.920	1.4097
14609	69.928	1.7499
14636	69.937	1.6631
14659	69.944	1.4250
14678	69.949	1.7596
14699	69.956	1.5902
14736	69.967	1.5551
14774	69.978	1.8527
14801	69.987	1.5780
14841	69.999	1.6954
14871	70.008	1.9746
14893	70.014	2.0041
14926	70.026	1.6532
14956	70.037	1.7865
14984	70.048	1.7444
15020	70.061	1.9134
15049	70.072	1.6458
15078	70.082	1.7564
15106	70.093	1.8808
15140	70.105	1.9359
15162	70.113	1.5424
15175	70.118	1.7352
15196	70.126	1.2346
15227	70.137	2.0845
15253	70.147	2.0346
15273	70.154	1.8094
15294	70.162	1.7435
15326	70.173	1.7561
15357	70.185	2.0493
15390	70.197	1.9154
15422	70.209	1.6814
15467	70.225	1.9778
15488	70.233	1.8551
15495	70.235	1.8603
15507	70.240	1.9630
15525	70.246	1.9155
15558	70.259	1.6126
15589	70.270	1.9903
15621	70.282	1.8710
15653	70.294	1.9712
15679	70.303	1.7815
15704	70.312	2.0061
15732	70.322	2.0165
15763	70.334	1.9444
15785	70.342	1.7791
15797	70.346	1.8166
15815	70.353	1.6533
15835	70.360	1.6841
15860	70.370	1.9091
15883	70.378	1.6601
15907	70.387	1.7711
15933	70.397	1.7718
15961	70.407	1.6781
15983	70.415	1.9785
16007	70.423	1.7584
16029	70.431	1.6739
16045	70.437	1.6919
16070	70.446	1.7524
16095	70.455	1.4446
16123	70.464	1.6696
16151	70.474	1.6123
16188	70.487	1.5982
16221	70.499	1.6808
16255	70.511	1.5884
16289	70.523	1.7659
16327	70.537	1.6375
16357	70.547	1.5172
16391	70.559	1.5044
16427	70.572	1.5478
16460	70.583	1.4707
16487	70.593	2.0328
16514	70.602	1.6794
16541	70.612	1.4463
16568	70.622	1.9525
16589	70.629	1.6536
16613	70.638	1.7160
16636	70.646	1.3917
16668	70.657	1.7772
16698	70.667	1.7109
16728	70.678	1.7804
16749	70.686	1.7527
16771	70.693	1.4985
16793	70.701	1.7940
16822	70.711	1.5747
16852	70.722	1.5862
16878	70.731	1.5508
16909	70.742	1.6247
16947	70.756	1.4906
16982	70.768	1.9368
17022	70.782	1.6601
17044	70.790	1.7268
17076	70.801	1.7226
17112	70.813	1.6176
17150	70.825	1.6738
17183	70.836	1.6354
17216	70.847	1.8128
17246	70.856	1.8573
17269	70.864	1.7806
17299	70.874	1.8706
17340	70.887	1.7382
17374	70.898	1.7572
17401	70.907	1.7995
17409	70.910	1.7959
17416	70.912	1.9366
17430	70.917	1.5922
17439	70.919	1.9005
17450	70.923	1.7949
17458	70.925	1.7464
17467	70.929	1.7223
17479	70.932	1.8208
17490	70.936	1.7750
17499	70.939	1.6836
17514	70.944	1.7518
17526	70.948	1.8530
17538	70.952	2.1067
17549	70.955	1.7752
17564	70.960	1.9470
17573	70.963	1.8262
17581	70.966	1.8600
17594	70.970	1.8464
17603	70.973	1.7539
17611	70.975	1.8869
17618	70.978	1.8356
17630	70.982	1.7907
17637	70.984	1.7120
17644	70.986	1.8824
17650	70.988	1.8647
17657	70.991	1.6174
17672	70.995	1.9156
17684	70.999	1.9260
17694	71.003	1.9290
17705	71.006	1.9263
17719	71.011	1.7786
17724	71.012	1.9412
17730	71.014	1.8060
17741	71.018	1.7177
17747	71.020	1.9934
17753	71.022	1.9451
17759	71.024	2.0168
17768	71.027	1.8522
17772	71.028	1.9136
17779	71.030	1.9750
17787	71.033	1.7297
17793	71.035	1.6345
17798	71.036	1.7710
17808	71.040	1.9977
17817	71.043	1.8704
17823	71.044	1.9943
17833	71.048	1.9349

17838	71.049	1.9903
17849	71.053	1.9085
17858	71.056	1.8074
17867	71.059	1.7777
17874	71.061	1.5936
17888	71.066	1.8717
17892	71.067	1.9788
17897	71.069	2.0125
17903	71.071	1.9531
17915	71.075	1.7679
17921	71.077	1.9710
17928	71.079	2.2410
17937	71.082	1.7706
17947	71.085	2.0427
17951	71.086	1.9704
17955	71.088	1.8741
17959	71.089	2.0863
17970	71.092	1.8737
17979	71.096	1.8737
17988	71.098	2.0336
17999	71.102	2.0216
18004	71.103	1.9749
18009	71.105	2.0676
18014	71.107	2.0661
18024	71.110	2.0000
18029	71.112	1.8360
18034	71.113	1.9524
18045	71.117	1.9937
18050	71.119	1.9024
18054	71.120	1.8719
18063	71.123	1.8719
18069	71.125	1.9320
18073	71.126	1.9181
18089	71.131	1.9361
18110	71.138	1.8209
18136	71.146	1.7432
18164	71.156	1.9479
18193	71.165	1.7372
18224	71.175	1.6139
18259	71.187	1.8029
18292	71.197	2.0939
18321	71.207	1.7225
18347	71.218	2.0449
18379	71.231	1.7646
18402	71.241	2.0314
18428	71.251	1.7641
18456	71.263	1.8598
18484	71.275	1.8659
18507	71.285	1.6414

Appendix D. Stable carbon isotope data of bulk carbonate

Zumaia

Depth (cm)	Age (Ma)	δ13C (‰VPDB)
-362		1.5726
-350		1.6928
-338		1.3829
-326		1.4066
-317		0.8845
-307		1.9649
-297		1.5104
-288		1.2281
-277		1.5800
-267		1.8809
-255		1.4233
-244		1.7305
-233		1.2141
-219		1.0927
-203		1.2578
-190		0.8065
-179		1.6498
-164		1.4552
-140		0.4821
-120		0.9739
-103		1.3033
-75		1.2279
-51		1.0486
-36		1.0304
-25		0.6205
-8		0.5228
5	65.968	1.6227
15	65.971	1.1878
24	65.973	1.1332
34	65.976	1.4031
45	65.979	1.2164
56	65.982	1.4173
71	65.985	0.7966
83	65.989	1.0035
92	65.991	1.0738
101	65.993	0.9288
111	65.996	0.7769
124	65.999	1.0630
136	66.002	0.9826
149	66.006	1.3368
162	66.009	1.0138
175	66.013	0.9819
189	66.016	0.1121
198	66.019	0.9318
205	66.020	0.4364
219	66.024	0.7791
236	66.028	1.1133
249	66.032	0.7411
261	66.035	0.7869
281	66.040	0.8957
292	66.043	1.4771
302	66.046	1.1956
313	66.048	1.2386
324	66.051	0.8304
334	66.054	0.6330
345	66.057	0.9819
355	66.059	0.7580
366	66.062	0.7605
377	66.065	1.0470
387	66.068	0.7382
398	66.070	0.8480
409	66.073	0.7356
419	66.076	0.8816
430	66.079	0.7683
440	66.081	1.0750
451	66.084	0.7729
462	66.087	0.5221
472	66.090	0.7267
483	66.093	1.1057
494	66.095	0.6735
504	66.098	1.0730
515	66.101	1.3579
525	66.104	0.9331
536	66.106	0.9278
547	66.109	0.8901
557	66.112	0.8620
568	66.115	0.7787
589	66.120	0.6718
601	66.123	1.3928
657	66.138	0.8091
710	66.152	1.3733
754	66.163	0.3886
790	66.172	1.4854
839	66.185	0.7375
880	66.196	1.2534
917	66.205	1.0386
961	66.217	1.3378
990	66.224	1.3485
1034	66.236	0.2037
1047	66.239	0.6303
1059	66.242	1.6581
1072	66.246	1.5430
1083	66.248	1.4985
1103	66.254	1.5722
1132	66.261	1.4741
1171	66.271	1.3545
1201	66.279	1.5570
1238	66.289	1.4033
1271	66.297	1.5469
1302	66.305	1.4146
1344	66.316	1.7111
1375	66.324	1.5921
1403	66.331	1.3624
1441	66.341	1.3787
1470	66.349	1.3888
1508	66.359	1.4428
1538	66.367	1.4942
1558	66.372	1.4697
1568	66.375	1.1658
1578	66.377	1.2529
1587	66.379	0.9725
1595	66.381	0.9922
1604	66.383	1.3318
1612	66.385	1.4650
1620	66.387	1.3495
1629	66.389	1.0706
1637	66.391	0.8569
1647	66.394	0.8791
1658	66.396	0.7404
1669	66.399	1.4699
1680	66.402	1.0115
1691	66.405	1.3255
1702	66.407	1.3075
1713	66.410	1.0365
1724	66.413	1.1079
1734	66.415	1.0064
1745	66.418	1.1017
1756	66.421	1.1852
1766	66.423	1.1647
1777	66.426	1.0832
1787	66.428	0.7936
1798	66.431	0.8890
1809	66.434	1.0595
1821	66.437	0.7721
1834	66.440	0.8780
1847	66.443	1.1204
1860	66.446	1.1624
1873	66.449	0.7009
1886	66.453	0.7775
1899	66.456	0.7843
1912	66.459	0.7542
1923	66.462	1.1082
1931	66.464	1.0678
1939	66.466	0.9555
1947	66.468	1.3717
1955	66.470	1.0101
1970	66.473	1.2254
1981	66.476	1.2293
1992	66.479	0.8962
2003	66.482	1.3265
2014	66.484	0.8990
2025	66.487	1.1592
2035	66.489	0.9980
2046	66.492	0.5650
2057	66.495	0.7789
2067	66.497	1.0254
2078	66.500	1.0790
2088	66.502	1.1304
2099	66.505	1.0136
2109	66.508	1.2105
2120	66.510	0.8305
2131	66.513	1.4521
2141	66.515	0.1958
2152	66.518	0.6798
2163	66.521	1.1528
2174	66.523	1.3127
2184	66.526	0.7031
2195	66.529	0.7773
2206	66.531	0.8374
2217	66.534	1.4321
2229	66.537	0.6467
2240	66.540	1.3128

2252	66.543	0.8477	3643	66.898	1.4587	6107	67.560	1.7273
2264	66.545	1.0867	3684	66.909	1.1480	6134	67.567	1.6313
2275	66.548	0.7476	3735	66.923	1.2609	6164	67.575	1.6580
2287	66.551	0.0223	3778	66.936	1.5846	6214	67.588	1.6649
2299	66.554	0.3628	3828	66.949	0.7296	6243	67.596	1.7570
2310	66.557	1.2131	3880	66.964	1.6076	6287	67.609	1.7906
2320	66.559	1.0830	3928	66.977	0.9890	6320	67.618	1.6081
2328	66.561	1.2803	3972	66.989	1.4808	6360	67.630	1.8478
2337	66.563	0.7447	4002	66.998	1.1193	6399	67.641	1.5703
2345	66.565	1.2403	4054	67.012	1.7109	6439	67.652	1.6728
2353	66.567	0.7252	4086	67.021	1.6457	6478	67.663	1.5689
2361	66.569	0.9909	4125	67.032	1.6018	6518	67.675	1.7786
2370	66.572	0.5904	4148	67.038	1.6504	6549	67.684	1.5514
2378	66.574	1.2677	4159	67.042	1.3369	6584	67.693	1.9003
2386	66.576	0.9973	4201	67.053	1.4887	6614	67.702	1.8083
2395	66.578	1.4797	4241	67.064	1.5108	6652	67.713	1.8596
2404	66.580	1.0725	4284	67.076	1.3921	6688	67.723	1.7190
2413	66.582	0.9394	4326	67.088	1.6132	6725	67.734	1.5028
2422	66.584	1.2867	4356	67.096	1.6813	6761	67.744	1.4720
2430	66.586	1.0896	4399	67.108	1.7842	6793	67.753	1.5014
2439	66.589	0.6693	4431	67.117	1.6971	6826	67.762	1.7085
2448	66.591	1.2101	4480	67.131	1.3693	6880	67.778	1.3453
2457	66.593	1.2757	4508	67.139	1.5450	6906	67.785	1.7902
2466	66.595	1.5611	4537	67.147	1.8887	6948	67.797	1.1174
2477	66.598	1.0313	4587	67.161	1.5781	6992	67.810	1.5749
2488	66.601	1.5664	4605	67.165	1.8531	7034	67.821	1.5161
2499	66.603	1.6393	4632	67.173	1.6671	7079	67.834	1.7916
2509	66.606	1.5300	4657	67.180	1.7120	7125	67.847	1.8575
2520	66.609	1.3840	4682	67.187	1.4827	7178	67.862	2.0040
2531	66.611	1.7755	4705	67.193	1.3286	7232	67.878	1.3808
2542	66.614	1.4668	4722	67.198	1.6353	7284	67.893	1.8447
2550	66.616	1.2239	4769	67.210	1.0104	7321	67.903	1.7699
2556	66.617	1.2672	4797	67.217	1.5441	7353	67.912	1.8434
2563	66.619	1.1599	4838	67.228	1.6292	7395	67.924	1.8632
2569	66.620	1.4948	4868	67.236	1.4963	7439	67.937	1.9454
2595	66.627	1.5162	4909	67.247	1.4571	7470	67.945	1.7947
2644	66.639	1.5710	4955	67.259	1.3659	7517	67.959	1.9191
2680	66.648	1.3819	4995	67.269	1.7289	7556	67.970	2.0421
2732	66.661	1.7323	5019	67.275	1.5346	7587	67.979	1.8132
2765	66.669	1.4931	5053	67.284	1.4550	7610	67.985	1.8060
2801	66.677	1.4472	5079	67.291	1.3865	7642	67.994	2.0882
2832	66.685	1.5616	5126	67.303	1.6585	7666	68.001	2.0213
2860	66.692	1.6448	5200	67.323	1.1101	7688	68.007	1.9054
2897	66.701	1.3540	5255	67.337	1.3966	7719	68.015	1.9222
2930	66.709	1.7719	5305	67.350	0.7090	7756	68.025	1.8312
2963	66.717	1.5057	5341	67.360	1.4199	7796	68.036	1.8090
3001	66.727	1.7060	5385	67.371	0.7895	7830	68.045	1.7743
3043	66.737	1.5335	5426	67.382	1.6428	7851	68.051	2.0382
3081	66.746	1.7100	5470	67.393	0.9003	7879	68.059	1.7764
3120	66.756	1.7417	5514	67.405	1.4818	7908	68.067	1.8634
3164	66.767	1.6588	5573	67.420	0.9816	7943	68.076	1.9892
3195	66.774	1.7516	5640	67.438	1.6298	7984	68.087	1.8806
3234	66.784	1.7463	5704	67.455	1.2805	8021	68.098	1.9199
3278	66.797	1.6607	5748	67.466	1.5933	8064	68.109	1.8108
3320	66.808	1.8468	5792	67.478	0.4786	8104	68.120	1.6103
3357	66.819	1.2482	5833	67.488	1.6699	8133	68.128	2.0816
3408	66.833	1.7572	5866	67.497	1.5246	8153	68.134	1.8059
3444	66.843	1.2743	5899	67.505	1.3073	8233	68.156	1.8458
3493	66.856	1.5241	5994	67.530	1.6621	8265	68.164	1.6577
3530	66.866	1.2820	6051	67.545	1.6250	8307	68.176	1.7058
3590	66.883	1.4499	6093	67.556	1.8390	8356	68.189	1.7470

8415	68.205	1.3842	10947	68.765	1.7617	12411	69.269	1.9910
8451	68.215	1.5872	10995	68.775	1.8701	12419	69.271	1.9853
8479	68.223	1.7408	11026	68.781	1.8727	12433	69.275	2.0270
8503	68.229	1.2863	11051	68.786	2.0339	12448	69.280	1.8676
8537	68.239	1.8337	11066	68.792	1.6724	12458	69.283	1.9518
8611	68.259	1.7298	11073	68.795	1.7998	12474	69.288	1.8533
8656	68.271	1.6463	11098	68.804	2.2319	12503	69.296	2.0107
8713	68.287	1.4151	11120	68.812	1.7864	12541	69.308	1.9093
8757	68.299	1.8656	11147	68.821	2.1466	12580	69.319	1.9177
8799	68.310	1.4470	11172	68.831	1.9091	12608	69.328	2.2092
8842	68.322	1.6203	11184	68.835	1.9893	12643	69.338	1.8359
8891	68.335	1.5590	11208	68.844	1.8566	12672	69.347	2.0126
8936	68.348	1.6074	11237	68.854	2.1047	12687	69.351	1.8506
8983	68.361	1.4658	11265	68.865	2.1130	12700	69.355	2.1844
9023	68.371	1.7854	11298	68.877	2.0211	12729	69.364	2.0325
9056	68.381	1.5467	11326	68.887	2.1946	12751	69.370	1.9500
9103	68.391	1.5308	11352	68.896	2.1539	12793	69.383	2.0727
9147	68.400	1.7491	11387	68.909	2.0972	12839	69.396	1.6120
9202	68.411	1.6908	11422	68.922	1.9714	12872	69.406	1.9342
9236	68.418	1.5655	11454	68.934	2.1075	12923	69.422	2.0012
9282	68.427	1.6916	11479	68.943	2.1562	12961	69.433	1.5356
9322	68.435	1.4915	11504	68.952	2.1104	13011	69.448	1.9557
9371	68.445	1.8748	11534	68.963	2.0467	13052	69.460	1.8671
9415	68.454	1.5779	11580	68.980	2.2329	13092	69.472	1.8124
9462	68.463	1.9238	11617	68.993	2.1342	13131	69.483	1.7752
9503	68.472	1.7726	11656	69.008	1.8261	13171	69.495	1.9688
9559	68.483	1.7185	11695	69.022	1.9778	13206	69.506	1.8103
9591	68.490	1.3162	11736	69.037	2.2284	13246	69.518	1.9855
9649	68.502	1.6398	11765	69.047	2.1369	13277	69.527	1.9207
9701	68.512	1.1182	11791	69.057	2.2338	13292	69.532	2.0603
9819	68.536	1.5732	11823	69.068	2.0508	13316	69.539	1.8228
9871	68.547	1.6354	11853	69.079	2.2310	13355	69.550	2.0188
9911	68.555	1.6459	11893	69.094	2.1579	13395	69.562	1.7973
9951	68.563	0.8578	11910	69.100	2.2696	13448	69.578	2.1325
9985	68.570	1.6823	11929	69.107	2.0417	13483	69.588	1.7807
10036	68.580	1.2743	11949	69.114	2.0803	13522	69.600	1.8069
10087	68.591	1.4953	11969	69.122	2.1629	13547	69.608	1.8614
10186	68.611	1.3691	11991	69.130	2.2805	13569	69.613	1.8375
10229	68.619	1.6364	12013	69.138	2.1378	13604	69.622	2.0668
10294	68.633	1.6742	12049	69.151	2.2554	13636	69.630	1.9583
10354	68.645	1.7665	12087	69.165	2.0219	13677	69.641	1.6082
10396	68.653	1.5996	12125	69.179	2.1768	13709	69.649	1.6498
10444	68.663	1.4963	12160	69.192	1.9041	13737	69.656	1.7270
10492	68.673	1.7478	12186	69.201	1.9807	13782	69.667	1.7784
10537	68.682	1.7701	12212	69.209	2.1274	13819	69.677	2.0697
10599	68.695	1.5647	12238	69.217	1.9243	13858	69.687	1.6468
10663	68.708	1.0663	12269	69.227	1.8443	13905	69.698	1.9348
10722	68.720	1.6990	12305	69.237	1.8343	14005	69.724	1.8625
10780	68.731	1.9997	12330	69.245	1.9720	14041	69.733	1.7424
10842	68.744	1.0571	12382	69.260	1.9227	14090	69.745	1.8867
10916	68.759	1.7415	12395	69.264	2.1540	13954	69.711	1.7300

Sopelana

Depth (cm)	Age (Ma)	δ13C (‰ VPDB)
13531	69.603	1.8137
13547	69.608	1.7424
13565	69.613	1.5283
13597	69.623	1.9031
13632	69.633	1.7571
13667	69.644	1.5485
13696	69.653	1.6602
13726	69.662	1.8200
13771	69.675	1.7475
13803	69.685	1.4526
13845	69.698	1.8709
13886	69.710	1.5884
13927	69.723	1.8822
13969	69.735	1.4933
14010	69.748	1.8453
14054	69.761	1.3608
14096	69.773	1.8417
14143	69.788	1.3589
14181	69.799	1.9421
14212	69.809	1.1506
14255	69.822	1.6705
14294	69.833	1.7048
14328	69.844	1.7994
14367	69.855	1.3568
14404	69.867	1.6545
14442	69.878	1.2533
14480	69.890	1.6394
14514	69.900	1.0124
14556	69.913	1.6201
14581	69.920	1.4097
14609	69.928	1.7499
14636	69.937	1.6631
14659	69.944	1.4250
14678	69.949	1.7596
14699	69.956	1.5902
14736	69.967	1.5551
14774	69.978	1.8527
14801	69.987	1.5780
14841	69.999	1.6954
14871	70.008	1.9746
14893	70.014	2.0041
14926	70.026	1.6532
14956	70.037	1.7865
14984	70.048	1.7444
15020	70.061	1.9134
15049	70.072	1.6458
15078	70.082	1.7564
15106	70.093	1.8808
15140	70.105	1.9359
15162	70.113	1.5424
15175	70.118	1.7352
15196	70.126	1.2346
15227	70.137	2.0845
15253	70.147	2.0346
15273	70.154	1.8094
15294	70.162	1.7435
15326	70.173	1.7561
15357	70.185	2.0493
15390	70.197	1.9154
15422	70.209	1.6814
15467	70.225	1.9778
15488	70.233	1.8551
15495	70.235	1.8603
15507	70.240	1.9630
15525	70.246	1.9155
15558	70.259	1.6126
15589	70.270	1.9903
15621	70.282	1.8710
15653	70.294	1.9712
15679	70.303	1.7815
15704	70.312	2.0061
15732	70.322	2.0165
15763	70.334	1.9444
15785	70.342	1.7791
15797	70.346	1.8166
15815	70.353	1.6533
15835	70.360	1.6841
15860	70.370	1.9091
15883	70.378	1.6601
15907	70.387	1.7711
15933	70.397	1.7718
15961	70.407	1.6781
15983	70.415	1.9785
16007	70.423	1.7584
16029	70.431	1.6739
16045	70.437	1.6919
16070	70.446	1.7524
16095	70.455	1.4446
16123	70.464	1.6696
16151	70.474	1.6123
16188	70.487	1.5982
16221	70.499	1.6808
16255	70.511	1.5884
16289	70.523	1.7659
16327	70.537	1.6375
16357	70.547	1.5172
16391	70.559	1.5044
16427	70.572	1.5478
16460	70.583	1.4707
16487	70.593	2.0328
16514	70.602	1.6794
16541	70.612	1.4463
16568	70.622	1.9525
16589	70.629	1.6536
16613	70.638	1.7160
16636	70.646	1.3917
16668	70.657	1.7772
16698	70.667	1.7109
16728	70.678	1.7804
16749	70.686	1.7527
16771	70.693	1.4985
16793	70.701	1.7940
16822	70.711	1.5747
16852	70.722	1.5862
16878	70.731	1.5508
16909	70.742	1.6247
16947	70.756	1.4906
16982	70.768	1.9368
17022	70.782	1.6601
17044	70.790	1.7268
17076	70.801	1.7226
17112	70.813	1.6176
17150	70.825	1.6738
17183	70.836	1.6354
17216	70.847	1.8128
17246	70.856	1.8573
17269	70.864	1.7806
17299	70.874	1.8706
17340	70.887	1.7382
17374	70.898	1.7572
17401	70.907	1.7995
17409	70.910	1.7959
17416	70.912	1.9366
17430	70.917	1.5922
17439	70.919	1.9005
17450	70.923	1.7949
17458	70.925	1.7464
17467	70.929	1.7223
17479	70.932	1.8208
17490	70.936	1.7750
17499	70.939	1.6836
17514	70.944	1.7518
17526	70.948	1.8530
17538	70.952	2.1067
17549	70.955	1.7752
17564	70.960	1.9470
17573	70.963	1.8262
17581	70.966	1.8600
17594	70.970	1.8464
17603	70.973	1.7539
17611	70.975	1.8869
17618	70.978	1.8356
17630	70.982	1.7907
17637	70.984	1.7120
17644	70.986	1.8824
17650	70.988	1.8647
17657	70.991	1.6174
17672	70.995	1.9156
17684	70.999	1.9260
17694	71.003	1.9290
17705	71.006	1.9263
17719	71.011	1.7786
17724	71.012	1.9412
17730	71.014	1.8060
17741	71.018	1.7177
17747	71.020	1.9934
17753	71.022	1.9451
17759	71.024	2.0168
17768	71.027	1.8522
17772	71.028	1.9136
17779	71.030	1.9750
17787	71.033	1.7297
17793	71.035	1.6345
17798	71.036	1.7710
17808	71.040	1.9977
17817	71.043	1.8704
17823	71.044	1.9943
17833	71.048	1.9349

17838	71.049	1.9903
17849	71.053	1.9085
17858	71.056	1.8074
17867	71.059	1.7777
17874	71.061	1.5936
17888	71.066	1.8717
17892	71.067	1.9788
17897	71.069	2.0125
17903	71.071	1.9531
17915	71.075	1.7679
17921	71.077	1.9710
17928	71.079	2.2410
17937	71.082	1.7706
17947	71.085	2.0427
17951	71.086	1.9704
17955	71.088	1.8741
17959	71.089	2.0863
17970	71.092	1.8737
17979	71.096	1.8737
17988	71.098	2.0336
17999	71.102	2.0216
18004	71.103	1.9749
18009	71.105	2.0676
18014	71.107	2.0661
18024	71.110	2.0000
18029	71.112	1.8360
18034	71.113	1.9524
18045	71.117	1.9937
18050	71.119	1.9024
18054	71.120	1.8719
18063	71.123	1.8719
18069	71.125	1.9320
18073	71.126	1.9181
18089	71.131	1.9361
18110	71.138	1.8209
18136	71.146	1.7432
18164	71.156	1.9479
18193	71.165	1.7372
18224	71.175	1.6139
18259	71.187	1.8029
18292	71.197	2.0939
18321	71.207	1.7225
18347	71.218	2.0449
18379	71.231	1.7646
18402	71.241	2.0314
18428	71.251	1.7641
18456	71.263	1.8598
18484	71.275	1.8659
18507	71.285	1.6414

Appendix D. Stable carbon isotope data of bulk carbonate

Zumaia

Depth (cm)	Age (Ma)	δ13C (‰VPDB)
-362		1.5726
-350		1.6928
-338		1.3829
-326		1.4066
-317		0.8845
-307		1.9649
-297		1.5104
-288		1.2281
-277		1.5800
-267		1.8809
-255		1.4233
-244		1.7305
-233		1.2141
-219		1.0927
-203		1.2578
-190		0.8065
-179		1.6498
-164		1.4552
-140		0.4821
-120		0.9739
-103		1.3033
-75		1.2279
-51		1.0486
-36		1.0304
-25		0.6205
-8		0.5228
5	65.968	1.6227
15	65.971	1.1878
24	65.973	1.1332
34	65.976	1.4031
45	65.979	1.2164
56	65.982	1.4173
71	65.985	0.7966
83	65.989	1.0035
92	65.991	1.0738
101	65.993	0.9288
111	65.996	0.7769
124	65.999	1.0630
136	66.002	0.9826
149	66.006	1.3368
162	66.009	1.0138
175	66.013	0.9819
189	66.016	0.1121
198	66.019	0.9318
205	66.020	0.4364
219	66.024	0.7791
236	66.028	1.1133
249	66.032	0.7411
261	66.035	0.7869
281	66.040	0.8957
292	66.043	1.4771
302	66.046	1.1956
313	66.048	1.2386
324	66.051	0.8304
334	66.054	0.6330
345	66.057	0.9819
355	66.059	0.7580
366	66.062	0.7605
377	66.065	1.0470
387	66.068	0.7382
398	66.070	0.8480
409	66.073	0.7356
419	66.076	0.8816
430	66.079	0.7683
440	66.081	1.0750
451	66.084	0.7729
462	66.087	0.5221
472	66.090	0.7267
483	66.093	1.1057
494	66.095	0.6735
504	66.098	1.0730
515	66.101	1.3579
525	66.104	0.9331
536	66.106	0.9278
547	66.109	0.8901
557	66.112	0.8620
568	66.115	0.7787
589	66.120	0.6718
601	66.123	1.3928
657	66.138	0.8091
710	66.152	1.3733
754	66.163	0.3886
790	66.172	1.4854
839	66.185	0.7375
880	66.196	1.2534
917	66.205	1.0386
961	66.217	1.3378
990	66.224	1.3485
1034	66.236	0.2037
1047	66.239	0.6303
1059	66.242	1.6581
1072	66.246	1.5430
1083	66.248	1.4985
1103	66.254	1.5722
1132	66.261	1.4741
1171	66.271	1.3545
1201	66.279	1.5570
1238	66.289	1.4033
1271	66.297	1.5469
1302	66.305	1.4146
1344	66.316	1.7111
1375	66.324	1.5921
1403	66.331	1.3624
1441	66.341	1.3787
1470	66.349	1.3888
1508	66.359	1.4428
1538	66.367	1.4942
1558	66.372	1.4697
1568	66.375	1.1658
1578	66.377	1.2529
1587	66.379	0.9725
1595	66.381	0.9922
1604	66.383	1.3318
1612	66.385	1.4650
1620	66.387	1.3495
1629	66.389	1.0706
1637	66.391	0.8569
1647	66.394	0.8791
1658	66.396	0.7404
1669	66.399	1.4699
1680	66.402	1.0115
1691	66.405	1.3255
1702	66.407	1.3075
1713	66.410	1.0365
1724	66.413	1.1079
1734	66.415	1.0064
1745	66.418	1.1017
1756	66.421	1.1852
1766	66.423	1.1647
1777	66.426	1.0832
1787	66.428	0.7936
1798	66.431	0.8890
1809	66.434	1.0595
1821	66.437	0.7721
1834	66.440	0.8780
1847	66.443	1.1204
1860	66.446	1.1624
1873	66.449	0.7009
1886	66.453	0.7775
1899	66.456	0.7843
1912	66.459	0.7542
1923	66.462	1.1082
1931	66.464	1.0678
1939	66.466	0.9555
1947	66.468	1.3717
1955	66.470	1.0101
1970	66.473	1.2254
1981	66.476	1.2293
1992	66.479	0.8962
2003	66.482	1.3265
2014	66.484	0.8990
2025	66.487	1.1592
2035	66.489	0.9980
2046	66.492	0.5650
2057	66.495	0.7789
2067	66.497	1.0254
2078	66.500	1.0790
2088	66.502	1.1304
2099	66.505	1.0136
2109	66.508	1.2105
2120	66.510	0.8305
2131	66.513	1.4521
2141	66.515	0.1958
2152	66.518	0.6798
2163	66.521	1.1528
2174	66.523	1.3127
2184	66.526	0.7031
2195	66.529	0.7773
2206	66.531	0.8374
2217	66.534	1.4321
2229	66.537	0.6467
2240	66.540	1.3128

2252	66.543	0.8477	3643	66.898	1.4587	6107	67.560	1.7273
2264	66.545	1.0867	3684	66.909	1.1480	6134	67.567	1.6313
2275	66.548	0.7476	3735	66.923	1.2609	6164	67.575	1.6580
2287	66.551	0.0223	3778	66.936	1.5846	6214	67.588	1.6649
2299	66.554	0.3628	3828	66.949	0.7296	6243	67.596	1.7570
2310	66.557	1.2131	3880	66.964	1.6076	6287	67.609	1.7906
2320	66.559	1.0830	3928	66.977	0.9890	6320	67.618	1.6081
2328	66.561	1.2803	3972	66.989	1.4808	6360	67.630	1.8478
2337	66.563	0.7447	4002	66.998	1.1193	6399	67.641	1.5703
2345	66.565	1.2403	4054	67.012	1.7109	6439	67.652	1.6728
2353	66.567	0.7252	4086	67.021	1.6457	6478	67.663	1.5689
2361	66.569	0.9909	4125	67.032	1.6018	6518	67.675	1.7786
2370	66.572	0.5904	4148	67.038	1.6504	6549	67.684	1.5514
2378	66.574	1.2677	4159	67.042	1.3369	6584	67.693	1.9003
2386	66.576	0.9973	4201	67.053	1.4887	6614	67.702	1.8083
2395	66.578	1.4797	4241	67.064	1.5108	6652	67.713	1.8596
2404	66.580	1.0725	4284	67.076	1.3921	6688	67.723	1.7190
2413	66.582	0.9394	4326	67.088	1.6132	6725	67.734	1.5028
2422	66.584	1.2867	4356	67.096	1.6813	6761	67.744	1.4720
2430	66.586	1.0896	4399	67.108	1.7842	6793	67.753	1.5014
2439	66.589	0.6693	4431	67.117	1.6971	6826	67.762	1.7085
2448	66.591	1.2101	4480	67.131	1.3693	6880	67.778	1.3453
2457	66.593	1.2757	4508	67.139	1.5450	6906	67.785	1.7902
2466	66.595	1.5611	4537	67.147	1.8887	6948	67.797	1.1174
2477	66.598	1.0313	4587	67.161	1.5781	6992	67.810	1.5749
2488	66.601	1.5664	4605	67.165	1.8531	7034	67.821	1.5161
2499	66.603	1.6393	4632	67.173	1.6671	7079	67.834	1.7916
2509	66.606	1.5300	4657	67.180	1.7120	7125	67.847	1.8575
2520	66.609	1.3840	4682	67.187	1.4827	7178	67.862	2.0040
2531	66.611	1.7755	4705	67.193	1.3286	7232	67.878	1.3808
2542	66.614	1.4668	4722	67.198	1.6353	7284	67.893	1.8447
2550	66.616	1.2239	4769	67.210	1.0104	7321	67.903	1.7699
2556	66.617	1.2672	4797	67.217	1.5441	7353	67.912	1.8434
2563	66.619	1.1599	4838	67.228	1.6292	7395	67.924	1.8632
2569	66.620	1.4948	4868	67.236	1.4963	7439	67.937	1.9454
2595	66.627	1.5162	4909	67.247	1.4571	7470	67.945	1.7947
2644	66.639	1.5710	4955	67.259	1.3659	7517	67.959	1.9191
2680	66.648	1.3819	4995	67.269	1.7289	7556	67.970	2.0421
2732	66.661	1.7323	5019	67.275	1.5346	7587	67.979	1.8132
2765	66.669	1.4931	5053	67.284	1.4550	7610	67.985	1.8060
2801	66.677	1.4472	5079	67.291	1.3865	7642	67.994	2.0882
2832	66.685	1.5616	5126	67.303	1.6585	7666	68.001	2.0213
2860	66.692	1.6448	5200	67.323	1.1101	7688	68.007	1.9054
2897	66.701	1.3540	5255	67.337	1.3966	7719	68.015	1.9222
2930	66.709	1.7719	5305	67.350	0.7090	7756	68.025	1.8312
2963	66.717	1.5057	5341	67.360	1.4199	7796	68.036	1.8090
3001	66.727	1.7060	5385	67.371	0.7895	7830	68.045	1.7743
3043	66.737	1.5335	5426	67.382	1.6428	7851	68.051	2.0382
3081	66.746	1.7100	5470	67.393	0.9003	7879	68.059	1.7764
3120	66.756	1.7417	5514	67.405	1.4818	7908	68.067	1.8634
3164	66.767	1.6588	5573	67.420	0.9816	7943	68.076	1.9892
3195	66.774	1.7516	5640	67.438	1.6298	7984	68.087	1.8806
3234	66.784	1.7463	5704	67.455	1.2805	8021	68.098	1.9199
3278	66.797	1.6607	5748	67.466	1.5933	8064	68.109	1.8108
3320	66.808	1.8468	5792	67.478	0.4786	8104	68.120	1.6103
3357	66.819	1.2482	5833	67.488	1.6699	8133	68.128	2.0816
3408	66.833	1.7572	5866	67.497	1.5246	8153	68.134	1.8059
3444	66.843	1.2743	5899	67.505	1.3073	8233	68.156	1.8458
3493	66.856	1.5241	5994	67.530	1.6621	8265	68.164	1.6577
3530	66.866	1.2820	6051	67.545	1.6250	8307	68.176	1.7058
3590	66.883	1.4499	6093	67.556	1.8390	8356	68.189	1.7470

8415	68.205	1.3842	10947	68.765	1.7617	12411	69.269	1.9910
8451	68.215	1.5872	10995	68.775	1.8701	12419	69.271	1.9853
8479	68.223	1.7408	11026	68.781	1.8727	12433	69.275	2.0270
8503	68.229	1.2863	11051	68.786	2.0339	12448	69.280	1.8676
8537	68.239	1.8337	11066	68.792	1.6724	12458	69.283	1.9518
8611	68.259	1.7298	11073	68.795	1.7998	12474	69.288	1.8533
8656	68.271	1.6463	11098	68.804	2.2319	12503	69.296	2.0107
8713	68.287	1.4151	11120	68.812	1.7864	12541	69.308	1.9093
8757	68.299	1.8656	11147	68.821	2.1466	12580	69.319	1.9177
8799	68.310	1.4470	11172	68.831	1.9091	12608	69.328	2.2092
8842	68.322	1.6203	11184	68.835	1.9893	12643	69.338	1.8359
8891	68.335	1.5590	11208	68.844	1.8566	12672	69.347	2.0126
8936	68.348	1.6074	11237	68.854	2.1047	12687	69.351	1.8506
8983	68.361	1.4658	11265	68.865	2.1130	12700	69.355	2.1844
9023	68.371	1.7854	11298	68.877	2.0211	12729	69.364	2.0325
9056	68.381	1.5467	11326	68.887	2.1946	12751	69.370	1.9500
9103	68.391	1.5308	11352	68.896	2.1539	12793	69.383	2.0727
9147	68.400	1.7491	11387	68.909	2.0972	12839	69.396	1.6120
9202	68.411	1.6908	11422	68.922	1.9714	12872	69.406	1.9342
9236	68.418	1.5655	11454	68.934	2.1075	12923	69.422	2.0012
9282	68.427	1.6916	11479	68.943	2.1562	12961	69.433	1.5356
9322	68.435	1.4915	11504	68.952	2.1104	13011	69.448	1.9557
9371	68.445	1.8748	11534	68.963	2.0467	13052	69.460	1.8671
9415	68.454	1.5779	11580	68.980	2.2329	13092	69.472	1.8124
9462	68.463	1.9238	11617	68.993	2.1342	13131	69.483	1.7752
9503	68.472	1.7726	11656	69.008	1.8261	13171	69.495	1.9688
9559	68.483	1.7185	11695	69.022	1.9778	13206	69.506	1.8103
9591	68.490	1.3162	11736	69.037	2.2284	13246	69.518	1.9855
9649	68.502	1.6398	11765	69.047	2.1369	13277	69.527	1.9207
9701	68.512	1.1182	11791	69.057	2.2338	13292	69.532	2.0603
9819	68.536	1.5732	11823	69.068	2.0508	13316	69.539	1.8228
9871	68.547	1.6354	11853	69.079	2.2310	13355	69.550	2.0188
9911	68.555	1.6459	11893	69.094	2.1579	13395	69.562	1.7973
9951	68.563	0.8578	11910	69.100	2.2696	13448	69.578	2.1325
9985	68.570	1.6823	11929	69.107	2.0417	13483	69.588	1.7807
10036	68.580	1.2743	11949	69.114	2.0803	13522	69.600	1.8069
10087	68.591	1.4953	11969	69.122	2.1629	13547	69.608	1.8614
10186	68.611	1.3691	11991	69.130	2.2805	13569	69.613	1.8375
10229	68.619	1.6364	12013	69.138	2.1378	13604	69.622	2.0668
10294	68.633	1.6742	12049	69.151	2.2554	13636	69.630	1.9583
10354	68.645	1.7665	12087	69.165	2.0219	13677	69.641	1.6082
10396	68.653	1.5996	12125	69.179	2.1768	13709	69.649	1.6498
10444	68.663	1.4963	12160	69.192	1.9041	13737	69.656	1.7270
10492	68.673	1.7478	12186	69.201	1.9807	13782	69.667	1.7784
10537	68.682	1.7701	12212	69.209	2.1274	13819	69.677	2.0697
10599	68.695	1.5647	12238	69.217	1.9243	13858	69.687	1.6468
10663	68.708	1.0663	12269	69.227	1.8443	13905	69.698	1.9348
10722	68.720	1.6990	12305	69.237	1.8343	14005	69.724	1.8625
10780	68.731	1.9997	12330	69.245	1.9720	14041	69.733	1.7424
10842	68.744	1.0571	12382	69.260	1.9227	14090	69.745	1.8867
10916	68.759	1.7415	12395	69.264	2.1540	13954	69.711	1.7300

Sopelana

Depth (cm)	Age (Ma)	δ13C (‰ VPDB)
13531	69.603	1.8137
13547	69.608	1.7424
13565	69.613	1.5283
13597	69.623	1.9031
13632	69.633	1.7571
13667	69.644	1.5485
13696	69.653	1.6602
13726	69.662	1.8200
13771	69.675	1.7475
13803	69.685	1.4526
13845	69.698	1.8709
13886	69.710	1.5884
13927	69.723	1.8822
13969	69.735	1.4933
14010	69.748	1.8453
14054	69.761	1.3608
14096	69.773	1.8417
14143	69.788	1.3589
14181	69.799	1.9421
14212	69.809	1.1506
14255	69.822	1.6705
14294	69.833	1.7048
14328	69.844	1.7994
14367	69.855	1.3568
14404	69.867	1.6545
14442	69.878	1.2533
14480	69.890	1.6394
14514	69.900	1.0124
14556	69.913	1.6201
14581	69.920	1.4097
14609	69.928	1.7499
14636	69.937	1.6631
14659	69.944	1.4250
14678	69.949	1.7596
14699	69.956	1.5902
14736	69.967	1.5551
14774	69.978	1.8527
14801	69.987	1.5780
14841	69.999	1.6954
14871	70.008	1.9746
14893	70.014	2.0041
14926	70.026	1.6532
14956	70.037	1.7865
14984	70.048	1.7444
15020	70.061	1.9134
15049	70.072	1.6458
15078	70.082	1.7564
15106	70.093	1.8808
15140	70.105	1.9359
15162	70.113	1.5424
15175	70.118	1.7352
15196	70.126	1.2346
15227	70.137	2.0845
15253	70.147	2.0346
15273	70.154	1.8094
15294	70.162	1.7435
15326	70.173	1.7561
15357	70.185	2.0493
15390	70.197	1.9154
15422	70.209	1.6814
15467	70.225	1.9778
15488	70.233	1.8551
15495	70.235	1.8603
15507	70.240	1.9630
15525	70.246	1.9155
15558	70.259	1.6126
15589	70.270	1.9903
15621	70.282	1.8710
15653	70.294	1.9712
15679	70.303	1.7815
15704	70.312	2.0061
15732	70.322	2.0165
15763	70.334	1.9444
15785	70.342	1.7791
15797	70.346	1.8166
15815	70.353	1.6533
15835	70.360	1.6841
15860	70.370	1.9091
15883	70.378	1.6601
15907	70.387	1.7711
15933	70.397	1.7718
15961	70.407	1.6781
15983	70.415	1.9785
16007	70.423	1.7584
16029	70.431	1.6739
16045	70.437	1.6919
16070	70.446	1.7524
16095	70.455	1.4446
16123	70.464	1.6696
16151	70.474	1.6123
16188	70.487	1.5982
16221	70.499	1.6808
16255	70.511	1.5884
16289	70.523	1.7659
16327	70.537	1.6375
16357	70.547	1.5172
16391	70.559	1.5044
16427	70.572	1.5478
16460	70.583	1.4707
16487	70.593	2.0328
16514	70.602	1.6794
16541	70.612	1.4463
16568	70.622	1.9525
16589	70.629	1.6536
16613	70.638	1.7160
16636	70.646	1.3917
16668	70.657	1.7772
16698	70.667	1.7109
16728	70.678	1.7804
16749	70.686	1.7527
16771	70.693	1.4985
16793	70.701	1.7940
16822	70.711	1.5747
16852	70.722	1.5862
16878	70.731	1.5508
16909	70.742	1.6247
16947	70.756	1.4906
16982	70.768	1.9368
17022	70.782	1.6601
17044	70.790	1.7268
17076	70.801	1.7226
17112	70.813	1.6176
17150	70.825	1.6738
17183	70.836	1.6354
17216	70.847	1.8128
17246	70.856	1.8573
17269	70.864	1.7806
17299	70.874	1.8706
17340	70.887	1.7382
17374	70.898	1.7572
17401	70.907	1.7995
17409	70.910	1.7959
17416	70.912	1.9366
17430	70.917	1.5922
17439	70.919	1.9005
17450	70.923	1.7949
17458	70.925	1.7464
17467	70.929	1.7223
17479	70.932	1.8208
17490	70.936	1.7750
17499	70.939	1.6836
17514	70.944	1.7518
17526	70.948	1.8530
17538	70.952	2.1067
17549	70.955	1.7752
17564	70.960	1.9470
17573	70.963	1.8262
17581	70.966	1.8600
17594	70.970	1.8464
17603	70.973	1.7539
17611	70.975	1.8869
17618	70.978	1.8356
17630	70.982	1.7907
17637	70.984	1.7120
17644	70.986	1.8824
17650	70.988	1.8647
17657	70.991	1.6174
17672	70.995	1.9156
17684	70.999	1.9260
17694	71.003	1.9290
17705	71.006	1.9263
17719	71.011	1.7786
17724	71.012	1.9412
17730	71.014	1.8060
17741	71.018	1.7177
17747	71.020	1.9934
17753	71.022	1.9451
17759	71.024	2.0168
17768	71.027	1.8522
17772	71.028	1.9136
17779	71.030	1.9750
17787	71.033	1.7297
17793	71.035	1.6345
17798	71.036	1.7710
17808	71.040	1.9977
17817	71.043	1.8704
17823	71.044	1.9943
17833	71.048	1.9349

17838	71.049	1.9903
17849	71.053	1.9085
17858	71.056	1.8074
17867	71.059	1.7777
17874	71.061	1.5936
17888	71.066	1.8717
17892	71.067	1.9788
17897	71.069	2.0125
17903	71.071	1.9531
17915	71.075	1.7679
17921	71.077	1.9710
17928	71.079	2.2410
17937	71.082	1.7706
17947	71.085	2.0427
17951	71.086	1.9704
17955	71.088	1.8741
17959	71.089	2.0863
17970	71.092	1.8737
17979	71.096	1.8737
17988	71.098	2.0336
17999	71.102	2.0216
18004	71.103	1.9749
18009	71.105	2.0676
18014	71.107	2.0661
18024	71.110	2.0000
18029	71.112	1.8360
18034	71.113	1.9524
18045	71.117	1.9937
18050	71.119	1.9024
18054	71.120	1.8719
18063	71.123	1.8719
18069	71.125	1.9320
18073	71.126	1.9181
18089	71.131	1.9361
18110	71.138	1.8209
18136	71.146	1.7432
18164	71.156	1.9479
18193	71.165	1.7372
18224	71.175	1.6139
18259	71.187	1.8029
18292	71.197	2.0939
18321	71.207	1.7225
18347	71.218	2.0449
18379	71.231	1.7646
18402	71.241	2.0314
18428	71.251	1.7641
18456	71.263	1.8598
18484	71.275	1.8659
18507	71.285	1.6414

Appendix E. Bed thickness record of the Zumaia and Sopelana sections

Zumaia

Danian

Cycle nr	limest. (cm)	marl (cm)	cycle (cm)
1	30	20	50
2	20	14	34
3	14	16	30
4	16	16	32
5	20	16	36
6	16	12	28
7	20	15	35
8	18	23	41
9	17	16	33
10	12	16	28

Maastrichtian

cycle nr	new cycle	limest. (cm)	marl (cm)	cycle (cm)
1	1		39	39
2	2	23	42	65
3	3	25	64	89
4	4	13	82	95
5	5	21	87	108
6	6	25	56	81
7	7	30	78	108
8	8	23	87	110
9	9	16	63	79
10	10	21	65	86
11	11	20	59	79
12	12	14	59	73
13	13	14	37	51
14	14	10	40	50
15	15	15	55	70
16	16	10	60	70
17	17	12	58	70
18	18	23	37	60
19	19	18	49	67
20	20	18	50	68
21	21	20	30	50
22	22	23	35	58
23	23	20	68	88
24	24	32	53	85
25	25	45	60	105
26	26	40	45	85
27	27	35	60	95
28	28	32	75	107
29	29	30	75	105
30	30	32	34	66
31	31	21	58	79
32	32	34	52	86
33	33	25	60	85
34	34	24	63	87
35	35	23	50	73
36	36	19	33	52
37	37	23	51	74
38	38	20	48	68
39	39	30	53	83
40	40	21	61	82
41	41	22	39	61
42	42	38	43	81
43	43	30	59	89
44	44	27	59	86
45	45	23	61	84
46	46	36	69	105
47	47	27	59	86
48	48	26	73	99
49	49	30	65	95
50	50	17	61	78
51	51	23	55	78
52a	52	20	16	36
52b	53	12	62	74
53	54	32	50	82
54	55	22	50	72
55	56	24	53	77
56	57	32	33	65
57	58	33	39	72
58	59	10	40	50
59	60	10	40	50
60	61	5	40	45
61	62	35	40	75
62	63	32	37	69
63	64	36	55	91
64	65	25	32	57
65	66	26	35	61
66	67	50	86	136
67	68	30	55	85
68	69	36	48	84
69	70	29	43	72
70	71	42	76	118
71	72	58	69	127
72	73	17	70	87
73	74	23	32	55
74	75	45	44	89
75	76	45	70	115
76a	77	17	18	35
76b	78	20	60	80
77	79	25	45	70
78	80	32	44	76
79	81	25	54	79
80	82	25	54	79
81	83	25	38	63
82	84	31	39	70
83	85	36	38	74
84	86	31	37	68
85a	87	29	0	29
85b	88	53	23	76
86	89	38	48	86
87	90	38	47	85
88	91	41	53	94
89	92	40	65	105
90	93	38	35	73
91	94	30	53	83
92	95	35	37	72
93	96	42	39	81
94	97	22	32	54
95	98	24	24	48
96	99	20	42	62
97	100	42	37	79
98	101	21	29	50
99	102	20	38	58
100	103	31	51	82
101	104	23	61	84
102	105	27	23	50
103a	106	12	9	21
103b	107	42	42	84
104	108	22	61	83
105	109	50	55	105
106	110	25	30	55
107	111	10	58	68
108	112	5	79	84
109	113	24	78	102
110	114	21	63	84
111	115	25	71	96
112	116	14	74	88
113	117	5	75	80
114	118	5	96	101
115	119	5	73	78
116	120	11	76	87
117	121	18	75	93
118	122	5	93	98
119	123	5	67	72
120	124	38	78	116
121	125	34	78	112
122	126	26	64	90
123	127	5	76	81

124	128	27	62	89	146	150	28	32	60	166	170	38	44	82
125	129	33	70	103	147	151	23	50	73	167	171	34	47	81
126	130	31	87	118	148	152	17	18	35	168	172	28	47	75
127	131	27	69	96	149	153	19	21	40	169	173	29	25	54
128	132	31	59	90	150	154	20	23	43	170	174	11	43	54
129	133	38	73	111	151	155	22	49	71	171	175	31	54	85
130	134	44	88	132	152	156	37	40	77	172	176	33	42	75
131	135	25	103	128	153	157	19	33	52	173	177	35	5	40
132*	136	62	50	112	154	158	26	27	53	174	178	40	30	70
133	137	24	25	49	155	159	38	23	61	175	179	46	32	78
134	138	20	30	50	156	160	27	34	61	176	180	23	45	68
135	139	19	29	48	157*	161	9	18	48	177	181	33	42	75
136	140	18	20	38		161	13	8	48	178	182	48	45	93
137	141	24	36	60	158*	162	15	15	65	179	183	57	30	87
138	142	17	17	34		162	10	25	65	180	184	56	37	93
139	143	19	36	55	159	163	34	46	80	181	185	49	70	119
140	144	16	46	62	160	164	26	31	57	182	186	28	55	83
141	145	23	42	65	161	165	32	25	57	183	187	30	37	67
142	146	14	37	51	162*	166	13	46	59	184	188	35	40	75
143	147	31	45	76	163	167	21	70	91	185	189	34		
144	148	40	38	78	164	168	9	70	79					
145	149	40	31	71	165	169	27	56	83					

Sopelana

cycle nr	new cycle	limest. (cm)	marl (cm)	cycle (cm)										
156	160	21	21	42	188b	193	18	20	38	225	232	19	35	54
157*	161	7	7	31	189	194	30	47	77	226	233	23	45	68
	161	8	9	31	190	195	24	33	57	227	234	27	49	76
158*	162	9	10	57	191	196	38	21	59	228	235	18	35	53
	162	10	28	57	192	197	31	36	67	229	236	19	53	72
159	163	30	65	95	193	198	21	41	62	230	237	32	26	58
160	164	40	60	100	194	199	27	33	60	231	238	40	20	60
161	165	40	25	65	195	200	21	40	61	232	239	25	35	60
162	166	55	35	90	196a	201	24	14	38	233	240	45	26	71
163	167	35	40	75	196b	202	12	40	52	234	241	35	51	86
164	168	20	60	80	197	203	17	30	47	235	242	33	50	83
165	169	25	40	65	198	204	14	33	47	236	243	32	36	68
166	170	25	55	80	199	205	29	35	64	237	244	40	50	90
167	171	25	40	65	200	206	29	38	67	238	245	21	30	51
168	172	23	60	83	201*	207	41	25	66	239*	246	10	8	78
169	173	20	20	40	202	208	34	32	66		246	20	10	78
170	174	20	60	80	203	209	29	36	65		246	15	15	78
171	175	22	50	72	204	210	27	24	51	240	247	40	25	65
172	176	19	43	62	205	211	26	31	57	241	248	35	21	56
173	177	20	11	31	206a	212	31	13	44	242	249	30	25	55
174	178	25	40	65	206b	213	7	25	32	243	250	20	20	40
175	179	30	40	70	207	214	20	26	46	244	251	20	20	40
176	180	18	55	73	208	215	26	22	48	245	252	27	20	47
177	181	28	41	69	209	216	32	22	54	246	253	30	30	60
178	182	42	40	82	210	217	22	27	49	247	254	30	42	72
179	183	43	41	84	211	218	10	28	38	248	255	35	20	55
180	184	41	49	90	212	219	21	33	54	249	256	28	32	60
181	185	28	59	87	213	220	19	42	61	250	257	20	28	48
182	186	24	43	67	214	221	29	40	69	251	258	31	24	55
183	187	43	32	75	215	222	25	47	72	252	259	26	20	46
184	188	38	40	78	216	223	25	36	61	253	260	11	19	30
185	189	33	46	79	217	224	33	39	72	254	261	20	18	38
186	190	23	54	77	218	225	24	32	56	255	262	23	44	67
187	191	21	32	53	219	226	13	42	55	256	263	27	34	61
188a	192	20	29	49	220	227	16	29	45	257	264	26	29	55
					221	228	16	35	51	258	265	29	17	46
					222	229	26	36	62	259	266	16	19	35
					223	230	16	26	42	260	267	25	11	36
					224	231	18	35	53					

Appendix F. Elemental, carbon isotope and geophysical data for selected intervals

Interval l	major elements (weight percent)									minor and trace elements (parts per million)																		isotope ratios (‰VPDB)	
level (m)	Na2O	MgO	Al2O3	SiO2	P2O5	K2O	CaO	TiO2	Fe2O3	Sc	Cr	Co	Ni	Cu	Zn	Ga	Rb	Sr	Y	Zr	Nb	Mo	Ba	La	Pb	Th	U	$\delta^{18}O$	$\delta^{13}C$
3.40	0.09	0.74	1.90	10.37		0.60	53.34	0.06	0.57	3.59	0.00	3.40	12.15	15.73	25.30	3.43	17.29	729.72	14.22	17.47	1.77	0.14	72.84	5.30	5.28	0.55	0.12	-2.94	1.68
3.35	0.09	0.69	2.01	10.95		0.69	51.45	0.06	0.65	3.73	1.27	4.28	11.49	5.73	23.70	3.37	19.97	726.11	14.29	20.46	1.80	0.33	81.36	7.79	4.94	0.01	-0.27	-2.55	1.60
3.28	0.09	0.71	2.12	11.68		0.74	51.51	0.07	0.70	4.14	1.78	4.20	13.52	6.46	24.02	3.83	22.31	711.46	13.91	20.54	2.02	0.60	86.25	6.80	6.20	-0.34	-0.29	-2.70	1.57
3.24	0.10	0.73	2.29	12.56		0.82	50.21	0.08	0.72	3.94	3.66	3.63	11.74	5.55	24.63	3.48	24.14	694.37	14.07	23.60	2.02	0.47	89.06	8.82	5.21	1.30	0.01	-2.93	1.59
3.09	0.09	0.75	2.29	12.38		0.80	50.57	0.08	0.68	5.10	2.38	3.82	11.18	9.09	22.92	4.41	23.44	648.19	15.07	22.82	1.87	0.58	48.96	7.32	4.83	0.61	-0.28	-2.49	1.33
3.04	0.17	0.92	4.24	20.06		1.56	41.01	0.13	1.16	5.53	7.13	4.81	19.75	8.70	28.82	6.42	48.61	598.13	13.51	43.46	3.45	0.35	98.91	7.90	7.02	2.18	0.78	-2.10	1.60
3.00	0.21	1.00	4.96	23.43		1.77	37.72	0.16	1.34	5.62	10.74	6.09	21.43	6.93	31.15	7.15	57.18	596.40	15.27	52.80	4.10	0.95	110.69	8.54	7.33	4.46	-0.16	-2.82	1.44
2.96	0.08	0.67	1.78	10.88		0.61	52.83	0.06	0.58	2.99	0.82	5.20	11.91	6.96	21.72	3.20	18.16	701.59	13.86	18.52	1.54	0.49	77.29	4.64	5.14	1.10	-0.91	-2.74	1.55
2.93	0.09	0.70	2.01	11.85		0.70	51.54	0.06	0.60	3.21	4.08	3.76	11.40	8.65	23.60	3.15	21.18	687.95	13.96	20.42	1.78	0.31	81.32	10.25	4.86	0.51	-0.62	-3.09	1.50
2.90	0.07	0.66	1.58	10.02		0.52	52.81	0.06	0.52	3.28	1.23	4.99	10.19	9.75	21.53	3.58	15.86	696.90	13.74	17.35	1.67	0.78	82.09	7.01	4.37	-0.11	-0.29	-2.69	1.50
2.70	0.19	0.92	4.24	19.83		1.53	40.83	0.14	1.11	5.53	7.15	5.65	21.21	11.17	28.13	5.83	47.53	588.77	14.97	45.68	3.40	0.41	75.16	8.55	6.92	2.78	-0.16	-2.39	0.89
2.66	0.07	0.62	1.58	10.64		0.53	52.35	0.06	0.56	4.96	4.27	2.45	9.76	4.62	21.36	3.24	16.75	741.29	14.25	18.29	1.90	0.26	44.41	8.45	4.18	-0.30	-0.43	-3.42	1.39
2.60	0.07	0.69	1.54	9.22		0.45	54.04	0.05	0.49	2.79	0.65	3.06	10.03	25.66	23.60	4.23	14.10	684.42	14.69	18.78	1.69	0.30	42.41	9.52	4.42	-0.69	-0.23	-2.67	1.46
2.56	0.07	0.67	1.33	8.28		0.38	55.34	0.05	0.48	3.34	0.89	4.20	9.02	28.23	22.48	2.70	12.20	683.36	14.84	15.28	1.34	0.65	36.36	7.75	4.89	-0.21	0.12	-2.90	1.36
2.51	0.07	0.70	1.63	9.95		0.51	53.27	0.06	0.52	3.23	0.62	3.82	12.53	7.01	23.00	3.45	14.97	659.59	15.89	18.18	1.61	0.16	38.25	5.11	5.74	0.18	-0.01	-2.85	1.28
2.42	0.35	1.42	8.60	34.35		2.63	26.13	0.28	2.29	8.29	20.96	8.48	39.75	7.69	41.49	11.56	98.04	459.77	16.78	91.06	7.13	1.23	122.71	13.51	11.15	5.98	0.63	-2.33	0.62
2.39	0.33	1.34	7.82	32.43		2.48	28.06	0.26	2.09	7.15	19.95	8.36	35.75	8.70	39.91	10.55	90.32	475.65	15.77	84.78	6.63	1.03	111.77	13.53	9.33	4.96	0.16	-2.49	0.66
2.35	0.19	0.95	4.31	20.36		1.52	40.46	0.14	1.09	6.35	6.73	3.97	21.34	12.03	31.41	6.35	47.91	613.30	16.01	46.00	3.77	1.08	74.40	10.81	7.64	2.37	0.31	-2.32	1.14
2.28	0.06	0.65	1.31	8.17		0.36	55.31	0.05	0.46	4.03	2.14	3.22	9.18	12.34	22.14	3.22	11.68	711.77	15.43	12.84	1.40	0.30	38.54	6.78	4.59	-1.15	-0.56	-3.06	1.20
2.23	0.05	0.60	1.06	7.55		0.29	56.45	0.05	0.43	3.30	-1.64	3.15	8.80	12.19	20.29	2.59	9.62	758.09	15.94	10.69	1.08	0.76	37.37	9.59	5.17	-1.67	-0.27	-3.45	1.30
2.18	0.08	0.66	1.57	9.94		0.48	53.40	0.05	0.48	3.59	1.99	2.91	11.88	7.84	23.21	2.81	14.12	727.93	16.66	16.58	1.44	0.55	41.23	8.05	5.22	-1.04	-0.78	-2.68	1.35
2.09	0.34	1.44	8.80	35.73		2.66	24.98	0.29	2.36	7.79	24.43	7.97	41.07	9.08	43.74	10.95	100.78	476.86	16.76	94.33	7.18	1.19	123.08	13.04	10.43	6.48	0.82	-3.02	0.43
2.06	0.30	1.34	7.73	32.11		2.45	28.48	0.26	2.00	8.26	18.90	6.99	35.21	9.62	39.83	10.67	88.73	501.23	16.69	84.29	6.38	1.25	110.81	15.84	9.15	6.01	-0.01	-2.84	0.79
1.95	0.08	0.66	1.59	10.09		0.49	52.90	0.05	0.54	4.58	0.99	3.82	11.02	6.16	22.46	3.75	15.19	663.52	15.41	17.87	1.32	0.50	41.27	6.53	5.48	-1.21	0.32	-2.36	1.29
1.91	0.09	0.69	2.15	12.51		0.77	49.66	0.07	0.68	4.17	0.13	5.14	13.24	10.54	23.62	3.68	22.64	707.35	15.03	23.15	1.85	0.30	50.90	8.08	5.77	0.36	0.31	-2.75	1.34
1.86	0.11	0.77	2.58	13.93		0.90	48.08	0.08	0.72	3.99	3.26	3.92	12.46	6.64	24.75	4.70	27.29	675.18	14.85	26.91	2.12	-0.04	54.34	9.11	5.94	-0.12	-0.28	-2.55	1.33
1.78	0.23	1.06	5.52	25.02		1.89	35.84	0.17	1.41	5.62	12.28	7.43	25.08	9.01	31.15	8.52	62.64	546.75	16.18	59.44	4.92	0.83	88.05	12.97	7.35	3.58	-0.09	-3.25	1.13
1.74	0.27	1.20	6.43	27.35		2.13	33.09	0.20	1.58	8.02	14.23	7.68	31.06	6.88	36.21	8.86	71.55	531.48	15.65	68.01	5.33	0.51	93.85	11.56	7.56	4.79	0.02	-2.86	1.04
1.71	0.29	1.24	7.21	30.31		2.35	30.54	0.23	1.53	7.36	17.32	8.73	32.59	10.47	37.09	9.50	83.04	516.47	16.46	75.66	5.94	0.69	103.19	13.42	8.83	4.23	0.58	-2.75	1.06
1.59	0.08	0.69	1.86	10.23		0.61	52.64	0.06	0.55	3.37	-0.23	4.22	10.81	5.97	22.46	2.91	17.68	691.04	13.82	18.34	1.85	0.21	41.96	6.04	4.85	-0.43	-0.49	-2.65	1.36
1.55	0.12	0.77	2.70	13.52		0.94	48.57	0.07	0.55	4.03	3.82	4.35	11.89	22.98	22.22	4.51	27.36	655.82	12.93	25.09	2.15	-0.09	50.75	6.29	5.73	-0.15	-0.56	-2.72	1.44
1.51	0.24	1.04	5.20	23.53		1.74	38.06	0.16	1.03	5.89	10.14	6.33	24.04	10.03	29.60	7.32	55.80	561.50	15.66	52.62	4.43	0.63	82.72	12.91	5.91	2.69	0.38	-3.28	1.08
1.47	0.21	1.03	5.05	22.36		1.78	38.22	0.16	1.14	8.28	8.75	8.20	26.00	9.40	30.38	7.28	56.47	554.18	14.80	53.24	4.30	0.68	75.52	11.37	7.32	3.95	-0.79	-2.27	1.17
1.44	0.15	0.85	3.37	16.92		1.16	45.07	0.10	0.64	5.44	4.85	6.27	17.00	18.72	26.18	4.71	34.85	597.99	13.86	37.13	2.99	0.99	62.42	8.99	5.29	1.99	0.30	-2.70	1.26
1.39	0.13	0.78	3.00	15.40		1.07	46.40	0.10	0.72	6.28	5.75	3.40	15.16	10.17	25.65	5.29	32.27	666.98	13.97	31.45	2.67	0.23	60.35	7.13	5.53	0.48	-0.06	-2.78	1.19
1.33	0.05	0.53	1.08	8.11		0.32	56.66	0.05	0.38	2.25	-0.99	1.52	6.10	5.78	19.32	3.49	10.07	729.35	12.24	12.66	0.93	0.61	39.28	6.97	4.34	-0.88	0.20	-3.04	1.18
1.27	0.05	0.51	0.87	7.26		0.24	57.88	0.05	0.37	4.13	0.98	2.59	6.99	5.70	18.82	2.92	7.96	746.03	12.04	11.66	1.13	0.47	39.42	6.86	4.06	-1.98	-1.01	-2.84	1.34
1.22	0.06	0.57	0.97	8.23		0.27	56.33	0.05	0.38	3.43	0.69	2.76	6.63	7.71	18.65	2.62	8.95	693.33	11.61	22.78	1.33	0.73	43.90	6.28	5.99	-1.55	-0.44	-4.64	0.80
1.15	0.29	1.29	7.37	31.03		2.37	29.53	0.24	1.86	5.98	16.84	8.75	35.33	9.15	40.25	9.40	84.68	493.70	15.50	79.11	5.88	0.70	106.34	10.57	8.79	5.77	0.26	-2.90	0.88
1.10	0.24	1.12	5.79	25.48		2.00	35.04	0.19	1.49	6.34	13.27	5.92	27.73	11.55	34.63	8.37	65.89	537.28	15.72	63.94	4.70	0.79	88.27	10.06	8.76	3.77	0.37	-2.56	0.90
1.04	0.13	0.89	3.36	16.80		1.18	44.40	0.12	0.93	6.30	8.84	6.72	18.35	13.20	29.88	4.98	35.86	615.82	15.20	38.44	2.93	0.63	61.35	7.63	5.94	1.19	-0.27	-2.35	1.16
0.96	0.06	0.62	1.24	8.50		0.36	56.05	0.05	0.43	1.85	2.92	3.92	8.78	15.67	20.53	3.17	10.93	690.87	13.81	14.59	1.10	0.31	40.86	4.70	3.87	-0.75	-0.15	-2.64	1.39
0.91	0.07	0.62	1.32	9.23		0.38	55.19	0.05	0.47	3.89	-0.73	5.43	10.02	7.13	21.48	3.25	12.19	697.56	14.69	16.48	1.37	0.58	39.96	8.62	4.74	-0.52	-0.41	-3.32	1.26
0.87	0.17	0.92	4.17	19.54		1.52	41.39	0.13	1.14	4.96	6.47	4.41	19.16	9.33	28.06	6.15	47.09	606.51	14.40	44.56	3.39	0.59	108.71	8.65	7.49	1.92	-0.62	-2.66	1.47
0.77	0.37	1.50	8.93	36.13		2.68	24.93	0.30	2.39	8.61	23.25	8.48	43.02	13.07	44.93	11.45	101.53	428.66	16.86	96.11	7.15	1.05	123.41	17.13	10.41	7.64	1.30	-2.67	0.35

	0.73	0.40	1.60	9.69	38.66		2.87	22.35	0.34	2.64	9.31	25.57	11.14	49.21	12.78	48.42	12.38	112.35	432.37	16.97	104.51	8.07	0.82	136.84	17.98	10.41	6.44	0.56	-2.82	0.20
	0.67	0.33	1.33	7.72	32.59		2.50	28.52	0.27	1.76	8.81	19.74	9.51	36.46	12.08	40.63	10.33	90.67	496.07	17.27	84.53	6.62	0.39	109.28	13.73	8.64	5.44	0.47	-2.62	0.76
	0.56	0.09	0.71	1.99	12.46		0.65	50.71	0.07	0.57	4.71	1.61	4.03	13.59	7.92	25.14	3.73	19.61	707.69	16.68	22.81	2.37	0.10	49.49	9.40	5.01	0.14	-1.22	-3.28	1.21
	0.51	0.05	0.59	1.06	7.92		0.28	57.30	0.05	0.43	2.31	-0.02	3.80	8.00	7.51	21.06	2.71	9.45	728.20	16.67	11.60	1.13	0.12	38.19	7.21	3.96	-0.43	-0.97	-3.14	1.27
	0.47	0.05	0.62	1.23	9.09		0.35	55.73	0.05	0.46	3.17	0.71	2.16	9.90	6.58	24.09	2.75	11.09	716.28	17.11	14.69	1.54	0.24	38.63	9.15	5.10	-0.59	-0.49	-3.05	1.28
	0.41	0.37	1.50	9.03	36.41		2.75	24.44	0.31	2.40	9.27	26.48	10.66	44.64	12.53	48.08	11.90	104.82	490.07	18.03	95.94	7.30	1.28	130.45	20.38	10.74	6.34	1.57	-2.87	0.16
	0.37	0.36	1.46	8.75	35.27		2.73	25.58	0.29	2.33	7.84	22.24	9.75	45.72	11.22	45.78	10.54	102.11	496.34	17.97	92.91	7.26	1.12	128.50	12.85	9.30	5.43	1.00	-3.06	0.32
	0.32	0.23	1.09	5.72	25.61		1.98	35.53	0.18	1.39	6.38	11.35	7.80	26.72	10.14	37.80	7.88	65.23	594.74	18.55	60.10	4.91	0.77	96.58	14.10	6.81	3.17	-0.06	-3.34	0.85
	0.23	0.07	0.62	1.49	10.19		0.46	54.12	0.05	0.52	2.24	1.52	2.98	10.00	6.37	22.97	2.47	14.17	760.45	18.34	16.66	1.28	0.26	47.37	6.03	4.36	-0.12	0.64	-4.26	0.88
	0.21	0.08	0.68	1.84	11.74		0.57	52.08	0.07	0.60	4.99	0.86	4.97	12.38	6.54	25.95	3.91	17.29	757.90	17.61	19.68	1.77	0.19	49.63	11.40	4.82	0.68	-0.96	-3.02	1.25
	0.17	0.14	0.84	3.42	17.57		1.22	44.63	0.10	0.90	3.41	5.26	6.23	19.28	9.87	29.71	5.85	36.91	696.91	17.90	34.80	2.77	0.32	67.91	11.60	5.35	2.92	-0.53	-2.96	1.09
	0.12	0.27	1.24	6.62	28.32		2.15	32.83	0.21	1.63	6.99	12.99	8.42	34.36	13.52	40.26	8.98	72.99	576.71	18.74	66.31	5.38	0.78	128.45	14.42	7.25	4.50	0.59	-3.24	0.75
	0.08	0.27	1.16	6.53	28.35		2.24	33.13	0.21	1.72	8.14	13.29	7.19	32.21	12.64	38.82	9.71	75.81	585.77	17.23	63.72	5.27	0.68	95.39	14.42	7.83	4.74	0.12	-2.71	0.78
	0.04	0.17	0.91	4.23	19.97		1.54	40.61	0.13	1.15	7.56	8.40	4.86	22.82	11.19	34.13	6.84	46.46	708.00	17.58	40.54	3.51	0.59	69.59	9.55	6.24	2.17	-0.70	-3.19	1.17
average		0.16	0.90	3.86	18.28		1.26	44.00	0.13	1.04	5.25	7.51	5.46	19.97	10.27	29.14	5.88	42.47	630.98	15.49	41.22	3.32	0.57	74.72	9.81	6.44	1.86	-0.06	-2.87	1.13

Interval II	major elements (weight percent)										minor and trace elements (parts per million)																		stable isotope ratios (‰VPDB)		geophysical properties		
level (m)	Na2O	MgO	Al2O3	SiO2	P2O5	K2O	CaO	TiO2	Fe2O3	Sc	Cr	Co	Ni	Cu	Zn	Ga	Rb	Sr	Y	Zr	Nb	Mo	Ba	La	Pb	Th	U	$\delta^{18}O$	$\delta^{13}C$	MS (SI)	L* (%)	a* (%)
0.05	0.82	1.13	7.96	29.43		2.59	28.01	0.23	2.37	8.22	23.27	9.79	37.66	30.31	67.71	10.79	88.01	678.21	16.50	63.55	5.99	1.16	155.37	13.27	10.45	3.60	0.06	1.62	-3.83	8.30	54.22	-1.5
0.15	30.27	0.47	4.64	19.68		1.92	22.15	0.20	1.96	7.03	25.21	8.01	33.59	24.20	66.98	10.82	90.29	671.04	16.48	64.54	6.07	0.81	138.87	12.58	11.62	3.19	1.02	1.19	-7.19	8.90	54.26	-1.6
0.24	7.90	0.92	6.48	25.00		2.23	30.05	0.19	1.91	5.97	20.78	8.74	26.74	20.55	62.78	10.03	77.92	707.46	16.70	54.88	5.56	0.83	136.84	14.57	10.46	3.86	-0.04	1.13	-4.77	9.50	52.66	-1.8
0.34	0.33	1.13	7.79	28.53		2.54	29.97	0.22	2.13	8.84	22.08	8.77	29.10	20.49	65.73	10.55	84.14	689.27	16.81	61.42	6.12	1.20	152.49	14.44	9.69	4.23	0.70	1.40	-4.14	5.20	57.37	-1.5
0.45	0.30	1.12	7.35	26.80		2.44	31.35	0.21	2.19	8.28	21.19	7.23	24.40	15.57	65.07	10.34	79.01	694.98	15.77	55.87	5.18	0.42	144.26	12.88	10.74	3.79	0.62	1.22	-8.29	9.00	48.17	1.9
0.56	0.32	1.16	7.98	28.50		2.62	29.19	0.24	2.38	7.52	22.43	9.05	26.09	10.92	65.35	11.30	86.73	667.81	16.16	60.36	5.71	1.13	156.93	17.16	11.13	3.32	1.29	1.42	-4.19	13.60	48.14	1.5
0.71	0.34	1.20	8.51	29.99		2.74	27.83	0.25	2.42	8.02	26.31	9.33	26.32	17.11	66.06	11.06	93.04	650.87	14.99	63.69	6.20	0.58	162.64	13.40	11.01	4.59	-0.03	0.80	-5.43	11.20	46.56	2.1
0.83	0.44	1.28	9.45	34.77		2.79	24.04	0.30	2.48	8.76	28.43	8.69	27.79	15.92	63.29	12.38	97.82	568.97	18.01	91.58	7.01	0.63	185.54	14.01	14.76	6.25	0.06	1.00	-6.99	9.20	46.46	1.3
0.92	10.54	1.05	8.14	28.29		2.63	23.58	0.27	2.66	9.52	30.16	8.04	28.61	17.26	66.15	12.58	100.93	589.06	17.08	71.36	7.19	0.65	175.15	16.48	12.37	5.28	0.64	1.07	-4.73	7.50	49.65	1.8
1.01	0.37	1.16	8.13	28.81		2.64	28.69	0.24	2.46	8.27	22.76	7.52	24.65	14.58	59.77	11.05	88.26	644.66	15.63	62.57	5.96	0.90	156.86	12.79	10.63	4.69	0.19	0.93	-4.83	12.35	46.32	2.6
1.11	0.33	1.10	7.63	27.68		2.51	30.19	0.22	2.26	7.07	23.60	7.96	20.32	14.06	57.55	10.22	82.12	682.67	15.65	60.77	5.96	0.50	147.37	13.50	11.87	4.13	0.01	0.78	-9.12	13.25	50.58	2.0
1.24	0.42	1.25	9.58	32.62		2.97	25.04	0.28	2.55	7.66	32.06	8.19	27.29	16.00	65.32	12.72	104.39	610.27	16.22	73.11	7.23	0.80	185.45	15.37	13.85	5.75	0.38	1.06	-4.42	13.90	47.22	1.4
1.36	15.59	0.95	7.87	27.64		2.63	21.33	0.27	2.67	8.59	29.23	11.88	30.90	18.17	67.99	13.35	109.12	578.99	17.37	75.54	7.22	0.74	186.97	15.61	16.11	5.11	0.90	0.98	-4.42	13.30	48.60	1.9
1.49	0.51	1.37	10.12	33.62		3.07	23.43	0.30	3.03	8.38	32.39	10.04	28.76	17.02	69.34	12.96	110.66	581.56	17.30	76.46	7.45	0.59	197.70	15.70	12.45	5.61	0.42	1.34	-3.93	14.90	40.52	2.1
1.62	0.45	1.42	11.04	37.14		3.18	20.50	0.36	3.12	9.37	36.09	7.91	28.07	17.48	71.70	14.29	118.45	533.37	18.36	90.81	8.36	0.82	218.06	18.19	13.86	6.86	1.08	1.01	-6.46	13.50	44.02	2.5
1.75	0.39	1.28	10.14	33.93		3.07	23.32	0.30	3.07	8.93	32.83	7.64	25.65	14.67	68.14	13.45	111.49	582.34	17.57	79.88	7.41	1.05	196.11	18.37	13.49	5.32	0.73	0.98	-4.44	10.95	45.93	2.4
1.89	19.63	0.75	6.63	24.37		2.35	22.64	0.24	2.56	8.07	27.88	6.43	21.65	19.87	61.11	12.32	99.50	613.33	16.95	69.22	6.52	0.65	162.05	12.32	13.35	4.14	0.71	0.11	-6.35	7.60	48.45	2.1
1.98	0.39	1.11	8.31	29.33		2.65	28.42	0.23	2.35	9.05	26.96	9.30	23.20	35.34	58.12	10.35	89.68	657.64	17.06	65.63	6.15	0.84	157.21	17.13	12.98	4.64	1.49	0.93	-8.27	12.85	51.11	2.3
2.05	0.54	1.25	9.52	32.10		2.91	25.32	0.28	2.68	9.03	29.50	7.38	22.49	23.15	63.54	12.27	103.68	610.89	17.28	71.46	7.05	0.87	174.91	17.40	13.56	5.42	0.79	0.44	-5.68	16.50	46.57	2.3
2.19	2.85	1.16	8.99	31.14		2.81	24.98	0.27	2.78	9.99	30.57	6.47	24.93	18.96	63.05	12.19	102.51	611.91	17.67	70.81	6.89	0.61	179.53	14.20	12.93	6.02	0.43	0.78	-4.37	12.20	50.20	2.7
2.36	6.45	1.28	10.58	34.69		3.10	18.97	0.35	3.39	9.57	39.19	12.74	32.94	29.95	72.63	15.38	126.04	534.02	19.49	85.18	8.21	0.88	221.58	20.05	16.61	7.63	1.46	1.11	-3.73	8.20	40.71	2.7
2.49	0.55	1.50	11.98	37.94		3.33	18.85	0.38	3.77	11.05	40.82	14.67	30.32	21.87	74.08	15.63	130.25	523.38	19.07	90.32	8.60	1.13	237.38	17.69	15.82	7.70	1.32	0.74	-5.13	18.10	50.57	2.8
2.61	0.49	1.49	12.14	38.32		3.30	18.91	0.38	3.31	10.36	38.87	22.26	34.98	18.91	72.34	15.54	127.73	545.60	20.08	93.45	8.84	1.04	236.25	19.69	19.18	7.65	1.05	0.79	-4.00	15.20	47.29	-0.2
2.81	0.44	1.47	12.63	40.55		3.43	17.80	0.40	3.13	11.37	43.40	19.46	35.56	17.95	75.96	15.78	133.57	534.75	18.35	94.47	9.15	0.40	256.98	22.56	20.51	8.97	1.80	0.90	-4.38	8.65	45.99	3.0
2.92	0.40	1.32	11.16	36.42		3.22	21.50	0.34	3.09	10.77	36.88	13.93	31.61	18.78	73.10	14.33	120.31	605.56	17.50	79.60	7.87	0.27	223.96	16.88	14.93	7.70	1.34	1.48	-4.03	15.35	41.54	2.4
3.02	0.36	1.26	10.18	34.50		3.04	23.80	0.30	2.88	7.90	31.83	11.50	27.26	18.48	67.37	12.53	110.43	629.84	18.34	73.72	7.55	0.41	197.27	16.24	14.28	5.98	0.80	1.20	-6.54	15.90	43.22	2.7
3.13	0.37	1.30	10.59	35.33		3.12	22.82	0.32	2.94	8.94	33.82	14.85	29.20	21.66	69.75	13.54	113.17	610.19	18.22	73.17	7.49	0.70	209.92	20.18	14.64	7.70	1.09	1.24	-3.92	12.45	43.06	3.1
3.24	0.37	1.37	11.53	37.80		3.28	20.46	0.36	3.19	10.07	37.82	12.17	30.73	17.89	73.75	15.01	124.87	583.71	17.91	80.55	8.28	0.72	233.03	17.41	15.23	7.27	1.48	0.83	-4.76	17.50	47.21	2.8
3.34	0.36	1.35	11.00	36.19		3.19	21.57	0.34	3.48	9.89	37.29	10.98	28.70	17.85	69.52	14.17	118.93	587.67	17.52	74.97	7.99	0.56	215.42	19.79	13.94	7.94	1.74	0.63	-5.25	15.20	49.19	1.9

3.45	0.35	1.36	11.24	36.71	3.21	20.69	0.35	3.80	9.72	37.34	9.50	28.55	16.06	69.04	14.82	121.11	567.25	19.22	83.19	8.35	0.81	232.89	20.58	14.92	7.62	0.84	0.98	-3.96	12.30	46.46	2.4
3.55	0.38	1.38	11.54	37.25	3.23	20.28	0.36	3.37	9.78	36.95	10.30	28.42	14.62	69.57	14.53	123.35	568.48	19.77	85.92	8.64	0.92	234.11	21.76	15.32	7.78	1.57	0.76	-7.38	16.20	44.47	2.4
3.66	0.40	1.43	12.16	38.84	3.38	18.27	0.38	3.71	9.80	40.56	15.06	33.19	17.07	73.04	15.18	132.25	529.94	20.80	94.95	9.20	0.80	245.14	19.99	18.39	8.28	1.55	0.76	-3.70	14.50	46.48	2.8
3.77	0.42	1.40	11.92	38.56	3.32	18.94	0.38	3.26	10.90	39.46	14.65	32.29	14.77	73.74	15.25	128.43	557.79	20.24	93.07	9.00	0.78	241.54	20.97	19.85	7.13	1.15	1.05	-3.98	11.40	41.54	3.1
3.87	0.39	1.31	11.43	37.37	3.28	20.40	0.35	3.38	9.64	42.18	17.75	30.37	15.36	72.71	15.61	125.44	590.99	18.98	84.21	8.48	1.09	231.82	17.45	16.64	6.20	1.33	0.74	-5.05	11.80	45.62	2.9
3.98	0.40	1.30	11.24	37.00	3.29	20.63	0.35	3.42	10.81	38.17	16.92	29.58	20.60	70.77	14.59	124.27	578.59	19.62	81.03	8.00	0.79	241.83	20.24	15.09	7.13	1.09	0.85	-5.01	12.60	42.17	3.1
4.09	0.37	1.28	10.88	35.93	3.21	21.59	0.32	3.38	8.62	35.34	13.13	28.68	15.69	70.53	14.48	120.55	601.05	17.79	76.49	8.16	0.87	231.36	19.49	14.61	7.40	0.72	0.74	-8.49	13.20	43.03	3.4
4.19	0.32	1.18	9.81	33.08	2.99	24.46	0.28	3.14	8.88	29.95	21.68	28.16	14.20	64.78	13.55	107.83	667.96	18.47	67.19	7.29	0.92	203.28	19.08	14.28	5.95	1.00	0.88	-5.13	12.95	43.96	3.4
4.30	0.34	1.25	10.32	33.84	3.08	23.56	0.30	3.18	8.38	32.57	11.65	28.01	14.15	68.61	13.57	112.83	662.02	17.46	69.68	7.41	1.03	211.53	15.85	16.55	6.31	0.95	0.77	-5.33	16.30	43.11	3.5
4.40	0.34	1.27	10.47	34.61	3.09	22.74	0.31	3.37	9.02	31.53	39.90	33.48	13.97	67.04	13.60	114.28	630.93	18.39	73.12	7.60	0.54	207.48	19.81	16.14	5.64	1.19	1.07	-4.45	17.25	45.10	3.4
4.51	0.34	1.31	11.20	36.07	3.22	20.91	0.34	3.72	10.95	36.18	14.25	28.26	13.41	69.19	15.60	122.44	601.26	19.14	81.79	8.19	1.09	217.72	22.06	15.02	7.49	0.94	0.77	-7.16	15.70	42.34	3.7
4.62	0.38	1.38	11.99	38.26	3.33	19.23	0.38	3.46	11.79	38.99	16.68	33.96	16.48	72.40	15.24	129.20	558.62	19.40	93.20	9.12	0.93	235.70	20.93	18.63	7.92	1.74	0.52	-5.20	13.70	43.91	3.1
4.72	0.38	1.35	11.73	37.82	3.26	19.97	0.36	3.27	9.37	38.74	17.05	33.95	15.82	72.28	15.00	123.84	581.55	20.93	90.08	8.62	1.57	229.60	21.33	17.58	6.67	0.60	0.73	-4.55	11.60	40.65	2.7
4.83	0.37	1.25	10.68	34.26	3.12	22.81	0.31	3.32	8.79	34.66	9.87	28.95	14.51	68.41	14.75	114.48	648.07	18.65	73.89	7.56	0.98	212.85	17.11	14.33	6.06	0.86	1.11	-4.55	15.70	44.38	3.2
4.94	0.36	1.20	10.35	33.82	3.04	23.64	0.30	3.00	8.59	32.61	15.93	27.38	13.24	65.99	12.89	109.92	657.47	17.69	73.75	7.33	0.84	213.31	16.96	12.81	6.59	1.83	0.67	-5.53	9.90	45.41	2.6
5.04	0.34	1.17	10.08	33.29	3.02	24.35	0.28	2.88	8.40	33.23	10.25	26.93	18.06	67.32	13.46	108.84	681.62	16.43	70.20	7.31	0.81	213.61	18.57	13.39	8.48	0.54	1.07	-7.69	10.10	44.71	3.4
5.15	0.34	1.12	9.65	33.07	2.90	25.07	0.28	2.68	9.16	31.43	12.86	24.74	15.85	64.00	13.31	103.88	687.74	17.83	69.38	7.15	0.83	195.27	18.27	13.16	5.64	1.34	1.36	-4.54	16.20	52.44	3.3
5.25	0.37	1.20	10.52	34.89	3.14	22.75	0.30	3.03	9.57	33.95	11.43	28.64	21.95	69.65	14.04	116.92	654.47	17.48	72.27	7.66	0.85	222.90	14.23	14.97	7.10	0.89	0.93	-5.07	16.15	46.55	2.8
5.36	0.39	1.29	11.57	37.31	3.33	20.41	0.34	3.21	10.90	39.44	11.00	30.05	18.43	74.22	14.75	128.14	616.62	18.11	78.76	8.21	0.47	247.98	16.91	15.68	7.01	1.08	0.93	-4.85	11.60	45.45	3.4
5.47	0.38	1.34	11.77	37.70	3.38	19.70	0.35	3.58	11.23	37.56	11.27	30.79	16.03	74.81	15.88	131.62	610.93	18.89	76.97	8.33	0.66	243.28	19.79	18.00	7.54	0.72	0.89	-4.49	14.05	49.94	1.6
5.57	0.41	1.35	12.27	38.59	3.42	18.78	0.37	3.70	9.22	41.93	14.83	33.13	14.33	76.30	16.36	135.41	596.37	18.53	80.65	8.80	0.88	239.40	18.82	16.12	7.20	1.78	0.86	-5.50	13.90	44.84	2.5
5.68	0.41	1.35	12.08	38.32	3.31	19.44	0.37	3.31	10.60	39.39	15.07	31.46	16.76	72.89	15.73	128.82	593.08	20.68	84.36	8.88	0.69	232.19	21.76	18.71	7.15	0.57	0.78	-4.20	13.60	46.03	2.0
5.79	0.37	1.33	9.37	40.62	2.39	21.13	0.38	2.78	9.06	30.62	26.60	25.21	12.00	54.23	10.99	88.27	468.42	23.21	150.73	8.43	1.09	189.86	18.57	13.39	8.84	1.36	-1.66	-4.70	8.60	47.06	2.3
5.89	0.40	1.32	12.11	38.92	3.31	18.30	0.38	3.92	10.16	43.30	16.51	29.89	15.38	72.13	16.66	129.98	610.14	19.82	90.27	8.85	1.27	240.86	21.83	16.57	7.28	1.17	0.67	-4.79	17.45	48.65	2.1
average	2.10	1.24	10.08	33.91	2.99	22.88	0.31	3.00	9.24	33.20	12.74	28.94	17.81	68.24	13.52	111.42	609.46	18.10	77.81	7.58	0.82	204.11	17.59	14.58	6.32	0.95	0.89	-5.26	12.77	46.61	2.20

Interval III	major elements (weight percent)									minor and trace elements (parts per million)																	stable isotope ratios (‰VPDB)		geophysical properties		
level (m)	Na2O	MgO	Al2O3	SiO2	P2O5	K2O	CaO	TiO2	Fe2O3	Sc	Cr	Co	Ni	Cu	Zn	Ga	Rb	Sr	Y	Zr	Nb	Mo	Ba	La	Pb	Th	U	**$\delta^{18}O$**	**$\delta^{13}C$**	MS (SI)	L* (%)	a* (%)
15.58	0.27	0.84	7.29	24.91		2.38	32.12	0.20	2.14	7.79	24.23	4.82	20.25	20.02	53.11	9.93	76.18	841.21	15.28	49.28	5.65	0.96	141.40	14.03	11.48	3.15	0.70	1.47	-3.62	7.10	50.54	2.18
15.68	0.27	0.86	7.58	25.78		2.44	31.26	0.21	2.29	8.22	20.45	5.88	20.58	13.93	53.39	10.25	79.88	843.62	15.18	54.05	5.40	0.87	154.52	12.94	12.53	3.26	0.24	1.17	-5.94	9.00	46.65	3.24
15.78	0.29	0.91	8.20	27.23		2.60	29.70	0.23	2.40	8.39	23.48	6.41	19.96	13.71	57.54	11.29	86.83	806.48	14.30	59.14	6.20	0.86	166.29	12.79	12.21	4.07	0.47	1.25	-4.36	10.15	53.79	2.24
15.87	0.25	0.77	6.27	22.21		2.11	35.40	0.16	1.97	6.60	16.04	3.50	17.63	12.75	49.14	9.27	64.94	921.11	14.24	42.66	4.89	0.89	118.15	11.59	11.15	1.72	-0.69	0.97	-4.51	8.90	45.28	2.84
15.95	0.28	0.79	6.87	24.01		2.26	33.46	0.18	2.00	6.43	21.00	4.38	17.00	15.83	49.42	9.44	70.59	857.08	13.91	48.69	4.85	0.70	138.74	10.24	12.37	2.25	0.92	0.99	-6.73	6.80	45.04	2.92
16.04	0.30	0.91	8.27	27.43		2.61	29.92	0.23	2.35	7.90	22.48	7.45	23.59	13.79	55.07	11.55	86.95	805.70	14.15	59.50	6.19	0.62	170.84	13.37	13.78	3.25	1.14	1.33	-4.05	10.30	52.52	2.33
16.12	0.29	0.90	8.41	27.84		2.59	30.25	0.24	2.06	7.67	22.87	7.90	25.13	15.06	54.61	10.93	86.24	805.82	15.89	60.50	6.19	0.74	167.42	14.22	18.53	3.42	1.35	1.46	-3.81	9.30	47.91	1.83
16.20	0.27	0.85	7.88	26.38		2.53	30.71	0.21	1.99	7.84	20.78	10.42	25.27	43.82	52.54	10.31	83.54	837.96	14.68	56.50	5.95	1.11	157.62	14.99	16.71	4.07	-0.07	1.35	-5.96	8.40	53.72	1.28
16.29	0.28	0.85	7.73	26.15		2.47	31.02	0.21	2.08	8.01	21.21	6.21	20.83	17.01	53.83	10.31	81.43	827.59	15.00	54.68	5.79	0.43	149.30	12.32	12.31	2.92	0.86	1.07	-4.44	10.30	53.66	1.59
16.37	0.30	0.88	7.84	26.38		2.50	30.68	0.22	2.16	7.31	21.22	5.70	21.88	13.81	54.63	11.25	82.68	823.60	14.23	54.67	5.93	0.89	160.10	12.83	11.49	5.13	0.84	0.86	-5.03	11.90	50.46	2.00
16.47	0.26	0.79	6.76	23.72		2.22	33.77	0.19	1.89	8.73	19.71	4.86	19.86	13.61	49.47	10.03	69.81	875.31	14.45	47.78	5.30	0.50	142.08	11.46	12.72	2.05	0.04	0.88	-7.84	8.10	46.61	2.30
16.58	0.21	0.72	5.84	21.44		1.97	36.19	0.16	1.76	6.30	13.89	6.72	17.48	11.54	45.90	8.80	60.04	909.83	14.40	41.16	4.67	0.58	130.38	8.14	11.08	1.23	0.12	0.74	-4.91	9.80	52.90	2.12
16.69	0.24	0.81	6.80	23.88		2.22	33.34	0.18	1.99	7.75	17.93	5.99	18.71	12.81	48.68	9.12	68.78	848.28	14.67	47.74	5.11	0.68	148.18	10.63	10.92	2.94	0.20	1.47	-4.31	9.40	51.48	2.41
16.80	0.30	0.96	8.63	28.23		2.68	28.53	0.25	2.45	7.46	29.23	6.49	23.17	18.48	57.70	12.05	90.70	777.95	14.78	60.42	6.77	0.93	179.04	14.57	12.25	4.58	0.75	1.01	-4.11	11.40	50.27	2.17
16.91	0.30	0.98	8.78	28.32		2.72	28.28	0.26	2.51	8.82	26.00	5.55	22.73	12.39	57.42	11.82	92.48	782.95	15.75	61.10	6.48	0.77	177.81	17.55	12.73	3.06	1.66	1.33	-5.49	13.60	46.43	2.68
17.02	0.36	1.08	10.38	32.48		3.05	23.99	0.30	2.70	9.69	35.90	9.90	28.58	16.13	65.13	13.88	109.94	708.56	17.04	74.38	7.74	0.97	211.62	16.74	17.19	5.92	0.65	1.31	-3.56	10.10	49.57	1.69
17.13	0.35	1.05	9.60	30.60		2.89	25.91	0.28	2.66	8.32	29.30	7.28	25.24	13.11	61.78	12.73	100.97	739.30	16.35	68.97	7.34	0.53	198.75	13.67	13.92	5.09	0.05	1.04	-4.10	11.10	53.92	1.83
17.24	0.28	0.92	8.05	27.04		2.51	29.99	0.23	2.28	7.88	20.58	7.56	21.71	10.87	54.06	11.23	83.21	807.76	15.55	58.26	5.99	0.70	161.27	14.91	12.71	3.12	0.75	1.11	-4.26	9.40	51.79	1.83
17.34	0.21	0.73	5.61	21.06		1.90	36.82	0.16	1.72	5.81	15.53	5.20	17.17	13.87	44.40	8.06	57.30	937.16	14.80	39.97	4.22	0.71	112.73	11.03	10.68	0.77	-0.02	1.01	-4.78	11.80	50.94	2.24

17.45	0.26	0.84	6.97	24.62	2.25	32.78	0.19	2.05	6.89	19.78	7.72	19.98	17.47	50.73	9.21	71.62	856.16	14.64	50.03	5.32	0.78	142.60	11.34	11.43	3.04	0.30	1.10	-6.47	11.60	51.32	1.90
17.56	0.24	0.83	6.67	23.91	2.17	33.60	0.19	2.01	8.03	17.81	4.56	17.61	12.30	49.53	9.51	68.73	866.02	15.42	48.85	5.26	0.73	133.63	11.26	11.86	2.54	0.06	1.19	-4.22	10.30	49.58	2.42
17.66	0.25	0.82	6.72	23.90	2.19	33.47	0.18	2.03	5.72	19.08	4.68	19.28	11.98	49.88	9.83	69.42	864.37	15.47	48.02	4.99	0.92	133.53	12.66	11.69	3.24	-0.84	1.16	-4.54	6.80	54.40	2.34
17.77	0.33	1.04	9.62	30.60	2.86	26.08	0.27	2.60	8.16	26.13	8.66	26.61	14.29	59.88	12.79	100.99	747.83	15.96	69.72	7.06	0.89	183.67	17.71	15.48	5.22	1.16	1.08	-3.73	9.20	51.33	2.49
17.87	0.38	1.11	10.46	32.85	3.00	23.72	0.31	3.07	10.15	31.34	8.43	26.06	14.67	63.63	15.11	109.66	695.15	17.49	75.31	7.62	0.75	208.50	18.55	15.24	5.97	0.84	0.79	-4.44	12.10	48.96	2.50
17.98	0.35	1.08	10.31	32.40	2.96	24.10	0.32	3.07	9.49	32.28	7.68	27.53	9.89	61.71	13.19	107.41	694.99	16.63	75.77	7.49	1.08	197.13	20.28	13.83	5.16	1.65	0.89	-3.91	10.75	49.67	2.68
18.09	0.37	1.07	9.93	31.24	2.93	25.09	0.29	2.86	9.35	29.67	8.96	26.40	17.77	61.91	12.66	104.39	709.65	16.10	71.37	7.20	0.68	193.10	15.84	14.54	5.25	1.03	1.06	-3.90	11.40	46.08	2.79
18.21	0.31	0.91	7.75	28.64	2.30	29.25	0.25	2.15	8.25	21.69	6.15	21.92	10.91	52.96	10.30	75.78	768.15	16.11	78.84	6.08	0.73	160.86	16.53	11.54	3.65	0.40	0.77	-4.90	7.10	49.19	2.21
18.34	0.22	0.75	5.76	21.50	1.91	36.53	0.16	1.77	6.93	16.25	6.15	15.75	11.68	44.41	7.60	58.17	910.11	14.85	39.75	4.24	1.02	114.97	9.51	11.07	2.14	0.65	0.88	-8.20	10.00	54.36	1.68
18.47	0.25	0.82	6.68	24.14	2.14	33.82	0.18	1.89	7.73	19.43	4.14	18.83	12.58	48.95	9.52	68.01	864.70	14.75	48.28	5.02	0.79	136.30	10.75	11.36	1.73	0.18	1.12	-4.20	9.00	49.00	2.07
18.60	0.28	0.86	7.35	25.83	2.32	31.66	0.21	2.11	7.59	20.08	6.03	19.74	16.14	51.11	10.03	75.31	808.16	14.06	54.69	5.80	0.83	143.04	14.94	12.51	3.86	0.16	1.16	-4.00	8.20	48.86	2.39
18.73	0.27	0.85	6.96	24.81	2.21	32.84	0.19	2.14	6.66	21.15	7.04	21.30	13.66	51.77	9.47	69.69	849.17	16.77	51.32	5.34	1.19	144.27	8.45	11.11	2.21	-0.15	0.70	-4.74	11.40	44.38	2.80
18.86	0.43	1.20	11.51	37.15	3.11	20.23	0.38	3.08	9.64	38.80	9.50	30.70	19.43	66.75	14.63	116.88	617.38	18.83	92.02	8.59	0.33	239.45	17.28	17.22	6.71	1.03	0.78	-5.34	9.60	44.80	2.32
18.99	0.38	1.18	11.40	35.20	3.16	21.28	0.35	3.27	8.17	36.88	9.34	29.94	16.81	65.51	14.71	118.07	623.70	18.83	82.89	8.80	0.87	214.70	20.06	17.31	6.75	-0.08	0.78	-3.67	8.25	46.27	2.22
19.12	0.43	1.26	12.28	37.34	3.32	19.14	0.38	3.30	9.47	40.29	11.03	30.96	26.64	69.22	15.34	128.16	595.77	18.83	90.68	9.08	0.98	239.31	22.06	21.32	8.65	1.41	0.75	-3.77	12.50	51.43	2.41
19.23	0.27	0.88	7.40	25.85	2.34	31.67	0.20	2.16	6.29	20.35	6.14	20.34	14.74	54.60	9.85	76.01	851.82	16.84	52.76	5.53	1.20	138.13	13.13	12.54	3.39	0.79	1.11	-4.38	10.60	50.78	2.03
19.31	0.27	0.88	7.36	26.48	2.28	31.35	0.21	1.99	7.11	22.31	4.96	19.02	12.81	53.49	10.48	74.23	818.31	15.91	61.45	5.41	0.71	140.18	12.01	10.97	3.49	0.30	1.07	-4.48	10.40	54.71	1.32
19.39	0.28	0.91	7.65	26.57	2.39	30.89	0.22	2.12	7.91	21.30	6.09	22.92	12.68	55.84	10.31	78.58	818.69	15.93	56.56	5.87	0.59	150.72	15.66	12.61	3.90	0.70	0.96	-5.40	7.50	48.50	1.88
19.47	0.28	0.94	7.91	27.04	2.43	30.31	0.22	2.27	7.03	22.58	7.51	21.83	11.88	57.98	10.71	80.58	802.34	16.69	58.61	6.07	0.80	163.10	13.35	13.13	3.74	0.86	1.37	-4.10	7.90	52.94	1.56
19.55	0.35	1.07	9.79	32.58	2.77	24.92	0.30	2.40	8.63	31.54	12.83	28.35	14.87	59.94	12.36	96.79	683.36	17.08	85.00	7.38	0.48	201.73	18.56	19.70	6.14	1.13	1.01	-3.86	9.40	50.36	0.98
19.70	0.43	1.20	11.88	36.96	3.18	19.94	0.38	2.83	9.38	37.54	14.87	33.73	17.82	68.40	15.24	119.78	616.45	19.50	91.86	8.76	1.46	231.43	20.69	23.38	8.00	2.15	1.23	-3.53	11.90	49.27	-0.31
19.81	0.39	1.19	11.59	35.26	3.23	21.15	0.35	3.12	9.27	37.72	12.17	32.77	23.80	68.14	15.53	121.45	655.38	18.13	82.49	8.31	0.87	233.36	19.87	18.60	6.01	1.24	1.23	-4.81	12.30	46.37	2.12
19.92	0.38	1.13	10.71	34.66	2.99	22.51	0.33	2.69	9.70	36.49	7.48	25.88	20.13	64.29	14.00	109.04	667.35	17.83	85.27	8.26	0.43	213.40	16.80	15.49	6.09	0.64	0.90	-4.31	13.00	46.82	2.17
20.03	0.29	0.97	8.60	28.37	2.63	28.68	0.24	2.45	8.71	24.56	6.25	24.39	19.81	58.59	12.22	88.79	794.52	15.73	59.85	6.13	0.93	175.93	14.04	12.20	3.07	0.70	1.33	-4.21	11.00	47.72	2.48
20.14	0.28	0.90	7.59	26.16	2.36	31.11	0.21	2.23	6.84	20.91	5.57	21.55	15.02	54.13	10.18	75.35	832.97	15.83	51.18	5.66	0.65	154.52	13.31	11.49	2.98	0.92	0.90	-4.65	13.50	46.35	2.50
20.25	0.26	0.86	6.92	24.37	2.20	33.11	0.19	2.07	7.44	20.25	5.22	18.18	13.13	53.28	9.38	69.78	856.65	14.53	48.22	4.94	0.10	143.44	9.01	11.50	2.84	0.57	1.16	-7.61	11.20	53.41	2.33
20.35	0.27	0.90	7.40	25.56	2.34	31.68	0.21	2.23	8.13	21.37	5.14	22.65	13.08	56.66	9.61	75.26	831.68	15.02	51.38	5.52	0.97	154.37	14.06	13.17	3.12	0.04	1.00	-4.73	8.00	44.25	2.23
20.46	0.29	0.95	8.21	27.75	2.52	29.50	0.24	2.40	9.27	23.33	5.43	23.03	13.56	58.89	11.04	84.75	801.15	14.71	57.46	5.99	0.97	169.14	16.90	12.19	2.99	1.12	0.56	-5.77	8.60	46.39	2.25
20.57	0.30	0.97	8.41	28.29	2.55	28.91	0.24	2.48	8.68	25.19	8.27	22.92	11.25	58.19	11.34	86.54	782.35	15.30	59.92	6.32	1.18	172.92	15.05	11.13	3.02	1.02	0.78	-4.57	13.50	48.47	2.42
20.67	0.30	1.01	8.93	29.37	2.69	27.31	0.26	2.70	9.40	26.10	6.14	24.00	11.09	60.38	12.45	91.78	736.80	17.01	65.95	6.70	0.65	189.84	14.71	12.84	4.49	1.19	1.03	-6.31	13.30	44.35	2.60
20.78	0.34	1.10	10.18	32.52	2.95	24.11	0.30	2.94	8.21	34.18	8.31	26.97	15.41	64.35	13.11	106.26	699.00	17.27	75.22	7.85	0.96	216.32	17.58	15.74	5.16	0.67	1.08	-4.05	13.20	45.67	1.86
20.88	0.33	1.07	9.94	32.12	2.90	24.54	0.29	2.97	8.43	32.22	8.04	27.10	14.64	62.73	13.57	103.65	713.28	16.74	74.47	7.58	0.69	205.87	16.95	14.02	4.26	0.39	1.13	-4.08	13.90	50.85	2.30
20.99	0.32	1.06	9.47	30.66	2.80	26.09	0.27	2.74	8.99	27.80	8.39	27.49	20.35	62.79	12.86	98.49	737.21	16.76	68.87	7.06	0.32	195.98	17.67	13.60	3.91	0.05	1.01	-4.58	14.30	48.07	2.34
21.09	0.33	1.02	9.02	30.17	2.67	27.02	0.26	2.44	7.29	28.09	7.31	25.73	17.74	61.43	12.30	91.62	759.56	17.70	70.59	6.63	0.99	185.11	15.64	15.67	4.09	1.36	1.21	-4.03	7.00	54.03	-0.28
21.20	0.29	0.99	8.61	28.91	2.60	28.05	0.25	2.55	8.43	27.10	6.84	22.83	17.93	59.93	11.26	87.76	773.43	15.85	62.30	6.30	0.71	173.09	14.86	12.74	4.10	0.54	0.83	-7.80	14.10	51.03	2.03
21.31	0.31	1.01	8.91	29.84	2.69	27.11	0.27	2.65	9.48	29.51	7.35	22.82	15.15	61.24	11.64	92.23	766.91	15.93	67.63	6.50	1.13	188.02	14.42	14.14	3.97	1.43	1.45	-3.72	12.70	49.02	2.40
21.41	0.30	0.99	8.25	29.76	2.45	27.91	0.26	2.45	7.01	23.39	6.05	23.11	15.59	59.26	11.11	83.63	754.82	16.84	75.89	6.76	0.86	175.67	16.84	13.96	5.49	1.76	0.20	-5.54	11.90	46.93	2.42
21.52	0.32	1.03	9.07	30.07	2.68	27.05	0.26	2.73	8.00	27.37	6.86	22.50	14.14	61.74	11.48	92.72	741.88	16.87	66.62	7.06	0.62	187.92	16.60	13.42	5.57	0.01	0.68	-4.56	12.60	47.00	2.78
21.63	0.32	1.06	9.51	30.85	2.81	25.72	0.27	2.93	9.45	30.80	5.62	24.69	16.05	63.31	12.74	99.23	721.19	17.36	69.60	7.22	0.62	192.25	18.28	13.85	5.79	0.58	1.15	-3.98	13.90	49.66	2.23
21.74	0.31	1.06	9.59	31.27	2.84	25.24	0.28	3.04	9.11	31.28	6.94	23.46	11.11	62.72	12.77	101.58	737.15	17.97	71.67	7.34	1.12	195.98	17.24	13.00	4.55	1.09	1.31	-5.47	15.60	47.32	2.56
21.84	0.40	1.17	11.24	37.53	3.04	19.71	0.38	3.47	9.80	39.11	8.63	28.34	12.49	66.88	14.36	116.61	610.21	19.35	93.83	9.05	1.16	228.56	18.32	15.46	6.89	1.21	0.70	-4.39	17.40	44.13	3.21
21.95	0.36	1.16	11.06	35.36	3.11	21.26	0.35	3.33	11.03	36.61	10.41	29.44	16.67	65.99	14.29	116.42	649.77	18.89	85.73	8.48	1.27	216.46	20.25	18.08	6.95	1.32	0.78	-4.35	12.70	41.62	2.74
22.06	0.37	1.14	10.67	34.26	3.04	22.51	0.33	3.13	9.26	33.94	8.91	29.06	16.57	66.30	14.19	112.19	682.07	16.79	79.19	8.25	0.82	214.30	18.11	15.31	7.44	0.64	0.84	-4.12	12.90	47.88	2.07
22.17	0.30	1.02	9.07	30.63	2.73	26.37	0.27	2.74	7.72	27.71	6.69	24.31	16.81	63.45	12.47	96.28	748.06	16.83	68.28	6.85	1.24	182.01	16.77	13.53	4.17	1.13	1.43	-3.75	14.50	48.95	2.23
22.29	0.33	0.98	8.82	29.97	2.63	27.30	0.26	2.55	8.37	27.03	7.68	24.54	18.09	60.63	11.07	89.93	764.06	17.48	65.67	6.51	0.27	172.12	16.11	13.01	4.32	0.86	0.65	-8.28	16.40	50.38	2.01
22.40	0.34	0.99	9.14	31.47	2.71	25.96	0.28	2.68	8.80	27.93	12.24	25.41	11.43	61.08	12.32	95.55	729.48	18.10	71.00	7.11	0.82	177.21	17.79	14.05	5.06	1.31	1.31	-3.78	12.75	48.42	2.24
22.52	0.31	0.99	8.86	30.59	2.69	26.63	0.27	2.72	8.19	29.67	12.44	26.30	14.51	61.66	12.28	93.91	734.27	18.10	69.15	6.93	0.86	175.95	16.06	13.58	4.03	0.75	0.85	-4.36	14.80	49.45	2.35
22.64	0.41	1.12	10.82	37.85	2.90	20.48	0.37	3.04	8.34	33.97	19.77	27.42	19.74	63.87	13.64	108.34	599.80	19.81	94.22	8.17	0.85	218.13	19.59	17.36	6.48	1.59	1.09	-3.93	12.10	45.40	2.59

22.75	0.38	1.20	12.08	37.30	3.27	19.16	0.38	3.78	9.03	37.94	15.38	30.69	15.95	67.33	15.78	127.07	606.22	19.92	88.28	8.91	0.81	236.06	20.98	17.03	7.22	1.18	0.75	-4.78	11.80	44.06	2.89
22.87	0.40	1.20	11.73	38.79	3.03	19.18	0.39	3.23	9.70	36.12	16.42	31.16	17.32	62.89	14.45	116.27	588.26	22.41	106.33	9.26	0.83	229.64	22.34	17.15	8.13	1.42	0.02	-3.95	10.80	51.46	2.45
22.99	0.40	1.28	12.53	38.32	3.34	18.29	0.40	3.65	10.07	39.35	14.11	31.52	20.33	67.63	15.72	129.82	576.01	19.59	93.79	9.38	0.82	233.83	19.94	17.56	7.91	1.87	0.36	-4.02	11.10	52.62	2.43
23.10	0.38	1.23	11.53	35.78	3.20	20.71	0.36	3.35	9.23	42.29	12.86	31.49	23.59	71.57	15.47	121.32	641.14	18.60	85.72	8.69	0.87	223.97	20.31	18.48	6.51	1.47	1.21	-3.61	14.10	48.42	2.68
23.20	0.30	0.99	8.63	29.37	2.60	27.83	0.25	2.55	8.09	25.35	11.77	27.63	13.83	63.15	11.57	88.75	810.61	16.78	61.63	6.20	0.75	166.96	16.17	12.32	4.37	1.37	1.08	-4.45	12.00	48.72	2.13
23.28	0.33	0.98	8.58	30.36	2.53	27.27	0.26	2.57	7.10	25.34	11.30	26.39	15.04	61.29	10.84	86.49	776.32	19.02	68.04	6.36	0.46	166.37	15.29	12.40	3.83	0.82	1.28	-6.05	11.30	47.46	2.30
23.37	0.32	1.05	9.72	33.43	2.87	23.46	0.30	2.75	8.64	30.62	7.01	27.14	17.02	64.44	13.56	104.48	703.21	18.89	79.27	7.73	0.81	190.30	18.64	15.57	6.47	0.64	0.74	-4.70	14.60	51.23	1.34
23.45	0.31	1.01	9.03	30.44	2.69	26.47	0.27	2.94	8.15	29.09	9.69	28.09	13.59	63.08	12.02	94.43	777.29	20.26	67.10	6.93	0.89	178.01	16.36	12.66	4.30	1.44	1.24	-3.84	16.40	43.47	2.84
23.53	0.35	1.11	10.55	33.72	3.01	22.73	0.32	3.46	8.95	31.61	11.66	31.11	13.18	66.73	14.35	111.84	719.87	19.46	75.54	7.96	1.10	208.91	16.55	15.05	6.24	1.25	0.73	-4.42	16.45	52.62	2.12
23.61	0.39	1.20	11.83	36.54	3.25	19.82	0.37	3.56	9.89	39.55	13.09	31.14	15.01	67.68	14.23	123.27	623.63	18.70	83.58	8.65	0.55	233.27	17.93	17.86	6.43	2.11	0.99		8.90	40.90	3.14
23.70	0.41	1.21	11.98	37.69	3.20	19.20	0.38	3.52	10.66	38.09	14.25	30.33	17.26	67.79	16.02	123.88	649.96	19.83	97.84	9.28	1.45	223.06	19.43	18.41	6.99	0.44	0.59	-4.16	16.00	42.75	3.27
23.78	0.40	1.18	11.56	35.72	3.24	20.67	0.36	3.42	9.20	38.67	12.12	30.67	22.94	71.16	15.46	124.92	672.55	18.12	82.51	8.77	0.56	215.39	21.19	15.79	7.51	2.20	1.27	-3.83	13.30	45.60	2.57
23.86	0.31	0.97	8.48	29.05	2.60	28.11	0.24	2.52	6.90	27.97	10.39	25.66	15.04	61.28	11.55	89.43	793.07	17.08	62.11	6.24	0.97	157.30	15.47	12.83	3.82	0.74	1.00	-7.07	11.70	49.25	2.11
23.95	0.32	0.95	8.24	30.24	2.47	27.83	0.26	2.42	8.44	25.29	12.46	22.92	12.78	59.77	11.15	84.04	765.25	17.73	69.92	6.23	0.69	157.51	15.97	13.96	3.59	0.85	1.48	-3.97	9.90	47.99	2.02
24.04	0.30	0.94	8.31	28.84	2.55	28.55	0.24	2.44	8.57	25.21	11.26	25.31	14.79	59.88	11.21	86.98	778.91	16.75	63.70	6.14	0.88	154.67	13.90	12.51	5.15	0.68	1.07	-4.60	12.50	51.11	1.66
24.13	0.34	1.04	9.64	31.72	2.86	25.37	0.28	2.80	8.44	28.16	13.73	26.67	28.01	64.81	12.41	101.72	719.62	17.12	70.52	7.20	0.69	175.67	15.40	13.76	4.80	1.88	0.94	-4.32	15.00	46.18	2.25
24.22	0.39	1.15	11.12	35.22	3.17	21.70	0.35	3.00	9.85	36.12	14.16	31.55	15.56	67.48	14.95	118.93	664.79	20.95	84.59	8.26	1.07	205.78	16.98	18.82	6.99	1.66	1.29	-3.58	11.80	44.53	2.75
24.30	0.37	1.14	11.05	34.38	3.16	22.07	0.34	3.23	9.36	33.91	15.11	30.83	14.41	68.30	14.67	118.29	673.47	18.28	79.12	8.06	0.89	204.52	19.78	15.48	6.03	1.39	1.09	-6.91	12.70	49.45	2.00
24.39	0.38	1.13	10.90	34.30	3.15	22.20	0.33	3.27	9.43	35.71	12.18	31.33	13.27	69.39	14.67	118.16	684.46	17.76	79.16	8.26	0.98	202.75	22.61	16.22	7.10	1.30	0.67	-4.94	14.30	48.15	2.75
24.48	0.33	1.03	9.59	31.25	2.88	25.48	0.27	2.92	8.29	29.46	17.81	27.96	15.51	64.26	13.55	102.27	743.84	18.11	70.32	7.12	1.09	176.84	16.21	14.29	5.18	0.42	1.21	-4.17	13.00	46.83	2.34
24.57	0.36	1.09	10.19	32.59	2.98	24.13	0.30	3.04	11.30	32.16	12.20	29.09	14.80	68.61	14.25	106.89	712.21	18.79	72.33	7.75	0.94	191.66	16.44	13.35	5.42	0.38	1.28	-3.81	15.30	46.05	2.40
24.66	0.33	1.00	9.34	30.65	2.82	26.36	0.27	2.59	9.13	28.36	16.93	25.56	16.50	62.43	12.46	98.46	747.35	17.69	67.82	6.91	0.69	175.43	17.69	17.78	4.97	1.30	1.56	-3.70	10.60	51.18	1.73
24.77	0.30	0.91	8.02	27.58	2.51	29.50	0.23	2.51	8.39	22.00	9.40	23.09	17.13	57.91	11.16	84.48	819.69	16.47	57.40	6.15	0.98	155.35	15.10	12.51	4.60	0.43	1.03	-6.67	12.10	49.19	2.43
24.88	0.27	0.87	7.45	26.01	2.36	30.92	0.21	2.41	7.65	25.03	11.68	22.91	12.08	56.50	9.98	78.66	835.89	16.45	52.64	5.79	0.80	150.06	17.38	12.19	2.61	0.54	1.57	-4.00	10.60	51.46	2.00
24.99	0.27	0.89	7.66	26.56	2.43	30.32	0.21	2.46	7.39	22.57	13.91	22.74	20.87	57.60	11.06	81.62	838.40	16.06	54.94	5.60	0.91	160.72	14.08	11.79	4.29	0.40	1.64	-3.85	12.30	49.75	1.98
25.09	0.31	0.99	9.36	30.44	2.82	26.09	0.27	2.90	6.81	26.61	10.12	25.58	16.71	62.18	12.44	99.93	758.37	16.39	67.67	7.29	0.43	191.74	15.02	14.66	6.17	0.62	1.53	-3.31	10.80	46.73	2.25
25.20	0.35	1.02	9.92	32.61	2.90	24.38	0.30	3.00	8.46	29.46	9.67	26.88	16.90	62.22	13.03	104.65	725.58	17.83	76.43	7.48	0.88	202.32	17.86	13.91	6.11	0.65	1.38	-5.26	9.00	47.62	2.49
25.31	0.37	1.07	10.67	33.90	3.07	22.95	0.33	2.89	10.42	31.46	14.90	31.31	15.31	64.87	14.24	114.07	713.74	17.84	79.13	7.94	1.28	218.67	20.06	20.20	5.64	1.33	1.78	-3.20	11.45	48.88	1.61
25.42	0.33	1.03	9.98	31.95	2.96	24.64	0.29	2.96	8.41	31.97	10.86	25.97	17.98	62.91	13.73	107.12	747.14	16.84	70.96	7.47	1.11	203.80	16.28	14.16	5.16	0.52	1.47	-3.69	12.15	49.49	2.42
25.50	0.27	0.87	7.42	26.80	2.34	30.83	0.21	2.24	7.29	20.68	14.61	22.50	36.10	54.84	9.65	75.97	836.88	16.95	60.48	5.82	0.66	157.20	17.37	19.63	3.13	0.46	1.22	-4.02	10.50	47.32	2.39
25.56	0.27	0.87	7.44	26.49	2.37	30.91	0.20	2.27	5.40	20.80	12.84	23.20	16.15	55.58	11.34	77.90	841.31	16.03	57.56	6.03	1.08	158.88	16.43	12.52	4.05	1.45	1.27	-6.74	7.20	52.19	2.06
25.63	0.25	0.84	6.93	25.86	2.22	31.76	0.20	2.15	8.74	19.79	14.26	21.34	11.80	52.73	9.64	72.63	835.55	15.97	57.08	5.74	1.01	150.84	10.06	13.35	3.65	0.73	1.16	-4.51	8.00	52.66	2.25
25.69	0.28	0.91	7.71	27.60	2.39	29.92	0.24	2.31	9.24	24.88	8.37	21.32	12.97	55.55	11.02	79.63	803.56	17.60	62.30	6.26	0.79	166.99	15.55	13.40	4.09	1.00	1.49	-4.00	8.30	42.15	2.06
average	0.32	0.99	8.99	29.90	2.68	27.20	0.27	2.61	8.35	27.43	9.21	24.84	15.99	59.62	12.06	93.44	758.85	16.86	67.21	6.79	0.83	179.29	15.82	14.23	4.62	0.83	1.07	-4.68	11.36	48.77	2.22

Interval																											stable isotope ratios (‰VPDB)		geophysical properties		
IV	major elements (weight percent)									minor and trace elements (parts per million)																					
level (m)	Na2O	MgO	Al2O3	SiO2	P2O5	K2O	CaO	TiO2	Fe2O3	Sc	Cr	Co	Ni	Cu	Zn	Ga	Rb	Sr	Y	Zr	Nb	Mo	Ba	La	Pb	Th	U	**$\delta^{18}O$**	**$\delta^{13}C$**	MS (SI)	L* (%)	a*(%)
174.09	0.23	0.65	5.26	22.30	0.10	1.60	37.75	0.15	1.70	5.71	14.19	4.09	15.32	15.99	41.83	7.08	55.90	908.09	12.71	37.44	4.15	0.25	117.53	8.62	8.04	2.20	0.10	1.80	-3.22	6.85	56.86	-0.7267
174.16	0.30	0.73	6.19	24.95	0.07	1.94	34.64	0.17	1.82	7.16	13.71	6.35	19.72	13.24	44.74	9.77	68.51	888.25	12.69	45.01	4.86	0.97	156.54	12.83	9.61	2.35	-0.22	1.94	-2.85	4.53	58.70	-1.115
174.30	0.32	0.76	6.89	28.18	0.07	2.15	31.86	0.19	1.86	5.90	19.20	8.16	22.05	17.26	45.44	9.62	78.52	842.89	13.95	49.51	5.63	0.99	152.71	11.45	11.18	3.36	0.57	1.59	-3.21	6.20	57.48	-0.911
174.39	0.37	0.78	7.25	28.33	0.05	2.27	31.29	0.20	1.87	6.28	19.14	6.85	21.60	18.94	43.80	10.22	82.25	841.74	14.42	50.89	5.90	0.36	168.05	10.51	10.68	2.59	0.87	1.90	-2.72	7.15	58.14	-1.0369
174.50	0.42	0.90	8.89	33.11	0.05	2.63	26.53	0.25	2.12	7.44	28.74	8.54	26.74	22.12	48.94	12.38	100.92	821.87	14.18	60.97	7.03	0.97	207.91	11.15	12.91	5.45	0.77	1.79	-2.96	9.05	56.41	-1.0994
174.58	0.45	0.86	8.51	31.46	0.05	2.48	27.89	0.24	2.01	7.04	22.73	8.14	27.46	22.96	48.65	11.66	94.13	831.06	14.32	57.52	6.86	0.95	208.94	12.76	12.41	4.01	1.03	1.75	-3.30	7.68	56.26	-0.7215
174.67	0.41	0.83	8.05	30.01	0.05	2.29	29.44	0.23	1.91	7.94	24.56	11.47	25.10	41.56	51.63	10.47	87.25	827.10	13.00	54.29	6.35	1.23	163.66	12.85	15.99	4.16	0.70	1.72	-3.29	6.78	57.09	-0.8273
174.79	3.26	0.59	4.90	21.17	0.07	1.52	37.15	0.15	1.52	5.71	13.30	2.23	16.81	16.74	38.70	7.87	53.48	924.17	13.18	37.74	4.19	0.64	113.96	7.24	9.22	0.90	0.21	1.82	-3.33	8.08	54.44	-0.3149
174.90	0.30	0.62	4.74	20.53	0.10	1.46	39.35	0.14	1.53	5.79	10.93	3.95	15.69	15.22	38.99	7.66	49.82	906.87	13.06	36.49	4.09	0.49	108.36	10.55	9.04	1.99	0.83	1.78	-3.43	4.98	54.00	-0.3113
174.99	0.35	0.71	5.77	23.59	0.08	1.73	35.75	0.16	1.79	7.35	13.98	4.88	21.27	14.88	47.28	8.30	60.55	1065.62	13.27	42.25	4.88	0.59	157.94	11.43	9.60	2.53	-0.27	1.68	-3.29	7.63	56.33	-0.6487

175.14	0.40	0.80	7.52	29.31	0.07	2.26	30.44	0.21	1.97	8.23	18.43	7.58	23.92	14.34	47.48	11.07	82.50	815.10	14.67	52.47	6.00	0.49	178.65	12.63	11.15	3.80	0.05	1.75	-3.01	7.98	56.90	-1.0633
175.26	0.55	0.99	10.25	36.39	0.05	2.89	22.93	0.30	2.40	8.76	29.98	12.94	32.62	20.62	55.03	13.82	116.04	715.13	15.13	72.70	7.91	0.42	248.80	15.60	13.93	4.87	0.79	1.85	-3.08	9.68	55.95	-1.3345
175.38	0.62	1.05	11.10	38.73	0.05	3.11	20.55	0.33	2.55	9.73	36.49	13.58	34.60	29.92	58.33	15.43	127.66	685.16	16.14	77.47	8.65	0.76	260.34	16.91	19.02	7.29	1.08	2.11	-3.04	7.28	58.34	-1.2568
175.49	2.09	0.88	9.38	33.59	0.07	2.53	24.80	0.27	2.19	8.93	26.68	7.52	30.00	20.43	57.02	12.76	101.28	712.29	15.74	63.20	7.40	1.01	196.08	12.30	11.67	6.30	0.98	1.78	-3.41	9.03	61.76	-0.8576
175.64	0.26	0.65	4.64	20.40	0.11	1.42	39.41	0.13	1.66	5.84	10.15	3.20	14.02	14.57	38.78	6.78	48.19	924.52	13.13	33.13	3.92	0.48	113.51	10.16	7.92	1.47	-0.29	1.95	-3.70	4.55	57.30	-0.5091
175.73	0.27	0.67	4.50	19.84	0.16	1.39	39.67	0.14	1.78	7.25	10.11	2.91	15.54	11.40	41.05	7.02	47.71	909.49	15.45	32.64	3.59	0.49	98.63	8.04	7.43	2.29	0.43	1.83	-3.28	6.15	54.08	-0.5999
175.81	0.68	0.69	5.34	22.96	0.09	1.65	36.24	0.16	1.75	6.23	13.37	3.16	15.83	18.15	43.05	8.08	57.71	856.82	14.60	40.56	4.52	0.58	120.02	9.51	10.67	1.83	0.65	1.86	-3.15	7.50	56.95	-0.564
175.94	0.45	0.90	8.50	32.40	0.05	2.45	27.41	0.25	2.13	8.50	21.92	7.40	24.09	18.69	56.86	12.10	93.66	747.24	15.16	61.98	6.89	1.04	170.04	12.39	12.29	5.98	0.81	1.85	-3.26	6.18	59.05	-0.9592
176.03	0.48	0.95	9.48	34.50	0.04	2.75	24.92	0.27	2.27	8.75	28.89	7.19	24.74	18.40	53.97	12.63	107.24	745.36	14.78	65.79	7.57	0.78	238.87	15.31	14.25	4.41	0.57	1.75	-3.22	7.00	54.99	-1.1831
176.11	0.48	0.92	9.31	33.56	0.04	2.59	25.87	0.27	2.16	9.52	25.79	10.51	28.72	22.54	51.83	12.24	99.92	778.57	14.46	61.03	7.10	0.65	227.32	13.06	11.38	5.08	0.47	1.89	-3.05	9.30	56.16	-1.0203
176.18	0.45	0.87	8.49	31.27	0.05	2.46	27.87	0.24	2.02	9.06	22.43	7.04	25.65	19.14	52.19	10.89	93.71	822.19	14.09	57.63	6.59	0.30	205.67	12.09	11.86	4.81	0.64	1.84	-2.82	9.05	56.38	-0.5793
176.30	0.27	0.67	5.56	23.68	0.10	1.69	36.00	0.15	1.66	5.55	13.96	3.63	16.43	15.92	41.12	8.38	59.29	908.57	14.91	39.83	4.60	0.52	114.86	9.00	8.70	2.05	0.18	1.79	-3.39	5.25	54.24	-0.497
176.37	13.26	0.54	4.43	19.50	0.08	1.50	33.61	0.15	1.66	6.36	12.19	2.81	14.85	19.77	42.56	8.24	58.69	844.11	13.49	40.88	4.51	0.71	105.95	8.21	10.56	2.50	0.50	1.71	-3.49	7.18	57.61	-0.8282
176.44	0.58	0.67	4.73	20.55	0.27	1.50	39.19	0.14	1.63	6.78	9.81	3.61	15.53	17.36	38.56	7.01	50.69	860.20	16.89	35.18	4.03	0.60	128.17	10.69	8.15	1.85	-0.07	1.88	-3.27	4.50	55.72	-0.61
176.50	0.31	0.67	4.74	20.58	0.12	1.50	39.26	0.14	1.69	5.54	9.33	5.75	16.98	16.13	42.07	7.40	50.37	861.47	14.54	36.72	4.24	1.08	102.67	8.30	8.28	2.46	0.23	1.86	-3.40	5.38	54.71	-0.6038
176.57	2.49	0.67	4.95	21.11	0.12	1.56	37.38	0.15	1.76	7.27	11.42	2.72	17.19	16.68	44.16	7.41	54.13	841.53	15.60	39.30	4.35	0.99	105.84	11.35	8.52	2.38	0.55	1.62	-3.75	9.13	58.01	-0.8005
176.72	0.51	0.92	9.13	32.89	0.05	2.68	26.18	0.27	2.22	9.52	24.81	9.19	26.98	17.27	52.65	12.22	102.34	739.39	14.25	66.21	7.11	0.71	222.59	15.25	13.32	6.07	0.94	1.92	-2.95	8.73	55.24	-1.1784
176.84	0.54	0.99	10.27	36.55	0.04	2.90	22.81	0.30	2.45	9.45	29.45	7.86	29.16	17.50	53.50	12.75	114.18	694.78	14.72	71.79	7.65	0.82	252.42	16.19	14.68	6.73	0.29	1.93	-2.89	10.18	60.03	-1.2039
176.94	0.52	0.93	9.93	35.35	0.05	2.74	23.93	0.29	2.29	8.66	27.55	10.33	29.17	18.16	53.81	14.16	107.89	713.19	15.08	70.55	7.59	0.79	251.92	14.66	13.99	5.74	0.81	1.93	-2.87	6.80	57.01	-1.0251
177.05	0.45	0.81	8.14	30.48	0.05	2.32	29.09	0.23	1.93	7.63	23.25	5.23	18.81	29.01	49.46	10.89	86.61	825.41	13.71	57.44	6.55	0.49	216.08	11.31	15.60	4.57	0.29	1.93	-3.12	6.58	55.27	-0.8145
177.19	0.27	0.65	4.81	20.45	0.19	1.50	38.68	0.14	1.69	6.54	11.34	2.27	13.60	15.84	44.45	7.12	51.13	903.73	15.63	36.85	4.50	0.96	112.56	10.03	8.62	2.22	-0.14	1.78	-3.45	7.48	57.45	-0.5293
177.24	0.32	0.67	5.27	21.84	0.15	1.65	37.17	0.16	1.68	6.87	12.92	3.69	15.99	14.31	42.14	8.22	57.17	892.52	14.43	40.18	4.64	0.59	112.67	9.00	7.96	1.75	0.25	1.94	-3.06	5.23	54.74	-0.5357
177.30	1.23	0.75	6.17	24.91	0.10	1.88	33.54	0.18	1.72	7.48	14.74	2.82	17.33	15.95	45.91	8.61	68.37	845.07	14.53	49.08	5.53	0.53	148.80	10.72	11.63	3.66	1.17	1.81	-3.17	6.73	58.20	-0.553
177.41	0.42	0.82	6.88	27.02	0.07	2.05	31.79	0.20	1.91	6.22	18.19	5.92	24.80	14.98	50.68	9.42	75.56	824.54	14.61	53.19	5.52	0.55	204.85	11.65	11.58	2.94	-0.39	1.72	-3.61	4.23	56.04	-0.8033
177.47	30.13	0.33	4.72	20.11	0.04	1.78	22.94	0.20	1.97	6.56	22.42	32.63	28.89	18.13	50.72	11.65	90.57	772.60	13.69	59.37	6.57	0.75	201.73	10.04	13.63	5.27	0.46	1.99	-2.80	7.65	53.53	-0.9817
177.53	0.45	0.87	8.26	30.44	0.04	2.46	28.23	0.24	2.15	8.24	21.73	8.84	26.39	17.28	51.02	12.05	91.96	790.87	13.45	59.65	6.59	0.25	207.82	13.51	12.15	3.51	0.39	1.95	-2.81	7.53	58.52	-1.0628
177.59	0.42	0.81	7.39	27.81	0.05	2.27	30.99	0.20	1.94	6.54	19.49	8.34	23.03	17.37	46.03	11.00	81.97	842.05	14.01	51.63	5.93	0.78	181.22	12.57	10.42	3.41	0.51	2.02	-3.08	3.93	54.08	-0.9507
177.68	0.39	0.75	6.60	25.63	0.07	2.05	33.05	0.18	1.86	7.15	17.61	7.38	23.63	16.32	44.93	9.47	72.27	867.44	14.76	47.85	5.39	0.48	166.59	10.80	12.34	3.54	0.44	1.85	-3.18	7.00	56.19	-0.8038
177.72	0.42	0.76	6.88	26.55	0.07	2.15	32.10	0.19	1.84	7.72	19.78	8.22	19.97	25.94	46.83	9.59	77.08	857.66	13.76	50.16	5.37	0.63	154.90	11.85	10.73	4.05	0.59	1.91	-3.19	5.85	59.86	-0.9114
177.79	0.37	0.84	8.31	31.06	0.05	2.42	28.32	0.25	2.01	8.18	23.35	5.67	23.50	20.90	51.33	11.10	91.16	850.66	13.85	59.50	6.53	1.16	170.17	12.23	13.17	4.70	1.06	1.98	-3.48	8.25	57.29	-0.8027
177.87	4.63	0.54	4.05	17.97	0.11	1.39	39.19	0.12	1.39	5.47	11.59	1.94	11.60	11.27	35.14	6.81	47.71	937.20	12.46	30.95	3.74	0.60	121.30	7.85	8.49	1.64	1.17	1.73	-3.70	5.25	53.99	-0.3244
177.93	3.93	0.61	4.71	19.99	0.10	1.59	37.29	0.14	1.51	5.86	10.19	4.08	15.24	15.04	39.63	7.17	54.99	912.49	12.35	34.63	3.99	0.40	132.07	10.40	10.45	1.43	0.88	1.63	-3.75	7.03	58.13	-0.5012
177.98	0.51	0.80	6.56	25.49	0.08	2.06	33.47	0.18	1.82	7.46	16.95	5.33	18.11	15.61	45.27	8.70	71.36	848.82	13.52	45.69	5.07	0.52	172.54	13.24	10.82	3.06	0.20	1.77	-3.65	6.70	57.02	-0.9303
178.08	0.46	0.84	7.53	28.68	0.07	2.29	30.44	0.22	1.96	8.64	19.37	5.31	20.28	24.21	49.68	9.92	82.66	813.63	13.13	53.55	6.03	0.68	201.41	11.79	12.44	3.86	0.63	2.00	-3.43	7.78	58.20	-1.3394
178.17	1.27	0.77	6.72	26.23	0.07	2.11	32.14	0.19	1.91	6.63	20.19	4.33	20.54	17.98	45.50	9.59	76.07	833.63	13.82	45.91	5.64	0.83	177.81	12.11	12.51	2.80	0.99	1.87	-3.14	6.45	56.87	-0.9456
178.23	0.41	0.77	6.99	27.01	0.07	2.18	31.97	0.19	1.92	6.99	17.56	7.28	23.62	15.78	45.92	9.75	77.31	827.78	13.97	48.44	5.55	0.52	171.52	10.44	11.10	2.56	0.05	1.99	-2.97	6.18	53.09	-0.7933
178.33	0.46	0.87	8.30	30.56	0.05	2.51	28.35	0.23	2.12	9.25	23.79	6.94	24.42	17.99	48.70	11.37	92.70	790.88	14.61	56.33	6.42	0.88	207.88	10.76	12.79	4.39	0.39	1.93	-2.85	8.95	56.66	-1.1003
178.38	0.48	0.88	8.72	31.69	0.05	2.51	27.46	0.25	2.16	7.97	23.50	13.89	24.83	21.54	50.81	11.74	94.41	784.88	13.72	56.98	6.48	0.98	186.42	14.73	13.48	5.54	-0.29	1.99	-3.30	8.75	58.53	-0.8946
178.49	0.40	0.73	6.62	26.37	0.05	1.97	33.10	0.19	1.76	8.38	17.15	6.00	18.18	16.80	45.55	9.06	70.40	860.28	13.01	44.50	5.45	0.71	164.54	12.33	11.14	3.13	0.78	1.91	-3.08	5.60	53.72	-0.5952
178.58	0.38	0.66	5.28	22.54	0.08	1.64	36.98	0.15	1.64	7.04	12.52	5.55	16.39	17.80	41.42	8.13	56.77	891.25	12.93	36.13	4.27	0.35	138.69	10.11	8.68	1.54	0.53	1.81	-3.37	6.38	54.85	-0.5094
178.67	0.38	0.73	5.35	23.47	0.11	1.64	36.10	0.16	1.88	7.07	13.50	2.53	17.90	13.97	43.85	8.27	57.81	867.90	14.18	39.47	4.64	0.02	157.01	9.28	9.65	2.89	-0.05	1.78	-3.50	7.03	53.11	-0.507
178.74	0.45	0.81	6.68	27.10	0.07	2.03	32.20	0.19	1.97	7.10	16.90	7.58	21.52	25.68	49.96	9.46	73.25	827.10	14.33	49.24	5.35	0.68	178.52	15.67	13.05	4.74	0.27	1.59	-3.48	7.48	57.61	-0.8143
178.88	0.58	0.95	9.49	35.17	0.05	2.79	24.34	0.28	2.23	8.32	28.30	8.66	26.14	18.17	52.82	12.21	107.84	725.07	14.97	67.33	7.54	0.60	239.26	15.32	12.94	5.62	-0.04	1.87	-3.23	6.83	56.98	-1.2942
178.92	0.60	1.02	10.27	37.48	0.04	3.02	22.11	0.30	2.44	8.27	30.72	10.55	30.52	20.33	52.64	14.29	119.19	688.30	14.21	71.69	8.26	0.79	249.47	16.89	13.62	6.20	0.45	1.98	-3.05	6.85	57.20	-1.3549
178.97	0.56	0.91	8.73	32.56	0.05	2.53	26.46	0.25	2.21	7.71	24.16	7.68	30.81	23.48	52.73	11.90	95.75	750.67	14.07	57.69	6.98	0.60	221.49	10.94	11.40	4.88	0.32	2.01	-2.89	8.03	55.72	-1.1513
179.03	0.46	0.84	7.90	30.21	0.05	2.35	29.28	0.22	1.99	8.36	20.53	5.02	20.63	20.14	49.83	11.05	86.06	817.87	13.19	52.62	5.94	0.45	187.93	13.14	11.71	4.58	0.69	1.95	-2.87	6.55	57.75	-0.9299
179.15	0.33	0.68	5.47	23.02	0.11	1.72	36.45	0.15	1.71	5.92	14.27	5.00	16.66	21.70	40.07	8.38	58.27	887.01	14.74	36.35	4.57	0.37	134.12	8.82	10.26	1.81	0.39	1.77	-3.24	6.65	58.43	-0.6314
179.21	0.33	0.65	5.15	22.17	0.15	1.63	37.62	0.14	1.60	5.87	11.87	3.52	15.43	21.16	38.20	7.31	55.45	881.20	14.99	35.83	4.52	0.50	129.34	7.99	10.25	2.69	-0.05	1.97	-2.91	7.23	58.27	-0.5204

179.28	0.38	0.75	5.89	24.75	0.10	1.83	34.94	0.16	1.84	7.16	15.27	3.07	19.78	17.93	43.05	7.98	64.66	836.84	14.57	41.65	4.94	0.90	146.31	10.03	10.60	2.70	-0.10	2.24	-3.19	8.65	57.62	-0.7511
179.37	0.44	0.83	7.15	28.82	0.05	2.18	30.75	0.20	2.07	7.57	19.62	4.57	22.31	15.75	50.97	10.21	79.71	785.78	14.97	51.23	5.86	0.61	193.95	12.10	11.04	3.80	1.22	1.77	-3.72	7.20	58.14	-1.0266
179.47	0.54	0.92	9.07	33.89	0.05	2.61	25.60	0.26	2.21	8.52	27.00	10.51	28.19	23.13	52.71	12.70	100.07	745.83	14.89	63.18	6.67	0.50	229.72	15.53	13.21	4.79	0.47	2.04	-3.12	7.98	55.81	-0.9217
179.51	0.61	1.02	10.51	37.60	0.05	2.90	22.06	0.31	2.42	10.82	29.24	10.80	29.29	19.61	55.68	13.61	116.74	672.06	14.96	73.13	8.20	0.75	255.51	15.62	14.26	6.27	0.92	1.97	-3.48	9.15	55.33	-1.3902
179.55	0.60	1.01	10.79	37.60	0.04	2.87	21.90	0.31	2.31	9.85	32.40	8.81	27.05	24.63	58.09	13.56	115.72	673.76	15.22	74.72	8.17	0.81	249.20	17.11	17.04	6.09	1.56	1.87	-3.35	6.35	58.73	-1.12
179.59	0.54	0.93	9.13	33.53	0.05	2.57	25.86	0.27	2.16	8.27	24.67	9.15	30.44	24.43	56.28	12.54	99.19	745.17	14.21	61.54	7.08	0.43	215.10	14.27	14.94	5.48	0.59	2.09	-3.16	7.25	56.17	-0.9464
179.70	0.35	0.74	5.57	23.24	0.14	1.76	36.19	0.16	1.84	7.42	17.52	2.94	16.32	16.77	43.47	8.33	60.96	839.22	16.73	40.60	4.82	0.89	143.52	12.21	10.63	3.83	0.41	1.87	-2.94	4.70	55.88	-0.4766
179.79	4.81	0.75	5.80	24.40	0.08	1.79	32.47	0.17	2.02	6.87	14.57	4.18	21.05	15.48	49.79	8.58	67.63	811.97	14.84	47.72	5.15	0.93	158.65	10.20	9.12	3.07	0.72	1.87	-3.37	7.85	55.05	-0.8715
179.88	0.42	0.83	6.77	27.54	0.07	2.04	31.75	0.20	2.11	8.28	19.44	3.62	21.88	14.16	50.73	9.39	74.48	842.74	14.49	49.63	5.56	0.48	168.64	10.63	11.41	3.16	0.45	2.03	-3.08	6.60	60.28	-0.931
179.99	0.51	0.94	8.74	33.68	0.05	2.54	26.09	0.25	2.31	8.57	24.61	8.44	27.17	19.45	52.93	12.18	97.79	767.00	14.87	61.39	6.97	0.68	213.60	13.56	12.87	3.89	0.33	2.02	-3.07	9.35	58.14	-1.1801
180.04	0.62	1.01	10.08	36.46	0.04	2.91	23.12	0.29	2.32	9.45	29.98	10.15	29.83	24.73	54.66	13.80	116.25	698.66	14.32	69.96	8.03	0.61	241.35	13.22	15.25	5.55	0.59	1.97	-2.99	9.43	59.25	-1.3302
180.09	0.60	1.00	9.94	35.87	0.05	2.84	23.53	0.28	2.37	9.35	29.19	10.08	30.97	31.69	54.44	13.18	112.60	724.06	14.81	67.10	8.07	0.57	232.46	18.92	15.44	5.61	0.81	2.07	-3.38	7.85	57.95	-0.9596
180.14	0.48	0.86	7.80	30.19	0.07	2.35	29.25	0.22	2.04	7.98	20.06	6.85	22.68	22.90	48.86	10.66	88.24	822.43	14.53	53.87	6.57	0.82	186.83	10.95	11.57	4.61	0.45	2.07	-3.00	8.43	60.02	-1.0013
180.24	0.37	0.74	6.14	25.28	0.12	1.95	34.39	0.17	1.76	6.82	14.32	4.55	16.98	16.57	45.22	9.42	68.90	848.33	14.89	42.60	5.35	0.96	149.85	10.32	11.53	3.90	0.26	2.00	-2.92	6.70	57.03	-0.7017
180.29	0.49	0.86	7.73	30.51	0.05	2.35	29.08	0.22	2.05	7.73	22.15	7.73	24.06	16.90	49.35	10.59	87.90	786.05	13.11	54.77	6.16	0.85	184.66	12.05	12.27	4.26	0.36	1.84	-3.06	5.93	57.40	-0.8003
180.34	0.49	0.83	7.35	29.20	0.05	2.26	30.48	0.21	1.87	8.15	20.28	6.99	21.34	16.50	46.96	10.40	82.49	797.94	13.87	51.45	5.80	0.49	177.12	12.00	11.01	3.33	1.05	1.95	-3.13	7.78	62.60	-1.1336
180.45	0.53	0.86	8.11	31.54	0.05	2.47	27.92	0.24	2.06	7.85	23.37	7.57	27.32	16.51	47.50	11.60	94.37	790.73	14.27	57.03	6.75	0.73	197.14	12.76	11.93	3.36	0.07	1.99	-2.91	5.40	58.09	-0.9069
180.50	0.46	0.82	7.33	29.25	0.07	2.24	30.37	0.21	1.94	8.09	19.52	6.25	27.18	15.11	45.38	10.79	82.75	825.43	14.38	51.68	6.08	0.86	174.60	12.30	10.90	3.78	0.46	1.90	-3.42	7.40	55.89	-1.0569
180.54	0.50	0.85	7.61	30.12	0.07	2.27	29.61	0.22	1.93	8.78	21.34	7.13	23.49	21.37	47.81	10.23	84.01	799.79	14.86	53.99	6.45	0.25	178.90	9.84	11.64	4.05	0.44	1.87	-3.23	8.58	55.29	-0.6006
180.63	0.47	0.84	7.35	29.51	0.07	2.20	30.34	0.22	1.94	9.25	21.56	6.29	22.95	16.91	47.70	10.36	82.04	795.37	14.38	52.11	6.02	0.72	177.13	12.31	12.30	3.82	0.15	1.87	-3.14	7.75	60.03	-0.89
180.69	0.45	0.78	6.63	27.18	0.07	2.03	32.56	0.19	1.90	7.44	18.79	5.56	21.82	15.56	45.00	9.36	71.95	821.56	14.58	46.37	5.27	0.58	166.10	8.98	9.25	3.13	0.27	1.93	-3.25	5.65	57.35	-0.8167
180.73	21.02	0.47	4.90	21.53	0.05	1.74	27.36	0.18	1.92	6.57	17.22	5.91	20.92	17.57	45.96	9.62	76.76	802.54	14.29	48.40	5.84	0.69	157.57	10.16	9.61	4.12	0.74	1.92	-3.04	8.43	54.82	-0.9439
average	1.49	0.80	7.21	28.03	0.08	2.16	30.83	0.21	1.96	7.61	19.79	6.84	22.37	18.93	47.72	10.23	80.65	818.56	14.30	51.67	5.89	0.67	176.81	11.90	11.59	3.79	0.48	1.88	-3.20	7.13	56.88	-0.86